Using a multi-modal imaging platform to understand neutrophil-*Staphylococcus aureus* interactions

The University Of Sheffield.

Yin Xin Ho

Department of Infection, Immunity and Cardiovascular Disease

The University of Sheffield

Thesis submitted for the degree of

Doctor of Philosophy

November 2020

Acknowledgements

I would like to extend my sincere gratitude to my supervisors Dr. Lynne Prince and Professor Ashley Cadby for their guidance, support and kindness throughout my PhD journey. Lynne, for the constant encouragement and patience, and teaching me with everything neutrophil related. Ashley, for guiding me through all things optics, and giving me the opportunity to work with the coolest microscopes.

Thank you to The Florey Institute, University of Sheffield and MRC SHIELD consortium for funding my project and studentship.

I would like to thank the past and present Cadby lab members, with special mention to Elliot and Liyana who have provided immense help with the Cairnfocal work. Dylan, Olivia, and our BICEN neighbours Dr. Timothy Craggs and Ben Ambrose for all their help and support within and outside of the lab. Thanks for all the great lab meetings, coffee and laughter. I'd also like to express my gratitude to the past and present Prince group members, Beth, Becky, Callum, Georgia, Kim and Olivier for all their help and support. I'd also like to extend my thanks to Professors Alison Condliffe, Ian Sabroe and Dr. Lisa Parker, and their research group members Becca, Kirsty, Jo, Natalia and Zena for all their support and helpful discussions.

I am grateful to the blood donors and phlebotomists, without whom this work would not be possible. Special thanks goes to the IICD technicians, Dr. Mark Ariaans, Dr. Benjamin Durham, Katie Cooke and Jon Kilby for keeping the labs going. Big thank you to Dr. Darren Robinson and Dr. Christa Walther from the Wolfson Light

Microscopy Facility, and Dr. Colin Gray from the medical school microscopy core facility for their support in the microscopy work, as well as the invaluable assistance from the flow cytometry core facility staffs Kay Hopkinson and Sue Clark for everything flow cytometry-related. I'd also like to thank Dr. Victoria Lund and Professor Simon Foster for their advice and help with the fluorescence amino acid labelling work.

Thank you to all my friends outside of the lab, with a special mention to Laia, for all the coffee breaks and constant encouragements. I'd also like to thank my friends from the Florey and Imagine student cohort, for all the great times we had in the organisation of outreach activities, seminars and symposiums. Last but not least, I would like to render my deepest gratitude to my family, for their love and ceaseless support in my endeavours. To my partner Gim Seng, for his unwavering patience and faith in me. Thank you for putting up with me, and for fuelling me in this journey with an endless supply of cookies.

Abstract

Staphylococcus aureus is a multifaceted pathogen, and *S. aureus* infections remain a global health burden. Neutrophils are an essential component of innate immunity in response to *S. aureus* infections. Yet, *S. aureus* can evade the neutrophil response, ultimately leading to neutrophil death. Understanding neutrophil and *S. aureus* interactions at the sub-cellular level is crucial in developing new therapeutics.

This thesis aims to identify ways to enhance neutrophil killing of intracellular *S. aureus*, and to develop ways to visualise neutrophil and *S. aureus* interactions at sub-cellular level. To address the first aim, specific necrosis inhibitors were used to determine whether they enhanced neutrophil-mediated killing of *S. aureus*. Complemented by an unbiased approach, a subset of compounds (800 out of 2000) in the Spectrum Collection was screened by high-throughput flow cytometry. Four compounds without direct anti-staphylococcal activity: chlorambucil, 17-B-estradiol, phenylmercuric acetate, 4-aminophenylmercuric acetate (4-APMA) were identified and assessed for their ability to modify *S. aureus*-induced neutrophil cell death. Activation of matrix metalloprotease (MMP) by 4-APMA attenuated *S. aureus*-induced neutrophil cell death, but failed to promote neutrophil-mediated killing of *S. aureus*.

Next, a multi-modal imaging platform capable of studying *S. aureus* within neutrophils was developed. This enabled the switching between imaging modalities, from low photo-toxicity, low resolution modality through increasing illumination intensity to achieve live super-resolution imaging. This was applied to follow the intracellular

S. aureus dynamics. Early to late infection stages were followed using multi-colour confocal and structured-illumination, revealing heterogenous population of *S. aureus* in acidified and non-acidified compartments within single neutrophil. Furthermore, septum in *S. aureus* within non-acidified compartments were observed. New cell wall synthesis was confirmed by a novel *in vivo* fluorescence D-amino acid labelling approach.

This thesis identified possible roles of MMP in modifying neutrophil-mediated killing of intracellular *S. aureus*. Additionally, the multi-modal imaging technique revealed new cell wall synthesis by intracellular *S. aureus*. Combining biological and imaging approaches may contribute to the understanding of neutrophil-*S. aureus* interactions and future therapeutic strategies.

Table of contents

List of figures

List of tables

Abbreviations

4-APMA	4-aminophenylmercuric acetate
ADAM 10	A Disintegrin And Metalloprotease 10
Aur	Aureolysin
Bcl-2	B-cell lymphoma 2
BHI	Brain Heart Infusion
CA-MRSA	Community-acquired MRSA
CFU	Colony forming unit
CGD	Chronic granulomatous disease
CHIPS	Chemotaxis inhibitory protein of *S. aureus*
CHX	Cycloheximide
CLSM	Confocal laser scanning microscopes
CXCR4	CXC-chemokine receptor 4
DAMPs	Danger-associated molecular patterns
DIC	Differential interference contrast

DMD	Digital micromirror device
DMEM	Dulbecco's Modified Eagle's Medium
DPX	Distyrene, plasticizer and xylene
dsRNA	Double-stranded RNA
EAP	Extracellular adherence protein
ELISA	Enzyme-linked immunosorbent assay
ExM	Expansion microscopy
FBS	Fetal Bovine Serum
FcR	Fc receptors
FPR	Formyl-peptide receptor
FSC	Forward scatter
G-CSF	Granulocyte colony stimulating factor
GFP	Green fluorescence protein
GPCRs	G protein-coupled receptors
HA-MRSA	Hospital-acquired MRSA
hBD3	Human β-defensin 3
HBSS	Hank's Balanced Salt Solution
HlgAB	γ-hemolysin AB
HlgCB	γ-hemolysin CB

hMDM	Human monocyte-derived macrophage
HSCs	Hematopoietic stem cells
IFN γ	Interferon γ
Ig	Immunoglobulins
iNOS	Inducible nitric oxide synthase
ISM	Image scanning microscopy
LEDs	Light-emitting diodes
LFA1	Lymphocyte function-associated antigen 1
MLKL	Mixed lineage kinase domain-liked protein
MMPs	Matrix metalloprotease
MOI	Multiplicity of infection
MPO	Myeloperoxidase
MRSA	Methicillin-resistant *S. aureus*
MSIM	Multifocal structured-illumination microscopy
NA	Numerical aperture
NADPH	Nicotinamide adenine dinucleotide phosphate oxidase
Nec-1	Necrostatin-1
NETs	Neutrophil extracellular traps
NO	Nitric oxide

NSA	Necrosulfonamide
P/S	Penicillin/streptomycin
PAINT	Point accumulation for imaging in nanoscale topography
PALM	Photoactivated localisation microscopy
PAM	Programmable array microscope
PAMPS	Pathogen-associated molecular patterns
PBMCs	Peripheral blood mononuclear cells
PBS	Phosphate-buffered saline
PICD	Pathogen-induced cell death
PPP	Platelet-poor plasma
PRP	Platelet-rich plasma
PRRs	Pattern recognition receptors
PS	Phosphatidylserine
PSF	Point spread function
PSMs	Phenol-soluble modulins
PVL	Panton-Valentine Leukocidin
RBCs	Red blood cells
RCF	Relative centrifugal force
RIPK-1	Receptor interacting protein kinase-1

ROS	Reactive oxygen species
RPM	Revolutions per minute
RT	Room temperature
SAB	*S. aureus* bacteremia
SAg	Superantigen
Sbi	Staphylococcal binder of IgG
SCCmec	Staphylococcal cassette chromosome mec
SELX	Staphylococcal enterotoxin-like toxin X
SIM	Structured-illumination microscopy
SMLM	Single-molecule localisation microscopy
SNR	Signal to noise ratio
SOFI	Super-resolution Optical Fluctuation Imaging
SpA	*S. aureus* protein A
SRRF	Super-Resolution Radial Fluctuation
SSC	Side scatter
SSL5	Staphylococcal superantigen-like protein 5
SSTIs	Skin and soft tissue infections
STED	Stimulated emission depletion
STORM	Stochastic optical reconstruction microscopy

TLRs	Toll-like receptors
TNFα	Tumor necrosis factor α
WBCs	White blood cell

Chapter 1

Introduction

S. aureus is a Gram-positive bacterium, first discovered in 1880 by Sir Alexander Ogston from pus in surgical wound (Vanbelkum et al., 2009). A highly opportunistic pathogen in human, *S. aureus* is known to cause wide range of infections, such as skin and soft tissue infections (SSTIs), septicemia and osteomyelitis (Otto, 2010). *S. aureus* colonises roughly 30% of the human population, and preferentially adheres to nasal epithelial cells, thus facilitates its persistence in the anterior nares (Krismer et al., 2017; Mulcahy and McLoughlin, 2016). *S. aureus* has garnered major attention as a hugely successful pathogen due to its extensive antibiotic resistance profile and the virulence factors secreted. Neutrophils are immune cells that are critical in defending the host against *S. aureus* infections. However, *S. aureus* has evolved sophisticated mechanisms to evade neutrophil killing and persist inside neutrophils. Recent developments have cast light on this host-pathogen interaction, and yet our understanding of how *S. aureus* escape from neutrophil remains largely incomplete. It is important to understand the cellular and molecular events leading to *S. aureus* escape from neutrophils, which could potentially yield new strategies to combat *S. aureus* infections.

1.1 Neutrophils

Neutrophils are a component of the innate immune response, and they are the most abundant granulocyte in humans, accounting for 50-70% of the white blood cells in circulation (Edwards, 1994). Neutrophils have a short life span, surviving for 8-12 hours in the circulation; and up to 1-2 days in tissues (Dancey et al., 1976; Mayadas et al., 2014). Neutrophils are rapidly turned over, and their abundance and brief life span demands a high production rate. To meet this demand, it is estimated that a basal rate of 10^{10} neutrophils per day are produced from the bone marrow (Summers et al., 2010). Neutrophils are developed from hematopoietic stem cells (HSCs) in the bone marrow through a process known as granulopoiesis (Cowland and Borregaard, 2016). On average, granulopoiesis is estimated to take 14 days, before mature neutrophils are ready to be released into blood (Bainton, 1971). CXC-chemokine receptor 4 (CXCR4) expressed by mature neutrophils interacts with the chemokine SDF1α (CXCL12), thus retaining mature neutrophils in bone marrow (Semerad et al., 2002). Ninety percent of neutrophils are reserved in the bone marrow, creating a reservoir that enables rapid mobilisation of neutrophils into the circulation when there is an increased demand, such as during an infection. Granulocyte colony stimulating factor (G-CSF) downregulates CXCL12 expression, and by acting in concert with cytokines such as CXCL8, leads to the release of neutrophils from bone marrow into blood (Semerad et al., 2002; Soehnlein et al., 2017).

1.1.1 Neutrophil recruitment

Circulating neutrophils are quiescent, and pro-inflammatory mediators such as tumor necrosis factor α (TNFα), granulocyte-macrophage colony-stimulating factor (GM-CSF) and microbial products that are released upon infection mediates neutrophil

priming, a process which promotes a cellular response, thus allowing rapid and efficient neutrophil activation against invading pathogens (El-Benna et al., 2016; van Kessel et al., 2014). Circulating neutrophils are recruited to the site of infection via a process known as extravasation. To decelerate the neutrophils that are circulating at high speed, activated endothelial cells upregulate P and E -selectins to mediate binding of ligands such as lymphocyte function-associated antigen 1 (LFA1) on neutrophils, thus the "rolling" of neutrophils on blood vessels (Moore et al., 1995). Neutrophils then transmigrate across endothelium and travel along the chemotactic gradient, directing the neutrophils to the infection site (Figure 1.1). Although highly challenging and complex, using *in vivo* models provided the closest resemblance to biological environment. Besides, microscopy techniques such as intravital microscopy enabled the visualisation of these processes *in vivo*, which greatly advanced our understanding of neutrophil recruitment processes in different organs (Kolaczkowska and Kubes, 2013; Margraf et al., 2019). This contributed to recent paradigm shifts in neutrophil recruitment models, challenging previous assumptions on the recruitment steps that are extrapolated to all organs. Variation in neutrophil activation and recruitment steps, as well as chemokine expression shifts were unravelled in organ-specific models, such as in the lungs and kidneys, thus amending our understanding of neutrophil dynamics (Margraf et al., 2019).

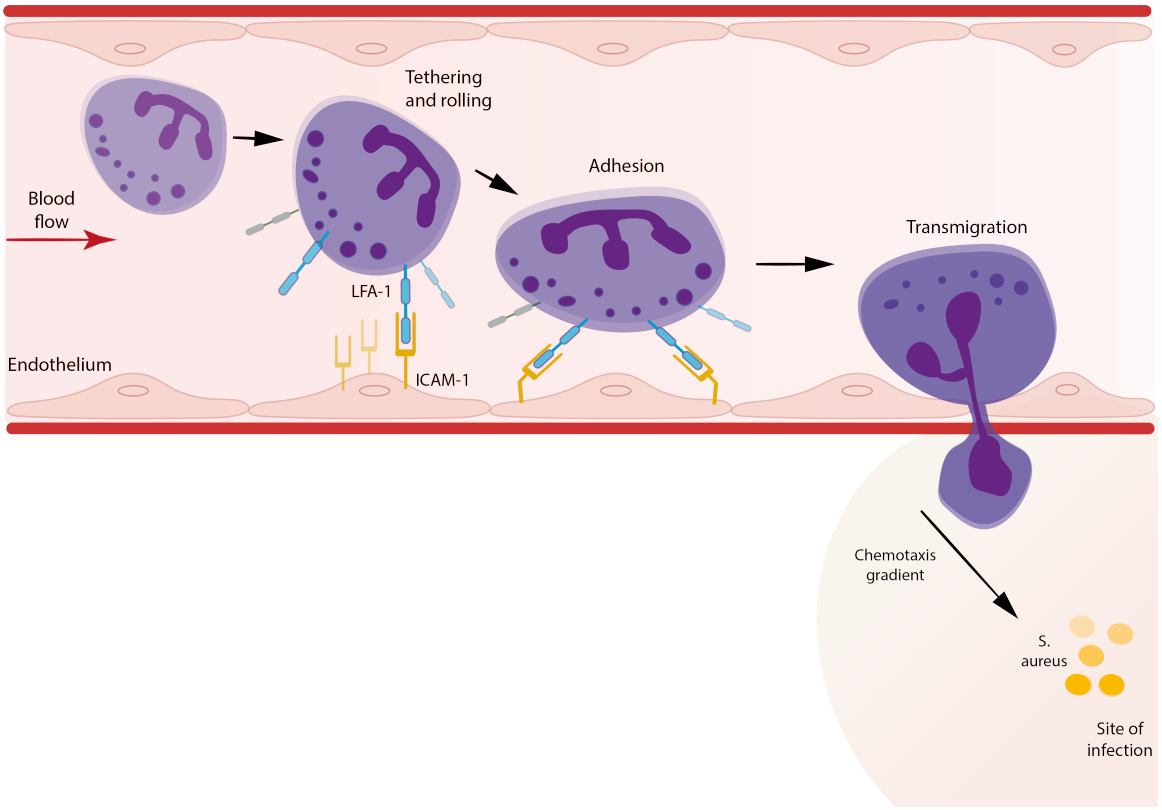

Fig. 1.1 **Neutrophil extravasation.** Neutrophil circulated at high speed are tethered to ligands on endothelium, which mediates rolling and adhesion processes, eventually transmigrating across endothelium and moving along the chemotaxis gradient towards infection site.

1.1.2 Pathogen recognition and killing

Neutrophil recognition of pathogen is a key step that precedes phagocytosis. Receptors on neutrophils, including Fc receptors (FcR), complement receptors and toll-like receptors (TLRs) are responsible for pathogen recognition. Immunoglobulins that are deposited on the *S. aureus* surface enabled its recognition by FcR on neutrophils. Similarly, complement components that opsonised the bacteria are recognised by complement receptors on neutrophils, thus triggering phagocytosis (McGuinness et al., 2016). Furthermore, TLRs on the neutrophil surface recognise and bind to microbe-specific pathogen-associated molecular patterns (PAMPS) such as lipoteichoic acid and

peptidoglycan (Mayadas et al., 2014). All TLRs are expressed by neutrophils, with the exception of TLR3, which recognise double-stranded RNA (dsRNA) expressed by viruses (Botos et al., 2009; Hayashi, 2003). Lipoteichoic acid and lipoproteins on *S. aureus* and lipopolysaccharide on Gram-negative bacteria such as *Escherichia coli* are recognised by TLR4 on neutrophils, which trigger downstream signalling cascades leading to inflammatory responses (Bubeck Wardenburg et al., 2006; Sabroe et al., 2003). Furthermore, complement factors C3a and C5a that are generated during complement activation are key components in inflammatory responses, as well as chemoattractants for neutrophils to site of infection (Sarma and Ward, 2011).

Invading bacteria are typically internalised and killed by neutrophils via phagocytosis, which is an important host defense mechanism. Phagocytosis is a receptor-mediated process which is initiated when receptors on neutrophils such as G protein-coupled receptors (GPCRs) and FcR recognise and bind to PAMPs on pathogens. This engagement initiates cytoskeleton rearrangement that leads to the formation of pseudopodia around the pathogen, which extends and encloses the pathogen, eventually forming a vacuole known as phagosome (Figure 1.2) (Mayadas et al., 2014). Unlike other phagocytes such as macrophages, neutrophils are able to internalise targets quickly. It has been shown that neutrophils are able to internalise IgG-opsonised particles in less than 20 seconds, and this rapid internalisation provides an upper hand to the host defense (Segal et al., 1980).

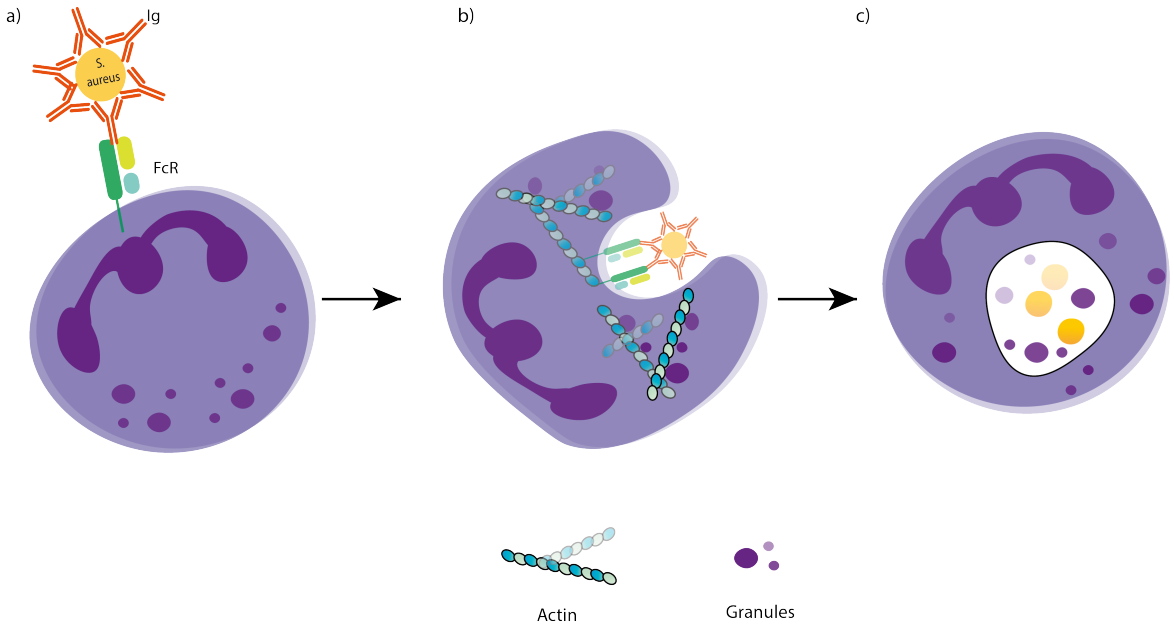

Fig. 1.2 **Neutrophil phagocytosis of *S. aureus*.** a) Opsonised *S. aureus* is recognised by Fc receptor (FcR) on neutrophil. b) Cytoskeleton rearrangements, such as actin remodelling lead to granules trafficking, as well as pseudopodia formation, which surrounds the pathogen. c) Extension and closing of pseudopodia, forming a phagosome.

1.1.3 Neutrophil oxidative and non-oxidative killing mechanism

Killing by oxidative and non-oxidative mechanisms are the two main microbicidal mechanisms of neutrophils. Degranulation, which is a non-oxidative killing mechanism is initiated when neutrophils are activated, as well as when granules are fused with phagosome.

Granules that are present in neutrophils can be grouped into peroxidase-positive granules (also known as primary granules) and peroxidase-negative granules, which further branch into secondary and tertiary granules. Each type of granule contains antimicrobial peptides, proteases and inflammatory mediators which are shown in

Table 1.1. The contents of different granule types are dependent on the timing of granulopoiesis (Faurschou and Borregaard, 2003). Azurophilic granules mainly constitutes of microbicidal proteins, hence critical in pathogen killing. For example, neutrophil elastase is vital in *S. aureus* killing, and this in turn, makes them a target of *S. aureus* immune evasion proteins like extracellular adherence protein (EAP) (Herdendorf and Geisbrecht, 2018; Herdendorf et al., 2020; Stapels et al., 2014). Specific and gelatinase granules have overlapping contents, and the proteins contained within these granules are required in neutrophil migration and extravasation (Yin and Heit, 2018). For instance, tertiary granule constituents gelatinase A and B, also known as matrix metalloproteases (MMP)-2 and MMP-9 degrades extracellular matrix, thus facilitating neutrophil extravasation (Faurschou and Borregaard, 2003). Neutrophil granules are released in an orderly manner and in consonance with neutrophilic functions. Proteins in specific and gelatinase granules are vital in neutrophil extravasation, thus released before encountering pathogen, whereas azurophilic granules are released upon pathogen contact (Cowland and Borregaard, 2016; Yin and Heit, 2018).

Types of granules	**Constituents**
Azurophilic (primary)	α-defensins, myeloperoxidase (MPO), lysozyme, elastase, proteinase-3, cathepsin G
Specific (secondary)	Lysozyme, lactoferrin, collagenase, gelatnase
Gelatinase (tertiary)	Acetyltransferase, gelatinase, lysozyme

Table 1.1 Components that are present in different types of neutrophil granules.

The release of granular constituents are dependent on the strength of degranulation stimuli. Presence of pathogens at infection sites contribute to the strong degranulation stimuli, hence the rapid release of azurophilic contents following neutrophils arrival

at the site of infection (Lodge et al., 2020). Following phagocytosis, phagosomes are formed within neutrophils, which subsequently leads to phagosomal maturation. Neutrophil granules such as azurophilic granules are rapidly delivered to the phagosome by translocation via microtubules (Sheshachalam et al., 2014). Fusion of granules with phagosome vesicles triggers the release of granule contents into the vesicles, which endow the phagosome with microbicidal abilities (Nordenfelt and Tapper, 2011). Furthermore, oxidative burst, where reactive oxygen species (ROS) such as hydrogen peroxide and hypochlorous acid, generated by the multi-component NADPH oxidase, are released occurs concurrently with degranulation, further enriching the phagosome for pathogen killing (El-Benna et al., 2016; Klebanoff, 2005; Nordenfelt and Tapper, 2011). Thirty minutes after phagocytosis, phagosomal pH has been shown to increase to pH 8-9, where proteases such as cathepsin G and MPO are activated in an alkaline environment, thus facilitating pathogen killing (Levine et al., 2015; Reeves et al., 2002). The alkalization of phagosomal pH is mediated by nicotinamide adenine dinucleotide phosphate oxidase (NADPH), in conjunction with oxidative burst (Jankowski and Grinstein, 2002). Following the brief alkalization, phagosomal pH gradually decreases, but the timing and pH levels remained controversial, as studying phagosomal pH changes are hindered by the sensitivity of fluorophores to the phagosomal microenvironment, hence quenching of fluorophore signals (Foote et al., 2017; Nordenfelt and Tapper, 2011).

The importance of granules in the antimicrobicidal activity of neutrophil is highlighted by Chediak-Higashi syndrome, a rare autosomal disease characterised by large, abnormal granules. Individuals with Chediak-Higashi syndrome have increased susceptibility to recurrent skin and respiratory infections, especially with *S. aureus* (Introne et al., 1999). In addition to antimicrobial activity, antimicrobial peptides that are found in granules have immunomodulatory functions. For example, LL-37 which kills

pathogens by permeabilisation of the cell wall can act as a chemokine for neutrophils, and it also plays an anti-inflammatory role by reducing IL-6 and TNFα production (Fabisiak et al., 2016; Nijnik and Hancock, 2009).

Other than degranulation, neutrophils can mediate oxidative-killing via generation of reactive oxygen species (ROS). NADPH oxidase, an enzymatic complex in the phagosomal membrane is activated following phagocytosis, leading to an immediate increase in oxygen consumption known as the respiratory burst. The production of superoxide anion (O_{2-}) from oxygen is catalysed by NADPH oxidase (Morel et al., 1991). Additionally, nitric oxide (NO) production is catalysed by inducible nitric oxide synthase (iNOS) in primary granules (Wheeler et al., 1997). These products are key components in pathogen killing by neutrophils. The importance is shown in chronic granulomatous disease (CGD), wherein patients suffer from recurrent *S. aureus* infections due to a respiratory burst defect caused by mutations in NADPH oxidase components (Goldblatt and Thrasher, 2000).

Neutrophil oxidative and non-oxidative mediated killing are often viewed as working in concert, or serving as a backup mechanism in the event in which one mechanism fails. However, the primacy of either mechanism remains enigmatic, as experiments are often focused on specific pathogens, which limits our ability to evaluate the relative contributions of either mechanism in mixed infections *in vivo*. In as much as oxidative and non-oxidative mediated killing are important in pathogen killing, these mechanisms require careful balancing as excessive oxidative or non-oxidative mediated killing can lead to collateral damage to the host. For example, high concentration of elastase and collagenase, which are enzymes in neutrophil granules can contribute to tissue damage in rheumatoid arthritis, an autoimmune disease characterised by inflammation in synovial tissues in joints (Navegantes et al., 2017). In lungs, unwarranted degranulation

leads to unregulated release of myeloperoxidase (MPO) and elastase, thus resulting in tissue damage that aggravates cystic fibrosis (Gray et al., 2018; Jasper et al., 2019).

1.1.4 Neutrophil extracellular traps (NETs) formation

Besides oxidative and non-oxidative mediated killing, neutrophils are capable of killing pathogens by releasing NETs. NETs are thought to function by trapping the pathogen with its network of chromatin and deploy antimicrobial peptides such as LL-37 and MPO to kill the pathogen (Papayannopoulos and Zychlinsky, 2009). NETs are comprised of decondensed chromatin and primary granule components such as elastase and MPO (Papayannopoulos et al., 2010). Upon activation of signalling cascades, neutrophil loses its nuclear membranes, and the expansion of chromatin fills the entire cell, subsequently leading to cell membrane rupture and chromatin expulsion (Brinkmann, 2018; Neubert et al., 2020, 2018).

S. aureus pore-forming cytotoxins such as SpA, PVL, LukGH and LukED have been shown to promote NETs formation (Hoppenbrouwers et al., 2018; Malachowa et al., 2013; Pilsczek et al., 2010). Although NETs have been described as a last attempt defense strategy, pathogens have also evolved ways to overcome NETs killing. Menegazzi and colleagues showed that live *S. aureus* and *Candida albicans* can be recovered after incubation with NET-forming neutrophils, suggesting that NETs entrap pathogens but do not kill them (Menegazzi et al., 2012). It has been suggested that extracellular adherence protein (Eap) enabled *S. aureus* to block NETs formation (Eisenbeis et al., 2018). Furthermore, Thammavongsa et. al showed that *S. aureus* secretes nuclease and adenosine synthase to degrade NETs, impeding macrophage entry to staphylococcal abcesses thus leading to persisting infections (Thammavongsa et al., 2013).

Despite various neutrophil killing mechanisms, Gresham et al showed that live *S. aureus* can be recovered from neutrophils (Gresham et al., 2000). This was independently verified by Voyich and colleagues, and the group also showed that phagocytosis of community-acquired *S. aureus* strains lead to upregulation of genes involved in oxidative stress and virulence (Voyich et al., 2005). For example, catalase, as well as superoxide dismutase SodA and SodM were among factors that were upregulated to facilitate *S. aureus* immune evasion (Beavers and Skaar, 2016; Voyich et al., 2005). How *S. aureus* has evolved numerous ways to manipulate neutrophils and evade immune responses will be discussed in section 1.2.3.3.

1.1.5 Neutrophil cell death programs

1.1.5.1 Apoptosis

Neutrophils undergo a tightly regulated form of cell death known as apoptosis, in order to limit the release of toxic cell contents. The release of toxic neutrophilic contents, if unregulated, can instigate undesirable consequences to the host, such as inflammation and tissue damage (Fox et al., 2010). For instance, unwarranted degranulation results in exacerbation of diseases like cystic fibrosis, as discussed in section 1.1.3. Moreover, the short half-life of neutrophils is a result of neutrophils being programmed to undergo apoptosis after circulating in blood for 8-12 hours, although the timing can be influenced by various factors (Iba et al., 2013; Summers et al., 2010). Apoptosis can be initiated through intrinsic and extrinsic pathways. The intrinsic apoptotic pathway primarily takes places at the mitochondrial level, wherein mitochondrial membrane permeabilisation leads to the release of cytochrome c into the cytosol. In cytoplasm, cytochrome c initiates downstream activities involving caspases 9 and 3 proteases, eventually leading to apoptosis (McCracken and Allen, 2014; Murphy et al., 2003). The extrinsic apoptotic pathway is driven by the binding

of ligands to death receptors such as TNF receptor on the cell surface, leading to cleaving of procaspase-8, further activating caspase-3 downstream that ultimately triggers apoptosis (Fox et al., 2010; McCracken and Allen, 2014).

Neutrophil apoptosis is manifested with morphological alterations, such as chromatin condensation and nuclear DNA fragmentation as a result of underlying biochemical shifts. Moreover, the plasma membrane of apoptotic neutrophils remains intact to prevent leakage of neutrophil contents (Iba et al., 2013). Pathogen-induced cell death (PICD) is a key form of apoptosis, triggered by phagocytosis of pathogen, which accelerates apoptosis and neutrophil clearance by macrophages. This clearing process is marked by changing of surface markers expression, for example, an increase in the 'eat me' signal phosphatidylserine, which recruits macrophages for clearance of apoptotic neutrophils through a process known as efferocytosis (Huynh et al., 2002). PICD is a ROS-dependent process, and this is highlighted in CGD patients, where PICD is attenuated, leading to the development of granulomas as a result of prolonged proinflammatory responses and tissue damage (Lawrence et al., 2020).

1.1.5.2 Necrosis and necroptosis

Unlike apoptosis whereby cell death proceeds in a regulated manner, necrotic cell death is turbulent. Neutrophils undergo necrosis as a result of exposure to insults such as trauma and pathogens (Zysk et al., 2000). Neutrophilic contents such as proteases and antimicrobial peptides, as well as danger-associated molecular patterns (DAMPs) such as heat shock proteins are released into the surrounding environment in an uncontrolled manner, leading to inflammation and tissue damage (Iba et al., 2013). Macroscopic morphology changes in necrotic neutrophils includes swelling of cells and disintegration of cell membrane. The damage and disintegration of cell membrane subsequently leads to the spillage of neutrophilic contents, hence inflammation (Rock and Kono, 2008).

Recently, necrosis is shown to occur in a controlled manner, and this process is known as necroptosis (Figure 1.3). Regulation of necroptosis occurs at the molecular level, wherein receptor interacting protein kinase-1 (RIPK-1), RIPK-3 and mixed lineage kinase domain-liked protein (MLKL) are activated sequentially (Galluzzi et al., 2018). Necroptotic cells exhibit necrotic morphological features, and necroptosis can be induced by TNF activation, as well as stimulation of death receptors such as IFNα receptors (Wang et al., 2018).

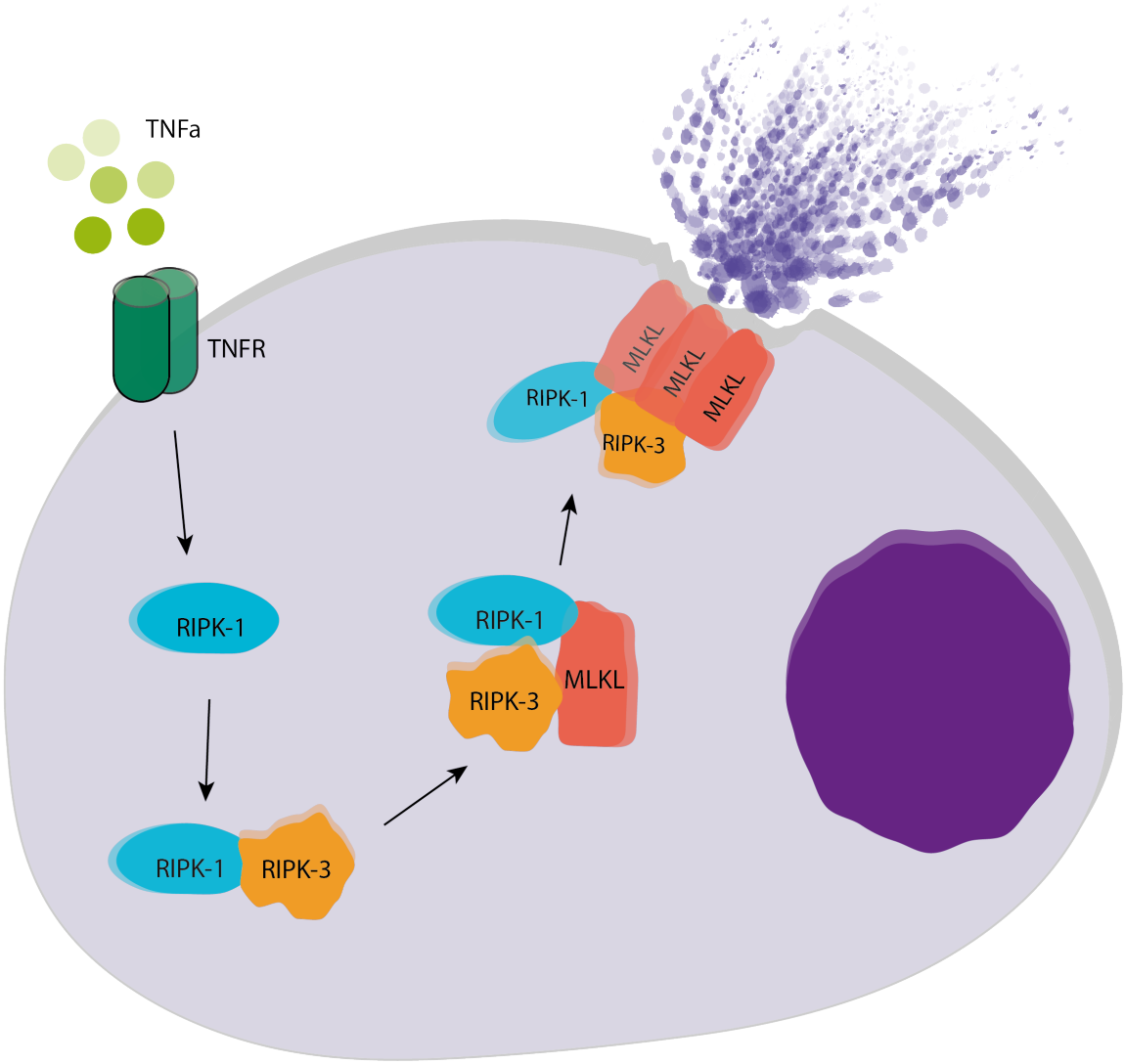

Fig. 1.3 **Necroptosis pathway in neutrophils.** Binding of TNFα to TNF receptor (TNFR) activates RIPK-1. RIPK-1 binds to RIPK-3, subsequently induces MLKL oligomerisation and translocation to plasma membrane, eventually triggering membrane permeabilisation and cell lysis.

It has been shown that *S. aureus* leukocidin and PSM can induce necrosis in neutrophils (Malachowa et al., 2013; Surewaard et al., 2013). Additionally, evidence suggests that neutrophil phagocytosis of *S. aureus* can induce necroptosis, and in MLKL knockout mice, clearing of *S. aureus* by neutrophils were incomplete (Greenlee-Wacker et al., 2017; Kitur et al., 2016). Recent work suggests that PSM triggers *S. aureus*-mediated neutrophil necroptosis, and blocking this using inhibitors such

as necrosulfonamide to block MLKL decreased neutrophil lysis (Zhou et al., 2018). However, this result contradicts with the work by Greenlee-Wacker and colleagues, which showed that *S. aureus*-induced necroptosis is RIPK-1 and MLKL independent (Greenlee-Wacker et al., 2017). This could be due to variation in neutrophil co-culture conditions, such as the use of *S. aureus* live bacteria and supernatant. There are limited studies on *S. aureus*-induced necroptosis in neutrophils, and the underlying mechanisms remained contentious. Therefore, further studies to unravel the mechanisms of *S. aureus*-induced neutrophil necrosis and necroptosis is essential, and this may lead to pharmalogical targeting of specific components for novel therapeutic means.

1.2 *S. aureus*

1.2.1 Clinical significance of *S. aureus*

A highly opportunistic pathogen, *S. aureus* is involved in extensive range of infections, including skin and soft tissue infections and bloodstream infections. As it preferably colonises human nares, *S. aureus* skin infections are the leading cause of bacteremia (Kwiecinski and Horswill, 2020). In fact, the incidence of *S. aureus* bacteremia (SAB) has grown significantly in the industrialised countries during the past decades. Since the development of methicillin-resistant *S. aureus* (MRSA) strain, MRSA infections have been an increasing burden in many countries, with particularly high prevalence in the United States and Asia (Lee et al., 2018). The high incidence of *S. aureus* infections can be attributed to its ability to acquire and develop resistance toward antibiotics (Otto, 2013). Unlike MRSA, the methicillin-sensitive *S. aureus* (MSSA) strain is susceptible to antibiotics treatment. However, the MSSA strain is more prevalent globally, and remains an important infection (Goss and Muhlebach, 2011). In

fact, patients with MSSA infections in hospital are more likely to develop bacteremia and sepsis (David et al., 2011).

1.2.2 *S. aureus* antibiotic resistant strains

The introduction of penicillin in clinical practices in the 1940s heralded the dawn of the antibiotic era. However, penicillin resistance began to surface just after a few years of widespread use, and this further developed into a major problem in hospitals. The introduction of methicillin, which is a penicillinase-resistant penicillin was quickly followed by the development of MRSA in 1961 (Deurenberg and Stobberingh, 2008). Since then, MRSA has disseminated globally and remained endemic in many healthcare facilities in the industrialised world (Chambers and DeLeo, 2009; Tong et al., 2015).

The first community-acquired MRSA (CA-MRSA) cases were reported in early 1990s in Australia (Udo et al., 1993). Healthcare-associated MRSA (HA-MRSA) affects individuals who are at risk of infection. Conversely, CA-MRSA is capable of infecting otherwise healthy individuals, therefore indicating that CA-MRSA has enhanced virulence compared to HA-MRSA (DeLeo et al., 2010). SSTIs are the most common clinical manifestations of CA-MRSA, accounting for up to 90% of CA-MRSA infections (Otto, 2010). Similar to all *S. aureus* strains, the transmission of CA-MRSA occurs by direct contact with the bacteria, for example via direct skin contact with infected individuals and contaminated environment (DeLeo et al., 2010; Stryjewski and Chambers, 2008). This has a profound consequence on the rapid spread of CA-MRSA in close communities. CA-MRSA carries staphylococcal cassette chromosome mec (SCCmec) type IV, which is more compact compared to other SCCmec variants in HA-MRSA. The compactness of SCCmec type IV is believed to reduce the fitness burden, thus explaining in part the ability of CA-MRSA to spread quickly in community (Otto, 2010, 2013).

CA-MRSA is a dangerous pathogen as a result of combining its extensive antibiotic resistance profile and the virulence factors secreted. Leukolytic toxins, also known also leukocidins, are toxins produced by *S. aureus* which kills leukocytes as well as erythrocytes (Rigby and DeLeo, 2012). Interest in leukocidins has surged as they are the focal point of efforts to understand the high virulence of CA-MRSA (Otto, 2010). Notably, Panton-Valentine Leukocidin (PVL), a bi-component toxin has been of great interest in the past decades. This is due to the presence of PVL-encoding genes in CA-MRSA isolates associated with infection (Boyle-Vavra and Daum, 2007; DeLeo et al., 2010). In addition to PVL, α-toxin is a pore-forming toxin that plays an important role in the virulence of CA-MRSA, and it has been shown that α-toxin is crucial in determining the virulence of clinically-relevant CA-MRSA isolates in pneumonia in mice model (Bubeck Wardenburg et al., 2007).

1.2.3 Virulence factors of *S. aureus* and how these virulence factors can facilitate *S. aureus* to overcome neutrophil immunity

S. aureus expresses a broad array of virulence factors that facilitates its adhesion and colonisation, evasion of host immune response, as well as acclimatisation to the host environment, which eventually cause infections (Foster, 2005; Foster et al., 2013). The specific and coordinated expression of multiple virulence factors are regulated at the transcriptional level by regulatory factors embedded within the core genome of *S. aureus*, and the selective expression of virulence factors is fine-tuned by various elements, such as growth phase and environmental cues (Bronner et al., 2004).

1.2.3.1 Inhibition of chemotaxis

The surface of *S. aureus* is decorated with surface proteins that are crucial in the adhesion to host cells, which is the first step of establishing itself in the host. Once *S. aureus* has established a foothold in the host, it is confronted by the host innate and then the adaptive immune response. Numerous virulence factors can act in concert to evade the host immune response effectively and to resist the killing of *S. aureus*. *S. aureus* infection leads to complement activation, which generates peptide fragments such as C3a and C5a. Furthermore, growing bacteria produces formylated peptides. Together with C3a and C5a, formylated peptides acts as chemoattractant to neutrophils, hence the migration of neutrophils to site of infection (Murdoch and Finn, 2000). To thwart neutrophils chemotaxis, chemotaxis inhibitory protein of *S. aureus* (CHIPS), an exoprotein secreted by 60% of *S. aureus* strains functions by binding to C5a receptor and formyl-peptide receptor (FPR) on neutrophils (Postma et al., 2004). Additionally, *S. aureus* secretes staphopain A, a cysteine protease that cleaves CXCR2 chemokine receptors on neutrophils, effectively inhibiting neutrophil recruitment (Laarman et al., 2012).

1.2.3.2 Inhibition of phagocytosis

Surface proteins and cell wall component such as teichoic acid and peptidoglycan are targeted by immunoglobulins (Ig), and binding of Ig to these components activate the complement system through classical and alternative pathway, and can lead to phagocytosis by neutrophils (Foster, 2005). To ensure its survival in the host, *S. aureus* secretes virulence factors that inhibit Ig recognition and complement activation, and also use multiple strategies to evade neutrophil phagocytosis and killing. One of the first steps of preventing phagocytosis is to block opsonisation. *S. aureus* that are opsonised by Ig or complement factors increases the efficiency of phagocytosis by

neutrophils. *S. aureus* produce SpA that blocks the recognition of Ig by neutrophils (Forsgren and Sjöquist, 1966). SpA, as well as Staphylococcal binder of IgG (Sbi) protein inhibit complement activation by binding to Fcγ region of IgG, rendering it inaccessible to complement components, thus blocking complement activation (Haupt et al., 2008; Laky et al., 1985). Recently, Tuffs et al. have shown that in addition to the ability to induce uncontrolled T cell proliferation, staphylococcal enterotoxin-like toxin X (SELX), a superantigen (SAg), also functions to inhibit IgG-mediated phagocytosis (Tuffs et al., 2017). This study is the first account of bifunctional SAg in *S. aureus*, and contributes to the growing research area on multifunctional *S. aureus* virulence factors.

Complement factors that are deposited on the capsular polysaccharide are rendered inaccessible to complement receptors on neutrophils. *S. aureus* capsular polysaccharide is proposed to be antiphagocytic, and yet the actual role remained debatable (O'Riordan and Lee, 2004). *S. aureus* strains with enhanced levels of capsular polysaccharide production have been shown to reduce neutrophil-mediated killing (Thakker et al., 1998). However, Gresham and colleagues showed that both microencapsulated and fully encapsulated *S. aureus* strains are able to gain entry and survive inside neutrophils (Gresham et al., 2000). In addition to the evasion of immune response, nutrient acquisition is also vital for *S. aureus* survival in host. Ferric uptake regulator (fur), which is sensitive to the iron levels in the environment mediates the upregulation of virulence factors such as Staphyloferrin A that scavenge iron, thus ensuring *S. aureus* survival in an iron-deficient environment (Hammer and Skaar, 2011; Torres et al., 2007).

1.2.3.3 Evasion of neutrophil-mediated killing

It is known that a subset of *S. aureus* survived within neutrophils using an array of immune evasion proteins. *S. aureus* uses superoxide dismutases SodA and SodM to breakdown O_{2-}, as well as using catalase to reduce hydrogen peroxide to water and oxygen, protecting the bacteria against toxic reactive oxygen species (Karavolos, 2003; Mandell, 1975). Furthermore, staphyloxantin, which is the carotenoid pigment that embellished *S. aureus* with its golden colour shields the bacteria from oxidative killing (Figure 1.4) (Liu et al., 2005). To evade non-oxidative killing of neutrophils such as defensin-mediated killing, *S. aureus* mprF gene modifies its membrane lipid composition by reducing the negative charge to repel cationic peptides (Peschel et al., 2001). Additionally, staphylokinase is secreted by *S. aureus* to bind to α-defensins, obstructing the bactericidal ability of α-defensins (Jin et al., 2004). Aside from its role in inhibiting complement activation, aureolysin plays a bifunctional role by cleaving cathelicidin LL-37, which aids in neutrophil killing evasion (Sieprawska-Lupa et al., 2004). Efflux pumps are efficient nanomachines that remove toxic substances from bacteria. Recently, Cheung et al. showed that Pmt, in addition to its function as a secretion system to export phenol-soluble modulins (PSMs) toxins, can eliminate LL-37 and human β-defensin 3 (hBD3), thus conferring resistance to neutrophil antimicrobial peptide killing (Cheung et al., 2018). This is the first account of an *S. aureus* efflux pump that eliminate human antimicrobial peptides, and further research on *S. aureus* and human antimicrobial peptides interaction is required.

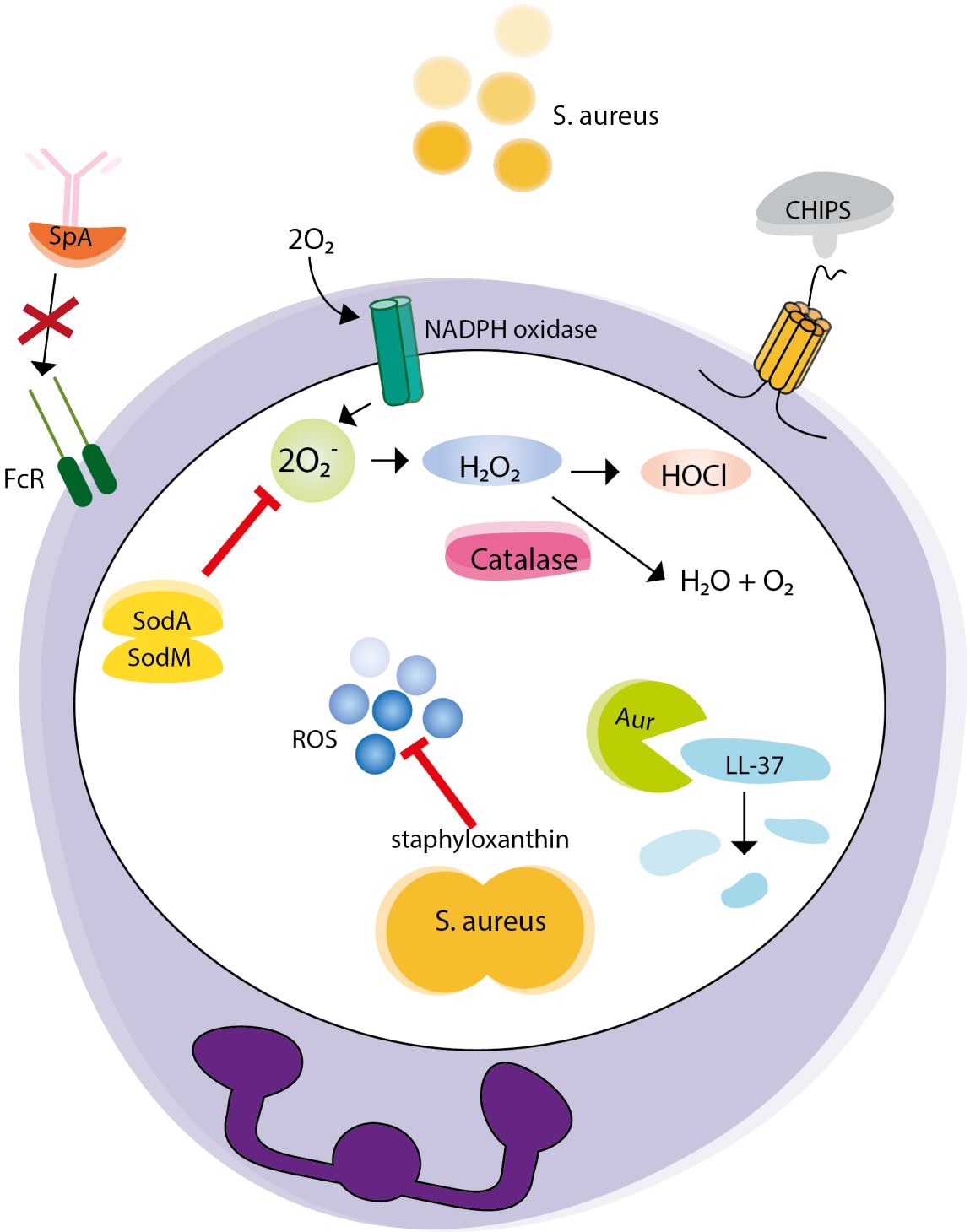

Fig. 1.4 **Various strategies used by *S. aureus* to evade neutrophil killing.** *S. aureus* uses CHIPS to circumvent neutrophil chemotaxis, and SpA to block neutrophil recognition. Within the neutrophils, catalase, staphyloxantin, as well as superoxide dismutase SodA and SodM protects *S. aureus* against reactive oxygen species. Furthermore, non-oxidative killing mechanisms circumvented by *S. aureus* includes the cleaving of LL-37 cathelicidin by aureolysin. CHIPS: chemotaxis inhibitory protein of staphylococcal; SpA: S. aureus protein A ; Aur: aureolysin; IgG: Immunoglobulin G

1.2.3.4 Virulence factors that induces neutrophil cell death

S. aureus toxins manipulates the host defense by killing neutrophils, as well as other innate and adaptive immune cells, and they are also key components in *S. aureus* pathogenesis. Tam and Torres have provided an in-depth review on the broad array of *S. aureus* virulence factors (Tam and Torres, 2019). Briefly, the α-toxin is a pore-forming toxin that is secreted as a monomer. It oligomerises to form a pre-pore structure upon binding to its target receptor, a zinc-dependent metalloprotease known as A Disintegrin And Metalloprotease 10 (ADAM 10), found in various host cells such as neutrophils, platelets and endothelial cells (Berube and Wardenburg, 2013). The pre-pore structure forms a hydrophilic transmembrane channel in host cell membrane, causing cell lysis (Seilie and Bubeck Wardenburg, 2017). Besides α-toxin, PSMs are peptides with cytolytic properties. It is found that PSMα leads to neutrophil lysis, thus facilitating intracellular *S. aureus* escape (Geiger et al., 2012; Surewaard et al., 2013). The mechanisms of intracellular *S. aureus* escape from neutrophils remained largely undefined.

Furthermore, *S. aureus* secretes bi-component leukocidins, which are pore-forming toxins that kill leukocytes. Although the discovery of leukocidins dates back to a century ago, leukocidins have amassed major attention in recent years as they are associated to CA-MRSA (Otto, 2010). Clinically relevant *S. aureus* isolates are able to produce up to five different leukocidins: PVL, LukAB, LukED, γ-hemolysin AB (HlgAB) and γ-hemolysin CB (HlgCB) (Thammavongsa et al., 2015). *S. aureus* deploy leukocidins such as LukAB to kill neutrophils by pore formation, leading to neutrophil lysis (DuMont et al., 2011). Additionally, it has also been shown that intracellular *S. aureus* uses LukAB to kill neutrophils, facilitating its escape from neutrophils and establishing infection elsewhere (DuMont et al., 2013). Recently, Niemann and colleagues showed that PVL produced by *S. aureus* lyse neutrophils, causing spillage of

neutrophil contents such as α-defensins, which activate platelets and subsequently lead to the aggregation of platelets and neutrophils. This provided a clue to the mechanism of the development of deep vein thrombosis that is linked to *S. aureus* osteomyelitis (Niemann et al., 2018).

It is not well understood why various leukocidins are produced and how these leukocidins act collectively to contribute to *S. aureus* pathogenicity. Perhaps as a way to counter the redundancy of the innate immune system, as well as to uphold the bacteria against the antigenic diversity in individual humans (de Jong et al., 2019). Majority of the leukocidin studies focused on a selected toxin and only few studies on *S. aureus* leukocidin interactions exist. For example, *S. aureus* leukocidins have shown to synergise to enhance its pathogenicity, wherein PVL and LukAB synergise to promote *S. aureus* cytotoxic potential (DuMont et al., 2013; Ventura et al., 2010). Moreover, it has been shown that PVL antagonise LukED cytotoxic activity, thus reducing *S. aureus* virulence in leukocytes and erythrocytes (Yoong and Torres, 2015). Species-specific tropism has been a major obstacle in the understanding of leukocidin interactions in human leukocytes, and the limited studies on *S. aureus* leukocidin interactions highlighted the need for further studies in understanding the collective action of the leukocidins. Recently, a new 'humanised' mouse model was described by Boguslawski and colleagues to study *S. aureus* toxins such as LukAB, thus paving way for further leukotoxin interaction studies (Boguslawski et al., 2020).

1.3 Light microscopy and the resolution limit

The microscope is an indispensable tool in biological research, enabling visualisation of interactions from molecular to multicellular level. For example, in the context of *S. aureus* and neutrophil host-pathogen interactions, microscopy techniques such as confocal microscopy allowed researchers to characterise the mechanisms of NETs

formation, and at the host level, intravital microscopy have greatly contributed to our understanding of neutrophil recruitment to *S. aureus* infection sites (Harding et al., 2014; Kolaczkowska and Kubes, 2013; Neubert et al., 2018; Thiam et al., 2020). Despite these advancements, our understanding of neutrophil and *S. aureus* at the molecular level remained limited. One of the challenges is due to the small size of cells, and the resolution limit of microscopes obstructs the ability to visualise the molecular interactions of neutrophil and *S. aureus*.

Resolution can be defined as the ability to distinguish two separate points, and in optical imaging systems, the resolution limit is fundamentally bounded by the diffraction limit of light. When a single point emitter, for example a fluorescent molecule is imaged on a microscope, a diffused spot with finite rings, known as Airy disk, is obtained, and the intensity profile of this spot is defined as the point spread function (PSF). To define resolution formally, if the distance between two point emitters is less than the width of PSF, then it does not satisfy the Rayleigh criterion for resolution, hence 'unresolvable' (Figure 1.5)(Rayleigh, 1903).

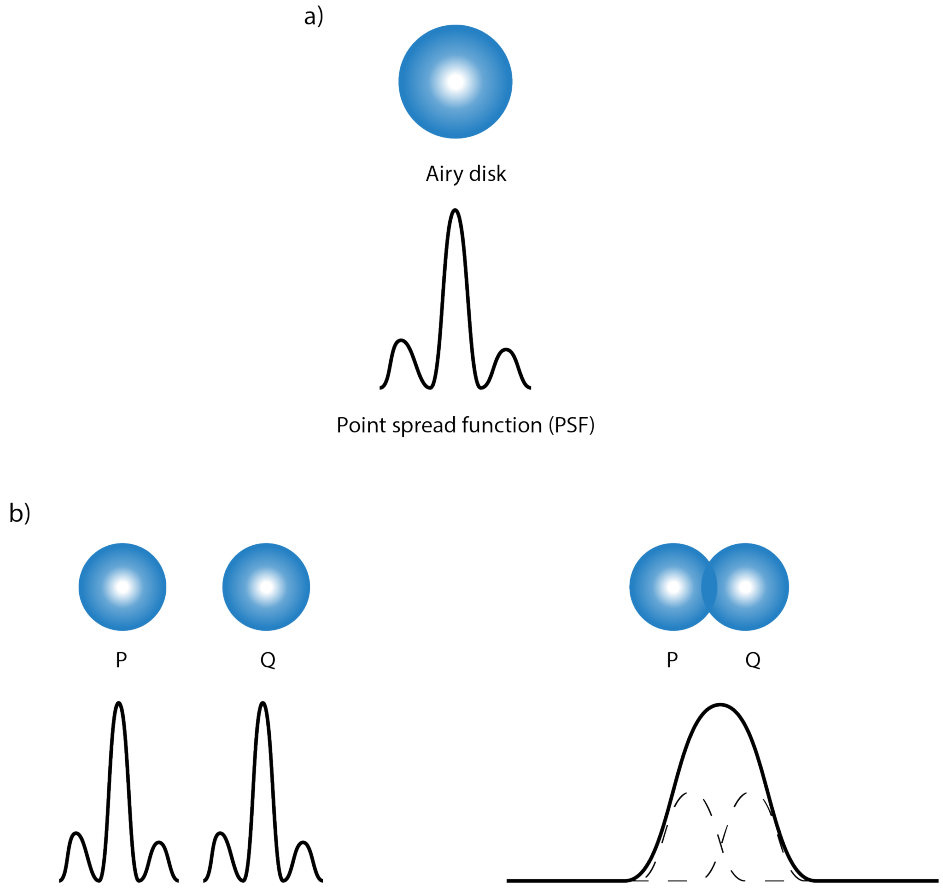

Fig. 1.5 **Resolution limit in light microscopes.** a) Patterns produced when light pass through an aperture, creating a diffused spot known as Airy disk. The intensity profile corresponding to the Airy disk is the point spread function (PSF). b) Two point emitters are 'resolvable' when the distance is greater than the width of PSF, whereas in (c), if the distance between point emitters P and Q is less than the width of PSF, it is 'unresolvable'.

The resolution limit of light, also known as Abbe limit, was recognised by Ernst Abbe, and his finding can be expressed by the following equation:

$$d = \frac{\lambda}{2n\sin(\theta)} = \frac{\lambda}{2NA} \tag{1.1}$$

stating that the wavelength of light (λ), as well as the numerical aperture (NA) of optics hindered the ability of microscope to resolve two objects within $\frac{\lambda}{2NA}$. The NA

of the lenses are defined by multiplying the refractive index of medium (n), and the aperture angles ($\sin(\theta)$) (Abbe, 1873).

For over a century, light microscopy was constrained by the resolution limit, which many have considered as a fundamental, unbreakable law of physics. Alternative to photons, the use of electrons in optical system steered the development of electron microscopes. The shorter wavelength of electrons conferred electron microscopes with higher resolution power that surpassed light microscopes. However, electron microscope samples are mainly visualised in vacuum, hence impossible to observe live samples (Gordon, 2014). Therefore, the ability to visualise live samples at nanoscopic scale remained a pipe-dream for many years. The development of super-resolution microscopes to circumvent the diffraction limit have heralded the dawn of new era in light microscopy, ushering new possibilities in biological research (Betzig et al., 2006; Gustafsson, 2000).

1.4 Fluorescence microscopy

Fluorophores are molecules with fluorescent properties. Immediately after absorbing light of shorter wavelength, fluorophores transition from low energy 'ground state' to high energy 'excited state'. The fluorophore returns to 'ground state' when the absorbed energy is eventually exhausted through the emission of fluorescence (Lichtman and Conchello, 2005). Coupling fluorophores to object of interests enhance the contrast, thus enabling objects to be distinguished from an otherwise dark background.

The development and application of green fluorescence protein (GFP) have propelled the use of fluorescence microscopy in biological investigations. Furthermore, broad spectrum of fluorescent probes were discovered subsequently, enabling a kaleidoscopic of proteins and structures to be visualised (Zimmer, 2009). In some instances, label-free fluorescence microscopy can be performed by imaging intrinsic fluorescence, or

autofluorescence within cells. For example, NADPH that are endogenous within macrophages can be visualised directly, and it is used to determine glucose metabolism in macrophages (Blacker et al., 2014; Kolenc and Quinn, 2019). However, introducing extrinsic fluorescent probes to label specific molecules is a more common approach, as it provides greater flexibility in terms of selecting the fluorophore spectrum to minimise crosstalk (Lichtman and Conchello, 2005).

Various techniques have been implemented to introduce fluorescent probes into cells, and a regular way is by genetically modifying protein of interests to express fluorophores. However, when genetic modification is not a feasible option, fluorescent probes can be introduced into cells by microinjections, and alternatively by using cell-permeable dyes to label specific organelles (Stephens, 2003). For example, cell-permeable dye such as MitoTracker are widely applied to label mitochondria for live cell imaging (Mitra and Lippincott-Schwartz, 2010).

1.4.1 Widefield microscopy

In widefield microscopy, the whole sample volume is illuminated by an excitation source, for example by light-emitting diodes (LEDs). Depending on the type of samples, illumination source originating from above (inverted microscopes) are commonly used for live samples, whereas fixed samples are illuminated from below using an upright microscope. Widefield microscopy encompass techniques such as phase contrast, differential interference contrast (DIC) and widefield fluorescence microscopy. Phase contrast and DIC microscopy are label-free techniques, in which bright light is used to illuminate and visualise transparent samples.

In widefield fluorescence microscopy, specific components are labelled with fluorophores, and the sample is illuminated with specific wavelength. Unlike label-free techniques like DIC, which enables quick visualisation of cell outline and position,

specific components, as well as images of improved contrast can be visualised using widefield fluorescence microscopy (Sanderson et al., 2014). Besides the low cost of implementation, the high temporal resolution, as well as minimal photodamage resulting from low illumination power requirement are among the advantages of using widefield fluorescence microscopy (Combs, 2010). However, a drawback of widefield fluorescence microscopy is the poor optical sectioning ability, where blurry images are formed as a result of background light generated from out of focal planes, as whole sample volume is illuminated at once.

1.4.2 Confocal microscopy

When visualising thick ($\geqslant$ 10 μm) samples, the contrast of images can be greatly compromised due to the production of out of focus light. Additionally, imaging thick samples can be further complicated by the scattering of light within samples. To overcome this problem, various techniques to improve optical sectioning abilities have been developed. The removal of out of focus light can enhance the contrast of an image, and this enabled better optical sectioning across the sample volume. In confocal microscopes, light is focused onto a spot in the focal plane using a laser beam, thus illuminating a small region in a sample. The emission from out of focal plane, as well as light scattering from samples are rejected by a physical pinhole, whereas the emission spot in focus is collected by an objective (Figure 1.6) (Conchello and Lichtman, 2005).

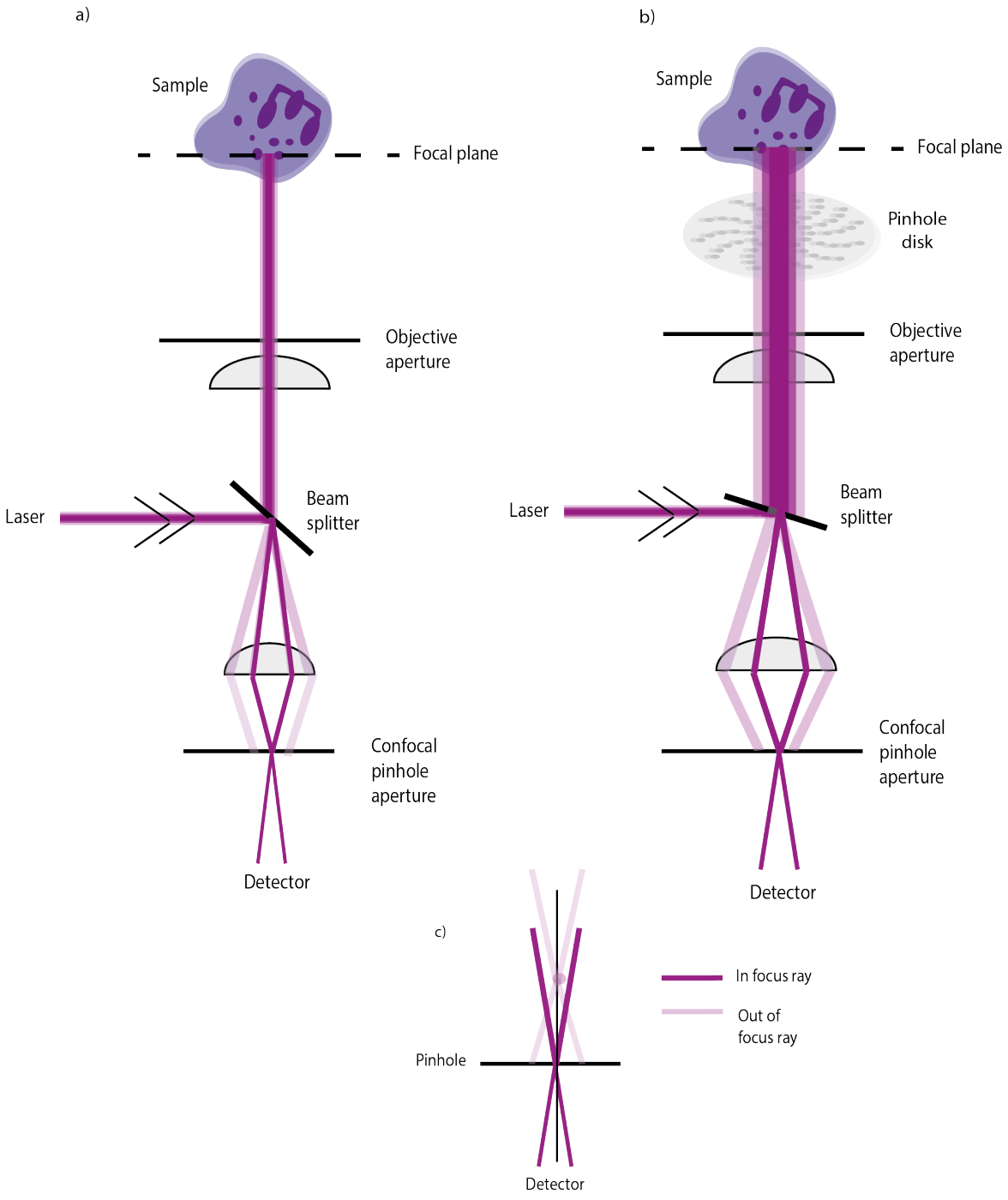

Fig. 1.6 **Principle of confocal microscopy.** a) In confocal laser scanning microscope, laser excitation is directed and focussed onto the sample. Emission from samples are separated from excitation light by beam splitter and appropriate filters, eventually passing through the pinhole where out-of-focus light is rejected, allowing in-focus light to reach the detector. b) In spinning disk confocal microscopes, multiple pinholes are used to excite numerous spots on a sample, and rejects out of focus light simultaneously. c) Ray diagram to demonstrate how pinholes are used to reject out-of-focus light, which enables optical sectioning.

In confocal laser scanning microscopes (CLSM), samples are scanned across with a laser beam by raster pattern, generated using a motorised stage, and eventually producing a confocal image (Carrington et al., 1990). To acquire volumetric images, image stacks across the z-direction are obtained and combined together to reconstruct the final 3D image. Due to the scanning of samples, images acquired using CLSM are generated gradually at one pixel a time, resulting in slow acquisition speed. Therefore, live imaging on CLSM is highly difficult.

One way to overcome the long acquisition time is by simultaneous illumination and collection of multiple emission spots. This forms the basis of spinning disk confocal microscopy, in which a disk with multiple pinhole apertures is used to excite numerous spots on a sample in parallel, and concomitantly rejects out of focus light from sample (Figure 1.6) (St. Croix et al., 2005). Acquisition speed is greatly enhanced by this method, enabling fast live cell imaging. However, early models of spinning disk confocal microscopes comes at the cost of transmission efficiency, where only partial of the excitation light is transmitted through pinholes. Furthermore, pinholes crosstalk occurred when rejected emission spots from sample leaked through adjacent pinholes, thus reducing image resolution (Conchello and Lichtman, 2005). These issues were later improved by the implementation of microlens array on the Yokogawa confocal scanning units. Positioning microlens array above the pinholes on the illumination side facilitates the focusing of light into the pinholes, hence greatly enhanced the excitation transmission of spinning disk confocal microscopes. Depending on the types of sample, the size and spacing of pinholes are adjusted in order to maximise the signal to noise ratio (SNR) and resolution of images. However, this flexibility is not offered by most commercialised spinning disks microscopes.

1.5 Super-resolution microscopy

The advent of fluorescence microscopes has improved our understanding of biological processes tremendously by allowing direct visualisation of components at cellular and subcellular scale. The ability to label specific elements and visualise them in live samples is a major advantage of fluorescence microscopy, hence an attractive technique to study biological processes. However, conventional fluorescence microscopy is restricted by its poor spatial resolution, due to the diffraction limit of light as mentioned in previous section. Studying subcellular structures in detail is difficult due to Abbe limit, as many of these structures are smaller than the wavelength of light (Huang et al., 2009). This hurdle can be overcome by techniques such as electron microscopy, which permits the study of detailed subcellular structures at higher resolution by using shorter wavelength, but compromised the ability to visualise these structures in live cells. Super-resolution microscopy modalities circumvent the diffraction limit by modulating illumination spatially or temporally, which will be further discussed in the following sections. Advancements in super-resolution fluorescence techniques in recent years have allowed us to overcome the obstacle imposed by diffraction limit, which opened up the possibility of observing finer structures, as well as studying interactions at molecular level in live cells.

1.5.1 Single-molecule localisation microscopy

Photoactivated localisation microscopy (PALM) and stochastic optical reconstruction microscopy (STORM), collectively known as single-molecule localisation microscopy (SMLM), are wide-field based technique and functions by stochastically switching fluorophores on and off through many repeating cycle.

The localised points collected throughout this process are then assembled and used to reconstruct super-resolved images that achieved 10-30 nm resolution (Betzig et al., 2006; Rust et al., 2006). To acquire images by switching fluorophores on and off, PALM requires photoswitchable fluorescent proteins, whereas organic dyes are used in STORM. The stochastic activation of fluorophores allows fluorescence signals to be distinguished temporally, rendering it suitable for measuring protein stoichiometries (Fricke et al., 2015).

Point accumulation for imaging in nanoscale topography (PAINT) is a technique that relies on the transient binding of fluorescent probes in solution to molecules of interest. Fast association of probes to molecules lead to emission of signals, and the signal disappears when probe dissociates, thus creating stochastic 'blinking effect' that enables spatial and temporal localisation of diffraction-limited spots (Sharonov and Hochstrasser, 2006). PAINT differs from other SMLM techniques such as STORM, where the fluorescent probes are bound to proteins of interest permanently. PAINT was originally demonstrated using Nile Red dye, but its biological application is limited due to the selection of compatible fluorophores available (Sharonov and Hochstrasser, 2006). Since then, variations of PAINT have been developed for broader biological applications. An example is DNA-PAINT, which uses single DNA strand to label structure of interests, and complementary DNA with fluorophores attached are subsequently introduced into the solution. Given the self-assembly nature of DNA, fluorescently-labelled DNA are rapidly associated and dissociated to its complementary strand on structure of interests, leading to 'blinking' that enabled localisation of diffraction-limited structures (Jungmann et al., 2010). DNA-PAINT is highly flexible, as the DNA structures can be customised with a palette of fluorophores that allow multicolour imaging (Jungmann et al., 2014; Schnitzbauer et al., 2017). Furthermore, the small size of DNA enabled

nanoscale structures of 5-10nm to be resolved, whereas in SMLM techniques such as STORM, resolution can be limited by the size of fluorophores used (Nieves et al., 2018).

Overall, SMLM techniques provide the highest spatial resolution, but the temporal resolution suffers as a result of the need to acquire large number of frames to reconstruct an image (Schermelleh et al., 2019). Additionally, the high illumination power requirement, as well as the necessity for special fluorophores in PALM and STORM limits the suitability SMLM in live cell imaging (Sydor et al., 2015).

1.5.2 Stimulated emission depletion microscopy

Stimulated emission depletion (STED) is a confocal-based super-resolution technique. In addition to the excitation laser, STED utilises a second donut-shaped laser to deplete fluorophores in outer region, therefore, only fluorophores present in the non-overlapping region of lasers will fluoresce. This technique allows resolution down to 50nm to be achieved in the lateral (xy) resolution (Hell and Wichmann, 1994). A distinctive feature of STED is that the resolution can be adjusted by tuning the laser power of the donut-beam. Given the spatial resolution, as well as its tunability, STED microscopy is commonly used in the studies of protein structures and organisations that were previously visible by electron microscopy (Müller et al., 2012). However, the donut-beam in STED requires high laser power, leading to effects such as photobleaching and phototoxicity (Hell, 2009). Live imaging is possible with STED, and this has been applied to visualise mitochondria crista and Golgi apparatus at nanoscopic level (Bottanelli et al., 2016; Stephan et al., 2019). However, the high laser power required in STED is toxic to live cells, thus limiting the duration of live imaging. Therefore, long term, live cell imaging with STED microscopy remained a challenge.

1.5.3 Structured-illumination microscopy

Structured-illumination microscopy (SIM) is a widefield-based technique, and it achieves resolution of 100-150 nm, which is approximately 2x the resolution limit of widefield microscopy. Classical SIM generates super-resolution images by using structured light pattern to illuminate samples. In a SIM set up, diffraction grating is placed at the excitation beam pathway, which generates interference stripes known as Moiré pattern on samples. Diffraction-limited structures are organised at high frequency in Fourier space. This high frequency information of unresolvable structures in sample is overlaid with high frequency of known illumination pattern, thus creating patterns with frequencies that can be collected by the objective in structured-illumination system. To acquire raw images, the same sample is repeatedly illuminated with patterns of various orientations, and all the raw images are eventually assembled, followed by computational reconstruction to obtain a final, super-resolution image (Fig 1.7) (Gustafsson, 2000).

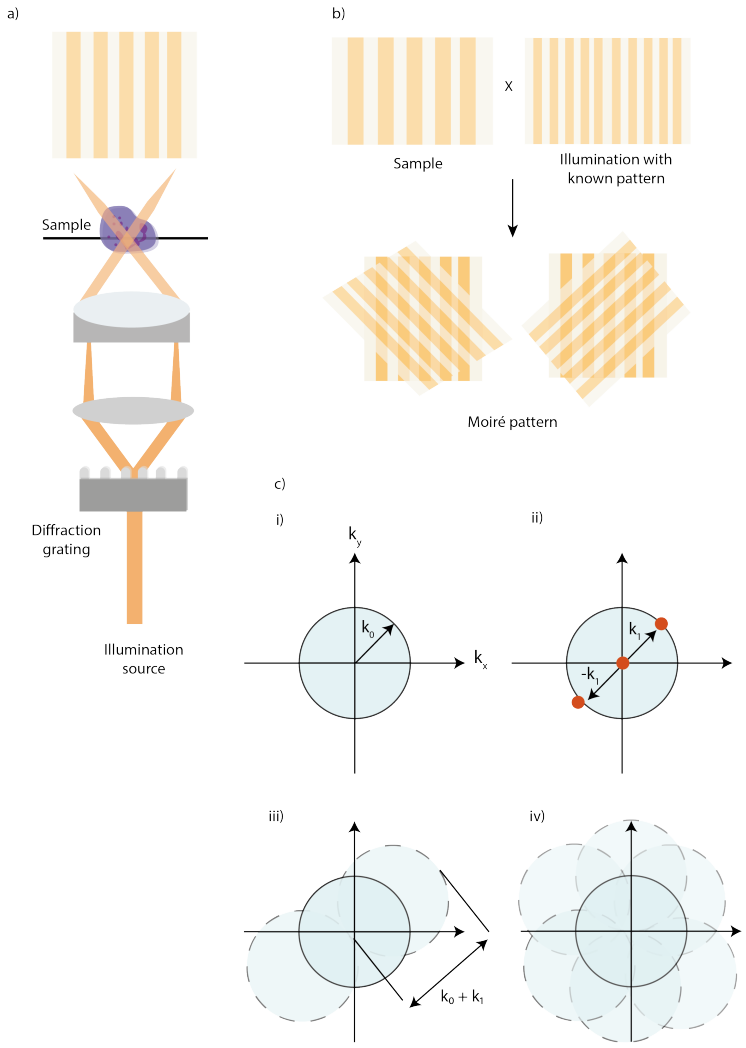

Fig. 1.7 **Principle of structured-illumination microscopy.** a) A diffraction grating is placed in front of an illumination source to generate interference stripe patterns. b) When high frequency information in the sample is overlaid with high frequency of known illumination pattern, this generates a Moiré pattern on samples, which can be collected by the system. c) i) The resolvable frequencies produced by objective in Fourier space is limited by the radius (k_0), and illumination pattern frequencies are marked by the three red circles in cii). iii) The resolvable region contains new frequencies (dotted circles) as a result of overlapping of frequencies, and higher spatial frequencies that were previously not resolvable are contained within the new frequencies contained. The resolution is now designated as $k_0 + k_1$. iv) Sample is repeatedly illuminated with patterns generated by orientating three phases at 120° to double the resolvable spatial frequency.

Point-scanning SIM, another form of SIM based on confocal setup, was theoretically proposed by Sheppard in the 1980s, and experimentally achieved in 2010 by Mueller

and Enderlein (J Cox et al., 1982; Müller and Enderlein, 2010). In the image scanning microscopy (ISM) set up by Mueller and Enderlein, an array detector with multiple pixels, instead of a point detector is implemented on a confocal microscope. Individual pixels in the array detector function as a confocal pinhole and detector simultaneously, thus each scanned image records the illumination spots at various positions. The illumination spots on the sample are recorded at different angles on each pixels, which creates a parallax effect, and the addition of all scanned images will result in final image that is blurry. Therefore, individual pixels needs to be reassigned, and this is done by shifting all the scanned images by a factor of ½ , followed by summing up using Sheppard summation algorithm to obtain a final high resolution image (Gregor and Enderlein, 2019; Müller and Enderlein, 2010).

Since then, different variation of point-scanning systems based on ISM, such as AiryScan, multifocal SIM (MSIM) and instant SIM (iSIM) have been introduced (Huff, 2015; York et al., 2013, 2012). In the MSIM setup, illumination pattern is generated using a digital micromirror device (DMD). The final, super-resolved images were acquired by post-processing the raw data digitally through deconvolution (York et al., 2012). Building on the MSIM setup, a lenslet array is implemented on the iSIM platform, circumventing the need to acquire and process images from multiple camera exposures, thus enabling faster imaging speed (York et al., 2013). Unlike the classical SIM, point-scanning SIM has better optical sectioning abilities, thus performs better at imaging thicker samples (Wu and Shroff, 2018). Although SIM only provides 1.7 to 2x improvement in resolution, the ease of sample preparation, compatibility with a broad range of fluorophores, as well as low photodamage in comparison to super-resolution techniques mentioned in previous sections makes it a suitable technique for live-cell imaging (Huang, 2010; Sydor et al., 2015).

1.5.4 Analytical-based super-resolution microscopy

Super-resolution techniques mentioned in previous sections required sophisticated optics setup, and this presents a challenge for non-optics experts to gain access. Furthermore, the high laser intensities required in these techniques further impedes long term live-cell imaging experiments. In addition to techniques in above sections, super-resolution imaging can also be achieved post-processing by analytical-based approaches, such as Super-resolution Optical Fluctuation Imaging (SOFI) and Super-Resolution Radial Fluctuation (SRRF) (Culley et al., 2018a; Dertinger et al., 2012).

SOFI works with the assumption that fluorophores emit signals stochastically. It can be performed on any imaging set up capable of fast acquisition to record fluorophore signal fluctuations over time, followed by performing correlation analysis to computationally enhance resolution (Dertinger et al., 2012). SOFI has been shown to improve resolution by order of 2, and theoretically, this approach is capable of achieving unlimited resolution. However, this is limited by factors such as the brightness of fluorophores, which in turn limits the resolution obtained by SOFI (Dertinger et al., 2013). Similar in principle to SOFI, SRRF can be performed on most imaging set up with fast imaging capabilities. SRRF is based on the assumption that PSF of fluorophore signals exhibits higher symmetry compared to its background, termed radial symmetry. Like SOFI, SRRF is done by rapid acquisition with high frame rates to record signals over time. This is followed by post-imaging processing, in which at sub-pixel level, the convergence of point source gradient, termed radiality, is estimated and analysed in individual frames in the acquired image series. The radiality is collated into a radiality stack, which is used to reconstruct the final SRRF images (Culley et al., 2018b; Gustafsson et al., 2016).

Analytical-based approaches can be performed without advanced optics set up, making it more accessible to researchers. For example, SRRF is applicable to LED and

laser-illuminated widefield microscopy, which is a commonly used technique available in many biological research facilities (Gustafsson et al., 2016). However, similar to other super-resolution techniques, analytical-based approaches risks generating artefacts. Furthermore, optical sectioning abilities of analytical-based techniques are limited, thus high resolution visualisation of volumetric samples can be challenging.

1.5.5 Expansion microscopy

Unlike other super-resolution techniques that rely on advancements in optics, expansion microscopy (ExM) is a recent technique pioneered by Boyden lab that focusses on sample preparation instead. Whole samples are preserved and physically expanded by polymers, and the enlarged samples are subsequently visualised using diffraction-limited microscopes (Chen et al., 2015). Sample preparation for ExM generally involves four steps, first is by labelling structure of interests with swellable hydrogel. This is followed by cross-linking of sample such that it is coupled to a polymer mesh, and the sample is subsequently homogenised either by enzyme digestion or chemical denaturation. Finally, the sample is immersed in water to allow swelling to occur. Using conventional microscopes available in most biological laboratories, this technique physically magnifies sample to enable visualisation of structures at nanoscopic level (Chen et al., 2015). The spatial organisation of structures in each sample are retained after expansion, and the samples can be expanded to 10 times of its original size, or even up to 20 times when using iterative expansion protocols (Chang et al., 2017; Truckenbrodt et al., 2019). ExM is advantageous as it involves simple implementation steps, and does not require complicated optics set up to acquire nanoscale resolution. However, ExM is only compatible for fixed, but not live sample imaging as it requires chemical fixation and expansion (Wassie et al., 2019).

1.5.6 Programmable array microscopy

Programmable array microscope (PAM) is a technique developed by the Jovin lab. A spatial light modulator, such as the DMD is utilised in the PAM set up to generate patterns for illumination and detection (Verveer et al., 1998). DMD is a device at the size of a chip, and its surface is embellished with millions of microscopic mirrors arranged in an array. The individual micromirror corresponds to each pixel of an image, and the micromirrors are positioned at +/- 12°, corresponding to 'on' and 'off' states. DMD is a highly flexible device, as individual micromirror can be controlled by switching it to 'on' or 'off' state, thus producing diverse illumination patterns. As micromirrors are easily directed, this permits specific control of illumination or detection patterns by software, which can be used to target patterns onto a specific site or the entire sample (Verveer et al., 1998). The use of PAM with DMD for optical sectioning has been demonstrated by the Jovin group, and they showed that different optical sectioning strategies can be adapted on a single set up to suit the sample type (Hanley et al., 1999).

In super-resolution microscopes, DMD was implemented on MSIM, which is a variation of ISM. Compared to confocal microscopes, higher resolution images (up to 1.7x resolution) can be acquired on ISM. Besides, ISM have improved optical sectioning abilities over classical SIM set up (Gregor and Enderlein, 2019; Müller and Enderlein, 2010). However, the long acquisition time on ISM hampers its live imaging capabilities. Therefore, a system that can perform multiple point scanning in parallel will greatly reduce image acquisition time. MSIM overcomes the long acquisition time of ISM by utilising a DMD to digitally generate illumination patterns, which enable multiple excitation spots to be simultaneously projected and collected on a sample. This improved the image acquisition speed that is beneficial for live imaging (York et al., 2012).

A more recent utilisation of DMD on imaging system is the Cairnfocal system, a versatile imaging platform developed in the Cadby lab. The platform uses a DMD to project different illumination patterns, swapping between various imaging modalities (Peedikakkal et al., 2018). It has been demonstrated that targeted STORM can be implemented on the platform, using this modality to visualise a specific field of view. Therefore, only the selected area suffers photobleaching, whereas the rest of sample remained unaffected. Furthermore, the versatility of this system was demonstrated by visualising a targeted field of view with multiple imaging modalities, including widefield, confocal and STORM, thus minimising photobleaching, as well as enabling long term live imaging (Peedikakkal et al., 2018).

1.6 Summary

This chapter begins with an overview of neutrophil functions and killing mechanisms, as well as the different cell death programs. This is followed by reviewing *S. aureus* and its clinical impact, with a resumé of *S. aureus* virulence factors, and how these virulence factors are used to evade neutrophil killing. This will provide the reader with a background on the biological investigation part of this thesis. Subsequently, a brief summary on the resolution limit of light and different fluorescence microscopy techniques was provided. This lead to the discussion of super-resolution modalities and PAM, which will aid in understanding the technology development side of the thesis. This chapter is concluded with a short summary of the preceding work on the development of a multimodal imaging platform, which paved way for the work presented in this thesis.

1.7 Aims

Neutrophil interaction with *S. aureus* is highly dynamic and complex. For example, the process whereby neutrophil granules fuse with vesicles and release their contents are tightly controlled, as uncontrolled release can lead to protease-mediated tissue damage and inflammation (Mayadas et al., 2014). Traditionally, processes such as phagosome maturation were mainly studied using electron microscopy, which provided high resolution but compromised the ability to study processes in live cells. Confocal microscopy has been implemented to follow early phagocytosis process in live macrophages, but the finer details and subsequent processes that requires higher resolution and long term live imaging remained challenging due to phototoxicity and photobleaching (Rashidfarrokhi et al., 2017). Therefore, the ability to visualise phagocytosis quickly within the range of seconds, as well as the ability to follow intracellular dynamics hours after phagocytosis at sub-cellular level, for example from 1μm to visualise intracellular *S. aureus*, down to nanometer range to study neutrophil receptor interactions with *S. aureus* using high resolution, and to perform long term live imaging remained a proving ground for both technology development and biological discovery.

The goal of the thesis is to identify compounds that attenuate *S. aureus* killing of neutrophils by library screen, and to further understand the changes in *S. aureus*-neutrophil interactions affected by the selected compounds at subcellular level using microscopy. Therefore, this requires two approaches: screening of a compound library to identify the compounds, and to develop a technique that enables long-term high resolution live imaging in neutrophils.

First, Chapter 3 presents the use of targeted and unbiased approach to identify compounds that modulate *S. aureus*-induced neutrophil cell death. This is followed by chapter 4, which details the development of a live imaging technique that enables

multicolour and multimodal imaging of human neutrophils. This chapter also discuss the selection of a most appropriate imaging modality for super-resolution imaging of neutrophils. Finally, chapter 5 presents the application of the multimodal imaging technique developed in chapter 4 to perform long-term live imaging of human neutrophils to visualise the neutrophil and *S. aureus* dynamics at high resolution.

Chapter 2

Materials and methods

2.1 Bacterial strains

S. aureus strains used in the experiments are shown in Table 2.1. The strains were stored in -80°C Microbank™ cryovials (Pro-Lab Diagnostics, Merseyside, U.K) and streaked onto Brain Heart Infusion (BHI) agar plates. The agar plates were kept at 4°C for up to two weeks for short term usage. For long term storage, a single colony of bacteria from a BHI agar plate was used to inoculate the Microbank bead stock and mixed thoroughly to allow bacteria adhesion to the beads, and the cryovial was stored in a -80°C freezer.

2.2 Cultivation of bacteria

A single Microbank bead containing bacteria was used to streak onto BHI agar plates, and incubated at 37°C overnight. A single colony of bacteria from the BHI agar plate was inoculated in 10ml of media (BHI or RPMI 1640), in a 50ml sterile Falcon tube. The cultures were incubated in 37°C with 5% CO_2, and with shaking at 350 revolutions per minute (rpm) overnight. The optical density of the overnight bacterial culture was

measured at a wavelength of 600nm (OD600) in a spectrophotometer (6100 Jenway, Staffordshire, U.K). A subculture was prepared by diluting the overnight culture with fresh media to achieve a starting OD600 of 0.05 and incubating for the desired time.

Strain	**Description**	**References**
SH1000	Wild type strain	(Horsburgh et al., 2002). Obtained from Natalia Hajdamowicz (Condliffe lab)
SH4276	JE2, derived from USA300 LAC strain cured of P01 and P03 plasmids.	(Fey et al., 2013).Obtained from Natalia Hajdamowicz (Condliffe lab)
SJF4622	SH1000 with mCherry chromosomal insertion.	Obtained from Dr. Tomasz Prajsnar (Foster lab)
GFP-SH1000	SH1000 with GFP chromosomal insertion.	Obtained from Dr. Paul Morris (Foster lab)
JE2-GFP	JE2 with GFP.	Obtained from Dr. Paul Morris (Foster lab)

Table 2.1 *S. aureus* strains used in this work

2.3 Generation of bacterial supernatant

A single colony of JE2 was inoculated in 10ml of BHI media, grown overnight and subcultured as described in section 2.2. To obtain the JE2 supernatant, the subculture was incubated at 37°C with 5% CO_2, with shaking at 350 rpm for 6 hours until stationary phase. The bacterial culture in a 50ml Falcon tube was sealed with parafilm and centrifuged at 4000 rcf for 10 minutes. The pellet was discarded, and the supernatant

filtered using sterile Acrodisc 0.2μm Supor Membrane syringe filters (Pall Life Sciences, Portsmouth, U.K). One hundred μl of the supernatant was made into aliquots and stored at -80°C.

2.4 Determination of bacterial colony forming units (CFU)

The Miles and Misra method was used to quantify the number of viable bacteria (Miles et al., 1938). Briefly, up to 7 series of ten-fold serial dilutions of the bacterial culture were made with sterile phosphate-buffered saline (PBS). Ten μl of each dilution was spotted in triplicates onto BHI agar, and left to dry in room temperature (RT) before incubating in 37°C overnight. The dilution series that yielded 20-80 discrete colonies were counted, and the colony forming unit CFU/ml was determined by the following formula:

$$\text{CFU}/ml = \frac{\text{average num. of colonies in selected dilution} \times \text{dilution factor}}{\text{volume spotted}}$$

2.5 Determination of bacterial growth curves

The growth dynamics of bacteria, in terms of bacterial growth phase and density were determined by generating a growth curve. Bacteria were grown following the procedures described in section 2.2. Bacterial subculture with a starting OD600 of 0.05 was incubated in 37°C with 5% CO_2, and with shaking at 350 rpm. Every hour, the bacterial culture was vortexed thoroughly and 1ml was removed to measure the optical density. One hundred μl of the culture was concurrently used for the determination of CFU using Miles and Misra method as described previously in section 2.4. Growth curves were generated by plotting the OD600 values against time. The progressive

growth phases of bacteria can be identified, and as the OD600 values were used to relate to the density of viable bacteria in culture, measuring OD600 of a culture can be used to estimate the concentration of viable bacteria.

2.6 Human neutrophil and mononuclear cell isolation and culture

2.6.1 Ethics

Experiments were performed using primary cells isolated from human peripheral venous blood. Peripheral blood was obtained from healthy individuals in accordance with a protocol approved by National Research Ethics Committee Yorkshire and The Humber-Sheffield, REC reference 05/Q2305/4. Informed and written consent was obtained from each volunteer.

2.6.2 Isolation and purification of neutrophils from peripheral blood

Neutrophils and peripheral blood mononuclear cells (PBMCs) were isolated by Plasma-Percoll density gradient centrifugation (Prince et al., 2017). All procedures were performed with rigorous care in a sterile class II biological safety cabinet to minimise contamination or neutrophil activation. Venous blood was drawn into a 50ml polypropylene Falcon tube containing 3.8% (w/v) sterile tri-sodium citrate (Martindale Pharmaceuticals, U.K) anticoagulant to a final concentration of 10% (v/v). The tube is inverted slowly and gently. The blood is centrifuged at 350 rcf for 20 minutes at RT to obtain platelet-rich plasma (PRP). PRP is aspirated into a clean 50ml Falcon tube and centrifuged at 2000 rpm for 20 minutes at RT to remove the platelets and

yield platelet-poor plasma (PPP). After centrifugation, PPP was aspirated into a clean Falcon tube and the remaining pellets were discarded.

Six ml of 6% (w/v) dextran (Sigma Aldrich, Dorset, U.K) was added to the remaining blood cells which was then topped up to 50ml with pre-warmed 0.9% sterile saline solution (Baxter, Newbury, U.K). The tube is gently inverted and excess blood was removed from the lid using a Pasteur pipette. The lid is loosened and the tube is left to stand at RT for 25 minutes, allowing the dextran (a high molecular weight polysaccharide) to bind to red blood cells (RBCs) and sediment them by gravity. After sedimentation of RBCs, the upper layer containing white blood cells (WBCs) is aspirated into a new Falcon tube and centrifuged at 320 rcf for 6 minutes at RT. The leukocyte-rich soft pellet obtained after centrifugation was carefully resuspended in 2ml of PPP.

The cells are further separated by their density using a plasma-Percoll gradient. The lower phase consists of 51% (v/v) Percoll/PPP, and it was prepared by mixing 1.02ml Percoll with 0.98ml PPP, whereas the upper phase consists of 42% (v/v) Percoll/PPP, prepared by mixing 0.84ml Percoll with 1.16ml PPP. Using a sterile Pasteur pipette, the upper phase is carefully overlaid onto the lower phase of Percoll to generate a discontinuous plasma-Percoll gradient. The resuspended leukocyte-rich pellet was overlaid carefully and slowly onto the upper phase Percoll. The gradient was centrifuged at 320 rcf for 11 minutes at RT without brake, and this yields three separate populations of cells: a top layer containing PBMCs, a middle layer containing granulocytes such as neutrophils, eosinophils and basophils, and a pellet of RBCs (Figure 2.1).

To obtain the different cell populations, PBMCs were first aspirated and removed carefully using a sterile Pasteur pipette into a new Falcon tube containing 10ml PPP. This is followed by aspirating the granulocyte layer into a separate Falcon tube con-

taining 10ml PPP. Hank's Balanced Salt Solution (HBSS) 1X, without Ca^{2+} and Mg^{2+} (Gibco®, Paisley, Scotland) was used to top up the volume to 40ml, and cell counts were quantified using a haemocytometer. Subsequently, the cells were centrifuged at 320 rcf for 6 minutes at RT. Neutrophils were resuspended in complete RPMI 1640 (+10% (v/v) heat-inactivated Fetal Bovine Serum (FBS) and 1% (v/v) Penicillin/Streptomycin) at $10x10^6$ cells/ml. For experiments where neutrophils were co-infected with bacteria, RPMI 1640 supplemented with 10% (v/v) heat-inactivated FBS (but without penicillin/streptomycin) was used. Granulocytes cannot be further separated by a Percoll gradient due to the similarity in densities. Therefore, it is important to determine the purity and viability of neutrophils to gain confidence in experiments where neutrophils were co-infected with bacteria to measure the killing efficiency. To do this, 100μl of the neutrophil suspension was used to prepare cytocentrifuge slides for purity assessment by morphological identification described in section 2.7.1. The percentage of neutrophil in the population should be greater than 95%, and cell preparation with high percentages of contamination by eosinophils or lymphocytes were discarded.

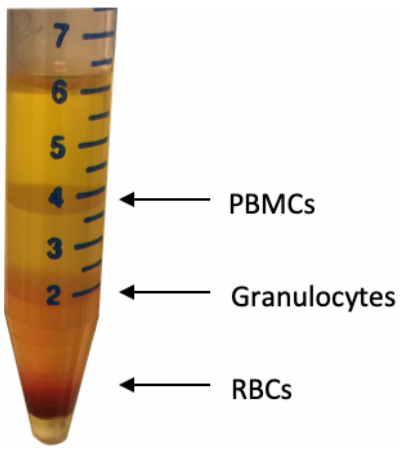

Fig. 2.1 **Plasma-Percoll gradient showing different cell populations.** Three distinct layers of cells: peripheral blood mononuclear cells (PBMCs), granulocytes and red blood cells (RBCs).

2.6.3 Neutrophil intracellular bacterial killing assay

Forty-five μl of neutrophils at 10x10^6 cells/ml were added to wells of a 96-well plate. The volume in each well is fixed at 90μl by adding the appropriate volume of RPMI (+10% (v/v) FBS), followed by incubation at 37°C with 5% CO_2 for 30 minutes prior adding bacteria. Frozen bacterial aliquots were thawed at room temperature and centrifuged at 6000 relative centrifugal force (rcf) for 7 minutes. The supernatant was removed and pellet was resuspended in appropriate volume of fresh RPMI 1640. Subsequently, 10μl of bacterial suspension was added to each well such that the multiplicity of infection (MOI) is 5. The exact starting CFU count of the bacterial aliquot is determined by incubating 10μl of bacterial in 90μl RPMI in absence of neutrophils. After 30 minutes of co-incubation, extracellular bacteria were killed by adding 40μg/ml of gentamicin to each well. Gentamicin was removed by washing after 30 minutes. This is done by centrifugation of cells at 400 rcf for 4 minutes and resuspending the pellet in fresh media. The cells were then promptly incubated until selected time points. At each selected time point (between 30-180 minutes), the samples were centrifuged at 400 rcf for 4 minutes, and the pellets were resuspended with 1ml of fresh alkali water (pH 11) and incubated at RT for 10 minutes, with vigorous pipetting and thorough vortexing to lyse the neutrophils. The viable intracellular bacteria load is quantified by Miles and Misra method described in section 2.4.

2.7 Assessment of neutrophil purity and viability

2.7.1 Morphological assessment for purity

After isolation of cell populations (section 2.6.2), 100μl of neutrophils were transferred to glass microscope slides fitted with cytospin chambers. Freshly-isolated neutrophils

were centrifuged at 400 rcf for 3 mins in a Cytospin4 centrifuge (Thermo Scientific, Waltham, USA). The cells were fixed with 1 drop of absolute methanol and stained with ReaStain Quick-Diff Red (Reagena, Finland) and Kwik Diff Solution 3 blue stain (Thermo Scientific, Loughborough, U.K) for 3 minutes respectively. This is followed by rinsing the excess stain with water and slides are left to dry. The slides were mounted with distyrene, plasticizer and xylene (DPX) (Thermo Scientific) prior to adding coverslips. The mounted slides were left in a fume hood overnight and then observed under light microscopes using x100 oil immersion objective.

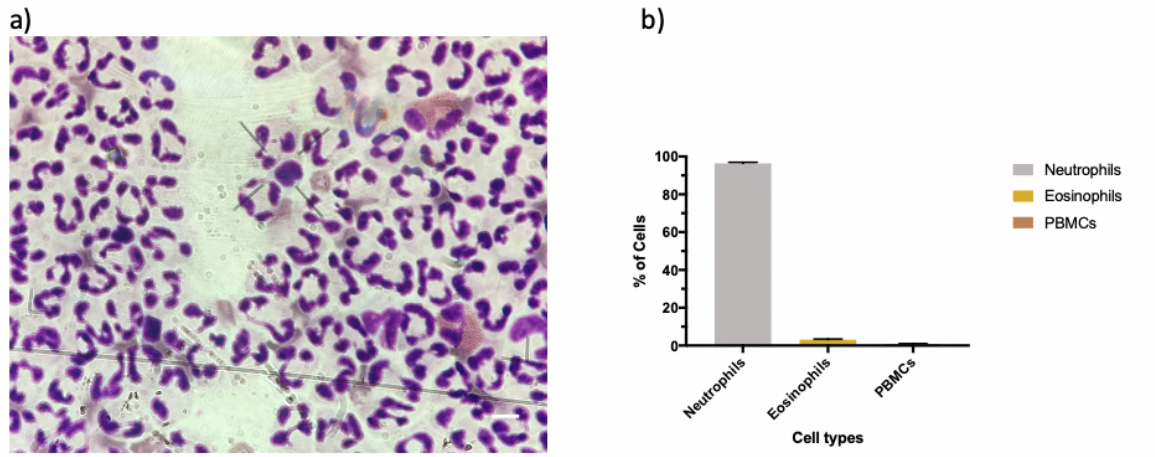

Fig. 2.2 **Morphological assessment of neutrophil purity.** a) Example of an area of the purity slides viewed under light microscope using x100 oil immersion objective. b) The percentage of neutrophils (grey bar), eosinophils (yellow bar) calculated by counting approximately 300 cells in each purity slides. The scale bar (white bar, bottom right) represents approximately 100μm. Data shown is a representative of 3 separate experiments. The mean values are shown and the error bars represent standard error mean).

2.7.2 Neutrophil viability assessment by LSRII flow cytometer

The viability of neutrophils were assessed by flow cytometry using BD™ LSRII (BD Biosciences), using To-Pro-3 dye (Molecular Probes, Invitrogen, Paisley, U.K). Cells

with compromised membrane integrity, for example necrotic cells, permit the entry of To-Pro-3, a cell-impermeant fluorescent dye that intercalates to, and stains, dsDNA. For each condition, the samples were recovered from wells by gentle resuspension, followed by centrifuging at 0.4 rcf for 3 minutes. The cell pellets were washed gently with sterile 1X PBS, and resuspended with ToPro-3 (1:10000 v/v) before immediate flow cytometry analysis. Neutrophils resuspended in 1X PBS without addition of ToPro-3 were used as negative control, wherein the autofluorescence of neutrophils were detected and used to set the fluorescence intensity threshold. Neutrophils subjected to freeze-thaw treatment to induce damage to cell membrane were used as positive control. Briefly, cell pellets resuspended in 1X PBS were frozen at -80°C for 10 minutes, thawed and vortexed vigorously prior adding ToPro-3.

2.7.3 Neutrophil viability assessment by Attune autosampler

The viability of neutrophils cultured in 96-well plates were assessed using the Applied Biosystem Attune Acoustic Focusing Cytometer (Thermo Fisher Scientific). Neutrophil controls and co-cultures were sampled by the Attune plate reader system at 500μL/min, and the aspiration was stopped once 70μL of individual samples were acquired.

2.7.4 Quantification of absolute viable cell number and ToPro-3 negativity cell count

Neutrophils in RPMI 1640 (+10% FBS) media control was used to confirm and quantify the neutrophil viability count in individual experiment, using Attune Cytometric Software v.2.1.0 (Thermo Fisher, U.K). Based on the forward scatter (FSC) and side scatter (SSC) profile, a gated region (R1) was drawn around healthy and viable

neutrophil population, to exclude debris and contaminating RBCs and PBMCs (Figure 2.3a). From the cell population in R1 gated region, another gated region (R2) was drawn to set up a threshold for ToPro-3 negativity (Figure 2.3b). The gates were applied to all samples in an experiment. The number of events in each function (i.e absolute viable neutrophil number and ToPro-3 negativity cell count) was determined by multiplying the concentration (events/μL) of individual gated region with the final volume of wells.

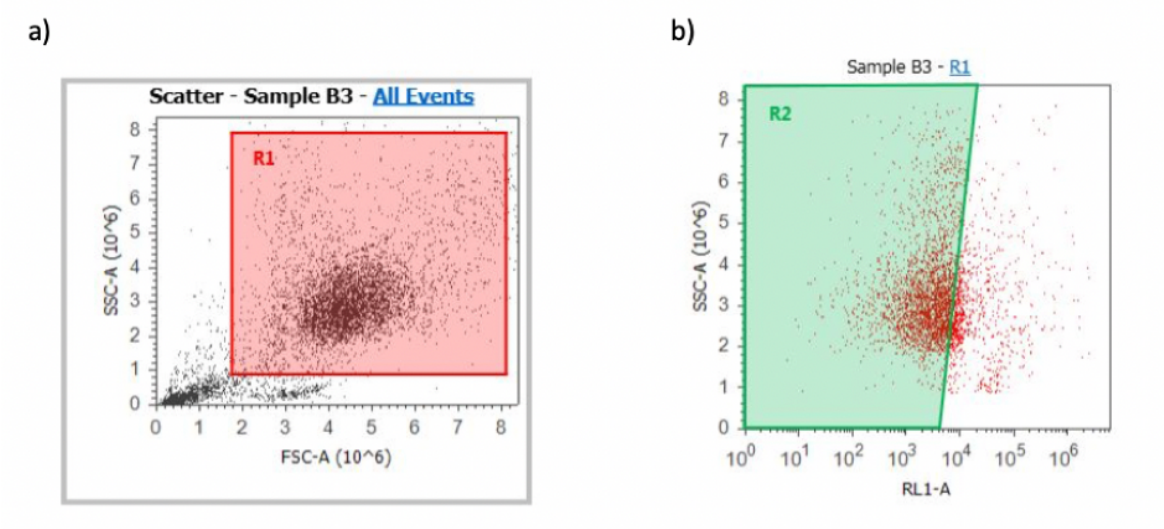

Fig. 2.3 **Gating strategies to assess neutrophil viability.** a) Gated region R1 drawn around viable neutrophils population based on the FSC and SSC profile b) R2 gated region showing the ToPro-3 negativity cell population.

2.8 Human monocyte-derived macrophages (hMDM) culture

Human monocyte-derived macrophage (hMDM) were obtained from peripheral blood mononuclear cells (PBMCs) isolated by Plasma-Percoll density gradient as described by Daigneault and colleagues (Daigneault et al., 2010). Briefly, the PBMCs were isolated as described previously in section 2.6.2, followed by resuspending PBMCs in RPMI

1640 supplemented with 1% (v/v) P/S at 4x10^6 cells/ml. PBMCs were seeded at cell density of 4x10^6 cells/ml on coverslips in 6-well tissue culture plates at 37°C with 5% CO_2. After 1 hour, the non-adherent cells were removed and the adherent cells were cultured in 1ml of complete RPMI. Media was exchanged with fresh media every two days, and the cells were ready to use after 7-10 days.

2.9 *S. aureus*-hMDM co-culture

HMDMs were cultured and maintained as described in section 2.8. On day 10-14, media from wells were aspirated and discarded, and the hMDM cells were washed with 1ml 1X PBS. Frozen *S. aureus* aliquots were thawed in room temperature and centrifuged at 6000 rcf for 7 minutes. The supernatant was removed and pellet was resuspended in appropriate volume of fresh RPMI 1640. To obtain a multiplicity of infection (MOI) of 5, 100μl of bacterial suspension was added to each well. The volume in each well is fixed at 1ml by adding appropriate volume of RPMI (+10% (v/v) FBS), followed by incubation in 37°C with 5% CO_2. for 1h.

2.10 HT-29 cell line culture

HT-29 human colorectal adenocarcinoma cell line was kindly provided by Dr. Martin Nicklin (Department of Infection, Immunity and Cardiovascular Disease, University of Sheffield). HT-29 cells were seeded in 75 cm^2 cell culture flask (Thermo Scientific) and cultured in high glucose Dulbecco's Modified Eagle's Medium (DMEM) (#D6429, Sigma Aldrich, Dorset, U.K) supplemented with 10% FBS and 1% P/S. The monolayer cell culture was incubated in 37°C with 5% CO_2. The cell culture was exchanged with fresh media every two days.

2.10.1 Passaging HT-29 cell line

Once the monolayer cell culture reached 80-90% confluency, the cells are ready to be passaged. Briefly, media was removed and the cells were washed with 1X PBS without Ca^{2+} and Mg^{2+}. The cells were detached using 1.5ml of Trypsin-EDTA and incubated in 37°C for 8 minutes. Trypsin-EDTA activity was stopped by adding 7.5ml of DMEM solution. The cell suspension was transferred to 15ml Falcon tube and centrifuged at 1000 rpm for 3 minutes. The supernatant was discarded and pellet was gently resuspended in 1ml of DMEM. 10μl of cell suspension was used for cell count using hemocytometer. Cells were seeded at 5 X 10^4 cells/cm^2 in 75 cm^2 cell culture flask and 2 X 10^4 cells/well in 24-well plate respectively.

2.10.2 HT-29 viability by flow cytometry

The viability of HT-29 cells were assessed by flow cytometry as described previously in section 2.7.2. For each condition, a cell scraper was used to recover the cells from wells. The cells were centrifuged at 1000 rpm for 3 mins, and the pellets were resuspended in ice cold 1X PBS supplemented with 10% FBS to prevent cell clumping, followed by resuspension with ToPro-3 (1:10000 v/v). The samples were put on ice and flow cytometry was performed within 30 mins after the samples were prepared.

2.10.3 Statistical analysis

All statistical analysis was completed using GraphPad Prism Version 7.0c. Analysis were performed using one-way analysis of variance (ANOVA), with Dunnett post-hoc test when appropriate. Significant differences were defined by reaching p value of < 0.05.

Chapter 3

Identification of compounds that modify *S. aureus*-induced neutrophil cell death

3.1 Introduction

Neutrophils are important components of the immune system to defend against *S. aureus* infections. However, *S. aureus* is able to overcome neutrophil response using multiple evasion strategies, notably by the production of leukotoxins that results in neutrophil cell death (Tam and Torres, 2019; Thammavongsa et al., 2015). The exact mechanisms that underlie *S. aureus*-induced neutrophil cell death pathway remained unclear. Necrosis and necroptosis are among the mechanisms that have been suggested to contribute to neutrophil cell death (Greenlee-Wacker et al., 2017, 2014; Kobayashi et al., 2010). Performing library-wide compound screen is a common approach to explore and to identify key components of specific pathways. For example, GSK' 872, an inhibitor of RIPK-3 was identified by performing compound screening (Kaiser et al., 2013).

The MicroSource Discovery System Spectrum collection compound library is made of 2560 compounds, and all existing compounds of US and International Drug Collection compounds are present within the collection library. Screening of spectrum compound collection library have contributed to applications in diverse fields, including the identification of new therapeutics for Alzheimer's disease and antiviral molecules (Edwards et al., 2015; Kim, 2015). Moreover, factors that play a role in oxidative death in primary neurons were identified from screening the Spectrum collection library (Aleyasin et al., 2015). This demonstrate that applying a compound library screen provides a powerful yet robust way to identify compounds as new therapeutics, as well as understanding the mechanism of specific signalling pathway.

The aim of this chapter is to identify compounds that can inhibit *S. aureus*-induced neutrophil cell death, as a strategy to identify ways to promote the ability of neutrophil to kill *S. aureus*. To address the aim, I have implemented two approaches, first by using specific necrosis and necroptosis inhibitors to determine whether it can attenuate *S. aureus*-induced neutrophil cell death. Secondly, a compound library screening protocol was optimised, followed by screening a subset of the spectrum collection compound library using high-throughput flow cytometry.

The use of high-throughput flow cytometry assay to study *S. aureus* and neutrophil interaction was established previously, as a technique to identify *S. aureus* mutants associated with the attenuation of neutrophil cell death (Yang et al., 2019). The parameters used to quantify neutrophil viability includes the neutrophil size and granularity, assessed by forward and side scatter respectively, as well as intensity of ToPro-3 dye.

3.2 Neutrophil-mediated *S. aureus* killing

It has been shown that laboratory *S. aureus* strains are able to survive and persist inside neutrophils (Gresham et al., 2000). Neutrophil intracellular killing assays were performed to show that JE2, a clinical MRSA strain is also able to survive inside neutrophils. JE2 was co-incubated with freshly isolated neutrophils at an MOI of 5 for 30 minutes. After 30 minutes, gentamicin was used to kill extracellular bacteria, thus allowing quantification of viable intracellular bacteria. The intracellular bacteria were quantified at 20, 40, 60 and 180 minutes post-gentamicin treatment as detailed in section 2.6.3. There was a drop in intracellular bacterial count (cfu/ml) at 20 minutes post-gentamicin treatment, followed by reduced viable intracellular bacteria at 40 and 60 minutes post-gentamicin treatment (Figure 3.1). The data showed the reduction of *S. aureus* inside neutrophils over time, but the clearance of intracellular *S. aureus* was incomplete even at the final timepoint, indicating that *S. aureus* may be able to overcome killing by human neutrophils.

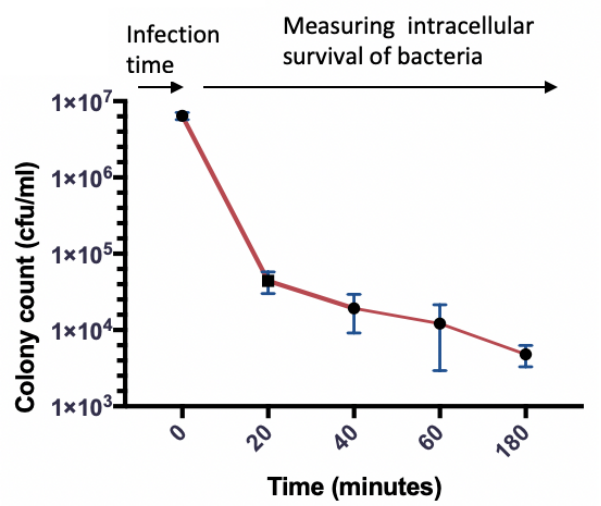

Fig. 3.1 **Neutrophil intracellular killing of *S. aureus* is incomplete after 3 h.** JE2 were co-cultured with neutrophils at MOI of 5. The number of phagocytosed bacteria were shown at 0 min. Gentamicin (40μg/ml) was added at 0 min to eliminate extracellular bacteria, and the intracellular bacteria load at different time were quantified. The data shown is a mean value of two separate experiments, and the error bars represent standard deviation (SD).

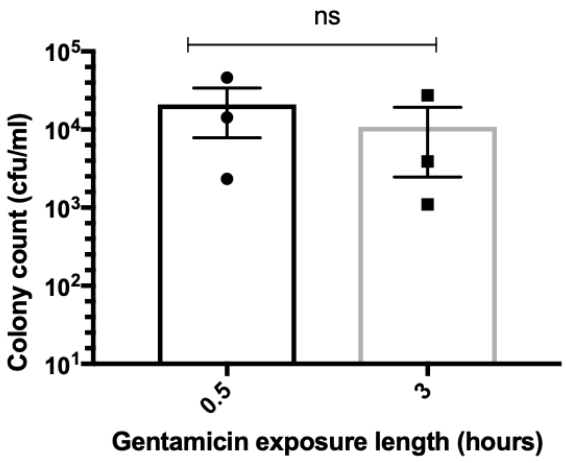

Fig. 3.2 **Gentamicin exposure does not affect intracellular bacterial viability.** Intracellular bacteria viability between 0.5 and 3 h of gentamicin exposure. Data shown is the mean and standard error of mean (SEM) of 3 independent experiments. A paired t-test was performed and there were no significant differences in bacterial intracellular viability.

Gentamicin is an antibiotic that functions by binding irreversibly to bacterial 30s ribosomal subunit, thus inhibiting protein synthesis (Tangy et al., 1985). Gentamicin is widely used in intracellular killing assays to eliminate bacteria that have not been phagocytosed (Gresham et al., 2000). Concerns were raised on the ability of gentamicin to cross the neutrophil cell membrane and kill intracellular bacteria (Hamrick et al., 2003). To assess whether the gentamicin exposure time affects the viability of intracellular *S. aureus* in neutrophils, JE2-neutrophil co-culture were exposed to gentamicin for different time points. Gentamicin was left for 0.5 h and then washed off. Intracellular bacteria were enumerated at 3 h. Figure 3.2 showed that there was no significant difference in terms of intracellular bacteria viability between 0.5 and 3 h of gentamicin exposure, thus does not affect the killing of intracellular bacteria.

3.3 Candidate approach to promote neutrophil killing of *S. aureus*

S. aureus can overcome neutrophilic immune responses by several means. Perhaps the most catastrophic way is to induce neutrophil cell death (de Jong et al., 2019). This is confirmed in Figure 3.3, where the low percentage of viable neutrophils and high ToPro-3 positivity shows that JE2 causes neutrophil cell death by lysis. The percentage of neutrophil viability was based on the FSC and SSC profile, where a gated region was drawn around healthy and viable neutrophil population to exclude debris and contaminating RBCs and PBMCs. Neutrophils incubated in media and stained with ToPro-3 was used to set the threshold for ToPro-3 positivity. As a positive control, neutrophils in media were freeze-thawed to induce membrane damage, which allows ToPro-3 to enter cells.

One of the mechanisms in which *S. aureus* does this is by necroptosis (Wang et al., 2018). For example, interfering the necroptosis pathway by blocking RIPK-3 has been shown to inhibit *S. aureus*-induced neutrophil lysis (Greenlee-Wacker et al., 2017, 2014). *S. aureus*-induced cell death pathway in neutrophils hitherto remained controversial in the literature. Therefore, targeting *S. aureus*-induced neutrophil cell death pathways using different cell death inhibitors is used here as a candidate approach to find new strategies to improve the ability of neutrophils to kill *S. aureus*.

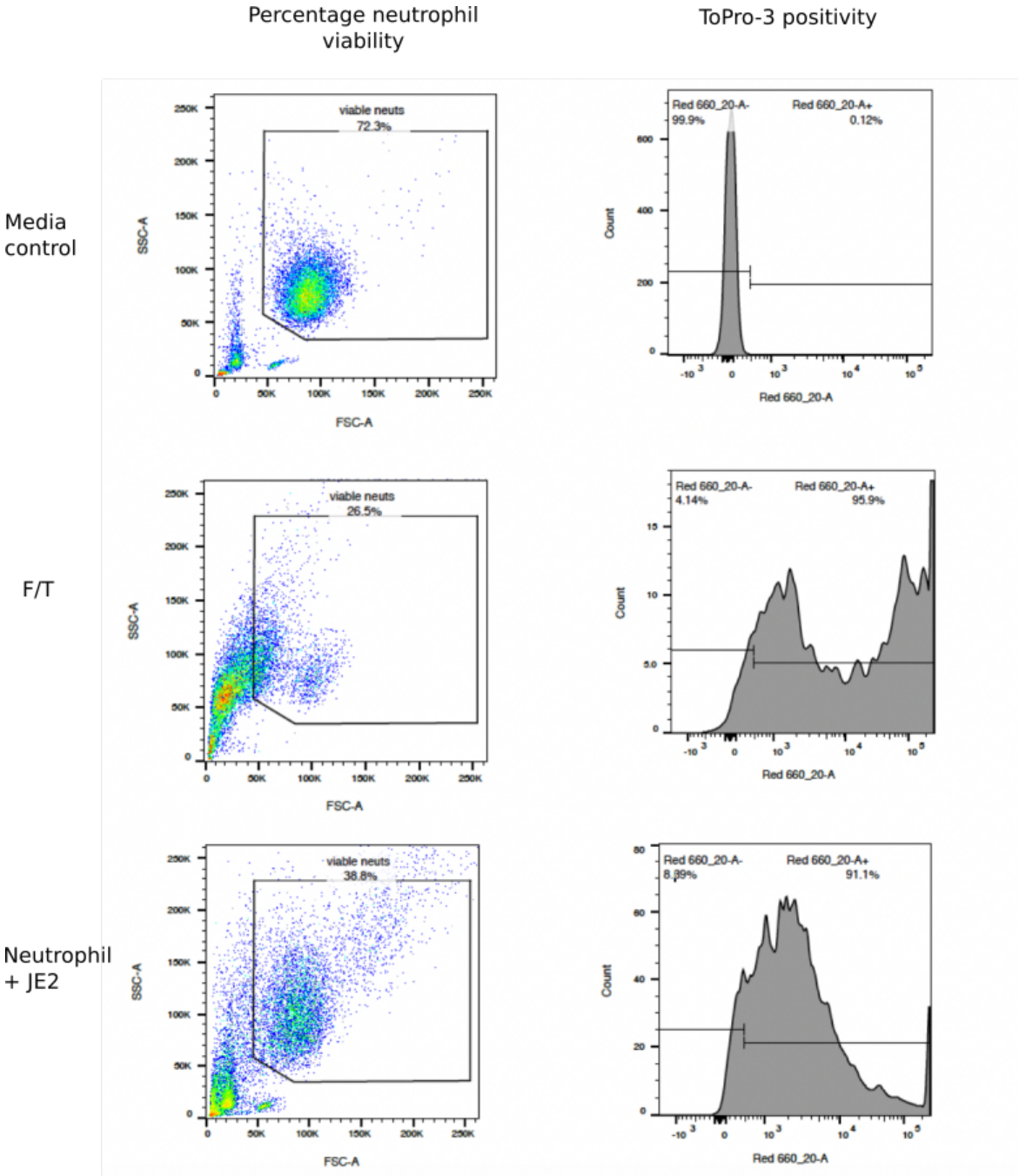

Fig. 3.3 **JE2-induced neutrophil cell death by lysis.** Neutrophils were co-incubated with live JE2 (MOI 10) for 2h, followed by addition of ToPro-3 (1:10000 in PBS). Media control: Neutrophils in RPMI (+10% FBS) media stained with ToPro-3. F-T: Freeze-thawed neutrophils stained with ToPro-3.

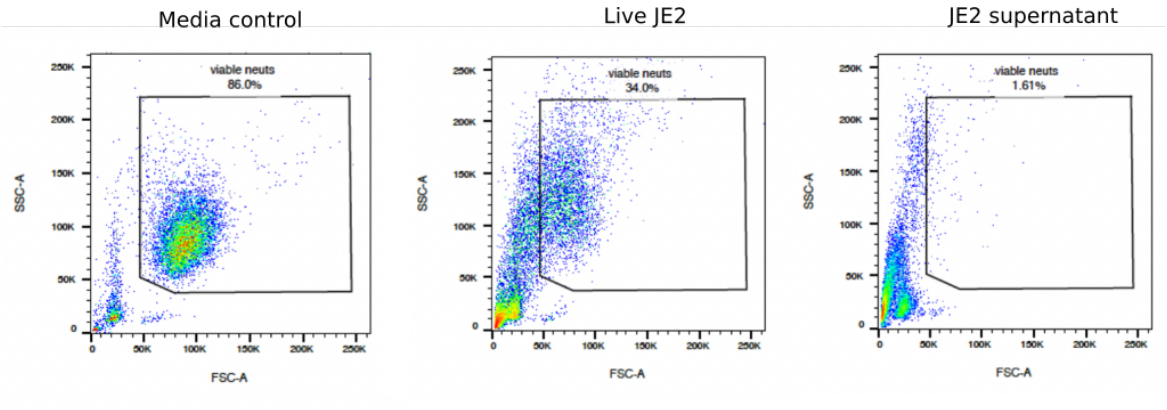

Fig. 3.4 **Neutrophil gating strategies using flow cytometry.** Neutrophil viability at 2h post-gentamicin treatment with media control, live JE2 (MOI 10) and 10 μL of JE2 supernatant were quantified using flow cytometry.

3.3.1 IM-54

Cell lysis consistent with necrosis have been suggested as a potential *S. aureus*-induced neutrophil cell death mechanism (McGuinness et al., 2016). IM-54 is a necrosis inhibitor that blocks oxidative stress-induced necrosis (Sodeoka and Dodo, 2010). To assess whether using IM-54 to inhibit necrosis can promote neutrophil-mediated *S. aureus* killing, freshly isolated neutrophils were incubated with IM-54 for 1 hour prior addition of JE2. The intracellular bacteria killing at 0.5 and 3 hours post-gentamicin treatment, as well as the viability of JE2-infected neutrophils 2 hours post-gentamicin treatment were assessed as above. Neutrophils were treated using IM-54 at 1, 5, 10 μM, which was based on the doses shown to reduced oxidative-stress induced cell death in neutrophil-like HL60 cells (Sodeoka and Dodo, 2010). Based on preliminary results, using different concentrations of IM-54 (1, 5, 10 μM) does not increase the viability of JE2-infected neutrophils (Figure 3.5). Additionally, IM-54 does not promote the ability of neutrophil to kill intracellular *S. aureus*, as there were no differences in viable intracellular bacteria count at 0.5 and 3h post-gentamicin treatment (Figure 3.6).

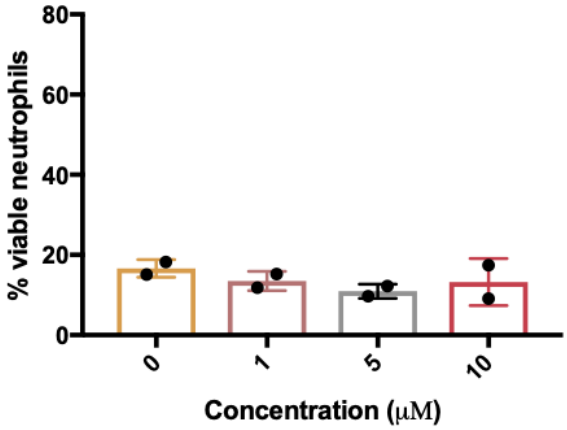

Fig. 3.5 **Cell death assay using IM-54.** Neutrophils were pre-incubated with IM-54 for 1h, followed by co-infection with JE2 at MOI 5 for 2h. Data showed the mean and error bars with SD of 2 independent experiments.

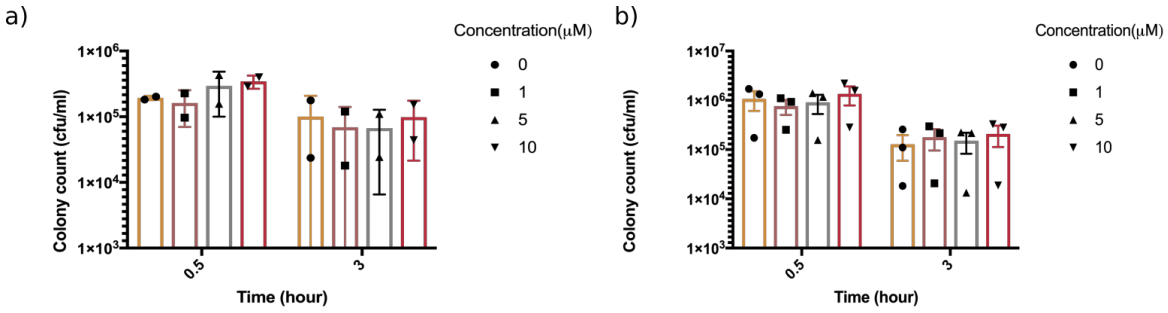

Fig. 3.6 **IM-54 neutrophil killing assay.** Neutrophil intracellular killing assay at 0.5 and 3h time points, using different concentrations of IM-54, a) MOI 5, data showing error bars and mean with SD (n=2) and b) MOI 10, data showing error bars and mean with SEM (n=3).

3.3.2 Necrosulfonamide (NSA)

Necrosulfonamide (NSA) is a necroptosis inhibitor that blocks mixed lineage kinase domain-like (MLKL) protein. The work of Greenlee-Wacker and colleagues suggested that the neutrophil plasma membrane was more fragile when a higher MOI is used (Greenlee-Wacker et al., 2014). Therefore, an MOI of 10 was used in addition to MOI of 5 to test the ability of NSA to inhibit neutrophil cell death and promote intracellular killing of *S. aureus*. Co-incubation of neutrophils with live JE2 or stationary phase

supernatant (see section 2.3) for 2h post-gentamicin treatment caused significant neutrophil cell death by lysis as measured by loss of viable neutrophils (Figure 3.4). Figure 3.7 showed that using different NSA concentrations prevent neutrophil cell death.

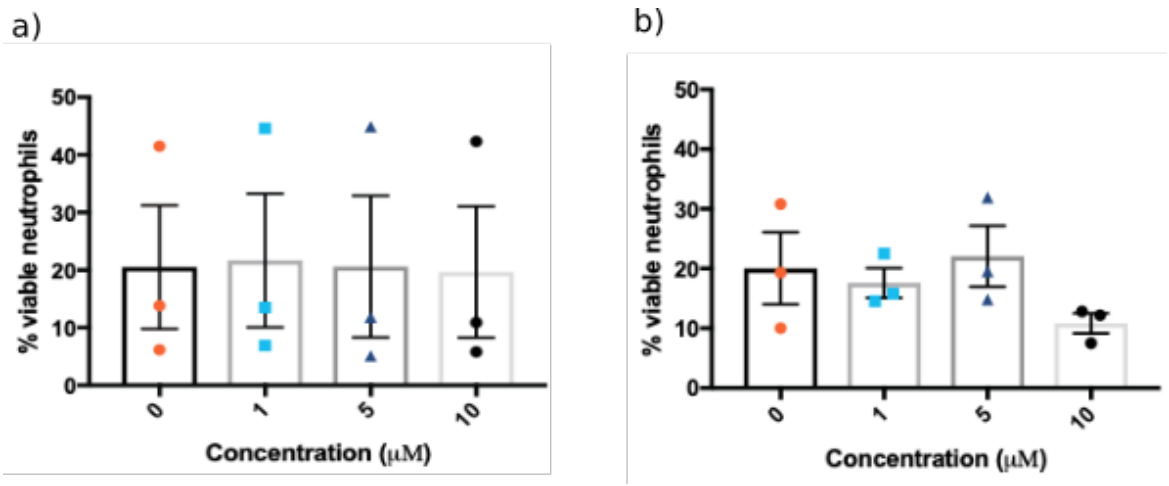

Fig. 3.7 **NSA neutrophil cell death assay.** Neutrophils were pre-incubated with NSA for 1h, followed by co-infection with JE2 at a) MOI 5 and b) MOI 10 for 2h. Data showed the mean with SEM of 3 independent experiments. One-way ANOVA was performed and no significant differences were found between neutrophil treated with different NSA concentrations.

It was also hypothesized that targeting cell death pathways to inhibit neutrophil cell death may promote the neutrophil-mediated killing of *S. aureus*. Therefore, different concentrations (1, 5 and 10μM) of NSA were used in neutrophil intracellular killing assay to determine whether blocking neutrophil cell death can promote the killing of *S. aureus* by neutrophils. Figure 3.8a showed the mean and individual cfu/mL values from three independent experiments using MOI 10. Taking an independent assay as example, there is a reduction of 93.83% of intracellular JE2 between early (0.5h) to late (3h) timepoint in untreated neutrophils. Similarly, the intracellular JE2 count between early and late timepoints when neutrophils were treated with 1, 5 and 10μM NSA were reduced by 88.13%, 92.21% and 99.91% respectively. This suggested that there were no significant differences in the intracellular bacterial killing between untreated

and NSA-treated neutrophils at both early (0.5h) and late (3h) timepoints, and NSA treatment does not promote intracellular bacterial killing in neutrophils. Figure 3.8b showed the mean and individual cfu/mL values from two independent experiments using MOI 5. Using values from an independent assay as example, the intracellular JE2 between early (0.5h) to late (3h) timepoint in untreated neutrophils was reduced by 76.12%, and the intracellular JE2 count between early and late timepoints when neutrophils were treated with 1, 5 and 10μM NSA were reduced by 45%, 64.19% and 49% respectively. These preliminary results suggested that NSA treatment does not promote intracellular bacterial killing in neutrophils.

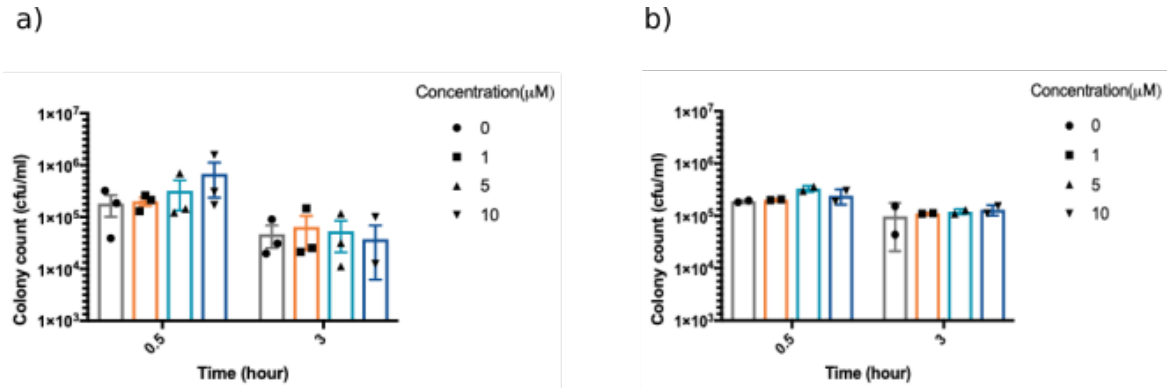

Fig. 3.8 **Neutrophil intracellular killing assay using NSA.** Neutrophils were co-infected with JE2 a) MOI 10, data shown is the mean with SEM of 3 separate experiments, and b) MOI 5, data shown is the mean with SD of 2 independent experiments.

To ensure that the compound was functional, a positive control experiment was carried out using human colorectal adenocarcinoma cell line HT-29. To determine whether NSA was able to reduce cell death, cell death assay was performed on NSA-treated HT-29 cells as described in (methods). Necroptosis of HT-29 cells were induced using tumor necrosis factor α (TNFα) and cycloheximide (CHX). Data from an independent assay was used to illustrate the gating strategies used to determine the percentage of viable cells, as well as the ToPro-3 positivity (Figure 3.9a), and the mean and individual values of four independent experiments were shown in Figure 3.9b and

c. Although the NSA-treated cells have comparatively higher cell viability percentages and lower ToPro-3 positivity, one-way ANOVA test showed no significant differences in the percentage of viable cells treated with 1 and 10 μM of NSA (p-values of 0.2075 and 0.4702 respectively), and there were no significant differences in the ToPro-3 positivity of 1 μM (p=0.2067) and 10 μM (p=0.2127) -treated HT-29 cells. This suggested that NSA may not be functional in reducing cell death, and it does not prevent *S. aureus* -induced neutrophil cell death. Therefore, a different cell death inhibitor was selected to determine whether it inhibits *S. aureus* -induced neutrophil cell death.

a)

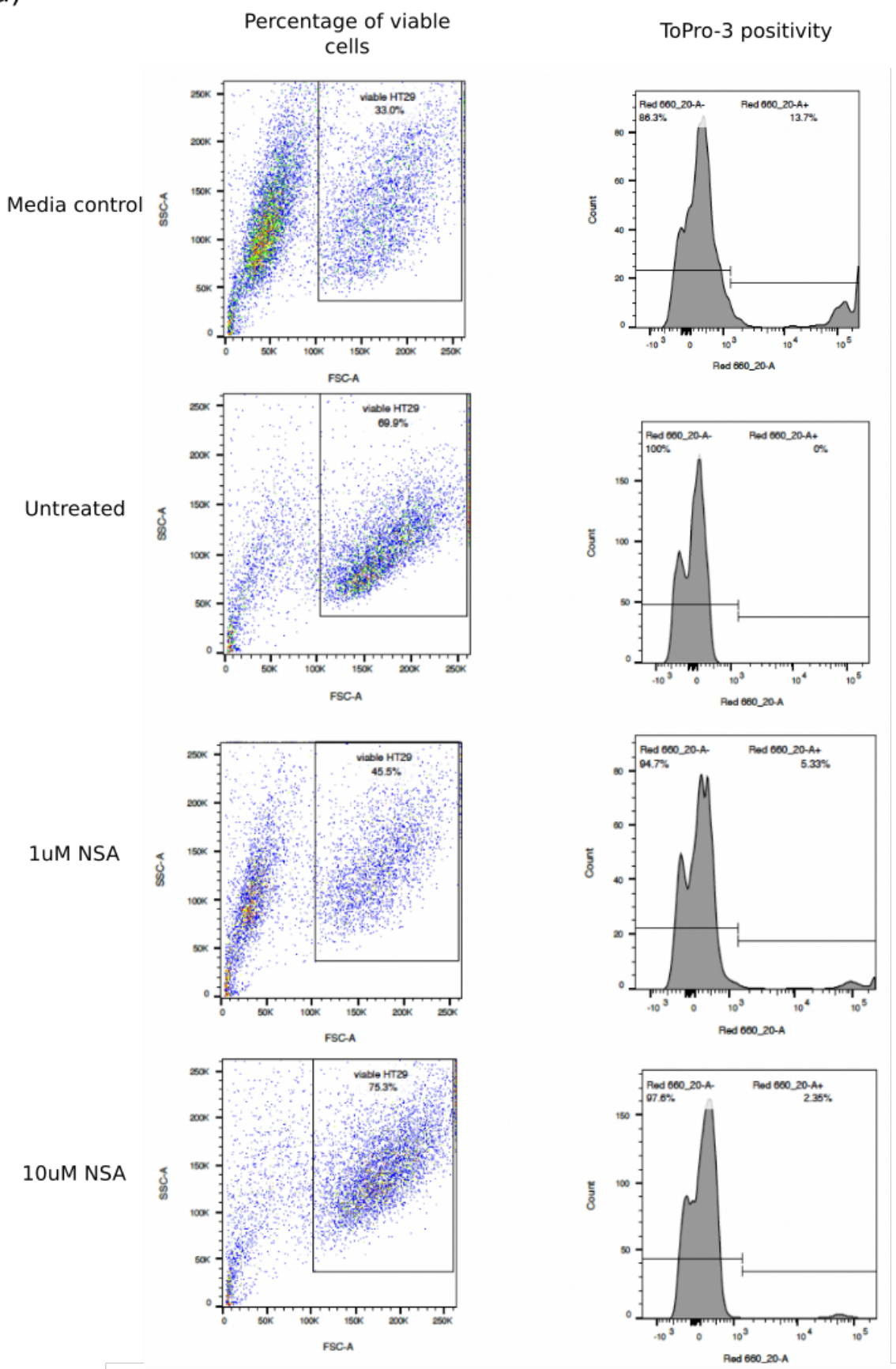
Percentage of viable cells
ToPro-3 positivity
Media control
Untreated
1uM NSA
10uM NSA
viable HT29
33.0%
69.9%
45.5%
75.3%
SSC-A
FSC-A
Red 660_20-A-
Red 660_20-A+
86.3%
13.7%
100%
0%
94.7%
5.33%
97.6%
2.35%
Count
Red 660_20-A

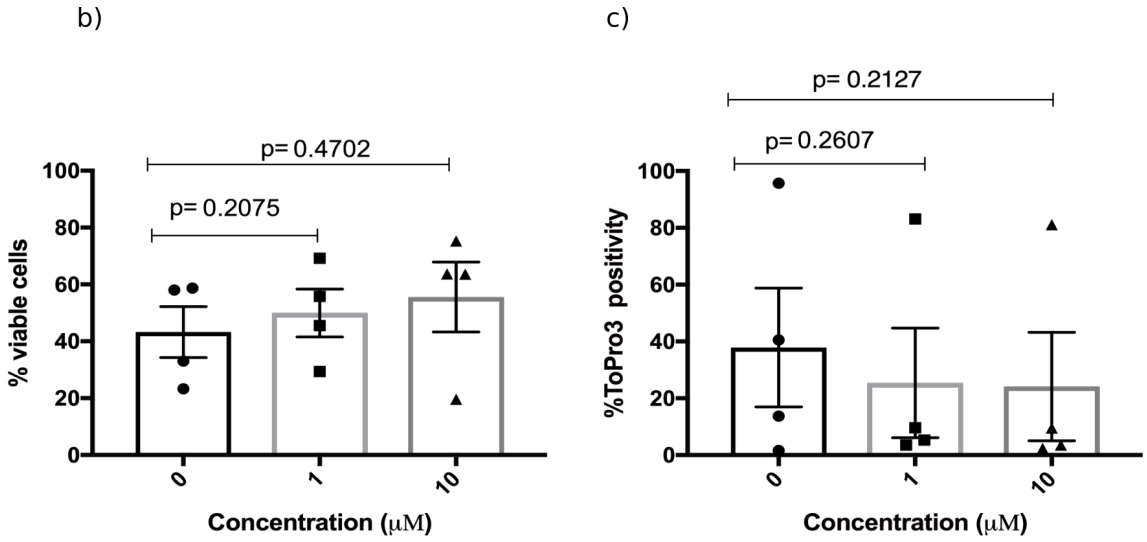

Fig. 3.9 **HT-29 cell death assay using NSA.** The ability of NSA to prevent cell death was tested in HT-29 cells, in which a combination of TNFα and CHX was used to induce necroptosis in HT-29 cells . A) Gating strategies used to determine HT-29 cell viability and ToPro-3 positivity. B) Percentage of viable cells and c) ToPro-3 positivity in HT-29 cells with and without NSA treatment. Data showed the mean with SEM from 4 independent experiments. One-way ANOVA was performed and no significant differences were found between HT-29 cells treated with different NSA concentrations.

3.3.3 Necrostatin-1 (Nec-1)

Nec-1 is a necroptosis inhibitor that selectively blocks the receptor-interacting serine/threonine kinase 1 (RIPK1) (Degterev et al., 2008, 2005). Nec-1 was used to assess whether blocking RIPK1 can inhibit *S. aureus*-induced neutrophil cell death. Neutrophils were incubated with Nec-1 for 1h prior addition of JE2, and the neutrophil viability was determined as previously (see section 3.3.2). Using different concentrations of Nec-1 does not rescue neutrophil viability at MOI 5 and 10 (Figure 3.10), and the use of Nec-1 does not promote neutrophil-mediated killing of *S. aureus* in early (0.5h) and late (3h) time points at both MOIs (Figure 3.11).

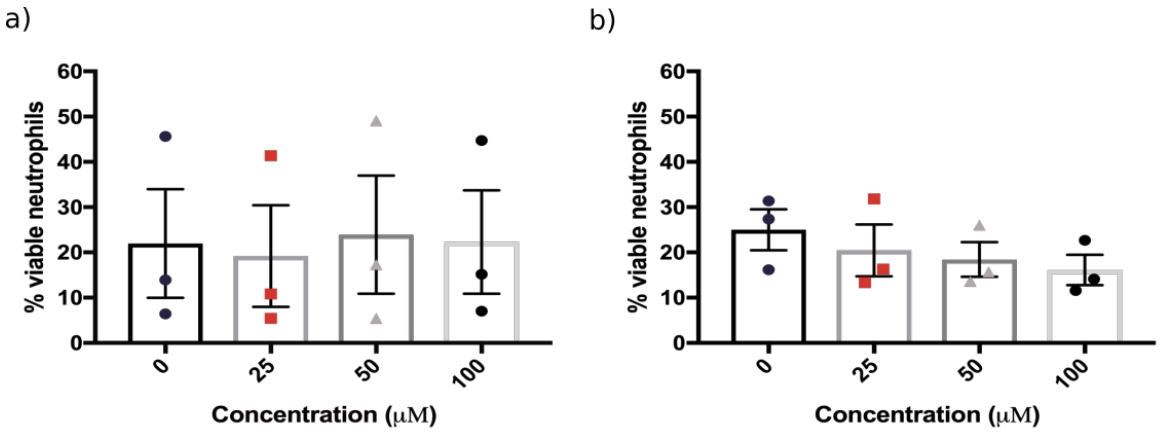

Fig. 3.10 **Neutrophil cell death assay using Nec-1.** Neutrophils were pre-incubated with Nec-1 for 1h, followed by co-infection with JE2 at a) MOI 10 and b) MOI 5, where data shown is the mean with SEM of 3 separate experiments. One-way ANOVA was performed and no significant differences were found.

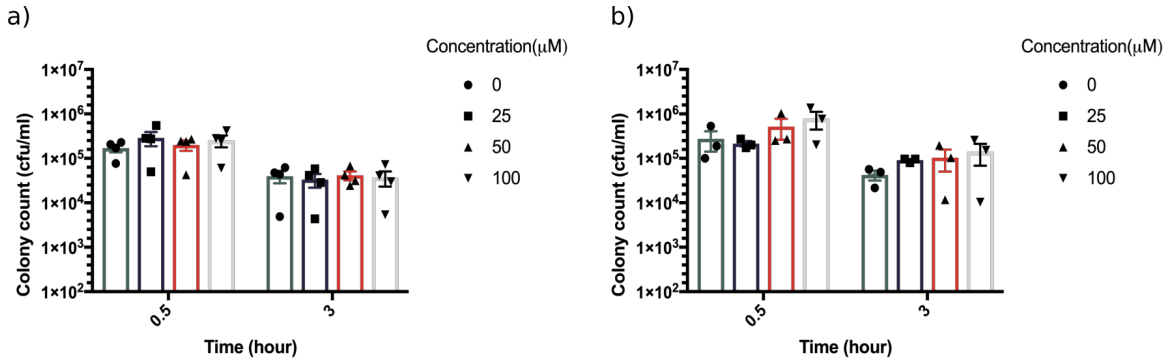

Fig. 3.11 **Neutrophil intracellular killing assay using Nec-1.** Neutrophils were pre-incubated with Nec-1 for 1h, followed by co-infection with JE2 at a) MOI 10 and b) MOI 5. Data shown is the mean with SEM of 3 separate experiments. One-way ANOVA was performed and no significant differences were found.

Similar to NSA, a positive control experiment was carried out using HT-29 cell line to ensure that the compound was functional. Cell death assay was performed on NSA-treated HT-29 cells as described in (methods). Necroptosis of HT-29 cells were induced using TNFα and CHX. Data from an independent assay was used to illustrate the gating strategies used to determine the percentage of viable cells, as well as the ToPro-3 positivity (Figure 3.12a), and the mean and individual values of

four independent experiments were shown in Figure 3.12b. There were no significant differences in the percentage of viable cells treated with 25 and 100 μM of NSA.

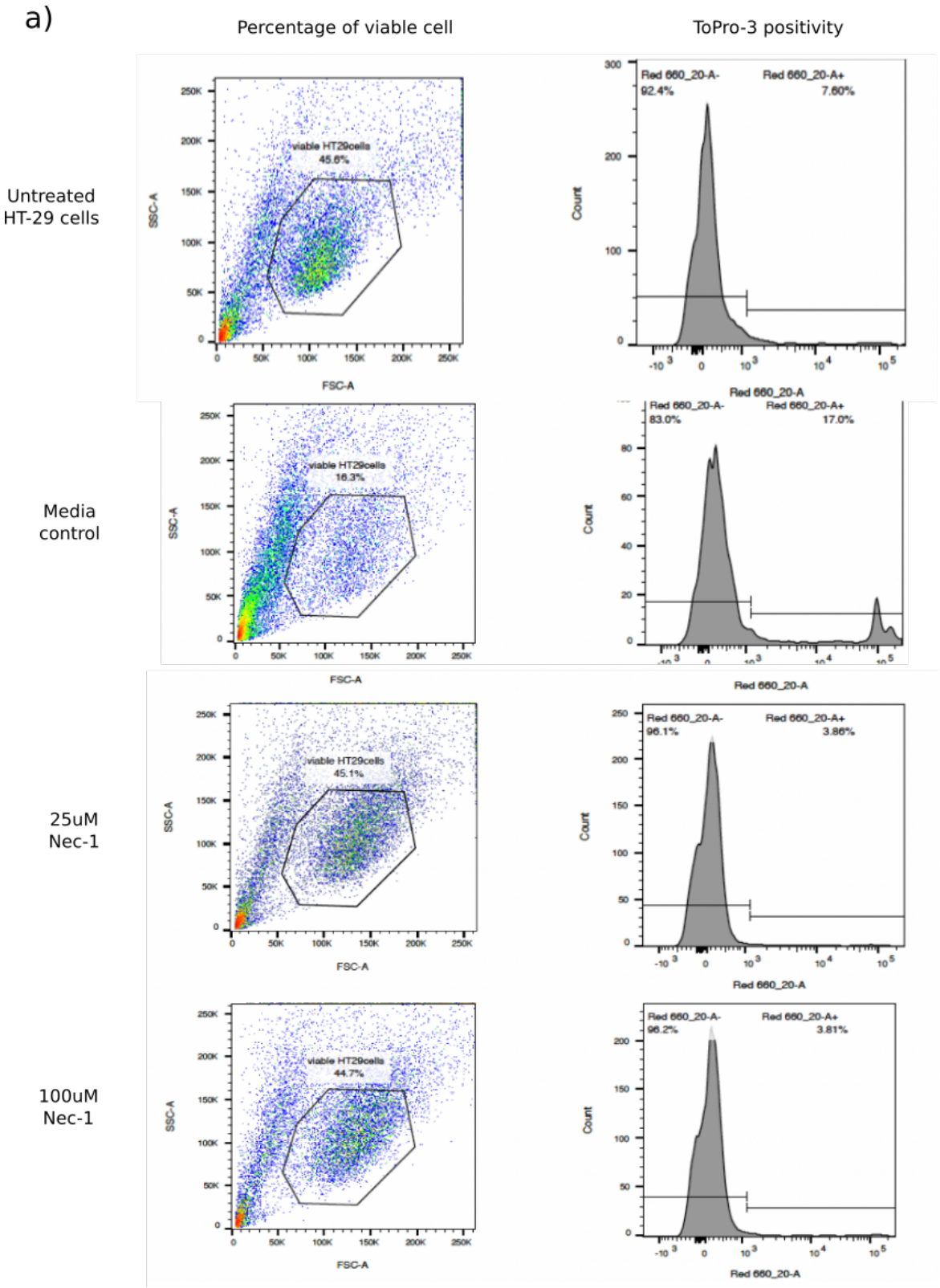
a)
Percentage of viable cell
ToPro-3 positivity
Untreated HT-29 cells
Media control
25uM Nec-1
100uM Nec-1
viable HT29cells
45.6%
viable HT29cells
16.3%
viable HT29cells
45.1%
viable HT29cells
44.7%
SSC-A
FSC-A
Count
Red 660_20-A-
92.4%
Red 660_20-A+
7.60%
Red 660_20-A-
83.0%
Red 660_20-A+
17.0%
Red 660_20-A-
96.1%
Red 660_20-A+
3.86%
Red 660_20-A-
96.2%
Red 660_20-A+
3.81%
Red 660_20-A

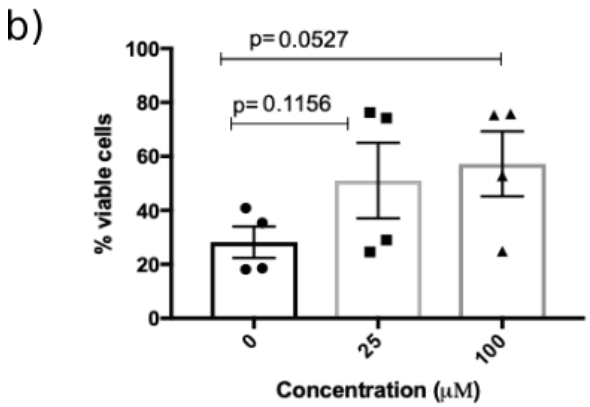

Fig. 3.12 **HT-29 cell death assay using Nec-1.** The ability of Nec-1 to prevent cell death was tested in HT-29 cells, in which a combination of TNFα and CHX was used to induce necroptosis in HT-29 cells . a) Gating strategies used to determine HT-29 cell viability and ToPro-3 positivity. b) Percentage of viable cells in HT-29 cells with and without Nec-1 treatment. Data showed the mean values with SEM from 4 independent experiments. One-way ANOVA test was performed, and no significant differences were found between HT-29 cells treated with different Nec-1 concentrations.

3.3.4 GSK' 872

RIPK-3 is central to necroptosis, and GSK' 872 is a small molecule that inhibits RIPK-3 activity (Mandal et al., 2014). Neutrophils were incubated with different concentrations of GSK' 872 for 1h prior addition of JE2, and the gating strategies used to quantify neutrophil viability was determined as previously (see section 3.3.2). Figure 3.13a showed the gating strategies to quantify neutrophil viability. Furthermore, the absolute neutrophil number was used in quantifying neutrophil viability. Together, figure 3.13b-g showed that GSK'872 can significantly inhibit *S. aureus*-induced neutrophil cell death at MOI 5 and 10.

a)

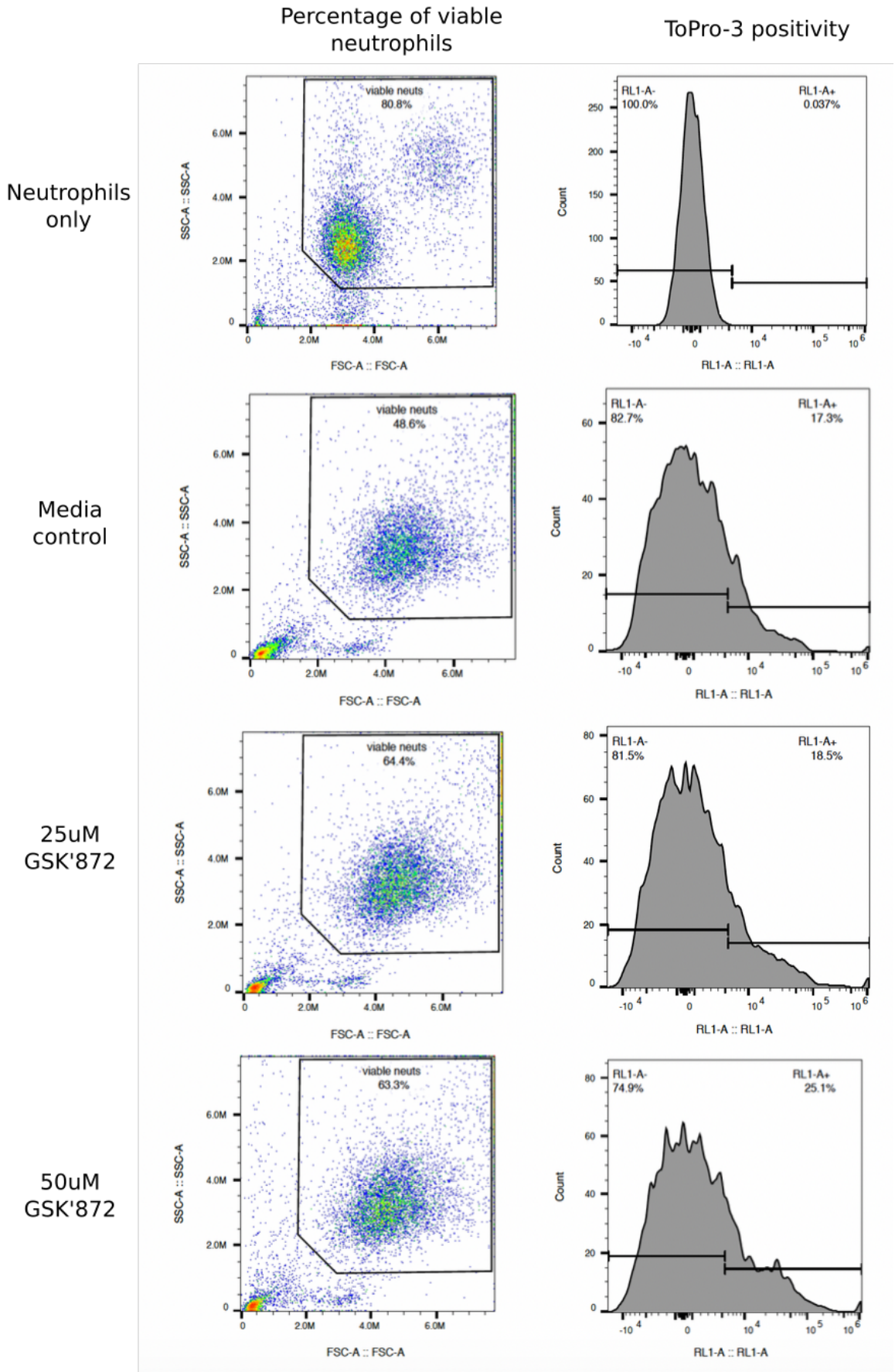
Percentage of viable neutrophils
ToPro-3 positivity
Neutrophils only
Media control
25uM GSK'872
50uM GSK'872
viable neuts 80.8%
viable neuts 48.6%
viable neuts 64.4%
viable neuts 63.3%
RL1-A- 100.0%
RL1-A+ 0.037%
RL1-A- 82.7%
RL1-A+ 17.3%
RL1-A- 81.5%
RL1-A+ 18.5%
RL1-A- 74.9%
RL1-A+ 25.1%
SSC-A :: SSC-A
FSC-A :: FSC-A
Count
RL1-A :: RL1-A

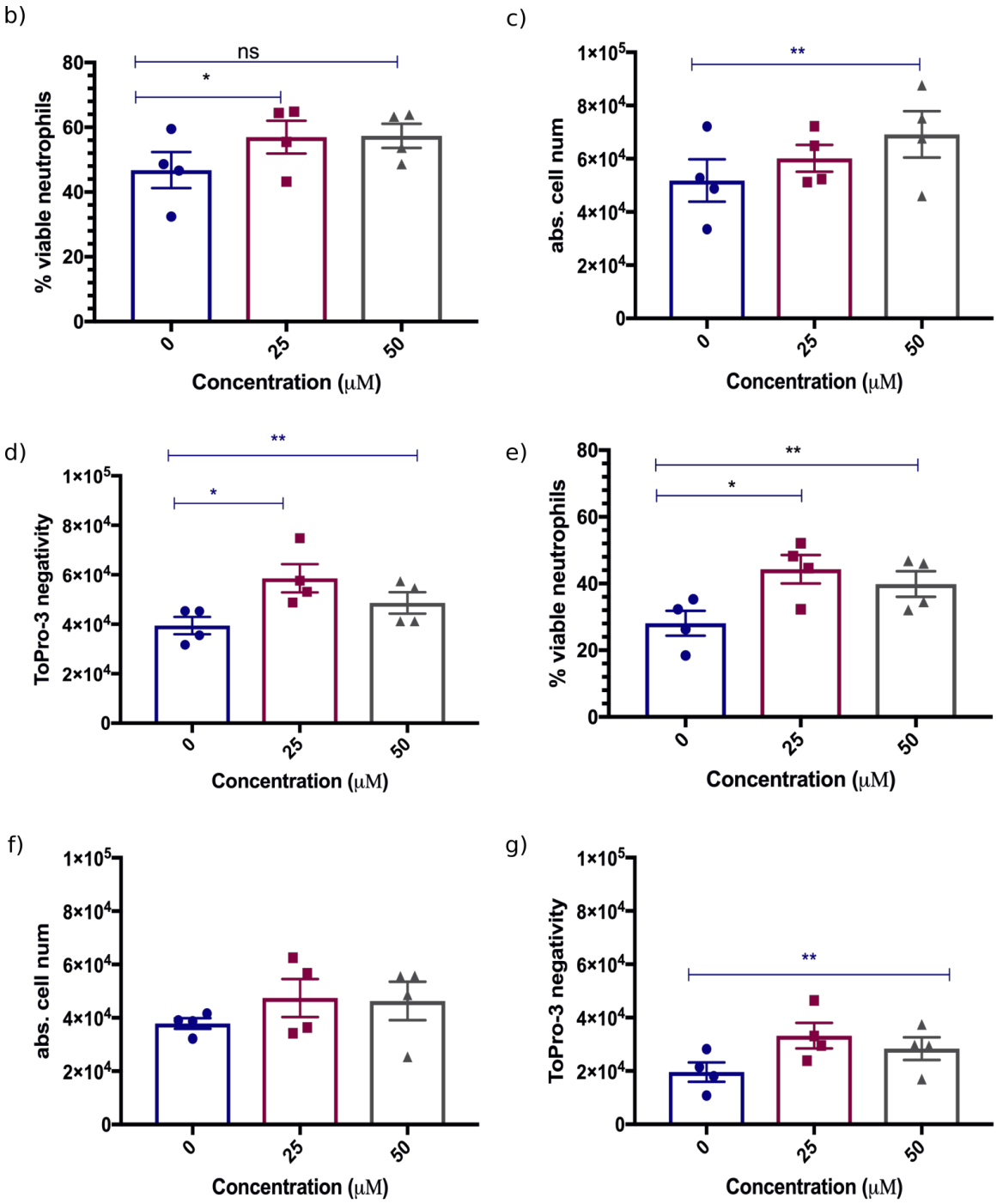

Fig. 3.13 **GSK' 872 cell death assays using Attune flow cytometer.** A) Representative gating strategies used to quantify neutrophil viability. The b) percentage of viable neutrophils c) absolute cell number d) ToPro-3 negativity of neutrophil co-infected with JE2 using an MOI 5, and the e) percentage of viable neutrophils f) absolute cell number g) ToPro-3 negativity of neutrophil co-infected with JE2 using an MOI 10. Data showed the mean values with SEM from 4 independent experiments. One-way ANOVA was performed, and the significant differences are indicated with * $p<0.05$ and ** $p<0.01$.

To test whether inhibiting neutrophil cell death using GSK'872 improves neutrophil-mediated *S. aureus* killing, neutrophil intracellular killing assay with early (0.5h) and late (3h) timepoints was performed as previously. Inhibition of RIPK-3 activity does not promote neutrophil-mediated *S. aureus* killing in either MOI 5 or 10, and the one-way ANOVA tests showed that there were no significant differences in the percentage of intracellular killing (Figure 3.14). Additional intracellular killing assay was performed at 2h timepoint, which is the timepoint used in cell death assay to determine whether increasing neutrophil viability enhances neutrophil-mediated *S. aureus* killing. Preliminary results showed that the use of GSK' 872 reduced *S. aureus*-induced neutrophil cell death (Figure 3.15a,b). In neutrophil intracellular killing assay, paired Student's t-test showed that there is no significant difference between GSK-872 treated neutrophils and media control (Figure 3.15c). Additionally, paired Student's t-test showed no significant difference in the percentage of intracellular bacterial killing in the control and GSK'872- treated neutrophils (Figure 3.15d). This suggests that GSK'872 does not enhance neutrophil-mediated *S. aureus* killing, even at an earlier timepoint.

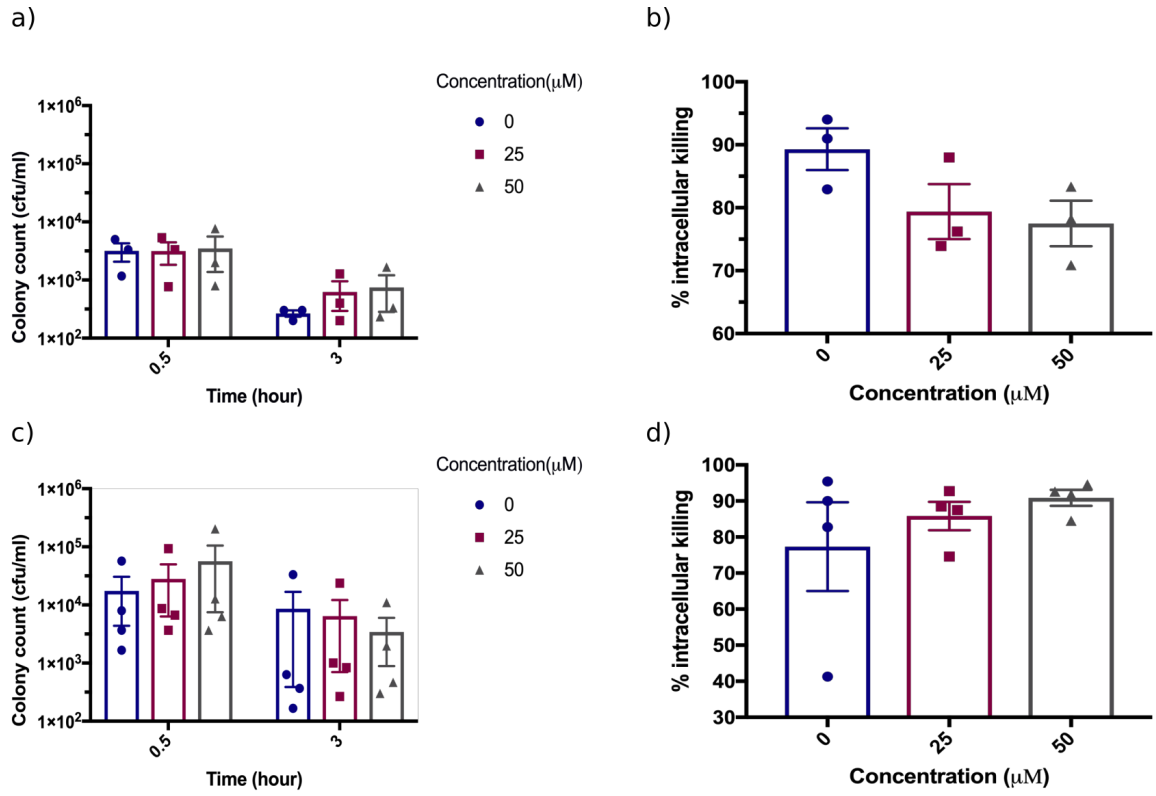

Fig. 3.14 **Neutrophil intracellular killing assay with different GSK' 872 concentrations at 0.5 and 3h time points.** Neutrophils were co-infected with JE2 at a) MOI 5, with error bars showing the mean with SEM (n=3), b) Percentage of intracellular killing of MOI 5, and at c) intracellular killing assay using MOI 10 and d) Percentage of intracellular bacterial killing at MOI 10, with error bars showing the mean with SEM (n=4). One-way ANOVA was performed, and no significant differences were found.

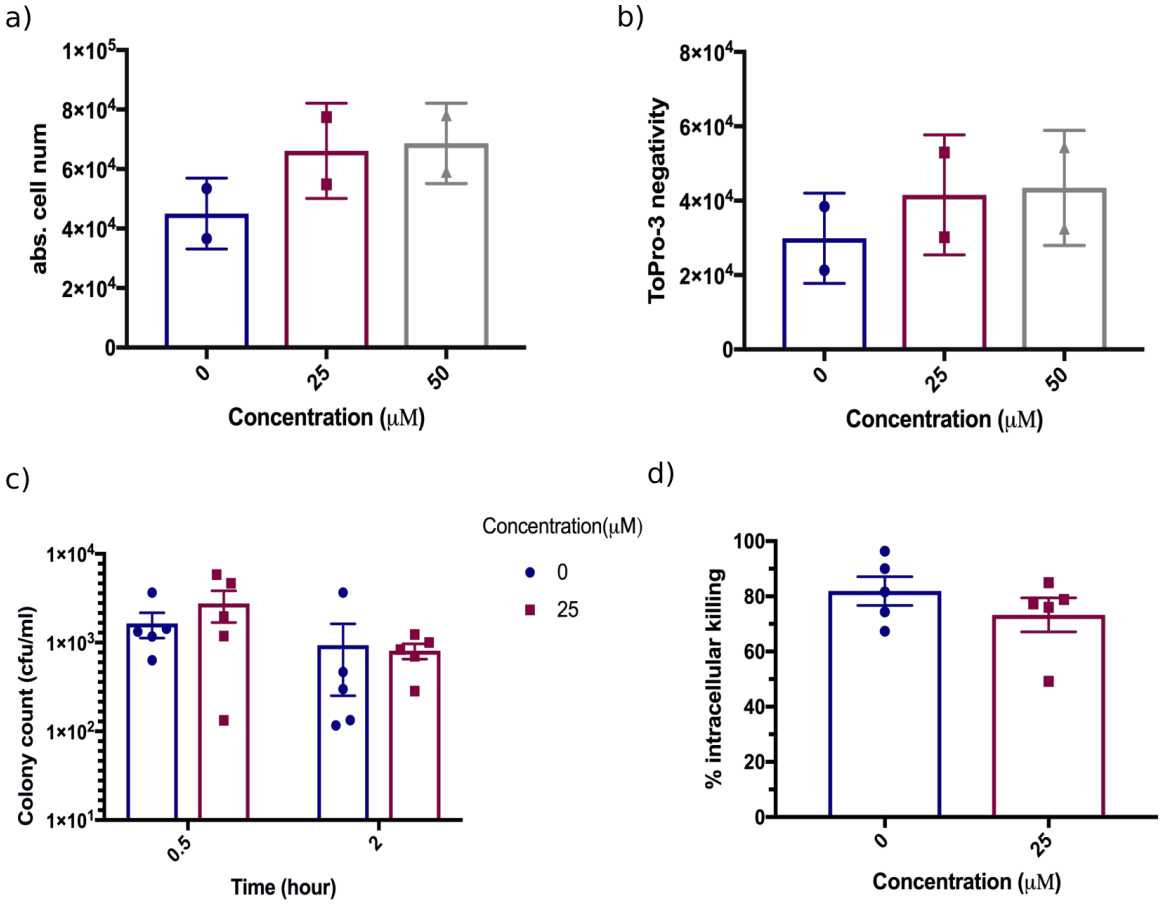

Fig. 3.15 **Cell death assay and neutrophil intracellular killing assay using earlier timepoint.** Quantification of the a) absolute cell number and ToPro-3 negativity at 2h timepoint. Intracellular killing assay at 0.5 and 2h time points using MOI 10. Data shown is the mean with SEM of 5 independent experiments. One-way ANOVA was performed and no significant differences was found. In intracellular killing assay, the intracellular bacterial load at different timepoints was shown in c), and the percentage of intracellular killing between control and GSK '872-treated neutrophils was shown in d). Data shown is the mean with SEM of 5 independent experiments. Student's paired t-test was performed and no significant differences were found.

It is interesting to note the preliminary results that showed an increased in the number of intracellular *S. aureus* recovered from GSK' 872-treated neutrophils at earlier timepoint (Figure 3.15a, b). It is possible that GSK' 872 treatment preserved neutrophil membrane integrity, whereas untreated neutrophils have compromised membrane integrity that allowed *S. aureus* escape, hence the lower intracellular *S.*

aureus load. To further investigate this, gentamicin was removed by washing with PBS after 30 mins, and neutrophil co-culture was resuspended and incubated in fresh RPMI 1640 media (+10 % FBS) until the 2h timepoint. At 2h time point, the neutrophil co-culture was spun at 0.4rcf for 4 mins, and the extracellular bacterial load was enumerated by performing Miles and Misra method using the supernatant. Paired Student's t-test showed that there were no significant differences in the extracellular bacterial load between media control and GSK' 872-treated neutrophils (Figure 3.16).

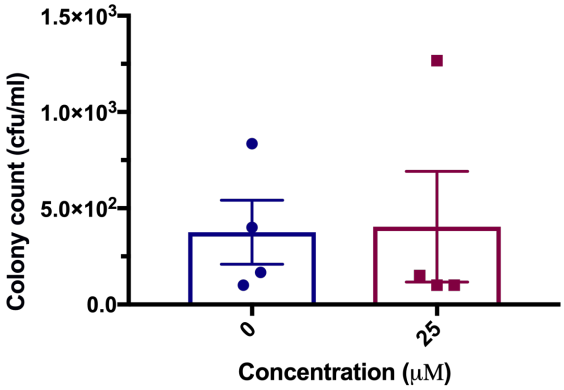

Fig. 3.16 **Extracellular bacterial load at 2h.** Neutrophils were co-infected with JE2 at MOI 10, and intracellular killing assay was performed as previously. The extracellular bacterial count at 2h was enumerated by Miles and Misra. Data shown is the mean with SEM of 4 separate experiments, and paired Student's t-test showed no significant differences.

So far, none of the candidate inhibitors tested have shown the ability to promote intracellular *S. aureus* killing by neutrophils. Although GSK'872 was able to inhibit *S. aureus*-induced neutrophil cell death, it does not promote intracellular bacterial killing. Therefore, an unbiased approach of screening a compound library was used to pursue the aim of identifying compounds that can prevent *S. aureus*-induced neutrophil cell death, thus promoting intracellular bacterial killing in neutrophils.

3.4 Unbiased approach

High-throughput compound screening is a commonly used method to explore and identify new strategies to modulate cell death pathways. For example, the screening of small molecule compound libraries have led to the identification of GSK' 872 as RIPK-3 inhibitor, used in the previous section (Kaiser et al., 2013). The Spectrum collection is a compound library that consist of 2000 bioactive compounds in the US and International drug collections (Microsource Discovery System). The aim of screening the Spectrum compound library was to identify compounds that can inhibit *S. aureus*-induced neutrophil cell death, and bring forward the compounds to test whether they can promote intracellular bacterial killing in neutrophils.

3.4.1 Determination of MOI and timepoint for Spectrum collection screen

The MOI and timepoint used in co-cultures were optimised to establish the Spectrum collection screen. This is to ensure adequate neutrophil cell lysis was induced by JE2, and to provide a window for identifying compounds that can reduce *S. aureus*-induced neutrophil cell death. To determine the optimal MOI and timepoint, neutrophils were co-cultured with JE2 at MOIs of 1,5 and 10 for 1,2 and 3h respectively. There is a significant drop in the percentage of viable neutrophils (Figure 3.17a), with the highest percentage of ToPro-3 positivity (Figure 3.17b) when neutrophils were co-cultured at MOI of 10 in all three timepoints. This indicated that MOI 10 causes the greatest level of cell death and ToPro-3 positivity.

In comparison to co-cultures at MOI 10, neutrophils infected with JE2 at MOI 1 maintained approximately 40% viable neutrophils and less than 20% ToPro-3 positivity across all three timepoints, indicating that there is appropriate amount of cell death,

but insignificant cell damage. At 2h timepoint, neutrophils co-cultured with JE2 at MOI of 5 retained 34.2% of viable neutrophils, which was approximately half of the neutrophil media control (68.1%), and the ToPro-3 positivity was higher (28.2%) compared to MOI 1 (12.1%). This showed that neutrophils co-cultured at MOI 5 for 2h induced sufficient cell death and cell damage, and thus was selected for the compound screen.

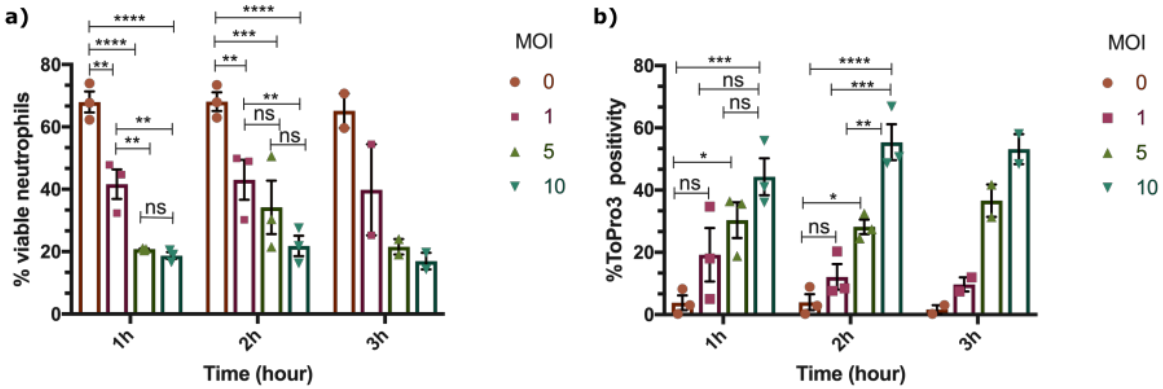

Fig. 3.17 **Selection of appropriate MOI and timepoint for screen.** a) Percentage of viable neutrophils and b) ToPro-3 positivity when neutrophils were co-infected with JE2 at different MOIs and timepoints. Data showing the mean with SEM (n=3) for 1 and 2h and mean with SEM (n=2) for 3h. Two-way ANOVA was performed, where Ns= not significant, *p<0.0332,** p<0.0021, *** p<0.0002 and **** p<0.0001 were indicated.

3.4.2 Determination of cell death variation across 96-well plate

The compounds in the Spectrum collection were provided in a 96-well plate format, and screening was performed using an autosampler plate reader on the Attune flow cytometer. Therefore, it is important to verify that the results of cell death assay is consistent across the plates before proceeding with the compound screen. Neutrophils were co-cultured with JE2 at MOI 5 for 2h, and the percentage of viable neutrophils across 96-well plate was determined. As a representative, Figure 3.18 showed minimal

cell death variation across a 96-well plate, thus providing confidence to proceed with the compound screen.

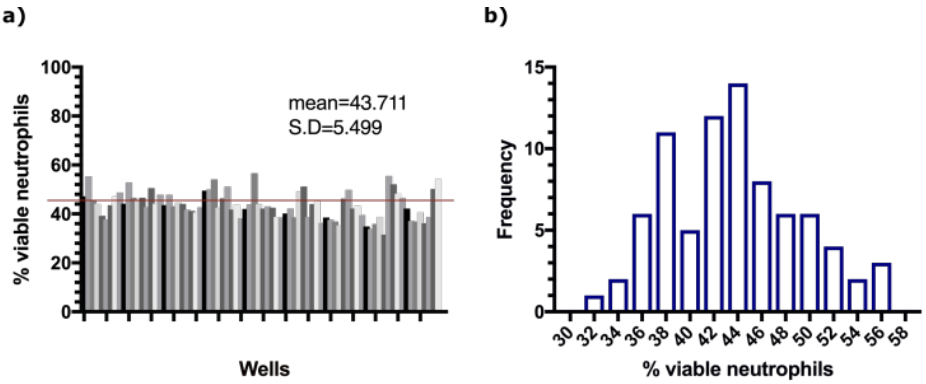

Fig. 3.18 **Representative graph of cell death variation across 96-well plate.** a) The percentage of viable neutrophils across individual wells in a 96-well plate. b) Histogram showing the frequency of the percentage of viable neutrophils.

3.4.3 First round screen

The first round of screening was performed after the screen conditions were established in sections 3.4.1 and 3.4.2. This was done by using JE2 strain at MOI 5 for 2h, and the number of viable neutrophils and ToPro-3 staining were quantified using high-throughput flow cytometry.

3.4.4 Strategies to identify of compounds that attenuated *S. aureus*-induced neutrophil lysis

The first round of screen was conducted with the goal of identifying compounds that can attenuate *S. aureus*-induced neutrophil lysis. Individual plates contained 80 compounds that were provided in a 96-well plate format, and the experimental set up is illustrated in Figure 3.19. The compounds were provided in stock concentrations of 2.5mM in DMSO, stored at -20°C. In each experiment, stock concentrations were thawed and compounds were transferred to a sterile 96-well plate, and dilutions were made with

RPMI 1640 (+10% FBS) such that the final concentration of compounds in each well is 1 μM.

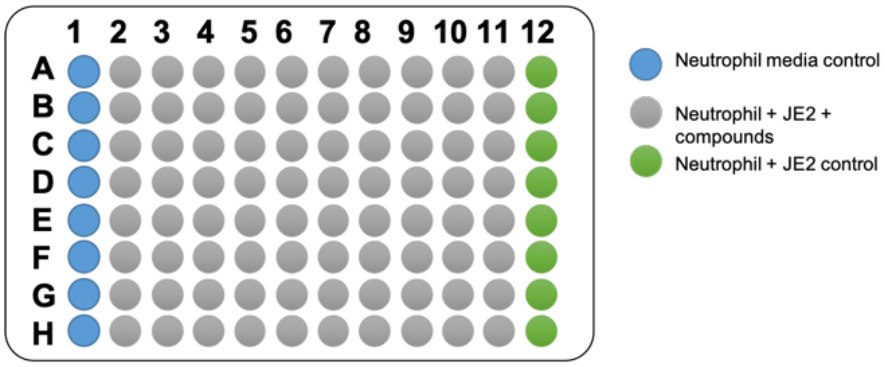

Fig. 3.19 **Illustration of 96-well plate set up.** Row 1 containing neutrophil media control and row 12 containing neutrophil and JE2 control.

The percentage of viable neutrophils, absolute cell number and ToPro-3 negativity cell count were criteria used to assess the compounds. The ToPro-3 negativity and absolute cell count were quantified using Attune NxT software, as described previously in section 2.7.4, whereas the percentage viable neutrophil was quantified using FlowJo analysis software. The mean value of individual plates was used as a benchmark, with the assumption that the majority of compounds do not attenuate *S. aureus*-induced neutrophil lysis. A threshold level is drawn by using the following formula:

$$\text{Threshold} = 1.5 \times \text{standard deviation} + \text{mean value} \tag{3.1}$$

Individual plates were screened twice using neutrophils from two independent donors (n=2). Preliminary identification was done by identifying compounds that exceeds the percentage of viable neutrophils threshold level, and further verified by assessing that the absolute cell number and ToPro-3 negativity values are above threshold level. A custom-written code using Python, as described in section 2.6.6 was used to perform analysis on individual plates, and to identify compounds that are greater than threshold

set in all three criteria. The workflow of identifying potential 'hits' from screen is summarised and illustrated in Figure 3.20.

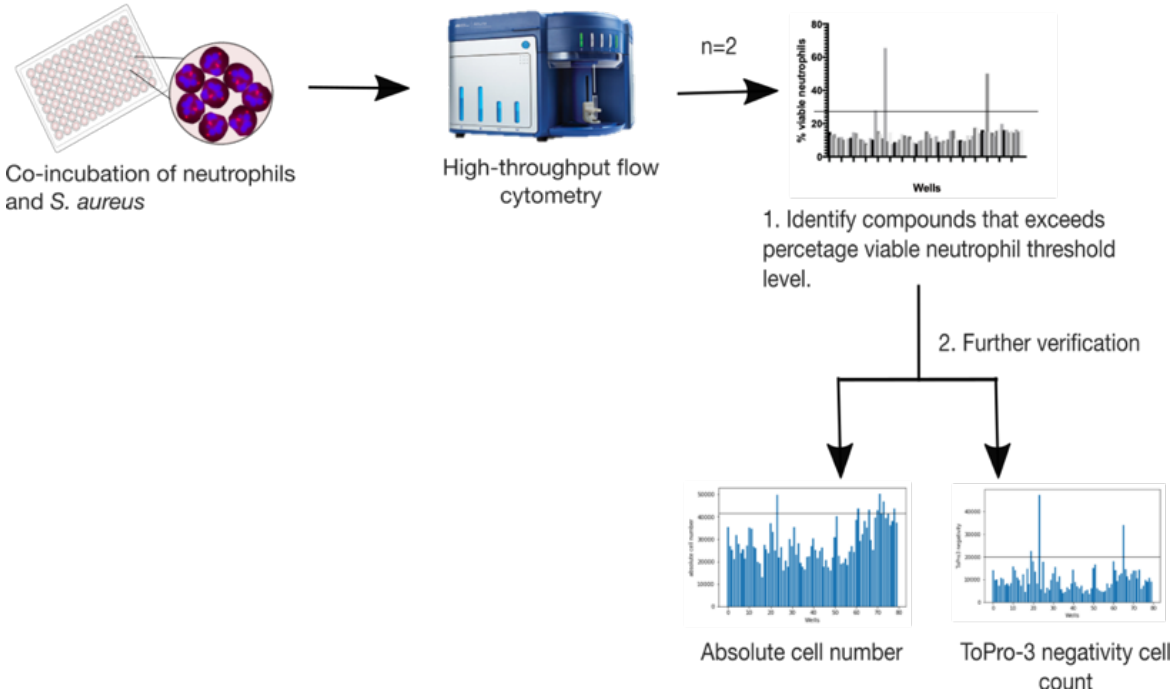

Fig. 3.20 **Representative flow assay plots and workflow of the compound screen.**

3.4.5 Identification of potential hits from first round of screen

Eight hundred compounds from the Spectrum collection were screened. Individual plates consist of 80 compounds, and each plate was screened twice using neutrophils from two independent donors. Twenty experiments were performed in total to complete the screening of 800 compounds. Figure 3.21 showed an example of two independent experiments of the same plate. The screen was carried out with the assumption that majority of the compounds present within each plate were unable to reduce *S. aureus*-induced neutrophil cell death. Therefore, using the overall mean values of individual plate, indicated as the plate average (yellow line, figure 3.21), a threshold level was set and compounds that exceeded the threshold level are identified as 'hits'. Additionally,

the absolute neutrophil number and ToPro-3 negativity values of untreated neutrophils co-infected with JE2 (green line, figure 3.21), as well as uninfected neutrophils in media (red line, figure 3.21) were used as controls. The figures of all 20 experiments can be found in the appendix (Appendix A).

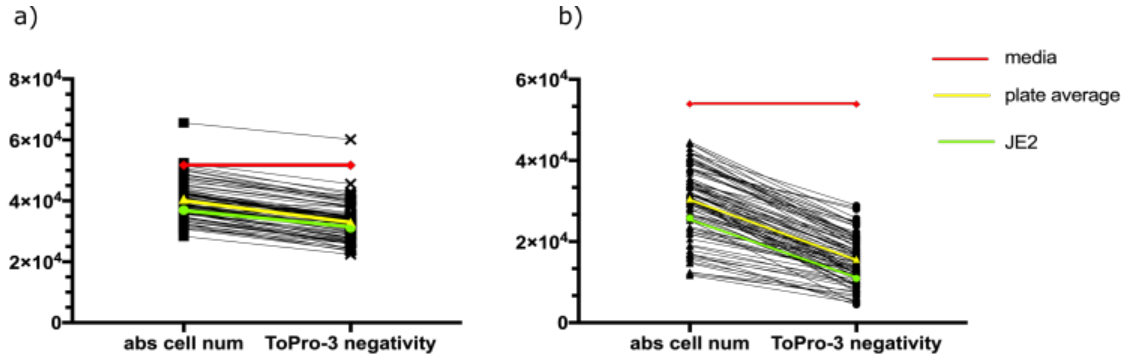

Fig. 3.21 **Representative plots of the compound screen.** An example of screen results from plate 9. The plate was screened twice using cells from two independent donors (n=2), a) donor 1 and b) donor 2. The yellow line indicated the threshold level, red line indicated uninfected neutrophils in media as control and the green line indicated untreated neutrophils co-infected with JE2. Each black line indicated the individual wells in each plate.

Using the strategies in section 3.4.4, a list of compounds that exceeds the threshold percentage of viable neutrophils, absolute cell number and ToPro-3 negativity values were returned. This was done on individual experiments, and compounds were identified as 'hits' if it is present in both lists returned from the two independent experiments of same plate. From this first round of screening, 31 compounds were identified (Table 3.1). To minimise false negative targets, compounds that exceeds the absolute cell number and ToPro-3 negativity cell count threshold, but were below the viable neutrophil percentage threshold were also included in the table. The screen was performed blindly so far, in which the compound names were not known, and individual compound was identified by the coordinates in 96-well plate. This is to reduce conscious bias of the screen.

Plate	**Wells**	**Compounds**	**Percentage of viable neutrophils**
1	Media control	-	55.05
	Neut. + JE2	-	18.55
	A3	Maprotiline hydrochloride*	19.45
	C3	Minocycline hydrochloride*	33.1
	E3	Novobiocin*	35.35
	H2	Puromycin hydrochloride*	21.55
2	Media control	-	51.7
	Neut. + JE2	-	16.15
	F3	Meclocycline sulfosalicylate*	23.5
	H3	Finasteride	21.6
3	Media control	-	77.05
	Neut. + JE2	-	45.4
	D4	Clarithromycin*	52.3
	E8	Rifaximin*	59.3
	H6	Testosterone propionate (Testoviron)	50.15
	H8	Eniconazole*	46.95
4	Media control	-	59.7
	Neut. + JE2	-	43.3
	H3	Chlorambucil	44.6
	H8	Chlorhexidine*	50.85
5	Media control	-	73.4

	Neut. + JE2	-	26.55
	B4	Clindamycin hydrochloride*	49.25
	F2	Diethylstilbestrol*	31.8
	H9	Erythromycin ethylsuccinate*	32.9
6	Media control	-	84.4
	Neut. + JE2	-	21.8
	C5	Gentian Violet*	58.15
7	Media control	-	85.7
	Neut. + JE2	-	28.45
	E3	Rifampin*	64.15
	G9	Tetracycline hydrochloride*	45.95
	H9	Tolbutamide *	34.8
	H10	Tranylcypromine sulfate*	34.35
8	Media control	-	67.5
	Neut. + JE2	-	34.35
	B11	Vancomycin hydrochloride*	43.35
	C8	Phenylmercuric acetate	49.55
	H11	Mebeverine hydrochloride	42.05
9	Media control	-	75.2
	Neut. + JE2	-	52.9
	A2	Aceclidine*	51.45
	A3	Capsaicin*	56.24
	A8	Estradiol propionate	57.5
	D4	Menadione	59.55
	E5	Fluoxuridine*	48.05

	H11	Halcinonide*	58
10	Media control	-	75.25
	Neut. + JE2	-	56.05
	H2	Tacrolimus*	60.1
	H6	Ethylnorepinephrine hydrochloride	57.5

Table 3.1 Potential hits identified from first round of screen.
*indicates that compound have known antimicrobial effects.

Compounds were screened without prior knowledge of their targets. Once targets were revealed, compounds that were well-known antibiotics served as internal positive controls for the screen. For example, antibiotics such as vancomycin, minocycline and tetracycline are widely used in *S. aureus* infections treatment, and as expected, were able to increase neutrophil viability (Table 3.1) (Bowker et al., 2008; Gardete and Tomasz, 2014; Trzcinski et al., 2000). As the aim of this project is to identify new strategies to enhance neutrophil-mediated *S. aureus* killing, compounds with known anti-staphylococcal bioactivities were excluded from further investigations. Of the 31 compounds, 8 compounds remained and were brought forward for a second round of screening (Table 3.2).

Compounds	**Bioactivity**
Finasteride	Anti-androgen
Testosterone propionate (Testoviron)	Androgen, antineoplastic
Chlorambucil	Antineoplastic
Phenylmercuric acetate	Antifungal
Mebeverine hydrochloride	Muscle relaxant

Estradiol priopionate	Estrogen
Menadione	Prothrombogenic agent
Ethylnorepinephrine hydrochloride	Bronchodilator

Table 3.2 Compounds for second round screen.

3.4.6 Second round screen

Eight compounds that were identified from first round of screening were taken forward for a second round screen. The second round of screening was carried out by performing three independent experiments (n=3), using the same techniques and strategies as the first round of screen (section 3.4.4). The concentration of compounds used in the first round of screen was 1μM, and two higher concentrations (2 and 5 μM) were used in the second round of screen to determine whether higher concentrations will improve the attenuation of *S. aureus*-induced neutrophil lysis. Two-way ANOVA test showed there are significant differences in the absolute cell number between untreated media control and using 1, 2 and 5 μM of phenylmercuric acetate (Figure 3.22a). Additionally, compared to untreated neutrophils, 2 μM of phenylmercuric acetate treatment in neutrophils increased the ToPro-3 negativity count, there is an increase in the overall percentage of viable neutrophils when neutrophils were treated with 5μM of phenylmercuric acetate. Together, results from these parameters suggest that phenylmercuric acetate could potentially improve neutrophil viability.

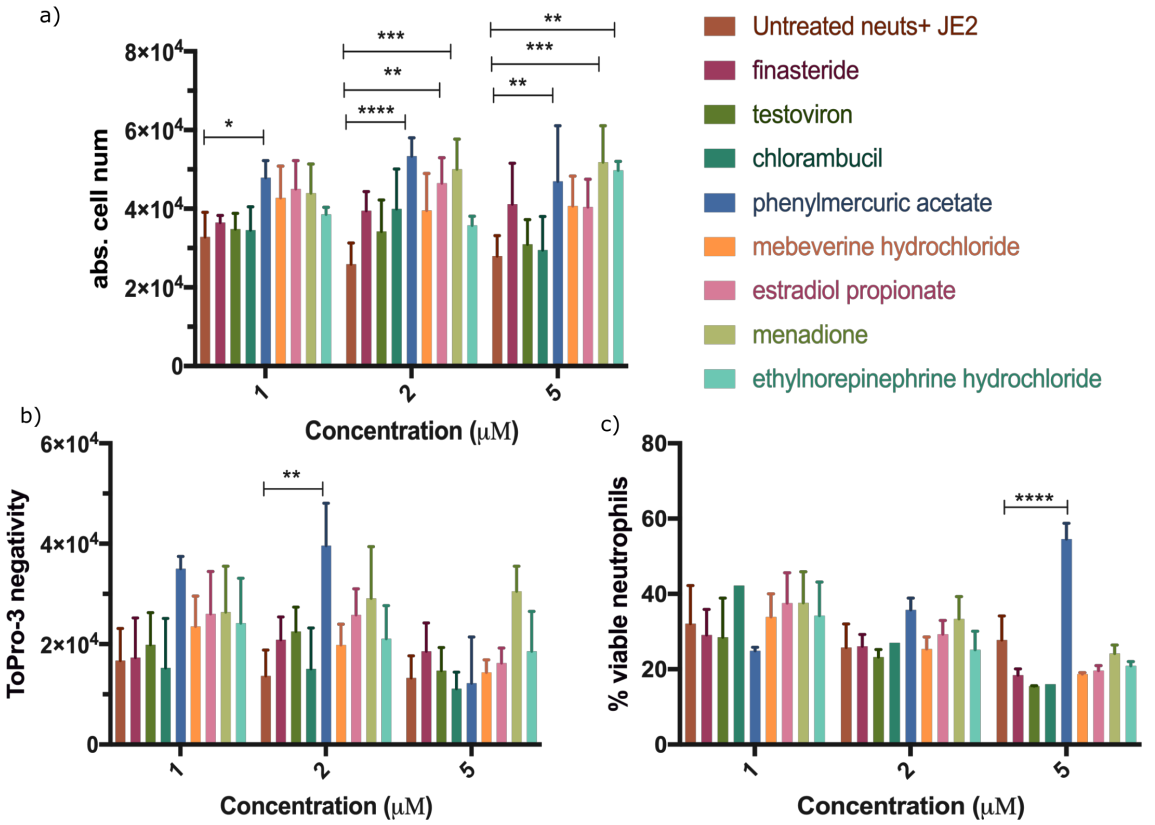

Fig. 3.22 **Second round screen of hits using different concentrations of compounds.** a) absolute cell number, b) ToPro-3 negativity and c) percentage of viable neutrophils when neutrophils were treated with different compounds of varying concentrations (1, 2, 5μM) and co-infected with JE2 at MOI 5 for 2h. Data showed the mean with SEM (n=3), statistical analysis was performed using two-way ANOVA, where *p<0.0332,** p<0.0021, *** p<0.0002 and **** p<0.0001 were indicated.

3.4.7 Compounds selected for further assays

Following the second round of screen, three compounds that showed attenuation of *S. aureus*-induced neutrophil cell death and were brought forward for further assays. These are chlorambucil, estradiol propionate (also known as 17-β-estradiol) and phenylmercuric acetate.

Since the aim was to identify compounds that can promote neutrophil-mediated *S. aureus* killing, it is important to verify that the selected compounds do not have direct anti-staphylococcal activity and do not directly affect neutrophil viability. Additionally,

it is important to verify that the attenuation of *S. aureus*-induced neutrophil cell death as seen in previous sections were not due to the killing of *S. aureus* prior to neutrophil phagocytosis.

To determine whether the compounds contain anti-staphylococcal activity, JE2 was incubated with 2 μM of compounds for 1h, and the bacterial count was enumerated by Miles and Misra assay as detailed in section 2.6.3. Figure 3.23 showed that all four compounds does not have anti-staphylococcal activity. To determine the effect of compounds of neutrophil viability, neutrophils were incubated with the compounds at concentrations of 1 and 2 μM for 2h, and parameters to measure neutrophil viability such as absolute cell number and ToPro-3 negativity were obtained by flow cytometry. Preliminary data based on the absolute cell number and ToPro-3 negativity count suggests all four compounds do not affect neutrophil viability, as seen in Figure 3.24.

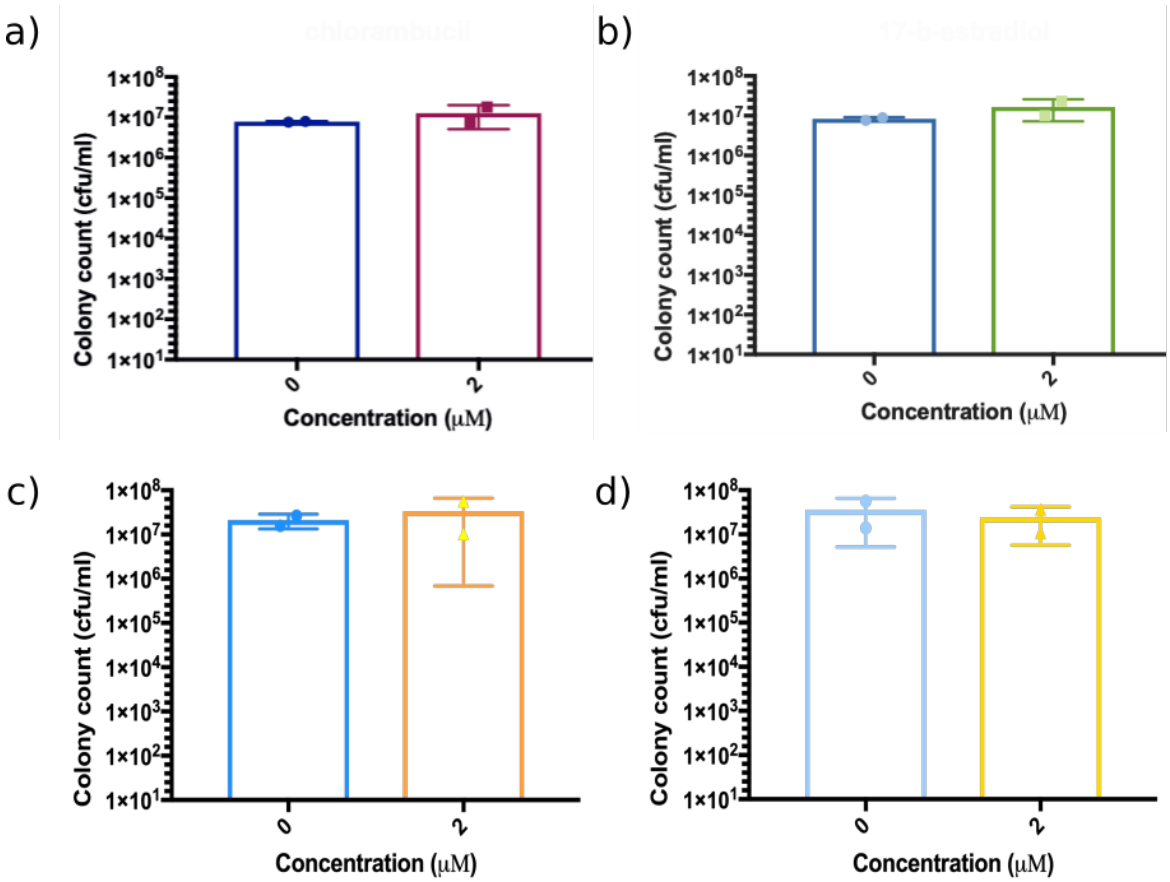

Fig. 3.23 **Anti-staphyloccocal activity assay.** Graphs to illustrate compounds do not have direct anti-staphylococcal activity. JE2 was incubated with a) chlorambucil, b) estradiol propionate, c) phenylmercuric acetate and d) 4-aminophenylmercuric acetate for 2h, followed by Miles and Misra to enumerate the colony counts. Data shown is the mean with SD of 2 separate experiments.

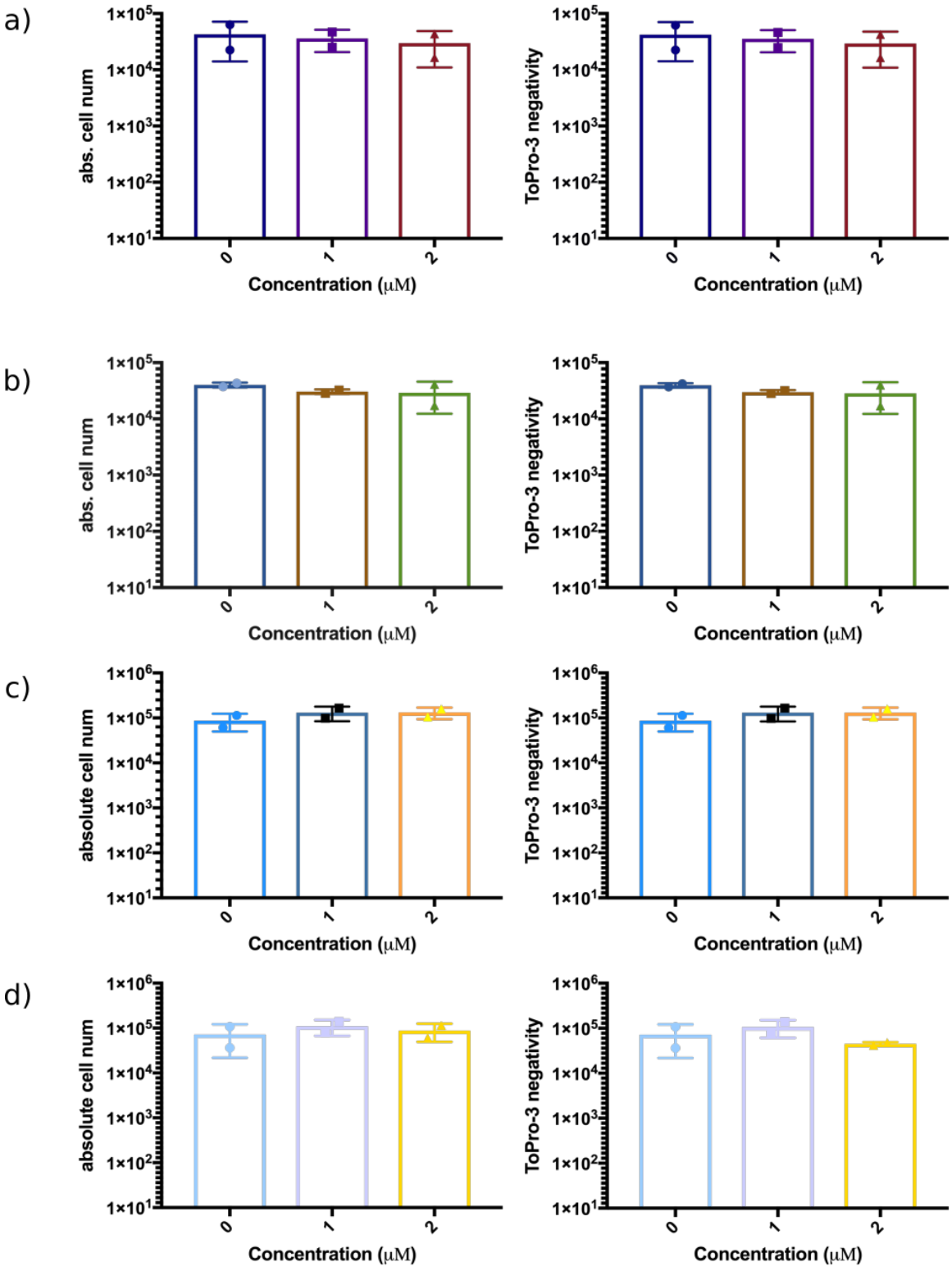

Fig. 3.24 **Compounds does not affect neutrophil viability.** The absolute cell number and ToPro-3 negativity of neutrophils when incubated with a) chlorambucil, b) estradiol propionate, c) phenylmercuric acetate and d) 4-aminophenylmercuric acetate for 2h. Error bars represent mean with S.D (n=2).

While performing literature searches on phenylmercuric acetate, a structurally related compound, 4-aminophenylmercuric acetate (4-APMA) was found to activate matrix metalloprotease 9 (MMP9) (Rosenfeldt et al., 2005). Matrix metalloproteases have important roles against staphylococcal infections, such as facilitating neutrophil transmigration to site of infections (Delclaux et al., 1996) but little is known on the direct effect of MMP-9 in cellular defences against *S. aureus*. Due to its anti-staphylococcal role, matrix metalloproteases like MMP9 are also actively targeted by *S. aureus* factors such as staphylococcal superantigen-like protein 5 (SSL5) (Itoh et al., 2010). Therefore, 4-APMA was selected for further tests.

3.4.8 Chlorambucil

Chlorambucil, also known as Leukeran is an anticancer drug used in the treatment of non-Hodgkin's lymphoma (Portlock et al., 1987). The exact mechanism of action is unknown, but chlorambucil can cross-link DNA to prevent cell proliferation (Begleiter et al., 1996; Di Antonio et al., 2014). Furthermore, chlorambucil is reported to accumulate cytosolic p53 protein, thus promoting apoptosis in chronic lymphocytic leukemia treatment (Di Antonio et al., 2014; Steele et al., 2008).

Neutrophil intracellular killing assay using neutrophils pre-incubated with chlorambucil at 1 and 2 μM for 1h was used to determine whether chlorambucil can promote neutrophil-mediated killing of *S. aureus*. Following the procedures described in section 2.6.3, neutrophil intracellular killing assay was performed using MOI 5 with 0.5 and 3h time points. There is an increased in percentage of intracellular bacterial killing between early (0.5h) to late (3h) timepoint in chlorambucil-treated neutrophils (Figure 3.25b). Taking an independent assay as example, the intracellular bacterial killing using neutrophil media control, 1 and 2 μM chlorambucil-treated neutrophil were 78.76%, 93.33% and 91.1% respectively. However, one-way ANOVA test showed that

there were no significant difference between media control and chlorambucil-treated neutrophils (Figure 3.25). This suggests a possible effect of chlorambucil in enhancing neutrophil-mediated *S. aureus* killing. Therefore, an earlier time point (2h) was used to determine whether a more significant effect in neutrophil intracellular killing can be detected. One-way ANOVA test showed no significant difference in the percentage of intracellular bacterial killing when 2h timepoint was used (Figure 3.26).

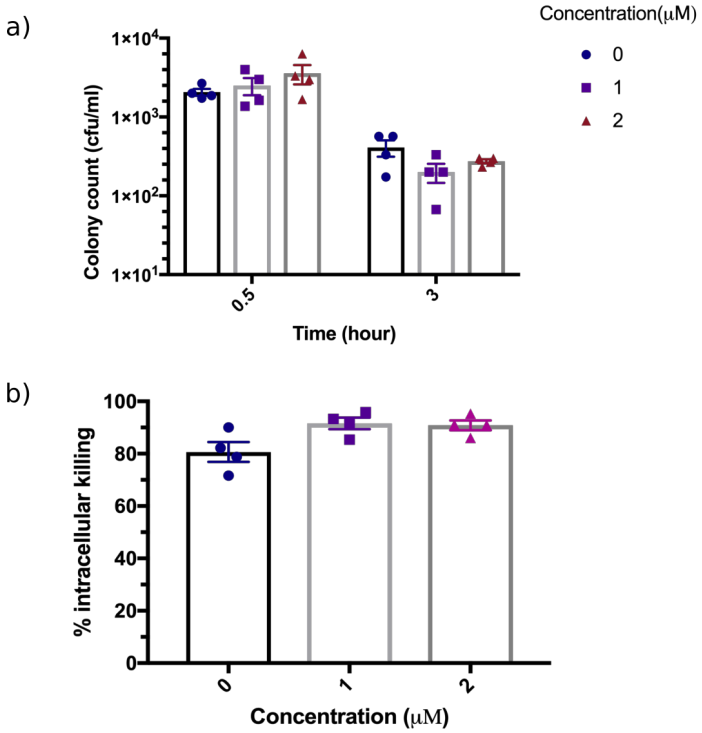

Fig. 3.25 **Chlorambucil-treated neutrophil intracellular killing assay.** Neutrophils were co-infected with JE2 at MOI 5. a) The intracellular bacterial load (cfu/mL) at different timepoints and concentrations of chlorambucil (1 and 2 μM) b) Percentage of intracellular bacterial killing in neutrophil. Data shown is the mean with SEM (n=4), statistical analysis was performed using one-way ANOVA and Dunnett's multiple test.

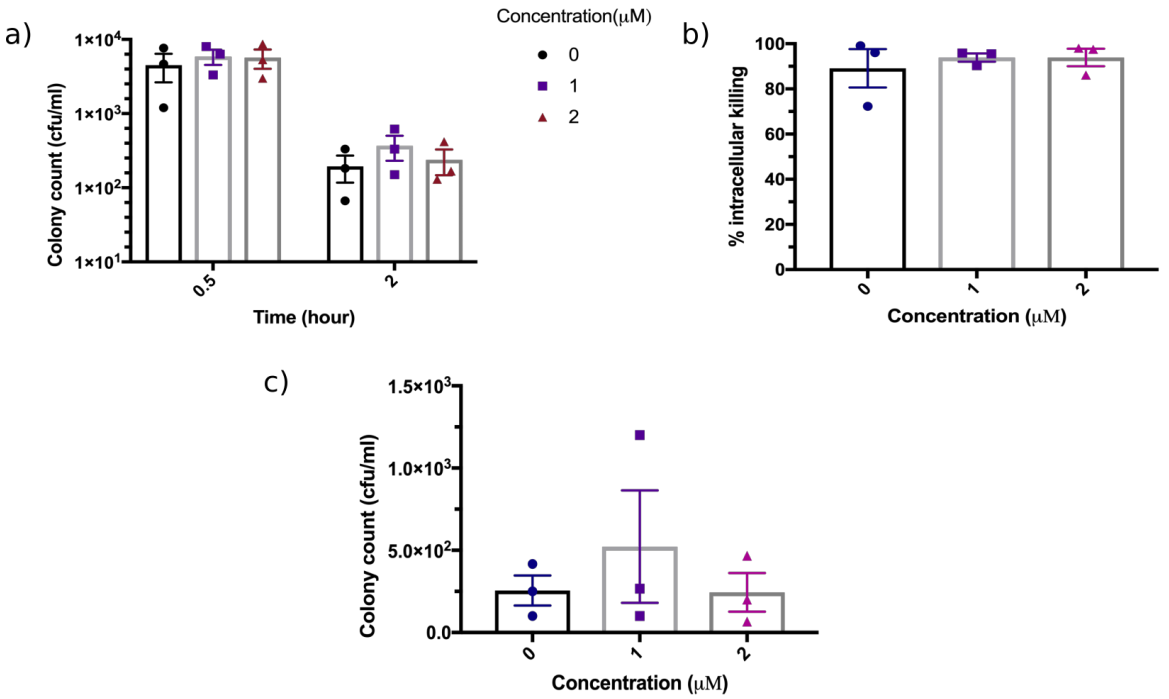

Fig. 3.26 **Chlorambucil-treated neutrophil intracellular killing assay using earlier timepoint.** Neutrophils were co-infected with JE2 and MOI 5. a) The intracellular bacterial load (cfu/mL) at different timepoints and concentrations of chlorambucil (1 and 2 μM), b) Percentage of intracellular bacterial killing in neutrophils and the c) extracellular bacterial load at 2h timepoint. Data shown is the mean with SEM (n=3), statistical analysis was performed using one-way ANOVA and Dunnett's multiple test.

Based on neutrophil cell death assay data in previous sections, ToPro-3 negativity in cells suggested that chlorambucil-treated neutrophils have more intact membrane compared to untreated neutrophils. It is possible that untreated neutrophils have compromised membrane integrity that allowed *S. aureus* escape, hence the lower intracellular *S. aureus* load. It is hypothesised that the extracellular bacterial load in chlorambucil-treated neutrophils is lower compared to untreated neutrophils. Hence the extracellular bacterial load at 2h was measured to further understand the effects of chlorambucil on neutrophil-mediated *S. aureus* killing. The measuring of extracellular bacterial load was performed in similarly as described in 3.3.4. Figure 3.26c showed the extracellular bacterial load at 2h, and one-way ANOVA test showed that there

were no significant difference in the bacterial load, suggesting that chlorambucil does not boost neutrophil-mediated *S. aureus* killing at an earlier time point.

3.4.9 Estradiol priopionate

Estradiol priopionate is an estrogen that can induce apoptosis by activating G-protein coupled receptor 30 (Yang et al., 2017). The increase of B-cell lymphoma 2 (Bcl-2) level has been associated with the use of 17-β-estradiol, contributing to proliferation of human thyroid cancer cells (Zeng et al., 2007).

Neutrophil intracellular killing assay was used to test whether neutrophil-mediated *S. aureus* killing can be enhanced by estradiol priopionate. Neutrophils were pre-incubated with estradiol priopionate at 1 and 2 μM for 1h, and co-infected with JE2 at MOI 5 for 0.5 and 3h, as described previously. One-way ANOVA test showed that there were no significant difference in percentage of intracellular bacterial killing between the media control and estradiol propionate-treated neutrophils (Figure 3.27). Additionally, an earlier time point (2h) was used to determine whether a more significant effect in neutrophil intracellular killing can be detected. Preliminary data suggested that there were no reduced intracellular bacterial load in estradiol priopionate-treated neutrophils compared to untreated neutrophil (Figure 3.28).

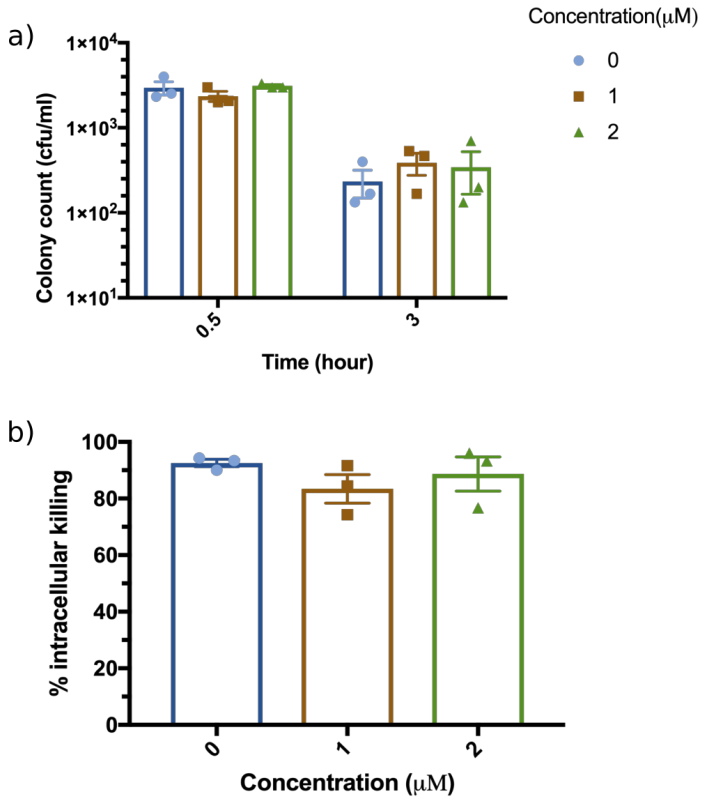

Fig. 3.27 **Neutrophil intracellular killing assay using estradiol propionate.** Neutrophils were co-infected with JE2 and MOI 5. a) The intracellular bacterial load (cfu/mL) at different timepoints and concentrations of chlorambucil (1 and 2uM) ba) Percentage of intracellular bacterial killing in neutrophil. Data shown is the Mean with SEM (n=3), statistical analysis was performed using one-way ANOVA and Dunnett's multiple test.

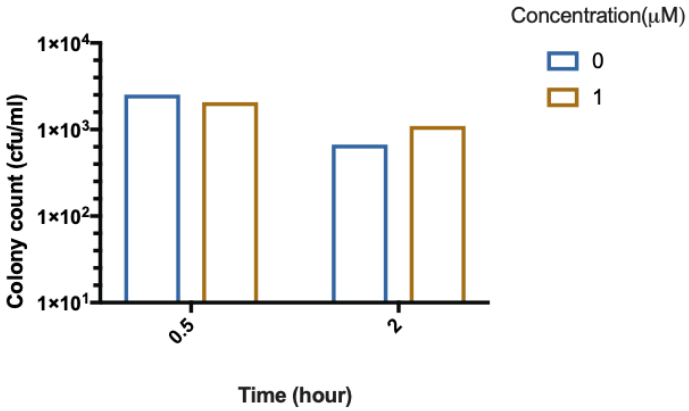

Fig. 3.28 **Neutrophil intracellular killing assay using estradiol propionate at 2h timepoint.** Data shown is the value of an independent assay (n=1).

3.4.10 Phenylmercuric acetate

Neutrophil intracellular killing assay using neutrophils pre-incubated with phenylmercuric acetate at 1 μM for 1h was used to determine whether it can promote neutrophil-mediated killing of *S. aureus*. Following the procedures described in previous sections, neutrophil intracellular killing assay was performed using MOI 5 with 0.5 and 2h time points. Paired Student's t-test showed that there were no significant differences in the intracellular bacterial load at specific timepoints, as well as the percentage of intracellular bacterial killing between phenylmercuric acetate-treated neutrophils and controls (Figure 3.29).

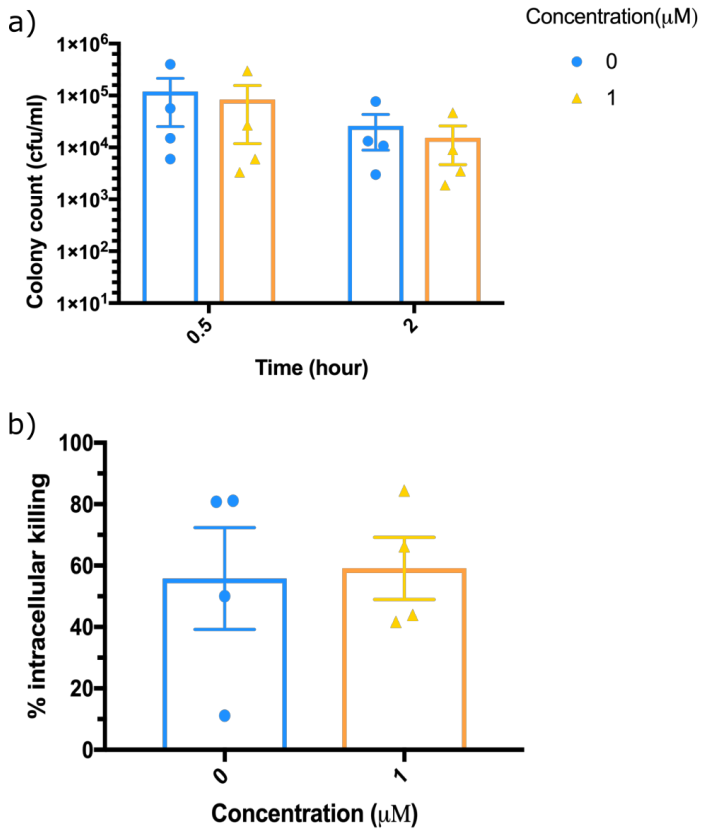

Fig. 3.29 **Phenylmercuric acetate-treated neutrophil intracellular killing assay.** Neutrophils were co-infected with JE2 and MOI 5. a) The intracellular bacterial load (cfu/mL) at different timepoints and b) Percentage of intracellular bacterial killing in neutrophils. Data shown is the mean with SEM (n=4). Statistical analysis was performed using paired Student's t-test.

3.4.11 4-aminophenylmercuric acetate (4-APMA)

Structurally related to phenylmercuric acetate, 4-APMA was included in the assays to test whether it improves neutrophil-mediated *S. aureus* killing. Matrix metalloproteases (MMPs) in eukaryotic cells is shown to be activated by 4-APMA (Rosenfeldt et al., 2005).

As the ability of 4-APMA compound to attenuate *S. aureus*-induced neutrophil cell death was not tested previously, cell death assay was performed using 2 different concentrations (1 and 2 μM) of 4-APMA. There is an increased in absolute cell

number in 4-APMA-treated neutrophils (Figure 3.30a), but minimal changes in ToPro-3 negativity when 1 μM 4-APMA was used, and decreased ToPro-3 negativity using 2 μM 4-APMA. One-way ANOVA test showed that there were no significant difference in terms of absolute cell number and ToPro-3 negativity between 4-APMA-treated and non-treated neutrophils.

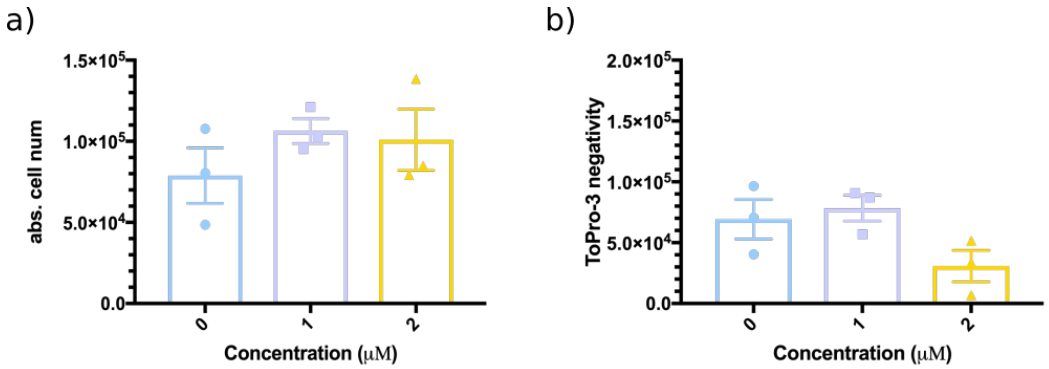

Fig. 3.30 **Neutrophil cell death assay using 4-APMA at different concentrations.** Neutrophils were pre-incubated with 4-APMA for 1h, followed by co-infection with JE2 at MOI 5 for 2h. Data shows the mean with SEM (n=3), and statistical analysis was performed using one-way ANOVA and Dunnett's multiple test.

Neutrophil intracellular killing assay using neutrophils pre-incubated with 4-APMA at 1 and 2 μM for 1h was used to determine whether 4-APMA can promote neutrophil-mediated killing of *S. aureus*. Following the procedures described previously, neutrophil intracellular killing assay was performed using MOI 5 with 0.5 and 2h time points. At 2h timepoint, there is an increased in the intracellular bacterial load in 1 μM 4-APMA-treated neutrophils compared to untreated neutrophils (Figure 3.31a), and one-way ANOVA test showed that it is statistically significant. Additionally, the percentage of intracellular bacterial killing between early (0.5h) to late (2h) timepoint decreased in 4-APMA-treated neutrophils (Figure 3.31b). Taking an independent assay as example, the intracellular bacterial killing of neutrophil media control, 1 and 2 μM 4-APMA-treated neutrophil were 90.91%, 75.84% and 72.22% respectively. One-way ANOVA test showed that the percentage of intracellular bacterial killing is significant

between control and 1 μM 4-APMA-treated neutrophil, but not significant between control and 2 μM 4-APMA-treated neutrophil. This suggests that 4-APMA does not improve, but impaired the ability of neutrophil to kill intracellular *S. aureus*.

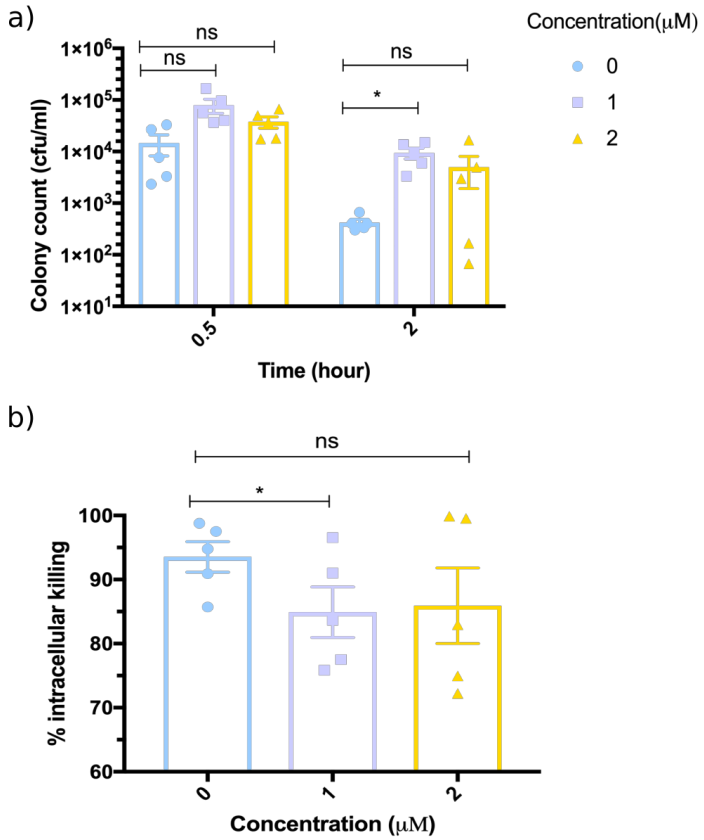

Fig. 3.31 **Neutrophil intracellular killing assay using 4-APMA.** Neutrophils were co-infected with JE2 and MOI 5. a) The intracellular bacterial load (cfu/mL) at different timepoints and b) Percentage of intracellular bacterial killing in neutrophils. Data shown is the mean with SEM (n=5). Statistical analysis was performed using one-way ANOVA and Dunnett's multiple test. Ns= not significant and *p<0.5.

3.4.12 Marimastat

Marimastat is a broad spectrum inhibitor of MMPs (Millar et al., 1998). In the previous section, it was suggested that 4-APMA impaired the ability of neutrophil to kill intracellular *S. aureus*. Following this, it was hypothesised that using an MMP

inhibitor will have an opposite effect of 4-APMA in terms of intracellular bacterial killing.

Firstly, to determine whether the marimastat contain anti-staphylococcal activity, JE2 was incubated with 5 μM of marimastat for 1h, and the bacterial count was enumerated by Miles and Misra assay as detailed in section 2.6.3. Figure 3.32 showed that marimastat does not display anti-staphylococcal activity. To ensure that marimastat does not affect neutrophil viability, different concentrations (1, 2, 5 and 10 μM) of marimastat was used to incubate with neutrophil for 2h, and the absolute cell number and ToPro-3 negativity was measured using flow cytometry. Preliminary results in Figure 3.33 showed that marimastat does not affect neutrophil viability at various concentrations.

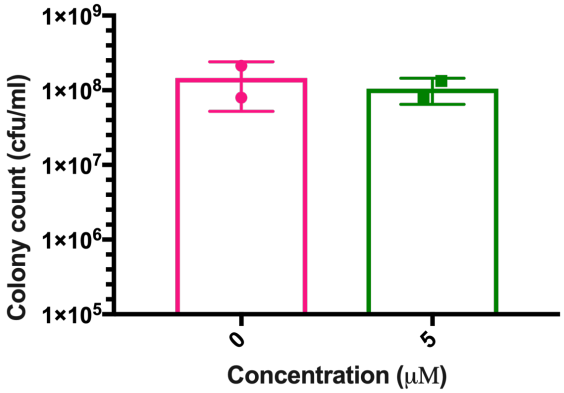

Fig. 3.32 **Marimastat do not have direct anti-staphylococcal activity.** JE2 was incubated with marimastat for 2h, followed by Miles and Misra to enumerate the colony counts. The error bars represent mean with S.D (n=2)

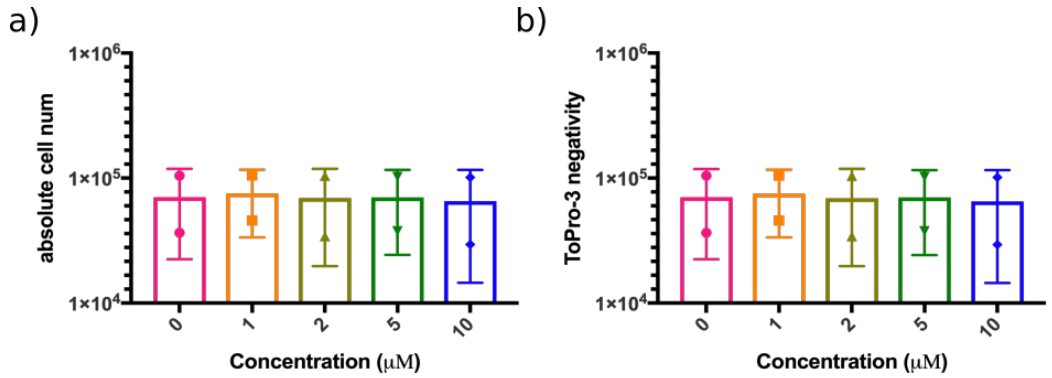

Fig. 3.33 **Marimastat neutrophil viability assay.** Neutrophil co-incubated with marimastat for 2h, followed by flow cytometry to assess viability. Error bars represent mean with S.D (n=2).

Previous section showed that 4-APMA treated neutrophil attenuated *S. aureus*-induced neutrophil cell death. To determine whether marimastat-treated neutrophil will have an opposite effect of 4-APMA, in which marimastat treatment increases *S. aureus*-induced neutrophil cell death, cell death assay was performed. Neutrophils pre-incubated with different concentrations of marimastat were co-infected with JE2 at MOI 5 for 2h, followed by flow cytometry to quantify absolute cell number and ToPro-3 negativity. Figure 3.34 showed that marimastat-treated neutrophils do not have reduced absolute cell count and ToPro-3 negativity. Furthermore, one-way ANOVA test was performed and showed that it is not statistically significant. This suggests that marimastat did not increase neutrophil cell death.

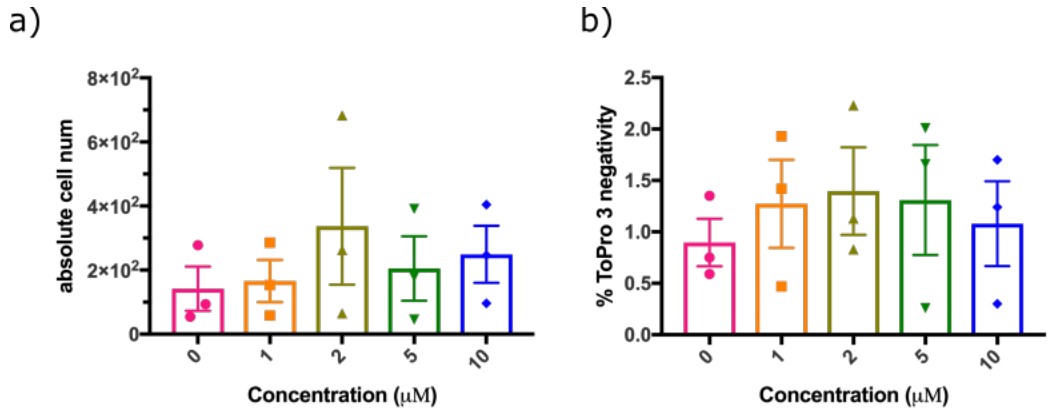

Fig. 3.34 **Neutrophil cell death assay using marimastat.** Neutrophil was co-infected with JE2 at MOI 5 for 2h, and the a) absolute cell number and b) percentage of ToPro-3 negative cells were determined. Data shown is the mean with SEM (n=3). Statistical analysis was performed using one-way ANOVA.

Neutrophil intracellular killing assay using neutrophils pre-incubated with marimastat at 1, 2 and 5 μM for 1h was used to determine whether marimastat can promote neutrophil-mediated killing of S. aureus. Following the procedures described previously, neutrophil intracellular killing assay was performed using MOI 5 with 0.5 and 2h time points. At 2h timepoint, there is an increased in the intracellular bacterial load in 2μM marimastat -treated neutrophils compared to untreated neutrophils (Figure 3.35a). However, one-way ANOVA test showed that it is not statistically significant. Additionally, the percentage of intracellular bacterial killing between early (0.5h) to late (2h) timepoint decreased in marimastat-treated neutrophils (Figure 3.35b). One-way ANOVA test showed that the percentage of intracellular bacterial killing is not significant between control and marimastat-treated neutrophil. This suggests that marimastat does not enhance neutrophil intracellular bacterial killing.

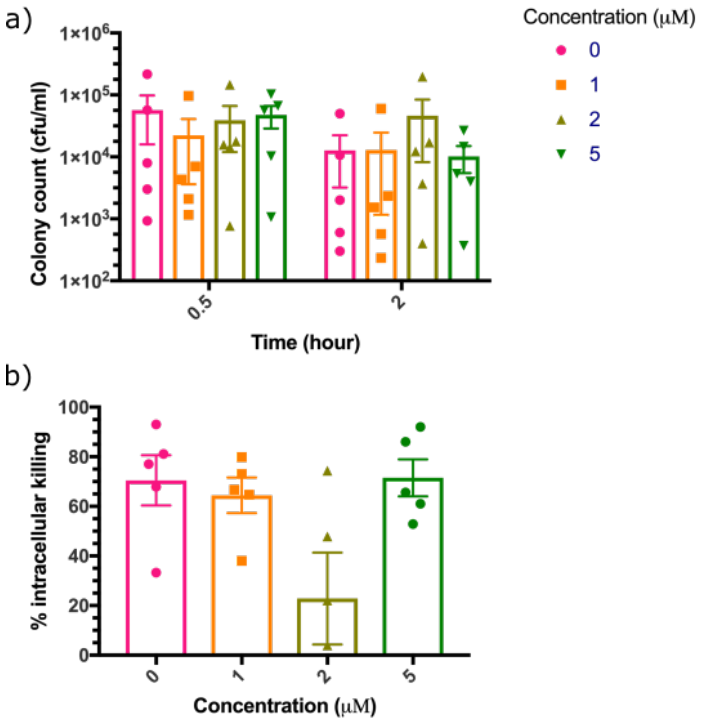

Fig. 3.35 **Neutrophil intracellular killing assay using marimastat.** Neutrophils were co-infected with JE2 and MOI 5. a) The intracellular bacterial load (cfu/mL) at different timepoints and b) Percentage of intracellular bacterial killing between 0.5 to 2h timepoints in neutrophils. Data shown is the mean with SEM (n=5). Statistical analysis was performed using one-way ANOVA test.

3.5 Discussion

The aim of this chapter was to identify compounds that can inhibit *S. aureus*-induced neutrophil cell death, and to test whether the compounds can promote the ability of neutrophil to kill *S. aureus*. This chapter showed that there is an incomplete intracellular killing of *S. aureus* in neutrophils after 3h, and JE2 caused neutrophil cell death by lysis. Candidate approaches using specific necrosis and necroptosis inhibitors does not enhance neutrophil-mediated killing of *S. aureus*. An unbiased approach in screening a subset of Spectrum compound library found that 4 compounds reduced

S. aureus-induced neutrophil cell death. Furthermore, 4-APMA and marimastat may identify a role between MMP modulation and neutrophil intracellular *S. aureus* killing.

3.5.1 Candidate approach

Our understanding of cell death induced by intracellular *S. aureus* remained incomplete. It has been shown that *S. aureus* lytic toxins such as PVL contributes to neutrophil cell death by necrosis (Genestier et al., 2005). In neutrophils, Kobayashi and colleagues have noted features of apoptosis, such as condensation of nuclei and membrane blebbing, occurring prior to neutrophil lysis. This leads to the suggestion that *S. aureus* induced neutrophil cell death by necroptosis, a programmed form of necrosis (Kobayashi et al., 2010). This observation of *S. aureus*-induced neutrophil cell death by lysis was subsequently confirmed by other studies (Greenlee-Wacker et al., 2017, 2014).

Neutrophil necroptosis involves RIPK-1, RIPK-3 and MLKL pathway (Wang et al., 2018). Kitur and colleagues used a mouse lung model to show that *S. aureus* toxins such as PVL and PSM induced neutrophil cell death by necroptosis, and using necroptosis inhibitors to block RIPK-1 and MLKL reduced neutrophil cell death (Kitur et al., 2015). In contrast, RIPK-1 and RIPK-3 inhibition in a mouse sepsis model impaired bacterial clearance (Kitur et al., 2016). Interestingly, Zhou and colleagues demonstrated that RIPK-1 was not involved in *S. aureus*-induced neutrophil cell death in mouse lung model (Zhou et al., 2018). Furthermore, Greenlee-Wacker et. al showed that RIPK-3, but not MLKL was required in *S. aureus*-induced neutrophil lysis (Greenlee-Wacker et al., 2017). Together, these studies suggested that *S. aureus*- induced neutrophil cell death could involve a novel pathway that may require RIPK-3. *S. aureus*-induced neutrophil cell death remained convoluted, and to dissect the *S. aureus*-induced neutrophil cell death pathways, four inhibitors that specifically targets necrosis and necroptosis were tested.

Neutrophil intracellular killing assays showed that the compounds Nec-1, NSA and IM-54 were unable to enhance the intracellular killing of *S. aureus* in neutrophils. Nec-1 and NSA inhibits RIPK-1 and MLKL respectively. A likely explanation for the inability of Nec-1 and NSA to improve neutrophil intracellular *S. aureus* killing could be due to the lack of RIPK-1 and MLKL involvement in *S. aureus*-induced neutrophil cell death pathways, as suggested by the works of Zhou et al. and Greenlee-Wacker et. al (Greenlee-Wacker et al., 2017; Zhou et al., 2018). It is also possible that the failure to use inhibitors to block *S. aureus*-induced neutrophil lysis is affected by the experimental conditions. For example, factors such as growth phase and media have been shown to have an effect on *S. aureus* bactericidal activity (DuMont et al., 2013; Lu et al., 2014). Moreover, *S. aureus* supernatant consists of different set of virulence factors as opposed to live bacteria (Oliveira et al., 2018; Oogai et al., 2011). Zhou and colleagues showed that *S. aureus*-induced neutrophil lysis in mice was blocked using Nec-1 and NSA, where Mueller-Hinton broth was used to grow *S. aureus*, and supernatant were used in the *S. aureus*-neutrophil lysis experiments (Zhou et al., 2018). In my experiments, *S. aureus* were grown in BHI broth, and live bacteria were used instead of supernatant. This could explain the failure to see an inhibition of neutrophil lysis using Nec-1 and NSA.

Interestingly, cell death assays showed that GSK' 872, a RIPK-3 inhibitor was able to inhibit *S. aureus*-induced neutrophil cell death. This is consistent with the work of Greenlee-Wacker and colleagues, where the authors have shown that blocking RIPK-3 decreased neutrophil cell death caused by *S. aureus* (Greenlee-Wacker et al., 2017). However, it is unknown whether there are any downstream effects, such as promotion of intracellular bacterial killing when neutrophil cell death is modified. As *S. aureus* triggers neutrophil premature cell death by lysis, it is possible that delaying neutrophil death, which prolongs the neutrophil lifespan can enhance the intracellular killing of *S.*

aureus. To address this hypothesis, neutrophil intracellular killing assay were performed at MOI of 10 using GSK' 872-treated neutrophils. Although not statistically significant, the results suggested an increase in percentage of intracellular *S. aureus* killing in GSK' 872-treated neutrophils when a late timepoint (3h) was used. This indicated that GSK' 872 may enhance the intracellular *S. aureus* killing in neutrophils. However, it is likely that significant damages, perhaps considerable membrane damage may have occurred in neutrophils at 3h, hence the minimal improvement in the percentage of intracellular *S. aureus* killing. Therefore, it was hypothesized that using an earlier timepoint (2h) in intracellular killing assay could see a larger increase in the percentage of intracellular *S. aureus* killing. However, the data does not support the hypothesis and did not show an improvement of intracellular *S. aureus* killing.

Using a candidate approach, which focused on selected inhibitors requires a priori knowledge on inhibitor functions and their relevance in cell death pathways. This approach could be powerful, provided that the *S. aureus*-induced neutrophil cell death processes are well-defined. However, the mechanisms of neutrophil cell death is highly complex, and it is insufficient to make predictions on the inhibitors based on our nascent understanding of *S. aureus*-induced neutrophil cell death pathways. Moreover, it is possible that *S. aureus*-induced neutrophil cell death involves a novel pathway, and not attributable to necrosis or necroptosis. These factors underscored the limitations of candidate approach, and highlighted the need for an unbiased approach to complement the identification of compounds to enhance intracellular *S. aureus* killing in neutrophils.

3.5.2 Unbiased approach

The aim of using an unbiased approach was to complement the candidate approach carried out previously in order to identify novel compounds that modify *S. aureus*-induced neutrophil cell death and boost the intracellular *S. aureus* killing in neutrophils.

This approach could benefit on two levels, where it could reveal novel pathways that underlies *S. aureus*-induced neutrophil cell death, and potentially identify new therapeutics for *S. aureus* infections. The optimal MOI and co-infection time of *S. aureus* and neutrophils was MOI of 5 and 2h respectively, and the cell death variation across a 96-well plate was minimal. The screen design was well-optimised to carry out the library screen.

Thirty one compounds were identified by screening 800 out of 2000 compounds in the Spectrum library. This included 23 compounds with known anti-staphylococcal activities. Eight compounds with no defined anti-staphylococcal activities were brought forward for a second round screen, which involves rescreening using the same method as 1st round, using neutrophils from 3 independent donors (n=3). Three compounds from Spectrum library: chlorambucil, 17-B-estradiol and phenylmercuric acetate, with addition of a phenylmercuric acetate structural-related compound, 4-APMA, were focused on for further investigations. These compounds were confirmed to have no direct anti-staphylococcal activities, validating that the reduced *S. aureus*-induced neutrophil cell death were not due to the killing of *S. aureus* by compounds before the bacteria are phagocytosed by neutrophils. Additionally, it was shown that the compounds are non-toxic and does not affect neutrophil viability. These results suggested that the compounds could possibly modify *S. aureus*-induced neutrophil cell death.

Unlike necrosis, a catastrophic form of cell death that exacerbates inflammation, apoptosis is a form of programmed cell death in which neutrophils remained intact to prevent spillage of granule enzymes (Savill et al., 1989). Phagocytosis-induced cell death (PICD) is a form of apoptosis in neutrophils that contains dead or partially dead microbes. PICD prevents spillage of cytotoxic components, thus facilitates tissue clearance and resolution of infections (Kennedy and DeLeo, 2009). Various intracellular pathogens, including *Coxiella burnetii* and *Neisseria gonorrhoeae* have been shown to

circumvent apoptosis to enable its survival and replication within neutrophils (Cherla et al., 2018; Kennedy and DeLeo, 2009; Simons et al., 2006). Our understanding of *S. aureus* engaging neutrophil apoptosis remained inconsistent. Kobayashi and colleagues observed that, characteristics of neutrophil apoptosis such as membrane blebbing and nuclei condensation occurred prior to neutrophil lysis (Kobayashi et al., 2010). Moreover, within 3h of *S. aureus* phagocytosis, elevated phosphatidylserine (PS) levels and reduction in mitochondrial membrane potential, both features of apoptosis were observed by Greenlee-Wacker and colleagues (Greenlee-Wacker et al., 2014). However, this was complicated by the observation of high CD47 level, a "don't eat me" signal that is usually depleted in apoptotic cells. Therefore, whether *S. aureus* induced neutrophil death by apoptosis remained controversial.

IL-8 is a chemokine that prevents neutrophil apoptosis by activating NF-kb and anti-apoptotic factors such as Mcl-1 (Sarkar et al., 2012). It has been shown that *S. aureus* reduced neutrophil IL-8 production using its two-component SaeR/S system, leading to cell death. Additionally, blocking IL-8 reduced bacterial clearance by neutrophils (Zurek et al., 2015). Chlorambucil and estradiol propionate are compounds from the screen that plays a role in apoptosis. Chlorambucil is reported to promote apoptosis by accumulating cytosolic p53 protein, leading to Bcl-2 associated X protein activation (Di Antonio et al., 2014; Steele et al., 2008). Activation of G-protein coupled receptor 30 by estradiol propionate have been shown to induce apoptosis (Yang et al., 2017). Furthermore, estradiol propionate is shown to associate with upregulating Bcl-2, which prevents apoptosis in human thyroid cancer cells (Zeng et al., 2007). Using a late timepoint (3h) in neutrophil intracellular killing assay, chlorambucil-treated neutrophils showed minimal increase in terms of the percentage of intracellular *S. aureus* killing. It is speculated that an earlier timepoint will see more profound effects in neutrophil intracellular bacterial killing, but this was not supported by the results.

Likewise, estradiol propionate treatment have minimal impact on the percentage of neutrophil intracellular *S. aureus* killing at 3h. This showed that chlorambucil and estradiol propionate were able to preserve neutrophil viability, but unable to improve intracellular *S. aureus* killing.

Neutrophils treated with phenylmercuric acetate have shown reduced *S. aureus*-induced neutrophil cell death, but there were minimal improvement in intracellular bacterial killing. Interestingly, 4-APMA-treatment compromised neutrophil intracellular *S. aureus* killing abilities. Activation of MMPs by 4-APMA in eukaryotic cells have been demonstrated (Rosenfeldt et al., 2005). MMPs are a collection of endopeptidases with a broad range of roles, including in chemotaxis and antimicrobial (Smigiel and Parks, 2017). Matrix metalloproteases have key roles in neutrophil-*S. aureus* interactions, where they facilitate neutrophil transmigration (Delclaux et al., 1996). For example, neutrophil chemoattractants such as CXCL5 and CXCL8 are upregulated by MMP- 8, 9 and 13, thus enabling neutrophil recruitment to inflammation site (Chakrabarti, 2005; Lin et al., 2008; Tester et al., 2007). Additionally, MMP-2 and MMP-9 have been shown to activate IL-1B, a cytokine critical in establishing neutrophil response against *S. aureus* (Cho et al., 2012; Schönbeck et al., 1998). Neutrophil MMPs are actively targeted by *S. aureus* toxins. For example, SSL1 and SSL5 toxins are broad range MMP inhibitors, and these toxins inhibited MMP-8 and MMP-9, blocking neutrophil migration (Itoh et al., 2010; Koymans et al., 2016). Neutrophils are only activated upon *S. aureus* infection. It is likely that pre-incubating neutrophils with 4-APMA prior *S. aureus* co-infection lead to neutrophil activation, thus reducing neutrophil intracellular *S. aureus* killing ability. It is unclear whether 4-APMA activates a specific MMP. Therefore, marimastat, a broad spectrum MMP inhibitor was used to test whether an opposite effect can be observed.

Marimastat is an anticancer compound, and it mimics MMP zinc substrate and prevents their binding to MMPs, thus preventing MMPs degradation of basal membranes (Rempel and Mikkelsen, 2006). Marimastat have been shown to reduce lung inflammation caused by *Pseudomonas aeruginosa* infections in cystic fibrosis patients (Sandri et al., 2018). However, there are no studies using marimastat in *S. aureus* infections treatments. Marimastat treatment did not improve neutrophil intracellular *S. aureus* killing abilities, suggesting that marimastat treatment do not have an opposite effect to neutrophils treated with 4-APMA. This also suggests that inhibiting MMPs does not improve neutrophil intracellular *S. aureus* killing.

Interestingly, neutrophil intracellular killing assay data suggested that using 2 μM of marimastat impaired the ability of neutrophils to kill intracellular *S. aureus*, an effect that was seen when neutrophils were treated with 4-APMA. Both 4-APMA and marimastat affects MMP activity, and these data suggests that activating and inhibiting MMP activities can impair neutrophil intracellular bacterial killing ability. It is unknown which MMP was specifically activated by 4-APMA, or inhibited by marimastat, leading to a reduction in neutrophil intracellular *S. aureus* killing abilities. Therefore, to dissect the relationship between specific MMPs activities and neutrophil intracellular killing, future work could include experiments to identify which MMP was upregulated or downregulated by 4-APMA and marimastat using techniques such as enzyme-linked immunosorbent assay (ELISA). Once particular MMP activities have been established, it can be further investigated using specific MMP activators or inhibitors to determine whether it can enhance neutrophil intracellular *S. aureus* killing.

3.5.3 Limitations and future work

In this work, Miles and Misra technique was used in the intracellular bacterial killing assay to measure the number of *S. aureus* that survive within neutrophils. This is a limitation in this work, as this technique is known to lack in sensitivity, for example, due the variability in diluting the bacterial lysates in selected timepoints. Additionally, this assay relies on the insusceptibility of bacteria to gentamicin killing, as well as the inability of gentamicin to permeate through neutrophil membrane (Edwards and Massey, 2011). Early optimisation assays in this chapter have shown that gentamicin does not affect the intracellular bacterial viability, even at the 3h timepoint. However, subsequent neutrophil cell death assay data suggests that *S. aureus* JE2 strain induced neutrophil cell death by lysis, indicating that gentamicin could permeate through the damaged neutrophil membrane. However, the intracellular bacteria remained viable, thus suggesting that JE2 is not susceptible to gentamicin killing. An alternative approach to investigate the survival of intracellular bacteria within neutrophils is by using the LIVE/DEAD bacterial viability kit, and to enumerate the number of live and dead intracellular bacteria using fluorescence microscopy (Johnson and Criss, 2013). This assay will provide a sensitive way to complement the intracellular bacterial killing assay in order to determine the intracellular bacterial survival.

In the candidate approach, only 4 compounds (Nec-1, NSA, IM-54 and GSK 872) were chosen for investigation based on the literature. This is a limitation in the study, as it did not include the analogs of selected compounds, which have been shown to have reduced off-target effects. An example is Nec-1s, a more specific analog of Nec-1, which have also shown to attenuate *S. aureus*-induced neutrophil cell death (Greenlee-Wacker et al., 2017). Furthermore, analogs of GSK'872, including GSK' 840 and GSK' 843, in which GSK'843 have been shown alongside GSK'872 to reduce *S. aureus*-induced neutrophil cell death, were not used in this work due to time constraint (Greenlee-

Wacker et al., 2017; Kaiser et al., 2013; Mandal et al., 2014). The effect of compounds on neutrophil viability is dose-dependent, and in this work, the concentration of IM-54 used was based on the doses that were shown to be effective in neutrophil-like HL-60 cells (Sodeoka and Dodo, 2010). However, this concentration could be variable in human neutrophils, and the concentrations that are effective on HL-60 cells may not be transferrable to neutrophils studies. Therefore, a dose-dependent curve in IM-54 could be performed to identify the concentration range that is most suitable for human neutrophil studies.

Alternative assays to detect cell toxicity, such as lactate dehydrogenase (LDH) cytotoxicity assay can be used to complement the flow cytometry assay using ToPro-3 in this work, which will enable the fast measurement of neutrophil viability. One limitation of both candidate approach and compound library screen was to detect neutrophil cell death using ToPro-3 dye as an indicator. However, it is unclear which form of cell death was modified by the compounds using ToPro-3. This can be further examine by supplementing the neutrophil cell death assays with apoptosis indicators such as Annexin V and Propidium iodide dyes in flow cytometry. In the compound screen, individual plates were screened twice using neutrophils from two different donors, and a compound was selected for a second round screen, only if it is presented as a 'hit' in the duplicated screen. This replicated screen introduced variations, such as experimental conditions, and the variability of neutrophils between donors. Therefore, this approach could potentially lead to the exclusion of compounds that may have an effect in improving neutrophil viability, but were not brought forward for second round screen as it does not qualify as 'hit'. Alternatively, an initial screen is performed once, followed by a more robust second-round screen to reduce the false-negativity in this screening approach.

The effect of marimastat and 4-APMA on neutrophil-*S. aureus* interaction will be further investigated by fluorescence microscopy techniques developed in chapter 4, where features such as neutrophil membrane damage and intracellular bacterial count can be validated at high resolution in live cells using a multimodal imaging platform. Ilomastat, an analog of marimastat, have been shown to block *Pseudomonas aeruginosa* elastase activity (Grobelny et al., 1992). This effect on *P. aeruginosa* protease activity was also confirmed using marimastat (Sandri et al., 2018). However, this effect has not been described in *S. aureus*, and it is possible that marimastat inhibits *S. aureus* protease activity, leading to better intracellular *S. aureus* killing by neutrophils. ELISA can be performed to determine whether marimastat inhibits *S. aureus* protease activities.

In vivo models, for example zebrafish, can be used to further explore the roles of MMP modulators such as 4-APMA and marimastat in neutrophil and *S. aureus* interactions. In terms of functionality and morphology, zebrafish neutrophils showed high level of similarities with human neutrophils (Lieschke et al., 2001). Moreover, understanding *S. aureus* pathogenesis using zebrafish embryo model have been established previously (Prajsnar et al., 2008, 2012). Optical transparency, as well as the ability to genetically modify zebrafish embryo makes it an attractive model for *S. aureus*-neutrophil interactions (Henry et al., 2013). In addition to understanding neutrophil intracellular *S. aureus* killing, effects of 4-APMA and marimastat on neutrophil chemotaxis and inflammation can also be studied by fluorescence microscopy using zebrafish embryo model.

Chapter 4

Development of live imaging techniques to visualise human immune cells and *S.aureus* interactions

4.1 Introduction

Human neutrophils are key immune cells to defend against *S. aureus* infections. The relatively small size of neutrophils ($\approx 10\mu$m), in addition to their short lifespan are among the challenges to visualise them by live microscopy (Allen, 2014; McCracken and Allen, 2014). A vital component as part of neutrophilic antimicrobial response against *S. aureus* is the production of reactive oxygen species (ROS). Following the phagocytosis of *S. aureus*, oxidative burst occurs in neutrophils, leading to the ROS generation by NADPH oxidase complex, which further activates neutrophil proteases that are essential in *S. aureus* killing (Nguyen et al., 2017). Besides *S. aureus*, ROS production can be

induced by illumination (Winterbourn et al., 2016). In live microscopy experiments, ROS generation is a major source of phototoxicity (Nguyen et al., 2017). Therefore, the illumination power used to visualise live neutrophils must be kept minimal (<10 mW) to reduce excessive ROS production and phototoxicity effects (Ettinger and Wittmann, 2014). Furthermore, neutrophils are non-adherent in unstimulated state, and it is important to keep neutrophils unstimulated prior the addition of bacteria in order to fully understand the mechanisms of neutrophil-mediated killing (Iba et al., 2013; Mayadas et al., 2014). The combination of all these factors make live imaging of neutrophils highly difficult, as minimal light invasion is required to reduce various confounding effects. High-resolution live imaging of neutrophil-like cell lines HL-60 and zebrafish neutrophils have been visualised using modalities such as lattice lightsheet and structured-illumination (Chen et al., 2014; Liu et al., 2018). However, there are no studies on live imaging of human neutrophils at high resolution at the time of this project. The aim of this chapter is to identify the most suitable microscopy technique to perform long term live imaging of neutrophils at highest resolution possible. To achieve this, samples were visualised with three different imaging modalities: widefield, confocal and structured illumination microscopy.

4.2 Materials and methods

4.2.1 Sample preparation using *S. aureus*-neutrophil co-culture

Freshly-isolated neutrophils as described in section 2.6.2 were added to 96-well plates. The volume in each well is fixed at 90μl by adding appropriate volume of RPMI (+10% (v/v) FBS), followed by incubation in 37°C with 5% CO_2. Frozen bacterial aliquots were thawed in room temperature and centrifuged at 6000 rcf for 7 minutes. The supernatant was removed and pellet was resuspended in appropriate volume of fresh

RPMI 1640 such that adding 10μl of bacterial suspension to neutrophils leads to MOI of 1, 5 and 10 respectively. This is followed by incubation in 37°C with 5% CO_2 for 30 and 60 mins. The samples were transferred to glass slides by centrifuging at 300 rcf for 2 mins in Cytospin4 centrifuge, and left to dry in RT. The slides were stained with DAPI with ProLong AntiFade Diamond Mountant (Cat no. P36931, Invitrogen, Paisley, U.K) before adding a coverslip, and the samples were left to incubate in the dark at RT overnight until imaging.

4.2.2 Imaging using hMDMs

HMDMs grown for 9-14 days were used for live cell imaging. One day prior imaging, cells were seeded into a high 35mm μ-dish with ibiTreat #1.5 polymer coverslip (ibidi, Martinsried, Germany). To detach cells from 6-well plates, media were discarded from wells and the cells were washed with 1X PBS for 3 times. This is followed by adding 750μl Accutase™ cell detachment solution (StemCell technologies, Cambridge, U.K) and left to incubate for 20 mins. After 20 mins, the cells were detached physically using a cell scraper, and collected into a 15ml Falcon tube. Complete RPMI 1640 was added such that the final volume is 5ml. The cells were centrifuged at 1500rpm for 6 minutes at 20°C. The pellet was resuspended in 1ml of complete RPMI, and cell count was performed using a haemocytometer. The hMDMs were seeded at 1 X 10^6 cells/ well in 35mm μ-dish, and incubated at 37°C with 5% CO_2. As complete RPMI 1640 was supplemented with 1% (v/v) P/S to prevent bacterial contamination, it is important to replace the media with RPMI free of P/S prior to *S. aureus* co-culture. Complete RPMI 1640 media was removed and the cells were washed 3 times with 1ml 1XPBS. This is replaced by phenol red-free RPMI 1640 supplemented with 10% (v/v) FBS and 25mM HEPES solution (Sigma Aldrich, Dorset, U.K) to buffer the pH in the solution.

4.2.3 Nile red staining

Nile red (ACROS organics, Geel, Belgium) was used to stain lipid droplets in plasma membrane of hMDMs and neutrophils. A working solution of 300 μM was reconstituted using PBS. Media from wells were discarded and the cells were washed with PBS for three times. This is followed by incubating cells in serum-free RPMI 1640 with fresh working solution for 15 mins in dark. After 15 mins of incubation, the media was discarded and cells were washed with PBS for three times, and replaced with fresh phenol-red free RPMI 1640 for live imaging experiments.

4.2.4 CellMask Deep Red stain

CellMask™ Deep Red plasma membrane stain (#C10046, Thermo Fisher, U.K) was used in hMDMs and neutrophils plasma membrane staining. Deep Red was freshly prepared for each use, and cells were incubated with 10 μg/ml of Deep Red stain in phenol-red free RPMI 1640 (+10% FBS) media for 20 mins in dark. After 20 mins, the media was discarded and cells were washed twice with PBS, followed by replacing with fresh phenol-red free RPMI 1640 (+10% (v/v) FBS) media, supplemented with 25mM HEPES solution.

4.2.5 Phase contrast microscopy

A Nikon TiE inverted microscope with temperature controlled stage was used for live cell imaging. Live cells were visualized every 10 min for the duration of 10-20 hours with an Andor iXon Ultra 897 EMCCD detector (Andor Technology, Belfast, U.K) and Apo Phase 60x/ 1.4 numerical aperture phase objective.

4.2.6 Widefield fluorescence microscopy

To visualise neutrophil phagocytosis of SJF4622, the samples were prepared as described in section 4.2.1. Widefield fluorescence microscopy was performed on Leica AF6000 inverted widefield fluorescence microscope in the Wolfson light microscopy core facility, University of Sheffield. The images were acquired using 100x/ 1.4 numerical aperture oil immersion lens and mercury lamp excitation, with A4 filter for DAPI and Y3 filter for mCherry.

For live cell imaging experiments, SJF4622 was added to hMDM co-culture as described previously in section 2.9, and the samples for live cell imaging were prepared as described in section 4.2.2. Widefield fluorescence microscopy was performed on the Nikon inverted Ti eclipse system in the Wolfson Light Microscopy facility. The system was equipped with temperature-controlled stage set to 37°C for live cell imaging. Cells were visualized every 10 min for the duration of 4 hours with Andor Zyla sCMOS detector and Apo 60x, 1.4 numerical aperture oil objective.

4.2.7 Super-resolution radial fluctuation (SRRF)

SRRF was carried out on a Nikon TiE inverted microscope and Andor iXon Ultra 897 EMCCD detector. To obtain a SRRF image, 19 frames were acquired with 488nm laser excitation and Texas Red filter set at 500 ms exposure time. The images were processed using NanoJ-SRRF plugin in ImageJ. SRRF analysis grouped 19 frames to generate 1 f.p.s super-resolution frame rates.

4.2.8 Confocal laser scanning microscopy with Airyscan

HMDMs differentiated to 10 days on coverslip in 6-well plate were used as samples for confocal laser scanning microscopy. The hMDMs were co-infected with SJF4622

at MOI of 5 for 1h, followed by removing the media and washed with 1X PBS for 3 times. Using a pair of tweezers, the coverslip was removed from 6-well plate and mounted with Vectashield Antifade mounting media (Cat. No H-1000-10, Vector Laboratories, Peterborough, U.K). The coverslip was sealed on the glass slide with nail polish. Imaging was performed using a confocal laser scanning microscope Zeiss LSM 880 system equipped with AiryScan detection unit in the Wolfson Light Microscopy facility. The image was acquired using Plan-Apochromat 63x, 1.4 numerical aperture oil objective and 488/561nm argon laser excitation. The images were acquired with 20 z-planes and saved as .czi format. The acquired datasets were processed using Zen 2.3 SP1 Black software.

4.2.9 Structured illumination microscopy (SIM)

Uninfected day 8 hMDMs were used as samples for SIM. The cells were stained with DAPI with ProLong AntiFade Diamond Mountant for super resolution imaging using SIM set up on a DeltaVision/GE OMX v4 optical microscope in the Wolfson Light Microscopy facility (University of Sheffield, U.K). The image was acquired on the set up using 60x, 1.42 numerical aperture oil objective, 436/31 filterset for DAPI and 405nm laser excitation, with 3 angles and 5 phases. The images were reconstructed using fairSIM plugin on ImageJ.

4.2.10 Confocal microscopy using Cairnfocal system

Freshly isolated neutrophil samples were co-cultured with GFP-SH1000 at MOI 10 for 30 minutes as mentioned previously in section 4.2.1. CellMask™ Deep Red stain was used to label plasma membrane according to the protocol in section 4.2.4, and the samples were transferred to coverslips by cytospinning at 300 rcf for 2 mins in a Cytospin4 centrifuge. The samples were fixed using 4% PFA pre-warmed in 37°C for

10 mins, followed by washing with PBS for three times. The samples were left to dry before adding DAPI with ProLong AntiFade Diamond Mountant. The samples were sealed with nail polish and left in RT in dark for overnight incubation. The samples that were not imaged immediately were stored in dark in 4°C for up to 1 month.

4.2.11 Structured-illumination live imaging

Freshly isolated neutrophils were pre-incubated on a 96-well plate for 1h at 37°C with 5% CO_2. This was followed by co-infection with GFP-labelled SH1000 *S. aureus* strain at MOI of 5. After 10 mins of co-infection, 10 μg/ml of fresh CellMask™ Deep Red Membrane label were added to cells, and the cells were incubated in dark for another 20 mins. After 30 mins of co-infection time, cells were gently aspirated and transferred to an Eppendorf tube. The cells were spun at 0.4 rcf for 3 mins, and the supernatant was discarded. The remaining pellet was resuspended with fresh phenol-red free RPMI 1640 (+10% FBS) media supplemented with 25mM HEPES solution, and seeded onto a 35mm imaging dish.

4.3 Results

4.3.1 Establishing a suitable imaging technique and experimental conditions

Samples using immune cells in this thesis were obtained from healthy volunteers according to the procedures and ethics in section 2.6.1. In addition to neutrophils, human monocyte-derived macrophages (hMDMs) are another population of cells isolated from blood (Daigneault et al., 2010). Like neutrophils, macrophages are also professional phagocytes that play a key role in controlling *S. aureus* infections (Kubica et al., 2008). Unlike neutrophils, which are cells that are easily stimulated upon

isolation, hMDMs are more resilient. Additionally, hMDMs have a longer lifespan and they are adherent cells that can be cultured on coverslips. Therefore, samples used at the beginning of this thesis in both live and fixed imaging were prepared using hMDMs instead of neutrophils, as the use of hMDMs simplifies the initial live imaging set up and optimisations.

4.3.2 Widefield microscopy to visualise hMDMs-*S. aureus*

One of the ways to label specific cell structure is by genetically encoding fluorescence tag to render it fluorescent. However, genetic modifications of primary human immune cells such as neutrophils and macrophages are not always possible (Progatzky et al., 2013). Macrophages are highly autofluorescent cells (Njoroge et al., 2001). Therefore, samples in initial experiments were prepared using hMDMs that were not fluorescently labelled.

To determine whether widefield microscopy can be used to visualise subcellular structure of macrophages containing *S. aureus*, samples were prepared as detailed in section 4.2.2, using unlabelled hMDM co-infected with mCherry (Em 560nm)-labelled *S. aureus* (SJF4622 strain). The samples were visualised on Nikon dual cam system using LED illumination for simultaneous red and green imaging. Signals of hMDMs were observed in both red and green channels (Figure 4.1), suggesting that may be due to light leaking from filters. However, mCherry- *S. aureus* (strain SJF4622) was observed in red channel only (white arrows, Figure 4.1), and not in green channel. Therefore, it is possible that the presence of hMDMs signals were due to autofluorescence from hMDMs. Imaging with samples fixed at a single timepoint is unable to reveal the dynamics between *S. aureus* and hMDMs, therefore live imaging is required for further investigations.

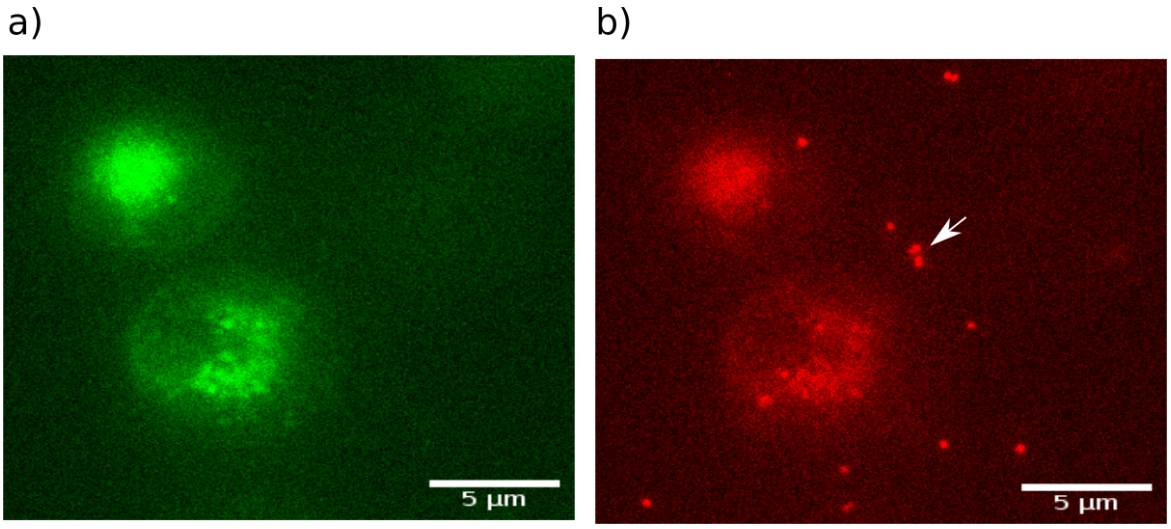

Fig. 4.1 **Visualisation of hMDMs-SJF4622 using widefield fluorescence microscopy.** Unlabelled hMDMs were co-infected with an mCherry-labelled *S. aureus* at MOI 5, and autofluorescence of hMDMs seen in green (FITC filter) channel (a). When hMDMs-*S. aureus* is visualised in red (TexasRed filter) channel, both autofluorescence from hMDMs and mCherry-labelled *S. aureus* (white arrows) were observed (b). The images were acquired on Nikon dual cam inverted Ti eclipse system in the Wolfson Light Microscopy facility, using 60x, 1.4 N.A oil objective.

4.3.3 Live imaging using widefield microscopy

In the previous section, fixed samples were used for imaging, but there is a limitation in terms of the number of time points used in sample preparation. Live imaging is required in order to better understand the dynamics and interactions between *S. aureus* and immune cells such as neutrophils and macrophages. Unlike imaging with fixed samples, live imaging brought a different set of challenges. For example, hMDMs are typically cultured and maintained in 37°C with 5% CO_2 incubator. Therefore, the imaging system needs to be equipped with appropriate conditions to be able to perform live imaging using hMDMs. However, the widefield microscopy system available was equipped with an incubator for temperature control but not CO_2. Therefore, it is important to assess whether hMDMs can tolerate live cell imaging under these conditions.

Firstly, hMDM live cell imaging sample was prepared as described in section 4.2.2, and 25mM HEPES was added to the media to buffer the pH in the absence of CO_2. Images from the start and end of the time-lapse imaging experiment were shown in Figure 4.2a, and the morphology of hMDMs were used to assess the hMDMs viability. The morphology of hMDMs remained largely unchanged, thus suggesting that the hMDMs remain alive under these experimental conditions (Figure 4.2b).

A key advantage of widefield microscopy is the flexibility, and it allows fast and gentle live imaging to be performed. To determine whether the interaction of hMDMs and *S. aureus* can be visualised by widefield microscopy, samples of hMDMs co-infected with *S. aureus* at multiplicity of infection (MOI) of 5 were used in live cell imaging experiment. The outline of hMDMs membrane and cytoplasm were observed (Figure 4.2c), indicated that the cells are alive and healthy. This is followed by co-infecting with *S. aureus*, and after 1h of infection, *S. aureus* interacting with hMDMs were observed (Figure 4.2d). After 4h, the number of *S. aureus* have increased and mainly surrounding the hMDMs. Furthermore, the morphology of hMDMs have changed, losing the distinct membrane outline that was observed earlier in the experiment (Figure 4.2e). As the lack of CO_2 system can be overcome by supplementing 25mM HEPES to the RPMI 1640 culture media, shown earlier in Figure 4.2a,b, it excluded the possibility that the health of hMDMs after 4h were compromised due to inadequate culture conditions.

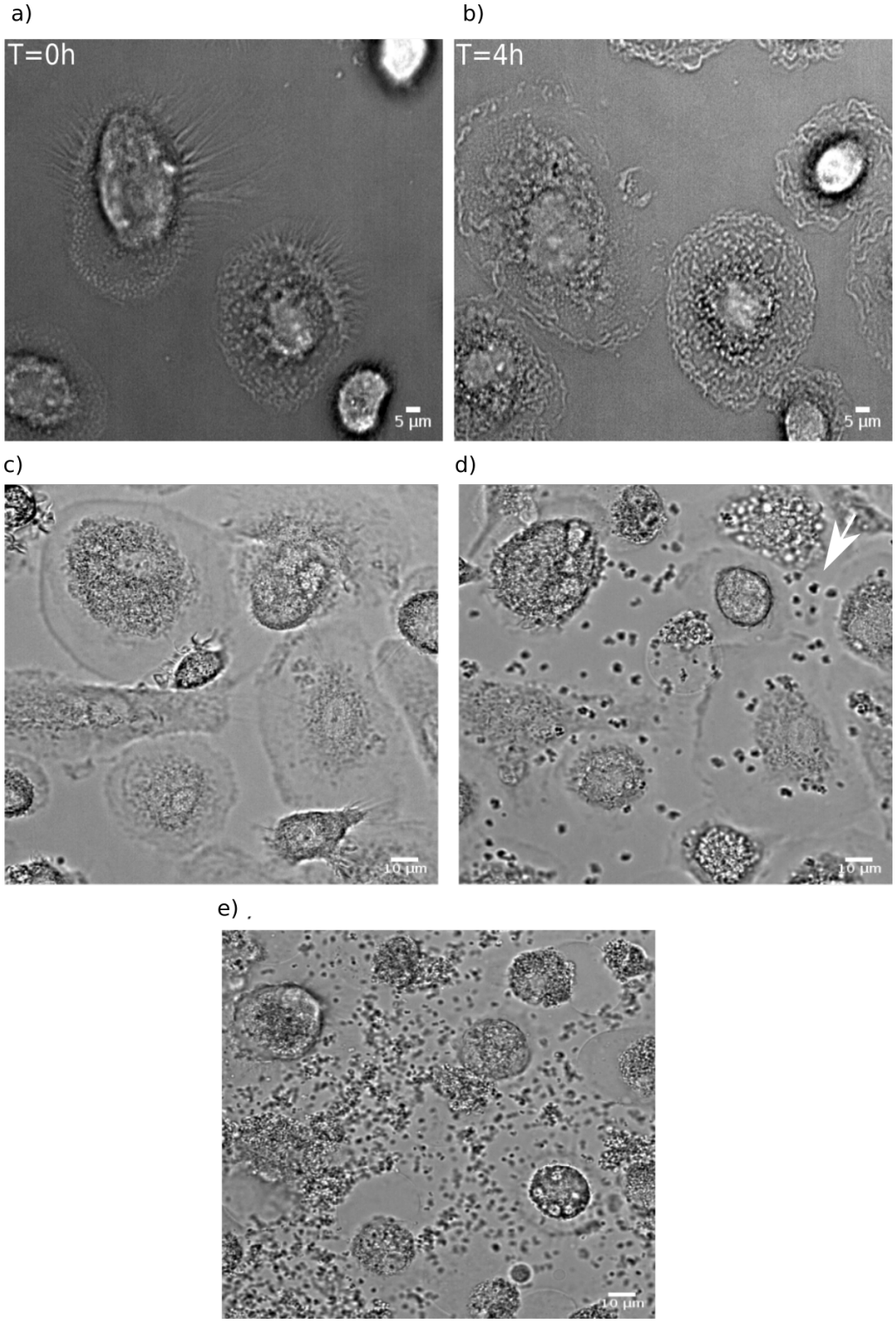

Fig. 4.2 **Time-lapse imaging of hMDMs and *S. aureus*.** Live imaging of uninfected hMDMs imaged without CO_2 at the a) T=0 h and b) T= 4 h. In live imaging of hMDMs and *S. aureus*, no *S. aureus* were observed at the start (T=0 h) of experiment (c), followed by observation of hMDMs phagocytosed *S. aureus* after 1h (d), and *S. aureus* surrounding hMDMs after 4h of time-lapse imaging (e). The morphology of hMDMs remained largely unchange after long-term live imaging, suggesting that they are alive under the experimental conditions without CO_2. Time-lapse imaging was performed by acquiring images every 10 min for 4 hours on Nikon inverted Ti eclipse system in the Wolfson Light Microscopy facility, using 60x, 1.4 N.A oil objective.

4.3.4 Fluorescence live imaging

Microscopy is an indispensable tool in biological investigations. In particular, fluorescence microscopy have the advantage over other light microscopy techniques such as phase-contrast microscopy, as fluorescence microscopy enables tracking of specific processes or protein by labelling them with fluorescent labels. Moreover, simultaneous visualisation of multiple components and biological interactions are made possible with access to a spectral range of fluorescent labels (Lichtman and Conchello, 2005).

As shown in previous section, hMDMs can be maintained for live imaging on the set up using 37°C without 5% CO_2, and 25mM HEPES was used to buffer the pH of media. Live imaging of label-free hMDMs and *S. aureus* were performed using widefield microscopy previously. However, to be able to visualise the bacterial localisation within cell, as well as to determine whether bacteria interacts with specific cell structures, fluorescently-labelled bacterial is needed for live imaging.

Live imaging was performed on label-free hMDMs co-infected with mCherry-labelled *S. aureus* at MOI of 5. Samples were imaged under 37°C conditions and the cell culture was buffered with 25mM HEPES, with images acquired at every 10 min overnight. Phase contrast microscopy, which gives a better contrast of cell outline and position compared to brightfield microscopy was used to visualise hMDMs at the start of experiment. The phase contrast and widefield images were overlaid to produce the series as seen in Figure 4.3. At the end of the time-lapse imaging (Figure 4.3c), the field of view was populated with red fluorescent signals, indicating that mCherry-labelled *S. aureus* have replicated over time.

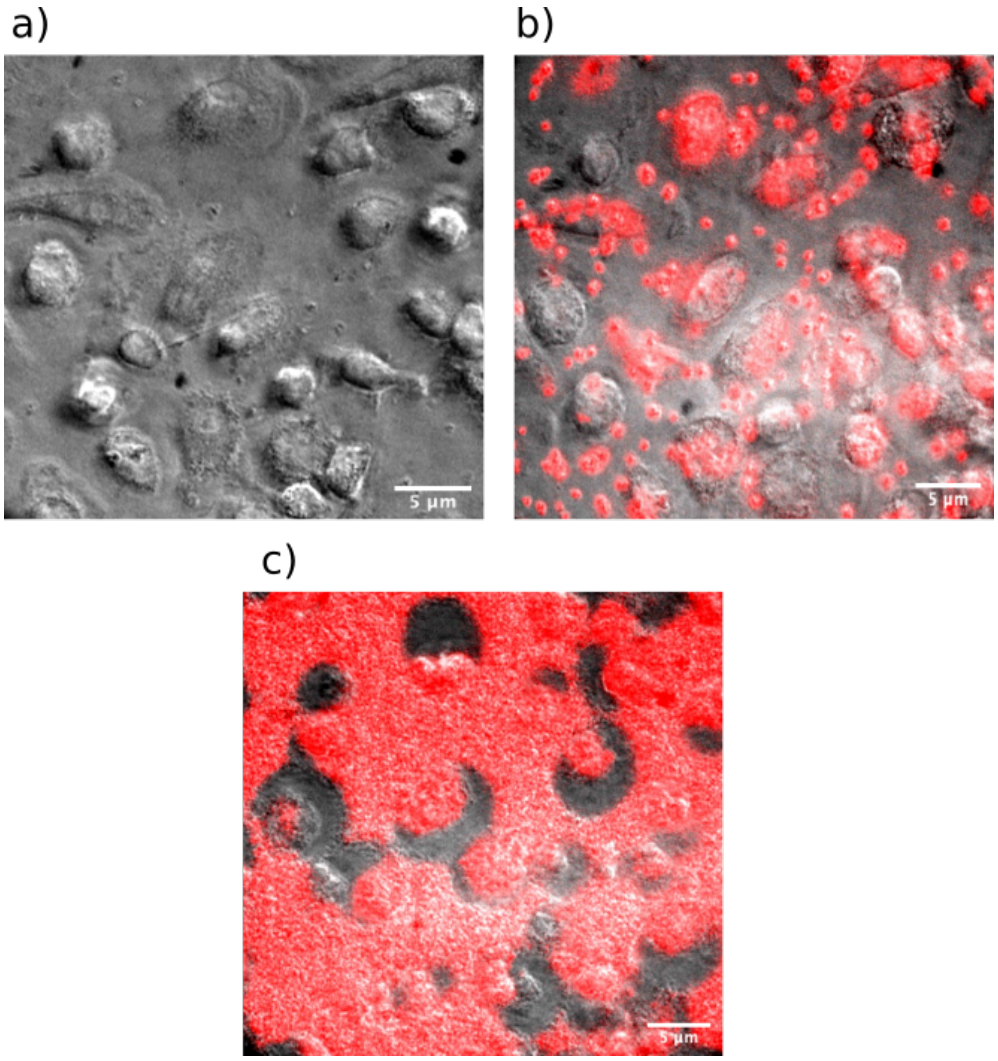

Fig. 4.3 **Live imaging of hMDMs and mCherry-labelled *S. aureus*.** hMDMs were co-infected with mCherry-labelled *S. aureus* at MOI of 5 for live imaging. a) The outline and position of hMDMs were observed at the start of time-lapse imaging (T=0h). b) hMDMs phagocytosed *S. aureus* (red fluorescence signals) after 1.5h. c) Large number of *S. aureus* surrounding hMDMs after 12h of overnight time-lapse imaging.

As the goal was to determine whether it is possible to perform live imaging on human immune cells at high resolution, computational-based super resolution microscopy was used to determine whether image of higher resolution can be acquired. Super-resolution radial fluctuations (SRRF) is a software approach to acquire super-resolution images from widefield microscopy. This method does not require complicated optical set

up and high laser power, thus suitable for long term live imaging (Gustafsson et al., 2016). SRRF is an alternative to hardware-based super-resolution microscopy, and factors such as the ease of use, as well as low implementation cost enables flexibility in live imaging if it can be implemented successfully. Therefore, SRRF algorithm was performed on the same set of data acquired using widefield microscopy to determine whether super-resolution images can be obtained. Figure 4.4 showed the comparison of images obtained using widefield microscopy and SRRF. The images acquired by SRRF showed better signal contrast of *S. aureus*, making it easier to distinguish individual bacterium.

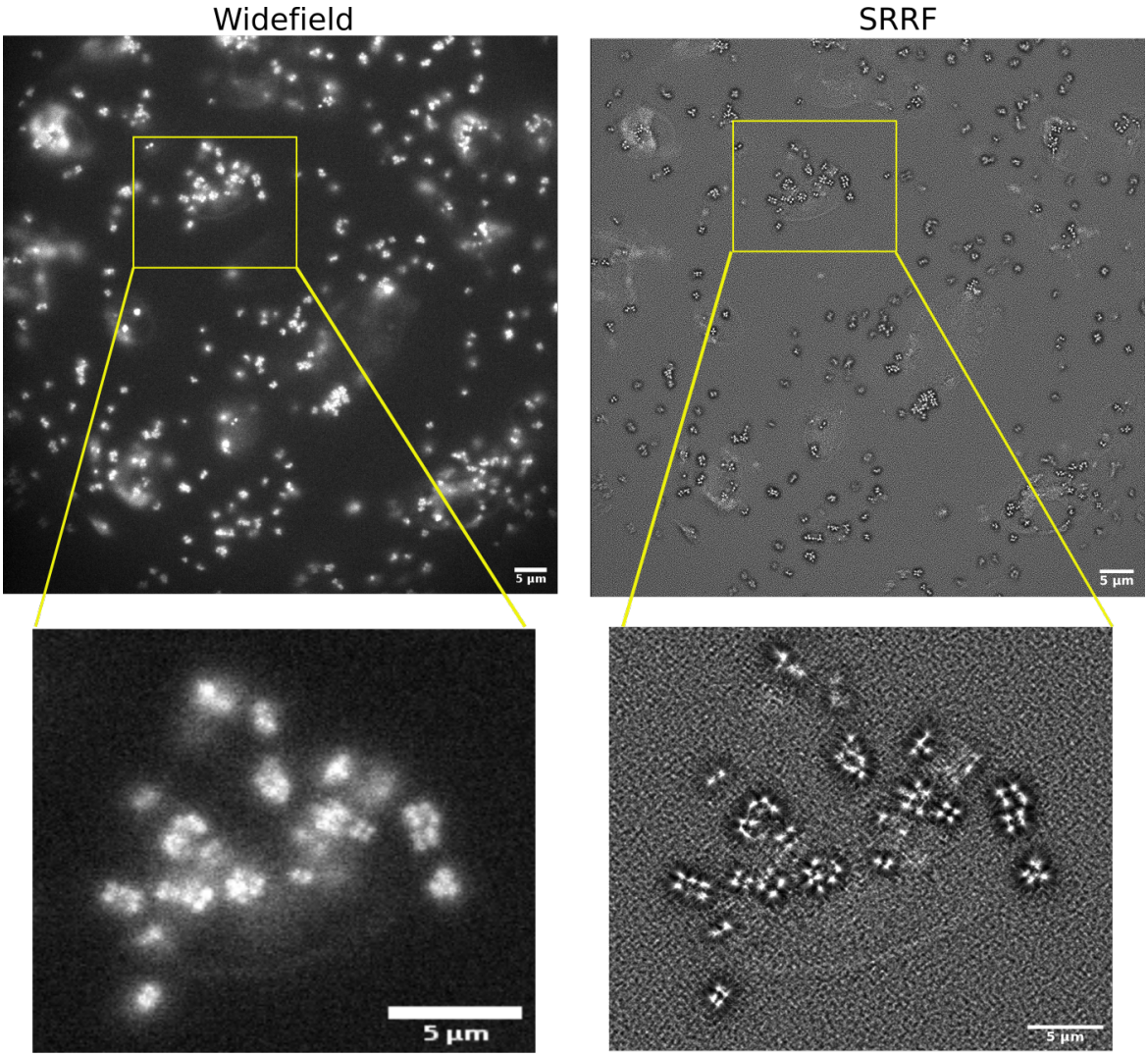

Fig. 4.4 **Widefield and SRRF imaging comparison.** Samples of hMDMs co-infected with mCherry-labelled *S. aureus* (SJF4622) was imaged using widefield microscopy (left), and processed using SRRF (right). Image on the right showed that SRRF provided better resolution to distinguish individual bacterium from the selected area (yellow box). However, background were introduced in the image following SRRF processing.

Specific labelling of cell structures and proteins allowed processes such as structural changes, protein interactions and localisations to be observed. However, fluorescent labelling of primary human immune cells are difficult as primary cells such as neutrophils cannot be transfected. Therefore, the selection of fluorescent labels that can be used are limited as the cells cannot be genetically modified for specific labelling. In fixed

imaging, the this can be overcome by immunofluorescence, where fluorescently-labelled antibodies are used to label specific structures in neutrophil. However, this method is invasive as permeabilization step is required for antibody staining (Allen, 2014). Therefore, only a limited number of cell permeable dyes are available for specific labelling of neutrophil structures.

To optimise an appropriate plasma membrane label for primary human immune cells, Nile red, a lipophilic dye for lipid droplets was used to dye hMDMs. HMDMs were stained with Nile red as mentioned in section 4.2.3, and the cells were co-infected with GFP-labelled *S. aureus*. Live cell imaging was performed by taking 30 frames every 3 minutes for 3.5h. Thirty frames was used to reconstruct 1 frame in SRRF imaging, and figure 4.5 showed an example of widefield and SRRF frames at 1.5h post infection, where intracellular structures in hMDMs such as nucleus and intracellular vacuole-like compartments were better defined in SRRF compared to widefield microscopy. However, SRRF algorithm highlighted the noise, and it is likely that artifacts, for example additional structures observable in the SRRF image were generated using SRRF. To determine whether resolution was improved using SRRF, fourier ring correlation (FRC) was calculated directly from the data, using FRC software on Fiji (Nieuwenhuizen et al., 2013). Based on the FRC software calculation, the Fourier Image Resolution (FIRE) value, which measures the image resolution was ∼166nm, thus a ∼1.8x resolution improvement compared to widefield microscopy (∼300nm).

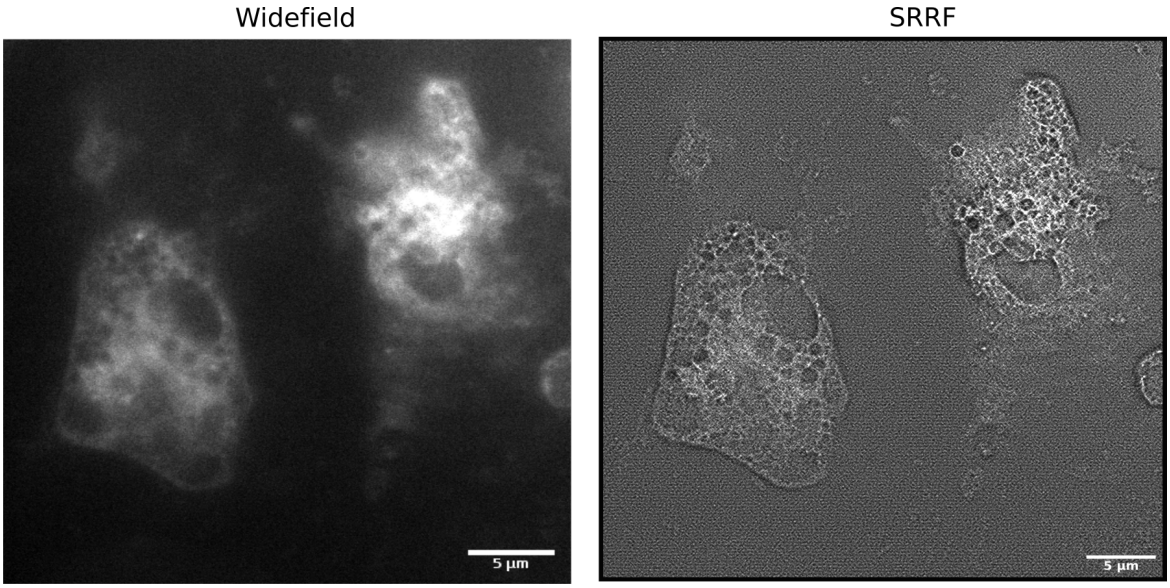

Fig. 4.5 **Live imaging using Nile red-labelled hMDMs with GFP-*S. aureus*.** SRRF improved the resolution, where compartmental-like intracellular structures that were not well resolved in widefield imaging (left) were better distinguished using SRRF (right image).

Optical sectioning is required in order to localise *S. aureus* within hMDMs, and to determine whether vacuole-like compartments in hMDMs contained *S. aureus*. However, widefield microscopy is limited in terms of optical sectioning, due to out-of-focus light from samples. As SRRF was used to generate super-resolution images using widefield microscopy, the limitation in optical sectioning persists. Although live imaging in low light conditions can be performed on hMDM and *S. aureus* samples using widefield microscopy and SRRF, the localisation of *S. aureus* within cells remained challenging.

4.3.5 Confocal microscopy to visualise hMDMs-*S. aureus*

Previous section showed the visualisation of live hMDMs-*S. aureus* samples using widefield microscopy and SRRF, but there were limitation in optical sectioning abilities of these methods, making it challenging to locate *S. aureus* within cell. Widefield microscopy illuminates the entire sample volume, thus producing images with low level

of contrast, as well as reducing sample details. Therefore, confocal microscopy was used to overcome the optical sectioning limitations in widefield microscopy (Carrington et al., 1990).

Unlike tradition confocal laser scanning microscopes, Zeiss Airyscan confocal microscope is a laser scanning microscopy technique that enables acquisition of improved signal-to-noise (SNR) ratio images (Huff, 2019). Furthermore, it also provides an improved resolution of up to factor of 1.7 (Huff, 2015). Airyscan confocal microscope was used to determine whether high resolution 3D images of neutrophil and *S. aureus* samples can be obtained. Nile red dye, previously optimised in hMDM samples were used on human neutrophils. Fixed neutrophils labelled with Nile red dye as prepared in section 4.2.3, and co-infected with GFP-labelled *S. aureus* were used as samples for Airyscan confocal microscopy. However, it is difficult to determine intracellular structures such as phagosomes in neutrophils (Figure 4.6). This indicated that Nile red may not specifically label neutrophil plasma membrane. To overcome this problem, CellMask™ Deep Red plasma membrane stain (Em 670nm) was used to label plasma membrane of human neutrophils. The CellMask™ stain showed more specific labelling compared to Nile red, where membrane and intracellular structures in neutrophils can be observed (Figure 4.6). Figure 4.7 showed an image of CellMask DeepRed-labelled neutrophils co-infected with GFP-*S. aureus* at MOI 5. Additionally, 4',6-diamidino-2-phenylindole, also known as DAPI was used to counterstain neutrophil and bacterial nuclei. DAPI is regularly used to label DNA in nuclei (Chazotte, 2011). *S. aureus* with weak GFP signal, counterstained with DAPI were observed in Figure 4.7, indicated by white arrow. Bleaching of GFP has been shown to indicate *S. aureus* cell death (Schwartz et al., 2009). Therefore, *S. aureus* with weak GFP signal and counterstained by DAPI may indicate *S. aureus* death within neutrophils.

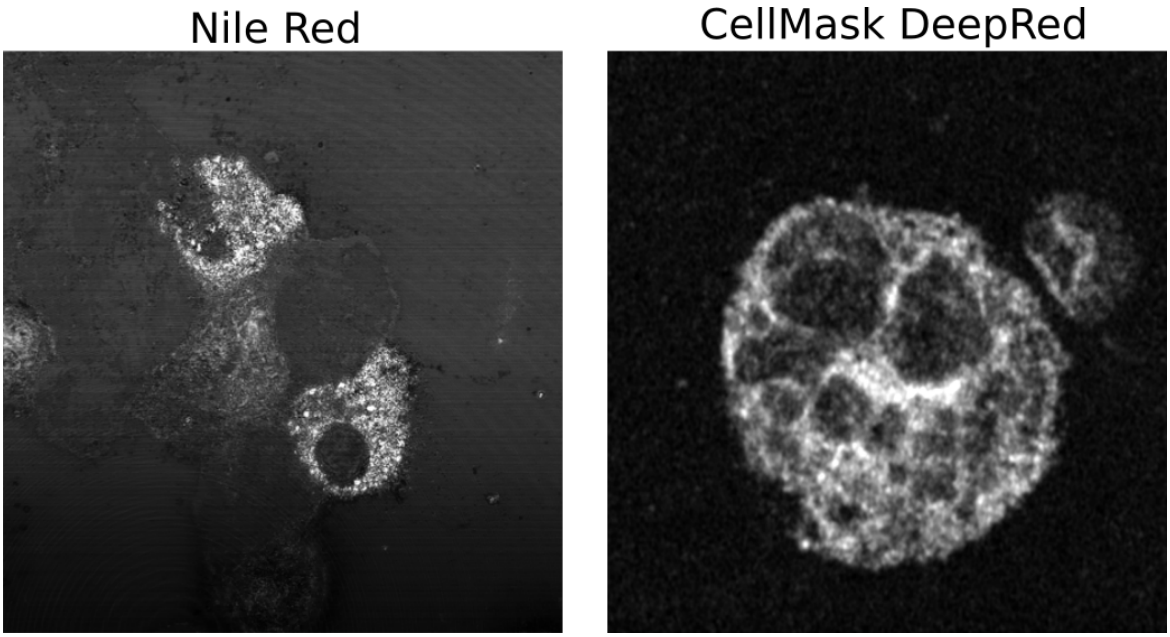

Fig. 4.6 **Neutrophils with different labelling dyes.** Neutrophils were labelled with Nile Red and CellMask DeepRed respectively. CellMask DeepRed showed specific labelling of neutrophil membrane compared to Nile Red, in which intracellular compartments can be observed when using CellMask labelling but not Nile Red. Images were acquired on Zeiss LSM 880 system equipped with AiryScan detection unit in the Wolfson Light Microscopy facility, using Plan-Apochromat 63x, 1.4 N.A oil objective and processed using Zen 2.3SP1 Black software.

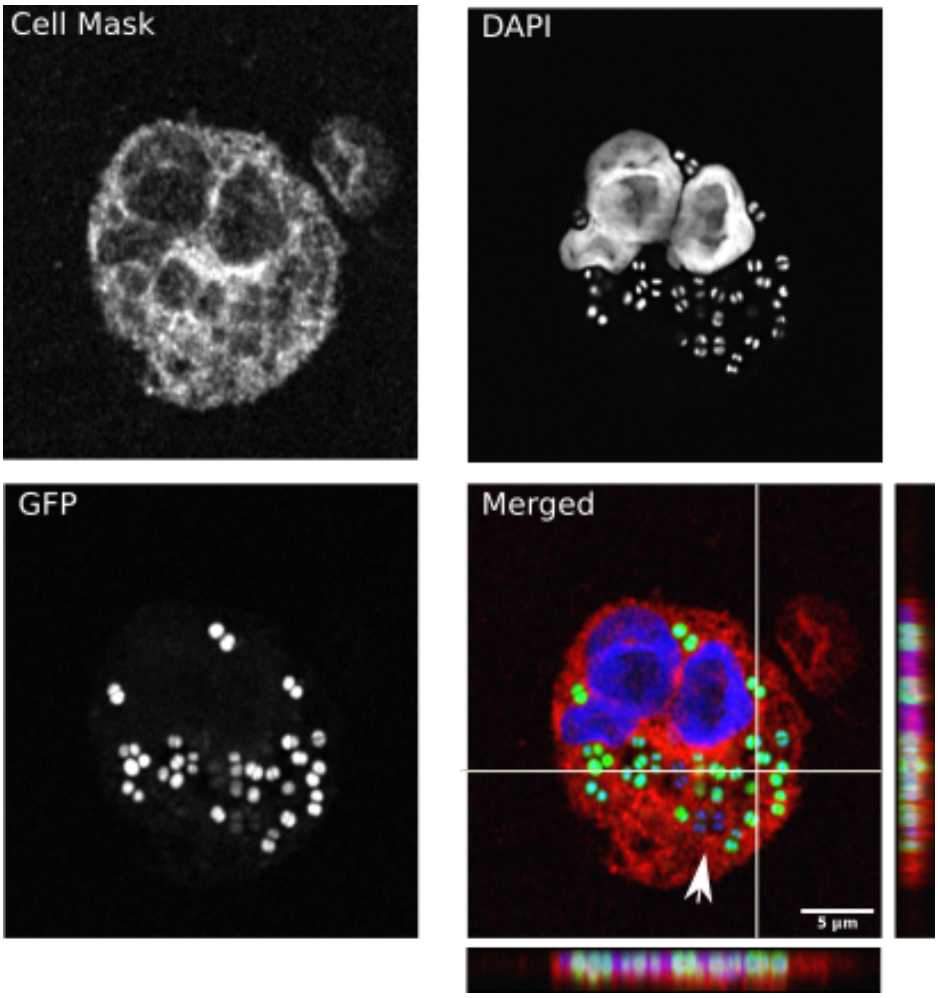

Fig. 4.7 **Airyscan visualisation of neutrophil-*S. aureus*.** Sample of Cell Mask DeepRed labelled-neutrophil with GFP-*S. aureus* and DAPI was used to counterstain neutrophil and *S. aureus* nuclei. Individual GFP-*S. aureus* can be distinguished (shown in GFP channel), and can be seen contained with intracellular compartments. The Z-stacks confirmed that *S. aureus* are located within neutrophil compartments.

Airyscan confocal microscope enabled high resolution image acquisition, where two bacteria separated by cell wall can be resolved. Additionally, z-stack was acquired and Figure 4.7 showed that *S. aureus* can be localised within neutrophil intracellular compartments. Together, this showed that high resolution and high SNR 3D imaging of neutrophil-*S. aureus* samples can be obtained using Airyscan confocal microscopy. However, it is challenging to perform fast and live imaging of neutrophil and *S.*

aureus samples as Airyscan is a laser scanning confocal microscope and requires high illumination power.

4.3.6 SIM to visualise hMDMs-*S. aureus*

Previous sections showed that unlike using widefield microscopy, high SNR and resolution images can be acquired using Airyscan confocal microscope. Airyscan confocal microscopy is able to improve the resolution by 1.7, whereas structured illumination microscopy (SIM) is theoretically able to surpass the diffraction limit up to factor of two (Gustafsson, 2000). Figure 4.7 in the previous section showed high resolution images acquired using Airyscan confocal microscopy, which theoretically is able to achieve lateral and axial resolutions of 140nm and 400nm respectively (Huff, 2015). Here, SIM was used to determine whether images improved to twice the theoretical resolution can be obtained.

Samples of hMDMs stained with DAPI, as described in section 4.2.2 were visualised using DeltaVision/GE OMX V4 microscope. Figure 4.8 showed a typical SIM illumination image, where the depth of the sample reduces the pattern contrast, which is an indication that the SIM reconstruction will be limited in resolution. Furthermore, artifacts were visible after image reconstruction (Figure 4.8b). This is most likely due to either autofluorescence in the sample or the poor depth penetration of the SIM pattern. Due to the poor optical sectioning abilities, as well as high illumination power required, SIM was not used to perform live imaging experiments.

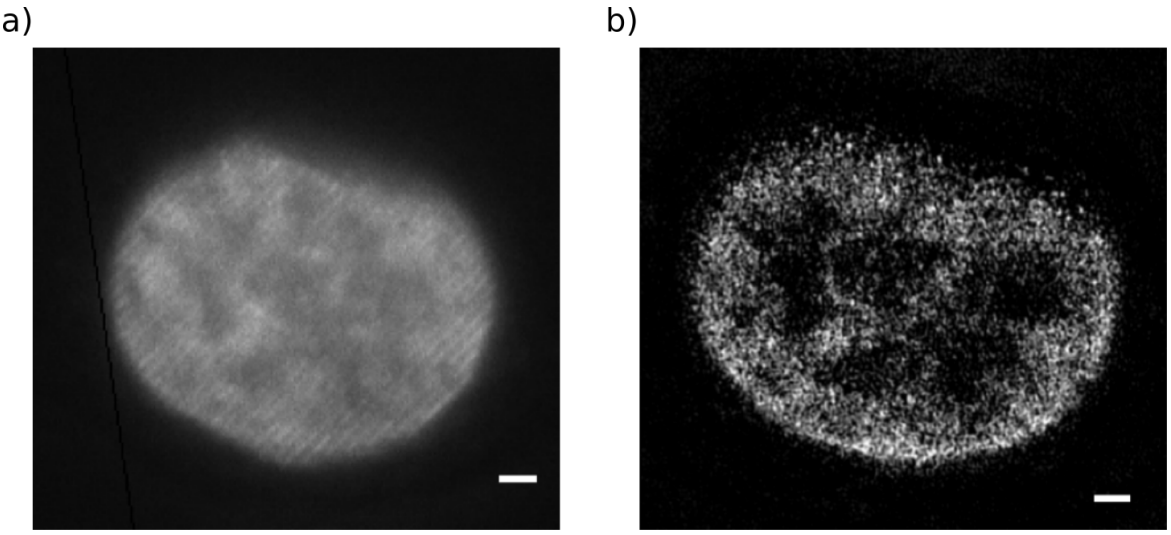

Fig. 4.8 **Visualisation of hMDMs using SIM.** a) Pre-reconstruction image where SIM patterns were visible. b) Artifacts visible post image reconstruction. Images were acquired on DeltaVision/GE OMX v4 in the Wolfson Light Microscopy facility, using 60x, 1.42 N.A oil objective. Scale bars are 2 μm.

In summary, modalities including widefield microscopy, SRRF, Airyscan confocal microscopy and SIM were used to image human immune cells samples. High SNR and resolution images can be acquired using Airyscan confocal microscopy. However, due to the high laser illumination requirement, as well as the long image acquisition time, it is challenging to perform long-term and fast live imaging expeirments using Airyscan confocal modality. Therefore, there is a need to develop new technologies that enable fast, long term and high resolution live imaging.

4.3.7 Adaptable imaging system

Various imaging modalities can be used to image human immune cell samples, but each of these systems have limitations, making fast and high resolution live imaging of human immune cells highly challenging. For example, previous sections showed that widefield microscopy can be used in long term live imaging with low light toxicity, but does not provide enough resolution to visualise intracellular *S. aureus*. Computational

approaches such as SRRF can be used to acquire better resolution images, but lacks optical sectioning ability to localise the *S. aureus* within human immune cells. It was shown that visualisation of neutrophil and *S. aureus* samples using Airyscan system provided high resolution to reveal subcellular structures, such as *S. aureus*-containing compartments in neutrophil. Additionally, *S. aureus* within the neutrophil compartments were confirmed by optical sectioning in Airyscan. However, using this technique requires high laser power that is unsuitable for long term live imaging. Moreover, Airyscan is a laser scanning microscope, which makes fast live imaging highly difficult. These results showed that there is a need for new imaging technology in order to visualise neutrophil and *S. aureus* interactions at the spatial resolution equivalent to Airyscan, with increase temporal resolution and at lower illumination power.

The Cairnfocal system is a versatile imaging platform developed in the Cadby lab. The platform uses a digital micromirror device (DMD) to project different illumination patterns, which allows switching between different imaging modalities (Dr. Liyana Valiya Peedikakkal, PhD thesis 2018). Using this platform, samples can be visualised in widefield at low illumination power, then transition to higher illumination confocal and structured-illumination based microscopy at selected timepoints. This reduces the light damage in live samples to allow long term imaging, and the confocal and structured-illumination based imaging will provide better optical sectioning and resolution to understand the interaction of *S. aureus* and human neutrophils.

4.3.8 Simultaneous widefield and confocal imaging of live neutrophils

To demonstrate the adaptability of the imaging system, simultaneous widefield and confocal live imaging in single colour was performed on neutrophils in the same field

of view. Neutrophils in the same field of view as visualised by widefield and confocal modalities in Figure 4.9 were approximately 15 μm apart. Neutrophil samples were illuminated with the same amount of light, and Figure 4.9 showed that confocal imaging provided a better contrast compared to widefield imaging. Other than demonstrating the flexibility, this showed that widefield and confocal modalities can be performed on the system. However, it is difficult to visualise neutrophil and *S. aureus* by performing single colour live imaging. Therefore, the next step is to set up two colour imaging on the platform to image neutrophil and *S. aureus*.

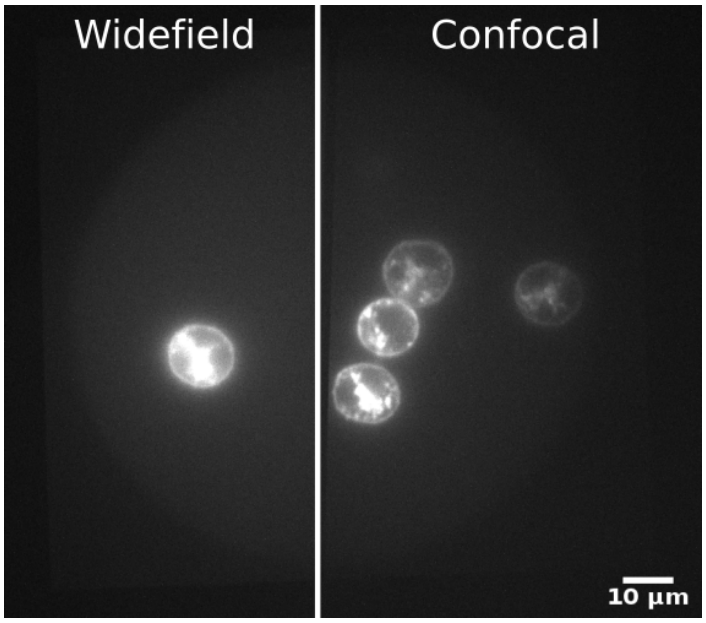

Fig. 4.9 **Simultaneous widefield and confocal imaging on Cairnfocal system.** Neutrophil samples in the same field of view were approximately 15 μm apart, labelled with Cell Mask Deep Red. Samples were imaged at every 2 mins for 2h. The ability to perform widefield and confocal imaging in parallel shows the versatility of the Cairnfocal system.

4.3.9 Live imaging of neutrophil-*S. aureus*

Previous section showed that single colour, live imaging of human neutrophils can be performed on our system. Next is to determine whether two-colour confocal live imaging can be implemented to visualise neutrophil and *S. aureus*. CellMask DeepRed-

labelled neutrophils were co-infected with GFP-*S. aureus* strain SH1000 at MOI of 5. To acquire time-lapse series, two-colour images alternating between using 470nm and 640nm laser lines on 89 North Laser Diode Illuminator (LDI) system were taken at every 5 s interval for 1 h. Figure 4.10 showed a time series of neutrophil phagocytosis of *S. aureus*. In the first two minutes in the time series, neutrophil can be seen migrating towards *S. aureus*, eventually engulfing and containing the *S. aureus*. However, the imaging was performed without the acquisition of z-stacks, making it difficult to located *S. aureus* within neutrophil phagosome. Therefore, two colour confocal live imaging in 3D was performed to localise *S. aureus* within neutrophils. Two-colour images with z-stacks were taken every 30s for 1h. Figure 4.11 showed a time series of neutrophil phagocytosis of *S. aureus*, with white arrow in the 2 min and 8 min snapshots showing the engulfment of *S. aureus* by neutrophil. A 3D projection of the snapshot at 25 min showed that *S. aureus* are contained within neutrophil.

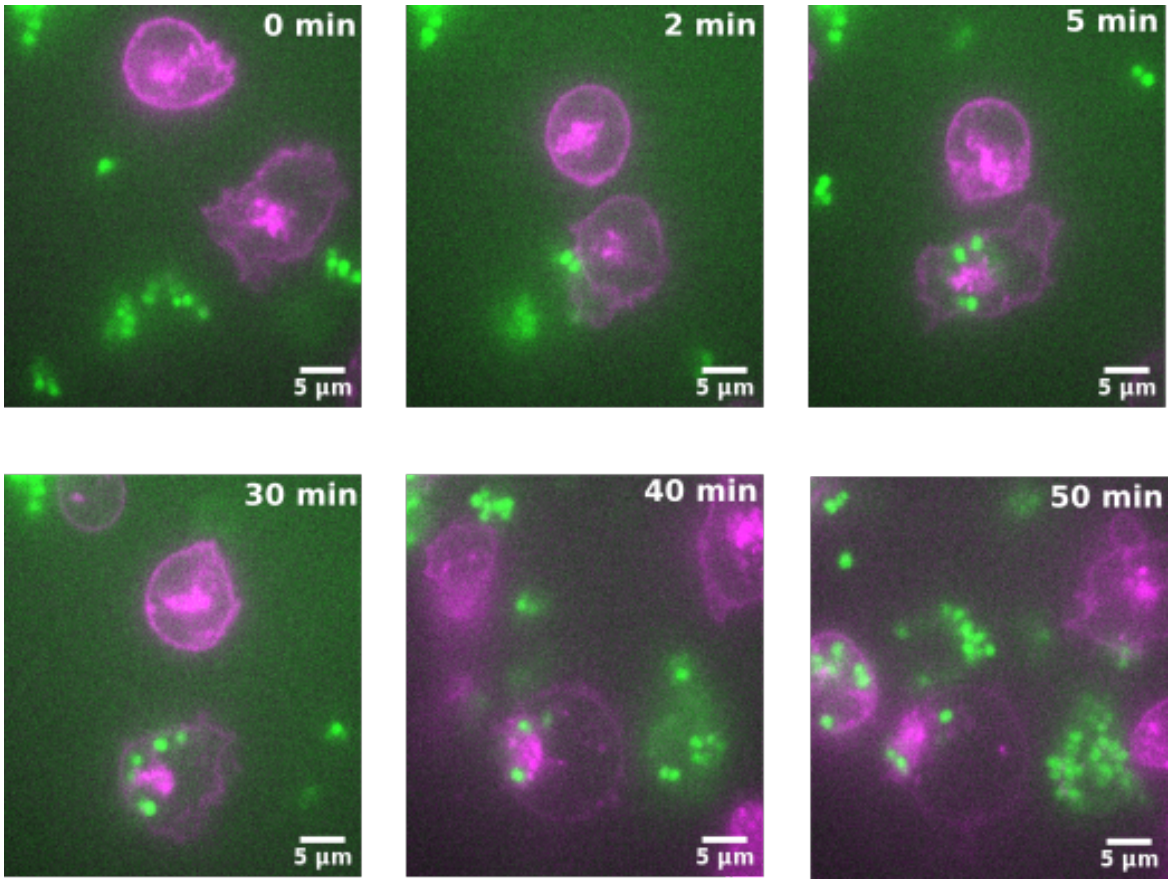

Fig. 4.10 **Confocal imaging of neutrophil-*S.aureus*.** Time series of 2-colour confocal imaging to follow the neutrophils phagocytosis of *S. aureus*. Neutrophils were co-infected with *S. aureus* at an MOI of 5. For example, at 2 min, neutrophil phagocytosis of *S. aureus* is observed, followed by the containment of *S. aureus* within the neutrophils at 5 min.

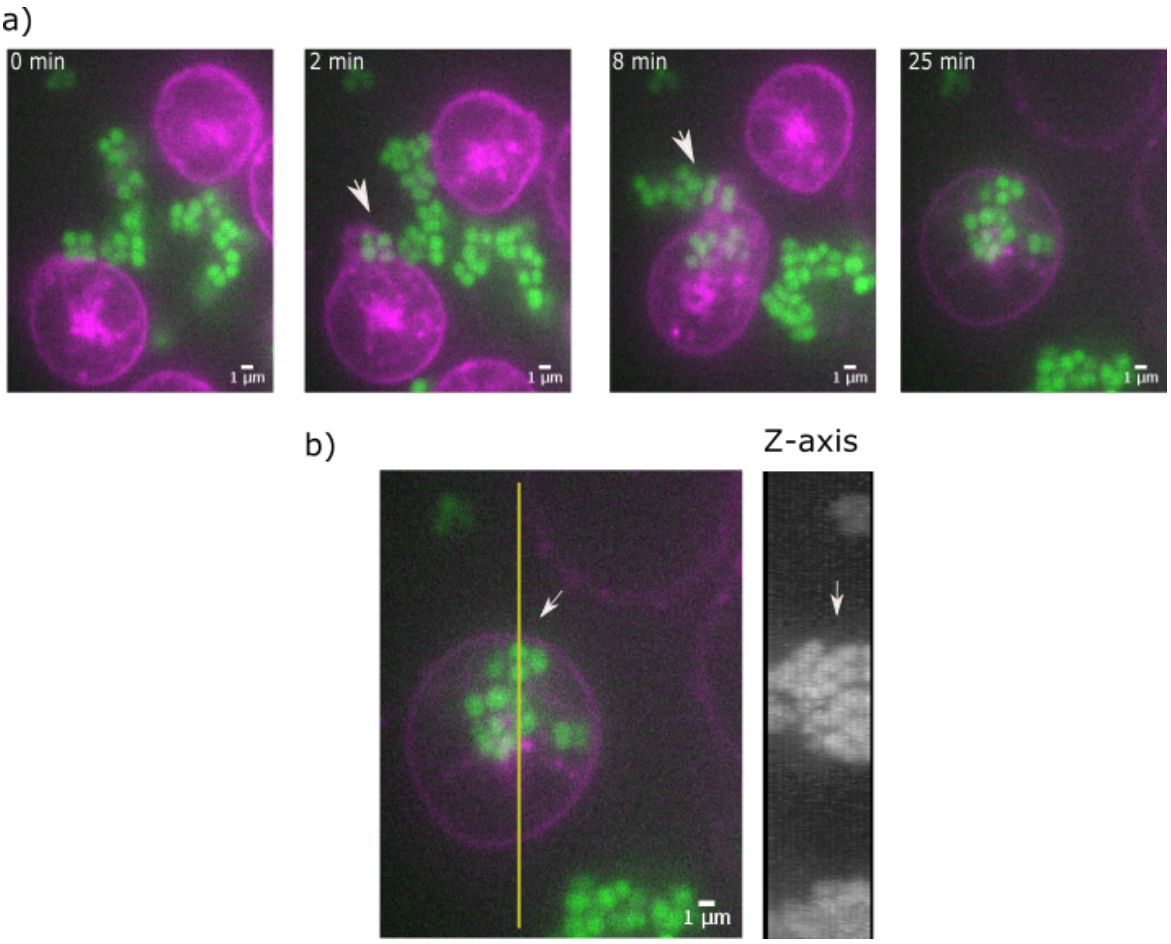

Fig. 4.11 **Two colour 3D confocal imaging of neutrophil-*S.aureus*.** a) Time series of neutrophil phagocytosis of *S. aureus*, where neutrophil phagocytosis of *S. aureus* can be observed at 2 min and 8 min (white arrows), and eventually the *S. aureus* is contained within neutrophils at 25 min timepoint. b) Z-projection of 25 min timepoint showed that *S. aureus* were contained within neutrophils.

In summary, widefield and confocal modalities can be performed either simultaneously or individually on the Cairnfocal system (Figure 4.9). Furthermore, results from Figure 4.10 and 4.11 showed that 2D and 3D two colour confocal imaging of live neutrophil and *S. aureus* samples can be imaged on our imaging platform, and z-stacks enabled the localisation of *S. aureus* within neutrophils.

4.3.10 Structured-illumination imaging of neutrophils

Fast live imaging of neutrophil and S. aureus were performed using confocal modality, as shown in previous section. The next step is to determine whether the Cairnfocal system is capable of performing super resolution imaging modality. Image scanning microscopy (ISM) is a confocal-based super resolution technique that increases the resolution by two-fold (Müller and Enderlein, 2010). Since its introduction in 2010, various forms of ISM have been implemented. Examples include multifocal SIM (MSIM), instant SIM (ISIM) and Airyscan (York et al., 2013, 2012). Two-colour confocal-based structured illumination imaging on our set up was used to acquire super-resolution images. Figure 4.12 showed a fixed sample of neutrophil and *S. aureus* visualised using two-colour structured illumination, where neutrophil compartments containing *S. aureus* can be clearly visualised. To obtain 1 structured illumination data frame, 100 frames of confocal pattern were acquired at 10ms. This was followed by reconstruction of ISM frames, first by identification and localisation of confocal spots using ThunderSTORM localisation plug-in on ImageJ, subsequently performing Sheppard summing algorithm to enhance resolution (J Cox et al., 1982; Ovesný et al., 2014).

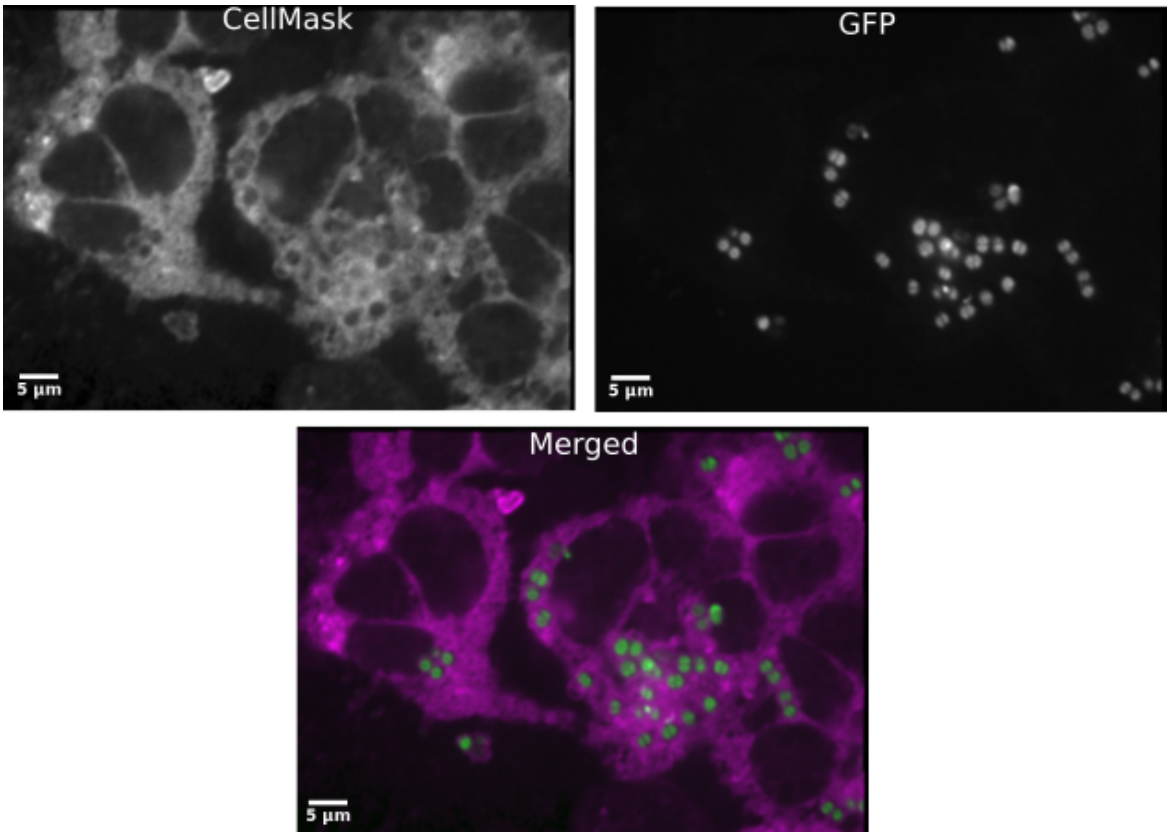

Fig. 4.12 **Fixed neutrophil-*S. aureus* samples imaging using two-colour structured illumination imaging.** The Cairnfocal system was set up to perform structured-illumination, and a fixed neutrophil-*S. aureus* sample was imaging using two-colour structured illumination imaging, where individual *S. aureus* can be resolved within neutrophil compartments.

4.3.11 Structured illumination live imaging

Previous section showed the use of structured illumination imaging on our platform to obtain super-resolution images of neutrophils. Next is to determine whether live structured illumination can be performed on the platform. Single-colour long term live structured illumination was first performed on CellMask DeepRed plasma membrane-labelled hMDMs, as hMDMs are more resilient cells compared to neutrophils. Figure 4.13 showed snapshots of hMDMs live imaging using structured illumination at an early and late timepoint. This showed that single-colour live structured illumination

imaging can be performed on hMDMs. Additionally, hMDM cell structures labelled with CellMask Deep Red plasma membrane dye was visible after 3.5h of imaging. This showed that CellMask Deep Red plasma membrane dye is photo-stable and suitable for long-term live structured illumination imaging. However, single-colour live structured illumination is unable provide further insights on bacterial interaction with human immune cells. For example, it is difficult to distinguish bacterial cells and hMDMs in single-colour imaging. Therefore, two-colour live structured illumination is required for this purpose.

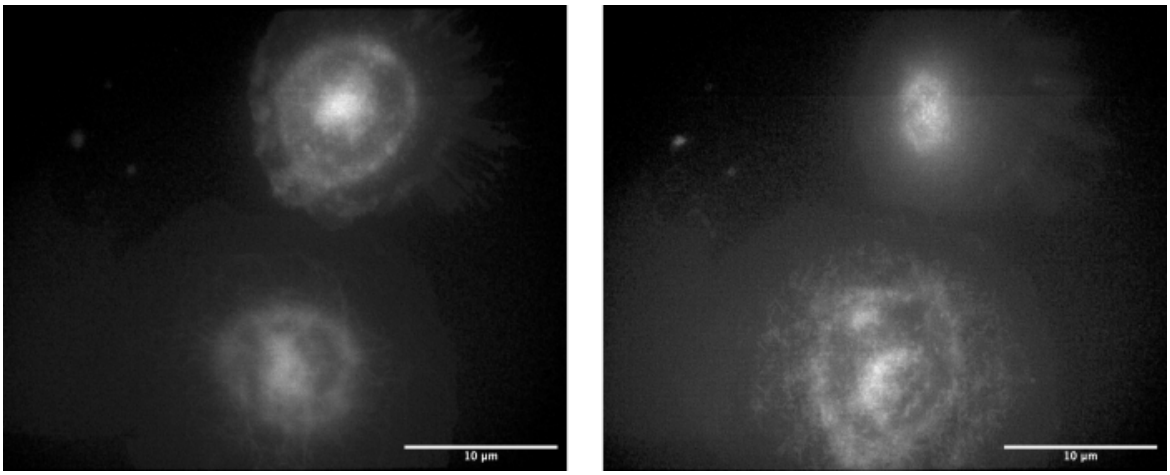

Fig. 4.13 **Structured illumination live imaging of hMDMs.** After structured-illumination modality was set up on the Cairnfocal, the system was applied to perform live imaging. A single colour structured illumination frame was acquired every 2 mins for 3.5h. CellMask DeepRed plasma membrane dye was used to label hMDMs. The left image is an early timepoint (T=0h) and the right image is at a late timepoint (T=3.5h).

4.3.12 *S. aureus*-hMDM 2 colour live structured illumination imaging

Next, the system was set up to perform two-colour structured illumination live imaging to image hMDMs and *S. aureus*. CellMask Deep Red-labelled hMDMs were co-infected with GFP-labelled *S. aureus* at MOI of 5. To reduce photodamage in samples, single

two-colour structured illumination frames were acquired every 2 mins for 3 h. Figure 4.14 showed that 2D, two colour structured illumination live imaging can be performed on the system, and it was used to follow *S. aureus* interaction with hMDMs.

At a later timepoint (3h) in the time series shown in Figure 4.14, intracellular structures in hMDMs can be seen disintegrating (white arrows, Figure 4.14). *S. aureus* is known to cause macrophage cell death by lysis, and this disintegration of structures observed in macrophages is likely due to cell death (Kubica et al., 2008). However, it is difficult to localise *S. aureus* contained within hMDMs. Moreover, it is challenging to determine whether the disintegration of internal hMDMs structures were due to *S. aureus*, as imaging was performed without the acquisition of z-stacks.

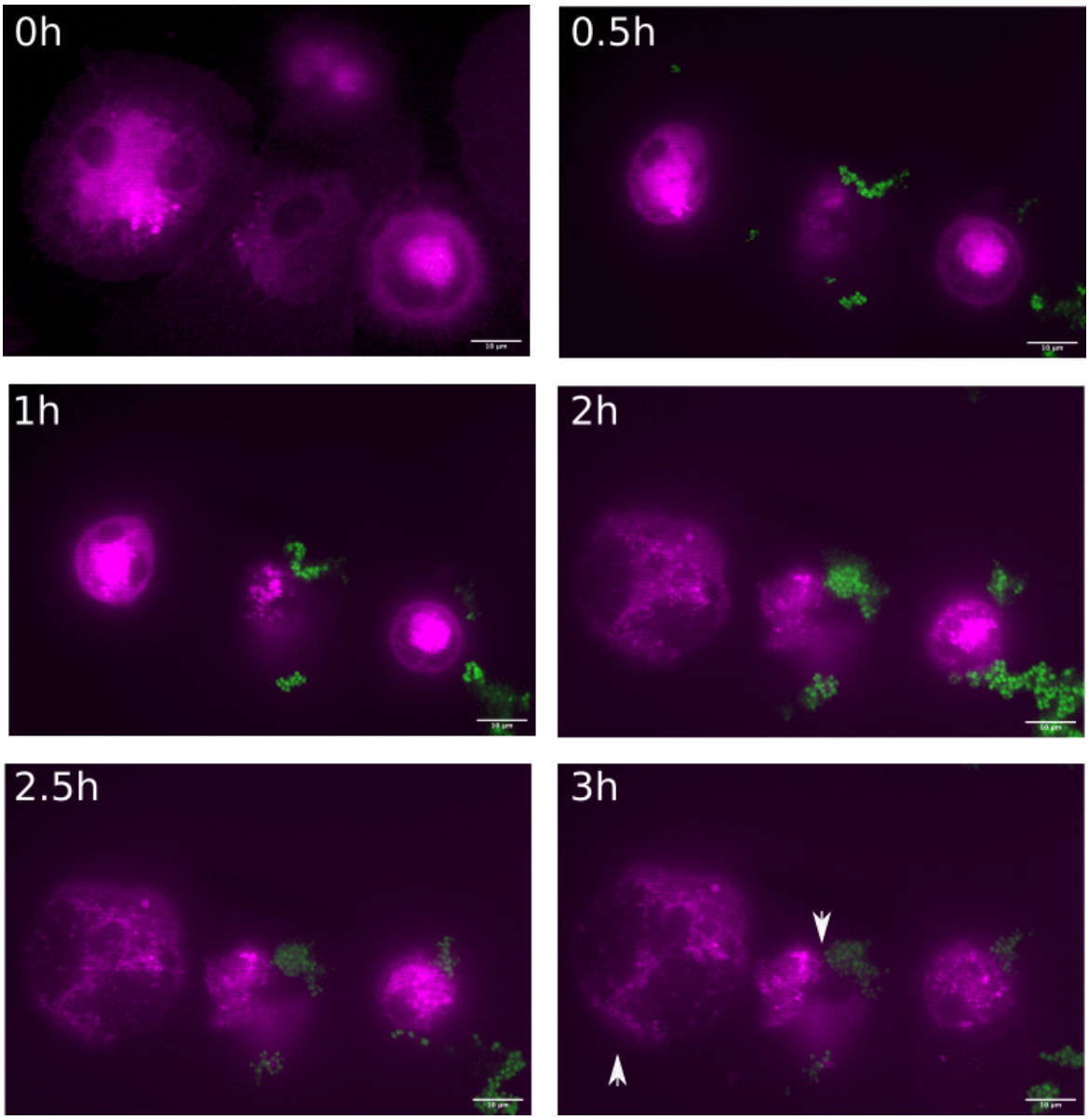

Fig. 4.14 **Two colour structured illumination live imaging of hMDMs and *S. aureus*.** Following single colour live structured-illumination imaging, the Cairnfocal system was set up to perform two colour live imaging. CellMask Deep Red was used to label hMDMs and co-infected with GFP-labelled *S. aureus* SH1000 strain for imaging. HMDMs were displayed in magenta and GFP *S. aureus* in green. White arrows show the disintegration of intracellular structures in hMDMs.

4.3.13 Structured illumination live imaging of neutrophils

Previous section showed that two-colour structured illumination live imaging can be performed on hMDMs to visualise its interaction with *S. aureus*. There are no current literature presenting live super-resolution imaging of human neutrophils, therefore it is not known whether neutrophils can withstand the high laser intensity used to acquire super-resolution images. To test this, live neutrophils were imaged using single colour structured illumination, with a single structured illumination frame taken every 2 mins for 2 h. Figure 4.15 showed the time series of neutrophil live imaging at the beginning and end of experiment. The number of neutrophils in the field of view differs between the time frames, and it is possible that this is due to the movement of neutrophils as they are loosely adherent to the imaging chambers.

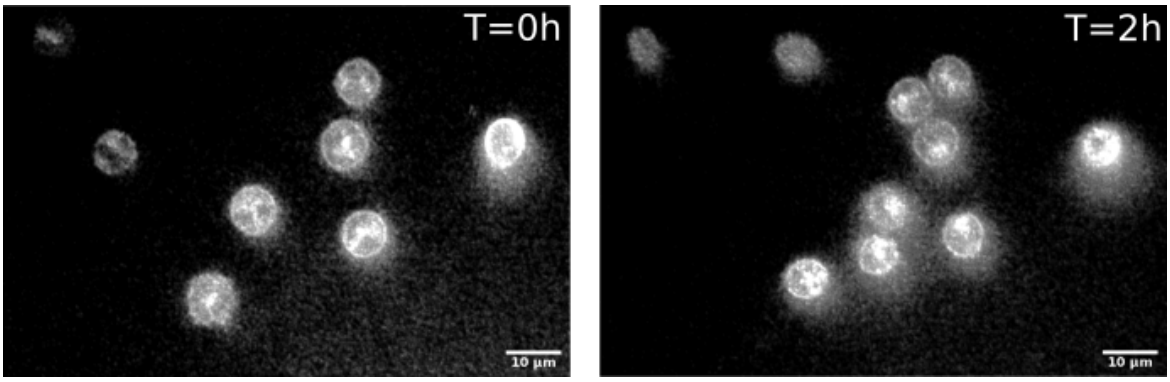

Fig. 4.15 **Live structured illumination of neutrophils.** The Cairnfocal system was optimised two perform live structured-illumination imaging using hMDMs previously. Here, neutrophils were labelled with CellMask Deep Red membrane dye, and visualised on the Cairnfocal system by live structured-illumination.

4.3.14 Neutrophil-*S. aureus* live structured illumination imaging

Following single colour live structured illumination imaging of neutrophils to show that neutrophils can survive the higher laser intensity required for imaging, next was to

implement two-colour structured illumination to visualise live neutrophil and GFP-labelled *S. aureus*. A single, two-colour structured illumination frame was acquired every 5s for 10 mins. Figure 4.16 showed time series of neutrophil containing *S. aureus*, where *S. aureus* can be seen contained within neutrophils. However, the localisation of *S. aureus* within neutrophils cannot be confirmed as z-stacks were not acquired. Therefore, 2 colour live structured illumination in 3D was implemented to visualise neutrophil and *S. aureus* samples.

Acquisition of z-stacks in two-colour structured illumination introduces greater light damage to cells, which can reduce the duration of live imaging. Therefore, two-colour structured illumination frames with z-stacks were acquired every 2 mins to reduce the photo-damage to cells. Within the neutrophil, intracellular *S. aureus* bounded by membranes were observable in Figure 4.17b (blue box). This suggested that *S. aureus* are within a compartment, perhaps a phagosome. Furthermore, z-stacks provided further confirmation, where *S. aureus* can be localised within the membranes (white arrow, Figure 4.17b).

This showed that 3D, two-colour structured illumination can be implemented on our system to perform live imaging of human immune cells and *S. aureus*. The application of this imaging system to understand *S. aureus*-immune cell biology will be discussed in the next chapter.

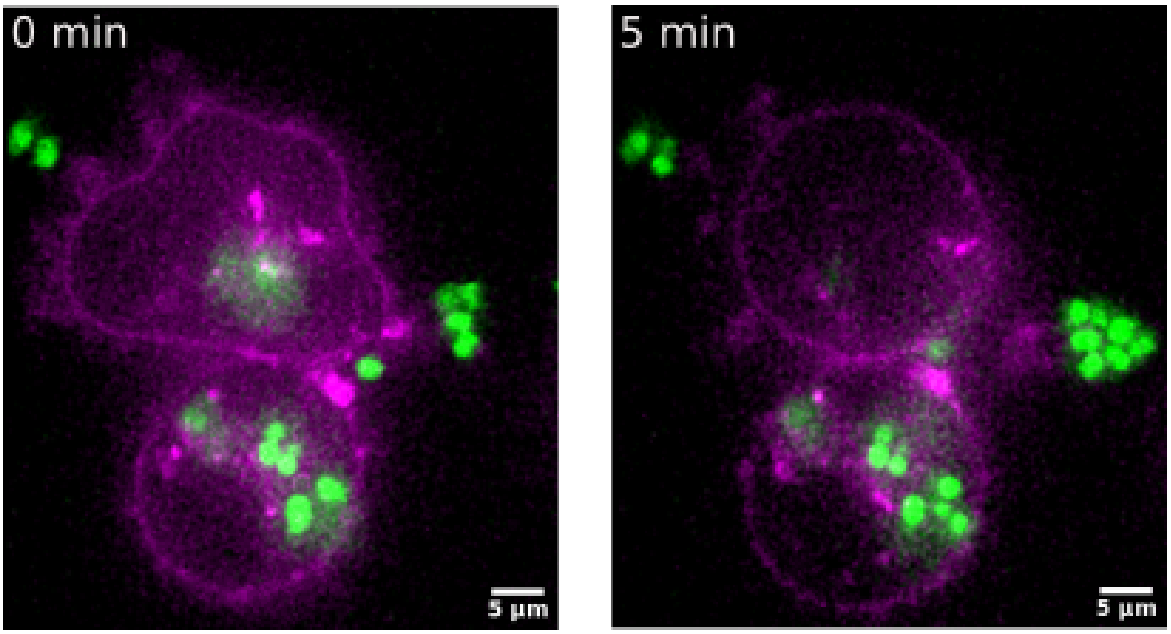

Fig. 4.16 **Two-colour 2D live structured illumination of neutrophil and *S. aureus*.** Neutrophil were co-infected with *S. aureus* at MOI 5. Live imaging were performed where a single two colour frames were acquired every 5s for 10mins.

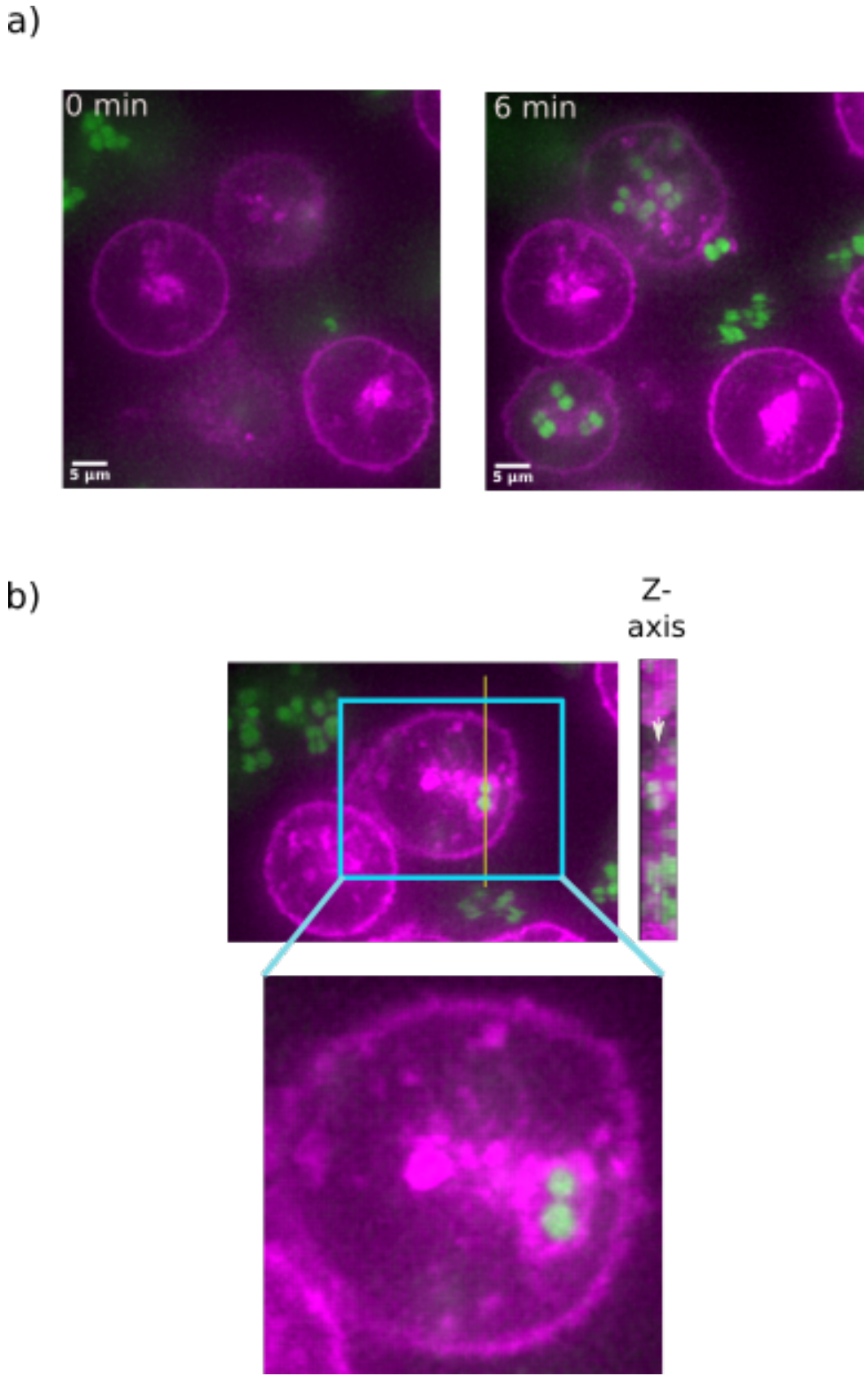

Fig. 4.17 **Two-colour structured illumination live imaging of neutrophil and *S. aureus* in 3D.** a) Snapshots of different timepoints to show the phagocytosis of *S. aureus* by neutrophils, where *S. aureus*-containing neutrophils were observed at 6 min timepoint. The localisation of *S. aureus* within neutrophils is shown in b), where two *S. aureus* can be resolved within a neutrophil compartment, and Z- stacks confirmed the presence of *S. aureus* within neutrophils.

4.4 Discussion

In this chapter, widefield microscopy, SRRF, Airyscan confocal microscopy and SIM were the modalities used to image human immune cells, including macrophage and neutrophil samples. Widefield microscopy was able to perform live imaging of hMDM-*S. aureus* at low illumination power for long term, but lacks in resolution. Using an analytical-based technique such as SRRF improved the resolution of data acquired from live imaging experiments performed on a widefield microscope. However, this technique is limited due to the introduction of noise artefacts. As the entire sample was illuminated using widefield microscopy and SRRF, thus reducing the depth sampling, these techniques lacked optical sectioning abilities to localise *S. aureus* within cells.

Next, *S. aureus*-immune cell samples were imaged at high resolution using Airyscan confocal microscopy, and the optical sectioning abilities of Airyscan allowed the localisation of *S. aureus* within neutrophils. However, Airyscan requires high illumination power which can cause photodamage in live cells, and the long acquisition time of Airyscan makes live imaging of neutrophil and *S. aureus* highly challenging. Fixed samples were also imaged on SIM, but live imaging were not pursued due to the high illumination power and poor 3D resolution of SIM. A summary comparing the advantages and disadvantages of the different imaging techniques used in this chapter is presented in Table 4.1. In addition to identifying the most suitable imaging technique to visualise human neutrophil and *S. aureus* samples, membrane labels were tested for labelling neutrophils. Unlike Nile red, CellMask DeepRed plasma membrane dye showed specific labelling of neutrophil membrane, and it is photo-stable for long term live imaging. Therefore, CellMask DeepRed was chosen as the dye to label neutrophils for future live imaging experiments.

Techniques	**Advantages**	**Disadvantages**
Widefield	• Fast acquisition • Low illumination requirement • Suitable for live imaging	• Poor optical sectioning • Diffraction-limited
SRRF	• Fast acquisition • Low illumination requirement • Suitable for live imaging • High resolution images	• Poor optical sectioning • Prone to artefacts
Airyscan confocal	• High resolution images • Improved optical sectioning abilities	• Slow acquisition • High illumination power requirement

OMX-SIM	• High resolution images	• High illumination power requirement • Poor optical sectioning abilities • Prone to artefacts • Slow acquisition

Table 4.1 Comparison of imaging techniques used in this work

Live imaging of human neutrophils is commonly performed using epifluorescence and confocal imaging modalities (Allen, 2014; Ellett et al., 2019). These techniques enable fast acquisition, and long term live imaging, but lacks the spatial resolution to visualise the intracellular *S. aureus* within neutrophils. Techniques that offer improved spatial resolution, including Airyscan confocal and OMX-SIM are not live-imaging friendly due to the high illumination power required. Various works comparing the different imaging techniques, and their application in live imaging have been performed (Godin et al., 2014; Jensen, 2013). However, the comparisons are typically performed on cell lines, and there were no comprehensive comparison of live imaging techniques using primary cells, in particular, human neutrophils at the time of this work.

This chapter begin by comparing different imaging techniques, and identifying the most suitable technique for live imaging of human neutrophils. It also highlighted the need for an imaging technique that provides the spatial resolution (< 250nm) to visualise neutrophils at subcellular level, with the ability to perform fast imaging every

minute, as well as introducing minimal light damage to cells that enable long term imaging for up to 3 hours. In summary, Airyscan confocal microscope was the most suitable technique in terms of spatial resolution, but performing live imaging is highly challenging. The main goal of the project is to be able to follow the process of *S. aureus* within live human neutrophils, and the criteria to achieve this objective includes:

1. Low illumination power to reduce photodamage and photoxicity in cells.
2. High resolution to visualise intracellular *S. aureus*.
3. Optical sectioning to localise the intracellular *S. aureus*.
4. Fast live imaging to visualise *S. aureus* dynamics.

Therefore, there is a need for a system with spatial resolution of Airyscan, but lower illumination power requirement and a shorter image acquisition time. The Cairnfocal system is an adaptable imaging platform that can be programmed to implement various imaging modalities for live imaging, such as confocal and structured illumination. This flexible platform enabled us to follow a biological process and switch modalities when an event occurs, thus reducing the illumination power introduced to live samples.

The work in this chapter showed that live imaging of neutrophil and *S. aureus* can be performed using 3D confocal and structured illumination modalities on the Cairnfocal system. This demonstrated the versatility of the platform to perform either confocal imaging with low illumination requirement, or short term structured illumination live imaging at higher illumination power. Using this imaging platform to switch between confocal and structured illumination modalities at specific timepoints to follow live neutrophil and *S. aureus* interactions are discussed in the following chapters.

Chapter 5

Multi-modal imaging reveals dynamic interactions of *Staphylococcus aureus* within human neutrophils

This chapter takes the form of a manuscript upon which I am the first author. I was the primary contributor to this manuscript, and my contributions included:

1. Experimental planning and design, with guidance from both supervisors.
2. Performed all the experimental work and data analysis.
3. Preparation of figures.
4. Writing of the manuscript, with reviews and editing by the co-authors where necessary.

5.1 Introduction

Staphylococcus aureus is a highly opportunistic pathogen that is known to cause wide range of infections, including skin and soft tissue infections, septicemia and osteomyelitis (Tong et al., 2015). As it preferably colonises human nares, *S. aureus* skin infections are the leading cause of bacteremia (Kwiecinski and Horswill, 2020). The high incidence of *S. aureus* infections can be attributed to its ability to acquire and develop resistance toward antibiotics (Otto, 2013). Since the evolution of methicillin-resistant *S. aureus* (MRSA) strain, life-threatening MRSA infections have been an increasing burden in many countries, with particularly high prevalence in the United States and Asia (Lee et al., 2018). Furthermore, *S. aureus* has garnered major attention as a successful pathogen due to its extensive arsenal of virulence factors, including the cytolytic toxins Panton-Valentine leukocidin and phenol-soluble modulins (Guerra et al., 2017).

Neutrophils are professional phagocytes constituting the body's first line of defence, and are critical in defending the host against *S. aureus* infections. Following neutrophil phagocytosis of *S. aureus*, the *S. aureus* are contained within the phagosomes, a compartment where most of the killing mechanisms occur. The presence of *S. aureus* within phagosomes triggers the phagosomal maturation process. This process involves the fusion of granules with the phagosome, deploying proteases and antimicrobial peptides into the phagosomal space (Mayadas et al., 2014). In addition, the production of reactive oxygen species (ROS) and nitric oxide (NO) within the phagosome creates a hostile environment and a critical element of pathogen killing (Morel et al., 1991; Wheeler et al., 1997). The decrease in phagosomal pH is another aspect of the maturation process and a fundamental part of the activity of key antimicrobial proteases such as myeloperoxidase and cathepsins (Foote et al., 2017; Nordenfelt and Tapper, 2011).

Despite various antimicrobial strategies, neutrophils fail to eliminate internalised *S. aureus* completely (Greenlee-Wacker et al., 2017; Gresham et al., 2000; Yang et al., 2019). *S. aureus* expresses a broad array of virulence factors that facilitates its adhesion and colonisation, evasion of host immune response, as well as acclimatisation to the host environment which eventually cause infections (Foster, 2005; Foster et al., 2013). To respond to elements such as environmental cues and host responses, the expression of specific *S. aureus* virulence factors are coordinated by underlying regulatory systems. For example, studies have shown that the two-component GraSR regulatory system are critical for *S. aureus* survival in acidic environment (Chaili et al., 2016; Flannagan et al., 2018).

Among the challenges of following the sub-cellular processes of intracellular *S. aureus* within human neutrophils is their relatively small sizes, which can only be circumvented by super-resolution imaging techniques. However, unlike other cell types, there is little application of super-resolution live imaging to the study of human neutrophils. In general this is due to the high illumination power required to implement super-resolution modalities which induces photo-damage in cells. Neutrophils are notorious for their sensitivity to imaging conditions (Allen, 2014). For example, the ROS production generated by high illumination power are toxic to cells, thus limiting the duration of live imaging (van de Linde et al., 2012). Therefore, low illumination power is required for imaging live neutrophils, and it is crucial in the context of neutrophil and *S. aureus* interaction studies, as ROS production is a key antimicrobial response against *S. aureus* (Nguyen et al., 2017). Therefore, we need to image neutrophils with minimal illumination power to gain an accurate understanding of intracellular *S. aureus* dynamics within human neutrophils.

5.2 Materials and methods

5.2.1 Neutrophils isolation and culture

Detailed description of the ethics and procedures of neutrophil isolation and culture are described in section 2.6.1 and 2.6.2 in Chapter 2.

5.2.2 Bacterial culture and labelling

USA300 *S. aureus* strain JE2 with GFP chromosomal insertion were grown in Brain Heart Infusion (BHI) broth at 37°C with 5% CO_2, with shaking at 350 revolutions per minute (rpm) until mid-log phase. The GFP-*S. aureus* were labelled with 2.5 mM pHrodo Red succinimidyl ester (Invitrogen) according to manufacturer's instruction.

5.2.3 Fluorescence D-amino acid labelling of intracellular *S. aureus*

Fluorescence D-amino acid labels were obtained from Dr. Victoria Lund and Professor Simon Foster (Department of Molecular Biology and Biotechnology, University of Sheffield) (Lund et al., 2018). Freshly isolated neutrophils ($5x10^5$ cells) were stained with 10 μg/ml of CellMask Deep Red plasma membrane stain (#C10046, Invitrogen), followed by co-infection with pHrodo-labelled GFP *S. aureus*, prepared as above, at multiplicity of infection (MOI) 5 for 30 mins. Extracellular bacteria were removed by centrifugation at 2000 rpm for 4 mins, and cells were resuspended in fresh phenol-red free RPMI (supplemented with 10% (v/v) heat-inactivated FBS and 25 mM HEPES). The cultures were left to incubate at 37°C with 5% CO_2 until specified time points.

To label the peptidoglycan of intracellular *S. aureus*, 1 mM HADA was added to the cultures 30 mins before specific time points. To remove excess dyes, cells

were centrifuged at 2000 rpm for 3 mins, followed by washing with fresh phenol-red free RPMI 1640 (supplemented with 10% (v/v) FBS). To preserve cell structures for widefield imaging, the cells were plated on poly-L-lysine-coated coverslips and fixed with 4% paraformaldehyde (PFA) for 10 mins at room temperature, followed by washing twice with phosphate-buffered saline (PBS). Vectashield Antifade mounting medium (#H-1000, Vector Laboratories) was added to the samples before mounting onto glass microscopic slides.

5.2.4 Neutrophil cell death assay

Neutrophil viability was assessed by flow cytometry using the Attune Autosampler (Thermo Fisher). Freshly isolated neutrophils (5x10^5 cells) were cultured in RPMI 1640 media and HADA (0.5, 1 and 2 mM) at 37°C with 5% CO_2 for 2h. ToPro-3 viability dye diluted to 1:10000 was added to the samples before flow cytometry. Forward scatter and side scatter profiles, as well as the ToPro-3 negativity of neutrophil media control were used to gate the viable neutrophils, which enabled the enumeration of absolute viable neutrophil and ToPro-3 negative neutrophil count. Flow cytometry analysis was performed using FlowJo software (TreeStar).

5.2.5 Morphological assessment of neutrophil viability

Apoptotic neutrophils display condensed nuclei morphology. Neutrophils were cultured in RPMI 1640 media and 1 mM HADA respectively at 37°C with 5% CO_2 for 2h. Cytospin slides of neutrophil cultures were prepared by cytocentrifugation, followed by Diff-Quick (Thermo Fisher) staining. The cytospin slides were visualised using a light microscope, and at least 300 cells were scored in each experiment to assess the percentage of neutrophils with apoptotic morphological features.

5.2.6 Live cell imaging

The live-cell confocal and structured-Illumination imaging was performed using the CairnFocal (Cairn Research, Kent, UK) based system described earlier. Excitation was delivered at 470 nm, 555 nm and 647 nm using the Laser Diode Illuminator (89-North, Vermont USA). The excitation light was filtered with a ZET405/470/555/640X quadband excitation filter (Chroma Technology, Vermont USA). A matching dichroic mirror, the ZT405/470/555/640RPC (Chroma Technology, Vermont USA) was used to separate the excitation and emitted light. Emitted light was filtered via the ZET/405/470/555/640M emission filter before being detected by a Prime 95B sCMOS camera (Teledyne Photometrics, Arizona, USA) (Peedikakkal et al., 2018). The system utilised an infinity corrected, 100x, 1.49 NA, oil immersion TIRF lens, mounted on an Eclipse Ti microscope frame (Nikon Instruments, UK). A 1.5X C-Mount Fixed Focal Length Lens Extender (Edmund Optics, North Yorkshire, UK) was placed between the DMD and the camera to ensure that the 11 µm pixels of the would be small enough to exceed the Nyquist criterion with a 100x lens. Z-stacks were performed by moving the sample using a Nano-Z100 z-stage (Mad City Labs, Wisconsin, USA). During imaging, cells were maintained at 37 °C using the UNO-T Stage-Top incubator (Okolab, Naples, Itally). The CO_2 levels were not controlled.

The camera was connected to the PC via the PCIe interface, allowing for frame-rates of up to 80 fps in full frame. Unless otherwise stated, experiments were run using the center 50% of the chip, allowing frame rates of up to $\sim$ 150 fps. Software control of the system was performed using the Micro-Manager 2.0-gamma software suite and custom software for control of the DMD. Acquisitions requiring more than XYCZT imaging (i.e., structured illumination) were performed using custom Micro-Manager Beanshell scripts.

Single structured illumination data frames were reconstructed from acquisition of 100 confocal pattern frames acquired with a 10 ms integration time. Reconstruction was performed by identifying and localising confocal spots using the ThunderSTORM ImageJ plug-in (Ovesný et al., 2014), and subsequently performing the Sheppard summing algorithm, via a MATLAB script, to enhance resolution.

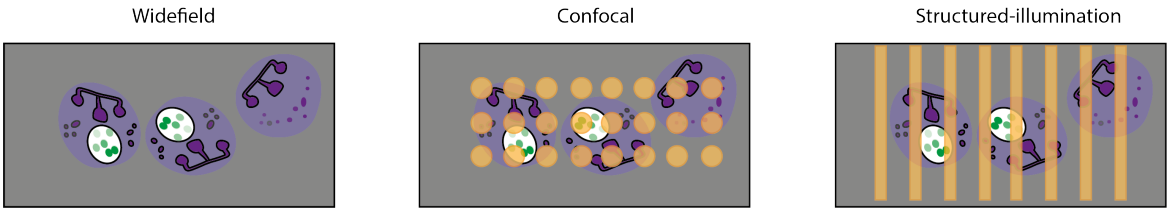

Fig. 5.1 **Illumination patterns generated by the DMD.** Different imaging modalities can be performed on the system by projecting various illumination patterns onto the sample using a DMD. For example, a uniform illumination pattern is projected onto the sample in widefield modality, multi-point pattern in confocal, and interference pattern in structured-illumination modality.

5.2.7 Image analysis

Image stacks were pre-processed in ImageJ. Maximum intensity Z- projections were used to represent the 3D stacks, and Gaussian blur filter with sigma 2.0, followed by multiplication was applied to subtract background. The images were enhanced using automatic brightness and contrast settings. To segment individual bacteria, automatic threshold and watershed algorithm were applied to single channel images. The circularity of bacteria were measured using the built-in plugin on ImageJ (Schindelin et al., 2012), and custom-written Python code was used to trace bacterial circularity across time.

5.3 Results

5.3.1 Multi-modal imaging platform setup

Implementation of a multi-modal imaging platform to adapt according to the biological samples was presented previously (Peedikakkal et al., 2018). Briefly, the system is built around the CairnFocal, a Digital Micromirror Device (DMD) based confocal system from Cairn Research Ltd. (Martin Thomas, 2017). A DMD is placed in an image plane between the camera(s) and the microscope, as well as in the illumination pathway, similarly to the disk in a traditional spinning disk confocal microscope (SDCM) (Inoué and Inoué, 2002; Toomre and Pawley, 2006). Any pattern displayed on the DMD will therefore be projected onto the sample, as well as determining which of the two cameras (dubbed the 'on' and 'off' side cameras) the emitted light is directed to. By displaying a pattern similar to the pinholes of a SDCM, a confocal image will be formed on the on side camera due to the groups of on pixels acting in the same manner as the pinholes of the equivalent spinning disk. This pattern can then be translated such that the entire sample is illuminated, either in a single camera frame to perform confocal or by synchronising the camera and DMD such that each frame displayed on the DMD is captured in a single camera exposure; this allows for a super-resolution image to be constructed via a Sheppard summing algorithm applied in post (J Cox et al., 1982). Other microscopy techniques can be applied by displaying different patterns on the DMD. In this work we use a combination of far field epi-fluorescent, confocal microscopy and super resolution microscopy by pixel reassignment (J Cox et al., 1982). (For more information see Supplementary.)

Here we demonstrate the versatility of a multi-modal imaging platform by applying it to visualise *S. aureus* and human neutrophils. Figure 5.2 shows the early stages of *S. aureus* and neutrophil interactions over 78 mins, where the 60 mins were visualised

using multi-point confocal modality, and the final 18 mins were visualised by switching to a structured-illumination modality.

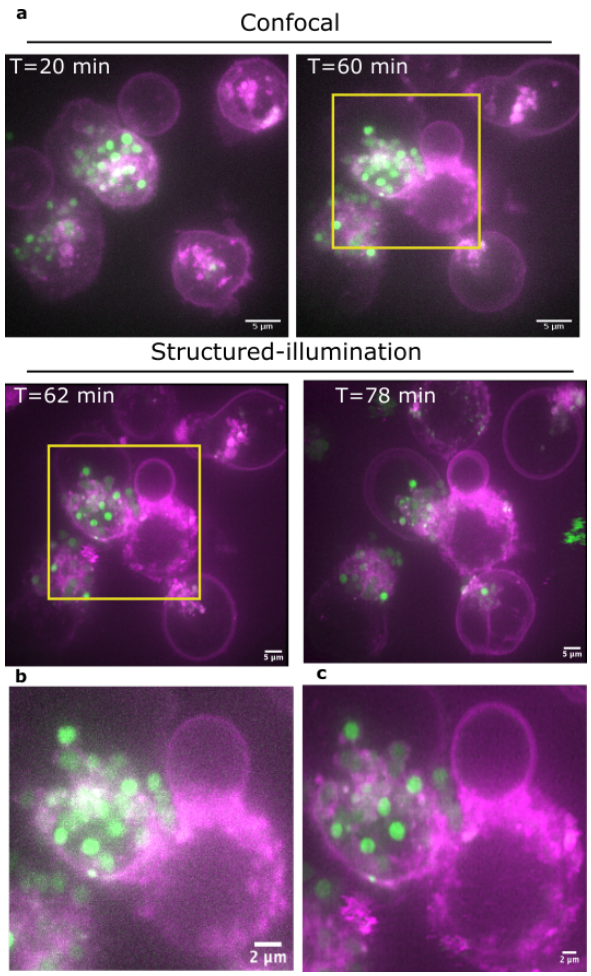

Fig. 5.2 **Multi-modal imaging.** a) Time series of neutrophil and *S. aureus* visualised using confocal modality at every 30 s for 1 h (upper panel), followed by structured-illumination modality at every 1 min for 20 mins (lower panel). The differences in resolution and contrast between b) confocal (T=60 min) and c) structured-illumination (T=62 min) of the neutrophil and *S. aureus* from the yellow boxes were shown. Neutrophils were labelled with CellMask DeepRed plasma membrane stain, and co-infected with GFP-labelled *S. aureus* at multiplicity of infection (MOI) of 5. Images shown are z-projects displayed at maximum intensity projections.

5.3.2 High resolution imaging revealed septum-like structures in intracellular *S. aureus*

The imaging platform described above gives us the ability to perform multi-colour super-resolution imaging allowing us to investigate the highly dynamic interactions between *S. aureus* and neutrophils. This, combined with active dyes allows us to follow processes in phagocytosis. For example, dyes sensitive to the neutrophil micro-environment can be conjugated to GFP-labelled *S. aureus* to understand their intracellular dynamics (Jubrail et al., 2016; Prajsnar et al., 2020). Here we used the pH sensitive pHrodo dye which allows us to understand the intracellular interactions between *S. aureus* and neutrophil.

GFP-labelled *S. aureus* were stained with pHrodo red prior to co-infection with neutrophils. This enabled us to identify populations of *S. aureus* within acidified (red fluorescence) and non-acidified (green fluoresence) phagosomes. The early stages of *S. aureus* and neutrophil interactions were visualised in three colours using a multi-point confocal modality for 1 h, where a heterogenous population of green and red *S. aureus* within neutrophils were observed (Supplementary Figure 5.4). Upon phagocytosis, the increase in oxidative burst leads to an initial alkalisation within the neutrophils, before gradually becoming acidic (Nordenfelt and Tapper, 2011). The presence of heterogenous *S. aureus* population within neutrophil suggests that some *S. aureus*-containing phagosomes failed to acidify.

Interestingly, switching to higher resolution imaging of the samples by using a structured-illumination modality revealed septum-like structures in green *S. aureus* (Figure 5.3), which was observed across 3 independent experiments (Supplementary Figure 5.4). Previously, the diffraction-limited cell wall components and structures of *S. aureus* have been visualised by a combination of biochemical approaches such as the

use of fluorescence D-amino-acid labels and super-resolution techniques (Lund et al., 2018; Saraiva et al., 2020). In the context of host-pathogen interactions, *S. aureus* within immune cells have also been visualised using various fluorescence microscopy technique. For example, *S. aureus* phagocytosed by neutrophil were visualised and quantified by confocal microscopy, and iSIM was implemented to localise *S. aureus* within dendritic cells (Berends et al., 2019; Hellebrekers et al., 2017). However, the presence of septum-like structures in *S. aureus* within host cells have not been observed previously.

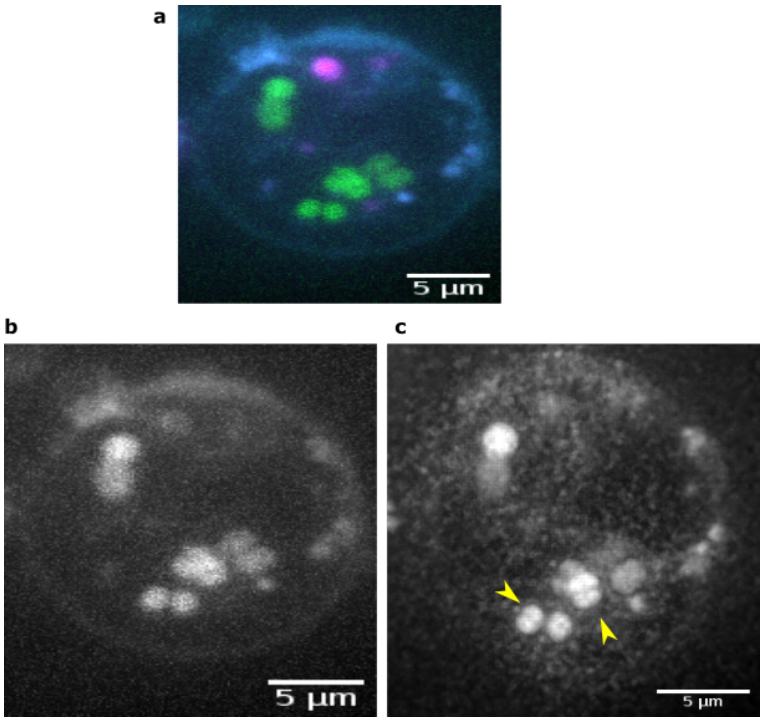

Fig. 5.3 **Confocal and structured-illumination live imaging of neutrophil and *S. aureus*.** a) Composite image of *S. aureus* and neutrophil visualised using a confocal modality. GFP-labelled *S. aureus* visualised using 470 nm laser line in b) confocal and c) structured-illumination modalities are compared to show the improvement in resolution using structured-illumination. The yellow arrows showed the *S. aureus* with septum structures observed in a structured-illumination modality. The images shown are z-projects displayed at maximum intensity projections.

5.3.3 Supplementary Note 1: Morphological variation between bacterial populations

In addition to septum-like structures, we observed morphological variation among bacterial populations using a structured-illumination modality. Green *S. aureus* exhibited ovoid morphology, whereas red *S. aureus* remained rounded (Figure 5.4). Therefore, the circularity of cell was used as a descriptor to quantify the morphological variation between bacterial populations. The bacterial circularity in structured-illumination time series were measured over time (Methods), with heat-killed GFP-labelled *S. aureus* as a control. We analysed images of *S. aureus* co-infected with neutrophils from three independent donors (Supplementary Figure 5.5.) Live red phrodo positive *S. aureus* situated within an acidified phagosome have higher circularity values, thus a more rounded morphology than green *S. aureus* across the time series, and for each bacterial population, there were minimal changes in the circularity values along the time series. Furthermore, the circularity of heat-killed GFP-labelled *S. aureus* time series is greater than both live *S. aureus* populations (Figure 5.5).

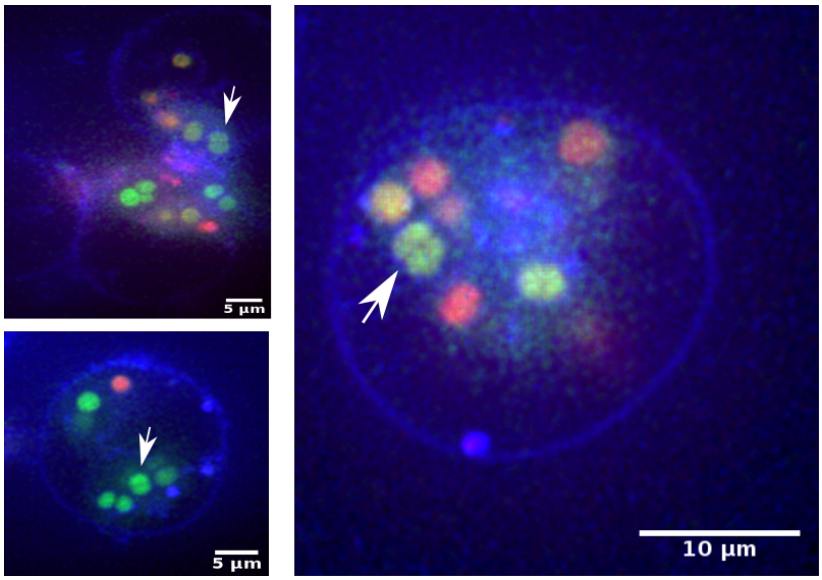

Fig. 5.4 **Visualisation of intracellular *S. aureus* in neutrophils.** Septum-like structures in intracellular *S. aureus* (white arrows) observed in 3 independent experiments using a structured-illumination modality. Neutrophils were co-infected with *S. aureus* at an MOI 5, and the neutrophil membrane was labelled with Cellmask Deep Red (falsed coloured to blue), GFP-labelled *S. aureus* in green and pHrodo red in red. Images are z-projects displayed at maximum intensity projections.

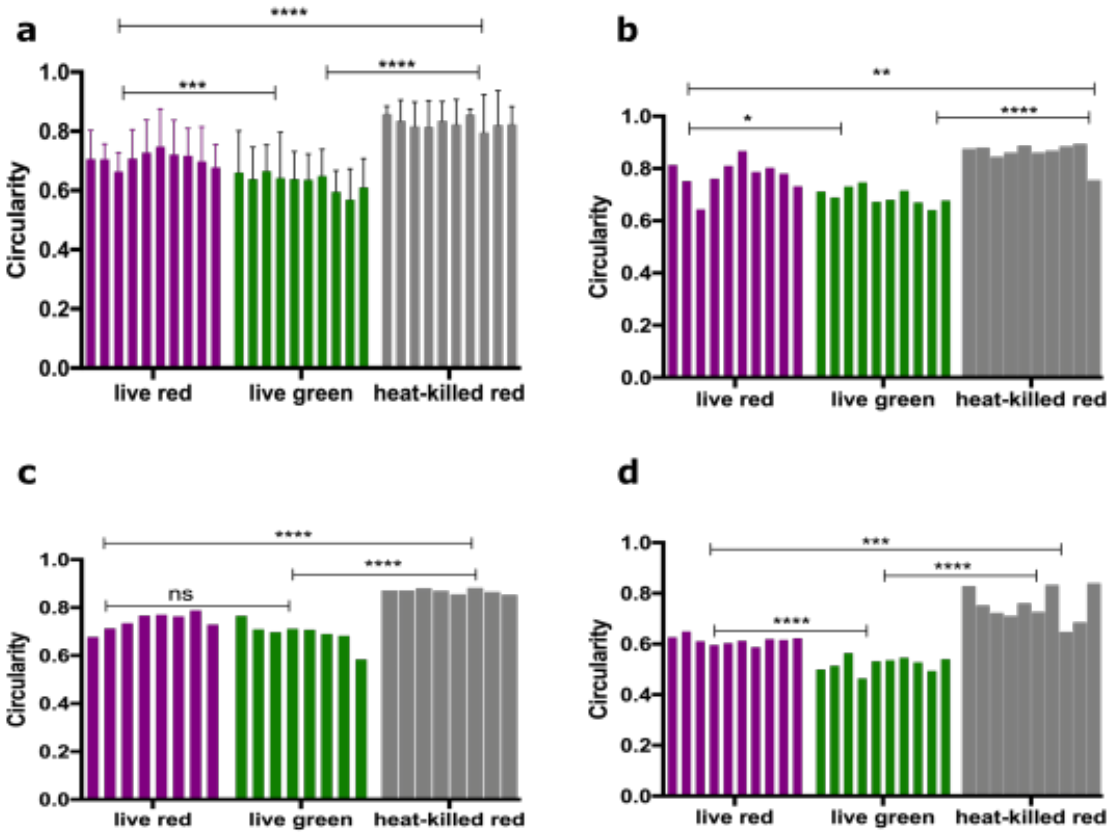

Fig. 5.5 **Comparison of the circularity between different bacterial populations.** The circularity of live red, green and heat-killed bacteria were measured and compared. Data shown in a) is the mean of 3 independent donors, and the measurements from independent donors b) donor 1, c) donor 2 and d) donor 3 were shown. Statistical analysis was performed using One-way ANOVA, **** $p<0.0001$,*** $p<0.0002$,* $p<0.0332$.

5.3.4 Fluorescence D-amino acid labelling to visualise bacterial cell division *in vivo*

The formation of a septum implies that cell fission occurs with in the neutrophil. To investigate this possibility we imaged *S. aureus* using dyes which specifically target new cell wall growth. Fluorescent D-amino acid dyes with intrinsic fluorophores attached, such as 7-hydroxycoumarin 3-carboxylic acid (HADA) enabled fast and real time

detection of peptidoglycan cell wall synthesis in extensive range of bacterial species including *S. aureus* (Kuru et al., 2012; Lund et al., 2018).

In vivo application of fluorescence D-amino acid was described previously (Siegrist et al., 2013). However, to our knowledge, there are currently no studies incorporating fluorescence D-amino acid labels to probe the peptidoglycan synthesis of intracellular *S. aureus* within human neutrophils. Therefore, it is important to ensure that the fluorescence D-amino acid labelling strategy used to probe the intracellular *S. aureus* dynamics does not affect neutrophil viability. We performed flow cytometry neutrophil cell death assay using ToPro-3 viability dye, and assessed the neutrophil morphology to determine the effect of fluorescence D-amino acid on neutrophil viability (Methods). Together, the flow cytometry and morphological viability assays confirmed that 1 mM of HADA used to label intracellular *S. aureus* does not compromise neutrophil viability (Supplementary Figures 5.7 and 5.8).

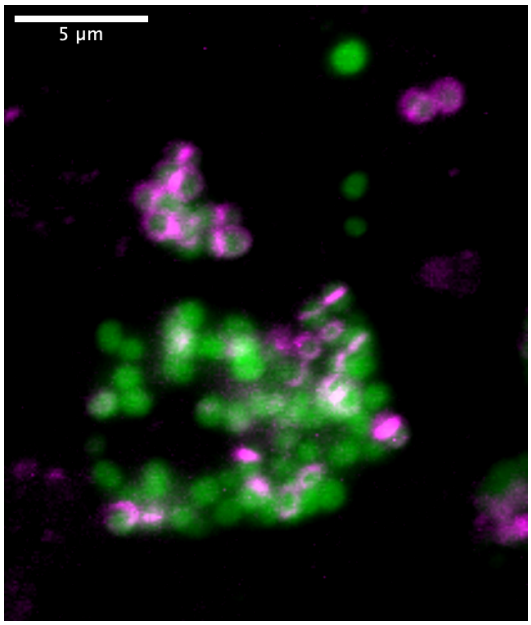

Fig. 5.6 **Fluorescence D-amino acid labelling of intracellular *S. aureus*.** Neutrophils were co-infected with GFP-*S. aureus* at MOI of 5 for 2h, and 1mM of fluorescence D-amino acid label HADA was added to the co-culture 30 mins prior fixation to label intracellular *S. aureus*. The presence of HADA (magenta) labelling in intracellular *S. aureus* (green) confirmed the new cell wall synthesis by *S. aureus in vivo*.The image shown is z-projects displayed at maximum intensity projections.

To determine whether septum-like structures observed in green *S. aureus* indicated that intracellular *S. aureus* undergoes cell division within neutrophils, HADA was used to label intracellular live and heat-killed *S. aureus*. Figure 5.6 showed HADA labelling of intracellular live *S. aureus*, confirming the ability to apply fluorescence D-amino acid labels to probe intracellular *S. aureus* in live neutrophils. Additionally, the incorporation of HADA in live intracellular *S. aureus* suggests that new cell wall are synthesised, and *S. aureus* are growing *in vivo*. This was further confirmed when neutrophils were co-infected with heat-killed *S. aureus*, and the absence of HADA in intracellular heat-killed *S. aureus* suggests that no new cell wall was synthesised (Supplementary Figure 5.9).

5.3.5 Supplementary Note 2: *In vivo* fluorescence D-amino acid labelling approach

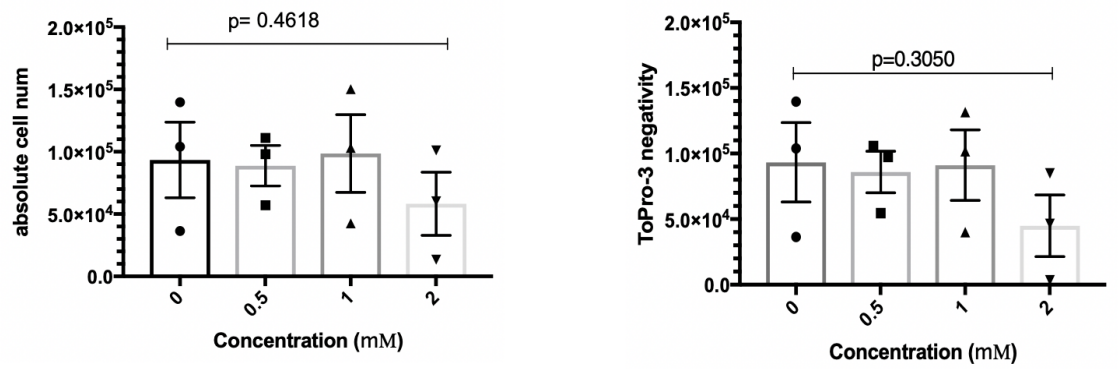

Fig. 5.7 **Neutrophil cell death assay.** Different HADA concentrations (0.5, 1 and 2mM) were used in co-incubation with neutrophils for 2h, and neutrophil viability was quantified using flow cytometry, using ToPro-3 as neutrophil cell death marker. The absolute neutrophil cell number and ToPro-3 negativity decreased when 2mM HADA was used, indicating that 2mM of HADA is toxic to neutrophils. Data shown is the mean with standard error mean of 3 independent experiments. Statistical analysis was performed by One-way ANOVA.

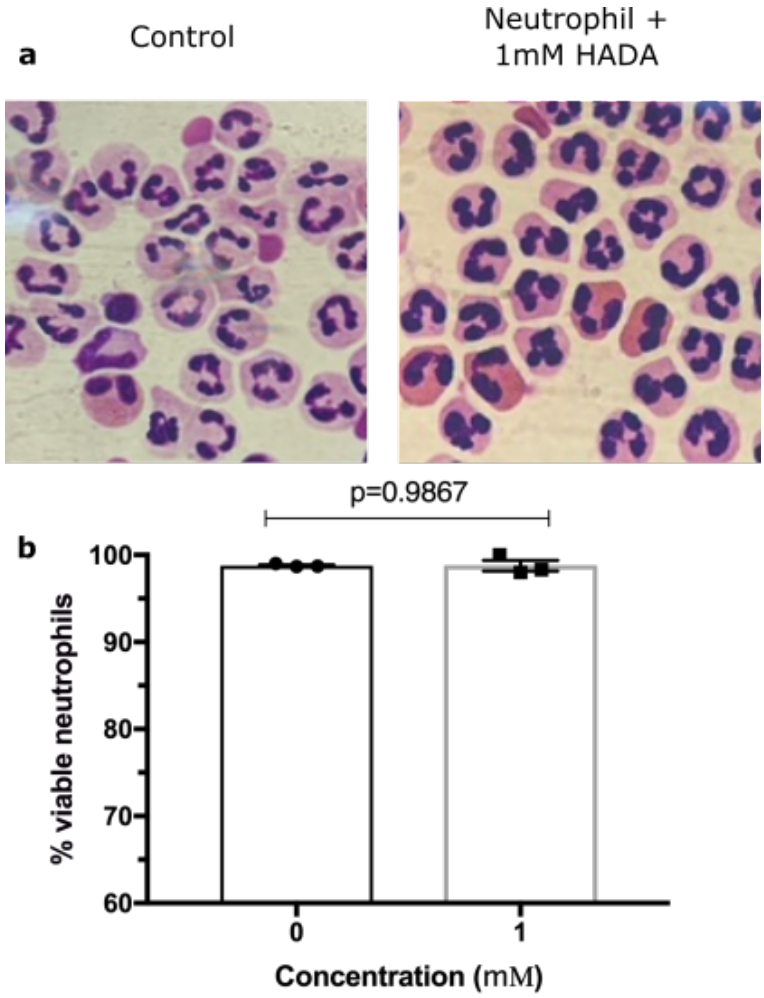

Fig. 5.8 **Neutrophil apoptosis assay.** a) Morphological assessment of neutrophils cultured in media as the control and 1mM HADA for 2h using light microscopy. b) The percentage of viable neutrophils between media control and 1 mM HADA treatment. Data shown is the mean with standard error mean of 3 independent experiments, and statistical analysis was performed by paired t-test.

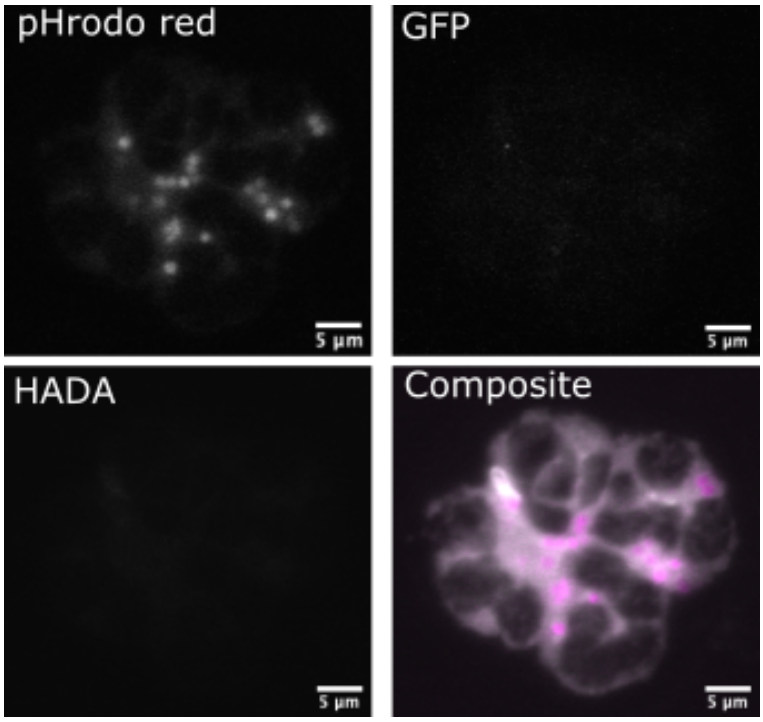

Fig. 5.9 **Fluorescence D-amino acid labelling of heat-killed *S. aureus in vivo*.** Neutrophils were co-infected with heat-killed pHrodo-labelled GFP-*S. aureus* (magenta) at an MOI of 5, followed by HADA labelling to probe new cell wall synthesis. HADA labelling is absent in heat-killed *S. aureus*, suggesting the lack of new cell wall synthesis. The neutrophil membranes were labelled with CellMask Deep Red plasma membrane label, and pHrodo red was false coloured with magenta in the composite image. Image shown is the maximum z-intensity projection, with background corrections performed on Fiji plug-in using a rolling-ball radius of 50.0 pixels.

5.4 Discussion

Our implementation of a multi-modal imaging platform enabled super-resolution live imaging of human neutrophils, revealing the dynamics of intracellular *S. aureus* within neutrophils. Using GFP-*S. aureus* labelled with pHrodo red revealed the presence of *S. aureus* in acidified and non-acidified neutrophil compartments, suggesting that a population of live *S. aureus* were able to resist acidification in neutrophil phagosome. Additionally, septum-like structures in green *S. aureus* was revealed by a structured-illumination modality. This suggests that *S. aureus* within non-acidified compartments

undergo cell division within the neutrophils. To further investigate this, a novel application of fluorescence D-amino acid labelling approach in human neutrophils was used, which revealed intracellular *S. aureus* dynamics within neutrophils. Our data showed that fluorescence D-amino acid labels are permeable to neutrophil membrane, enabling their incorporation to live intracellular bacteria. Furthermore, we confirmed that the fluorescence D-amino acid labelling approach does not compromise neutrophil viabilty.

The presence of fluorescence D-amino acid labelling in live *S. aureus in vivo* indicate that intracellular *S. aureus* are growing, and new cell walls are being synthesised within neutrophils. This was further confirm by the absence of fluorescence D-amino acid labelling in heat-killed *S. aureus*, indicating the lack of growth and new cell wall synthesise in intracellular *S. aureus*.

Together, using super-resolution live imaging and biochemical labelling approaches we show that live intracellular *S. aureus* in non-acidified compartments of neutrophils are growing as shown by new peptidoglycan cell wall synthesis occuring in the *S. aureus* within non-acidified compartments.

Chapter 6

Conclusion

6.1 Summary

Our understanding of neutrophil and *S. aureus* interactions remained nascent, hindered by the complexity of biological processes and the limitations in tools. Interdisciplinary effort that combine existing biological assays with techniques from other disciplines, such as imaging technologies, will enable us to gain insights into the neutrophil and *S. aureus* interactions. The work in this thesis involves the use of a high-throughput flow cytometry assay to investigate *S. aureus*- induced neutrophil cell death pathways, and the development of a novel imaging technique for multicolour and long-term live visualisation of *S. aureus* and neutrophil.

Candidate approach targeting *S. aureus*- induced neutrophil cell death pathway using Nec-1, NSA, IM-54 and GSK' 872, which are specific necrosis and necroptosis inhibitors did not enhance neutrophil-mediated killing of *S. aureus*. These findings were obtained by flow cytometry neutrophil cell death assay and intracellular killing assay, suggesting that *S. aureus*- induced neutrophil cell death may involve a novel pathway not attributable to necrosis or necroptosis. To complement the candidate approach, high-throughput flow cytometry assay to screen 800 compounds in the

Spectrum library was performed, and four compounds that reduced *S. aureus*- induced neutrophil cell death were identified. The identification of compounds with known anti-staphylococcal activities, for example antibiotics used in *S. aureus* infection treatments such as erythromycin and vancomycin validated the screen. Flow cytometry cell death assays showed that neutrophils treated with 4-APMA and marimastat have improved viability when co-infected with *S. aureus*. Yet, the neutrophils have reduced capability in terms of intracellular *S. aureus* killing in neutrophil intracellular killing assay. These findings suggest a potential role between MMP modulation and neutrophil intracellular *S. aureus* killing, where specific MMP is essential in neutrophil survival and intracellular bacterial killing function.

The delicateness of biological samples present a great challenge for the application of advanced imaging technologies to follow the subcellular processes in live cells. Therefore, a technique that involves switching between multi-point confocal and structured-illumination imaging modalities was developed to follow neutrophil and *S. aureus* dynamics at the subcellular level. The development stages of a multicolour, long-term live imaging method to visualise neutrophil and *S. aureus* presented in this work involves:

1. Epifluorescence microscopy
2. Super Resolution Radial Fluctuation (SRRF)
3. Confocal laser scanning with Airyscan
4. Linear structured-illumination microscopy
5. Multi-point confocal imaging
6. 2D novel form of structured-illumination live imaging
7. 3D multicolour structured-illumination live imaging

Applying the multimodal imaging system allows us to control the illumination power required for different modalities reduced the risk of photodamage. For example, imaging samples using high illumination power modalities such as structured-illumination may introduce photodamage and reduce the duration of live imaging. Therefore, this imaging platform allows us to switch between different illumination requirements of respective modalities in real time to enable long-term live imaging of neutrophil and *S. aureus*, as well as following the subcellular interactions in live neutrophils. Furthermore, the localisation of *S. aureus* within neutrophils can be achieved due to the ability to perform 3D imaging in confocal and structured-illumination modalities respectively.

The ability to perform multicolour live imaging of neutrophil and *S. aureus* using the multimodal imaging platform revealed heterogeneity of *S. aureus* within single neutrophils, as shown in chapter 5. Moreover, septum-like structures in *S. aureus* that are within non-acidified compartments were observed using structured-illumination modality, but not diffraction-limited multi-point confocal modality. This observation suggests that *S. aureus* may undergo, or have undergone cell division within neutrophils. Additionally, this showed that using super-resolution modality to follow *S. aureus* and neutrophil dynamics at subcellular level leads to interesting new observations.

6.2 Limitations

General limitations of the work in this thesis is that the inability to genetically manipulate primary human neutrophils limits the type of fluorescent probes, as well as applicable super resolution modalities. For example, labelling of specific neutrophil receptors using genetically-encoded fluorescent tags will allow better understanding of *S. aureus* and neutrophil interactions. Furthermore, the ability to genetically-encoded fluorescent tags will provide improved flexibility in multicolour imaging, as fluorophores with different spectral range and photostability can be explored to provide

the best results for live imaging (Thorn, 2017). Moreover, the restricted selection fluorescent probes in neutrophil limits the ability to observe subcellular interactions using modalities with higher resolutions, such as PALM is challenging, as it requires specialised fluorophores that can be photoactivated (Sydor et al., 2015).

The advantage of using primary human neutrophils is that it serves as a better model for understanding neutrophil and *S. aureus* interactions. Alternative models such as neutrophil-like cell lines HL-60 are commonly used to study neutrophil differentiation processes, but these cell lines lacked the antimicrobial properties of primary human neutrophils, thus inadequate for the purpose of studying host-pathogen interactions (Yaseen et al., 2017). Additionally, species tropism is an issue in host-pathogen interaction studies. For example, *S. aureus* toxins like LukAB only binds specifically to human receptors CD11b that is absent in mice models (Boguslawski et al., 2020). Thus, using primary human neutrophils overcome host tropism issues that may arise using alternative models.

6.3 Future work

The observation of *S. aureus* heterogeneity observed in this thesis showed that variation exists among individual bacterial within a single host cell. Therefore, future work could involve investigations to understand *S. aureus* dynamics within a single neutrophil.

Often, bacterial dynamics within host cells are studied as a whole population, but the behaviour of a single bacteria in a host cell could give rise to unintended consequences. How this heterogeneity relates to *S. aureus* survival within neutrophil, and the mechanisms that contributes to this variation are unknown.

A targeted approach can be used to further understand the *S. aureus* heterogeneity within single neutrophils. Briefly, selected *S. aureus* mutants, for example *S. aureus* ClpP strain that was shown to attenuate neutrophil cell death can be used to determine

whether the heterogeneity persists within neutrophils. Furthermore, an unbiased approach can be carried out to complement the targeted approach. This can be done by identifying the determinants of *S. aureus* variation in acidic and non-acidic compartments within neutrophils using a genome-wide screen of *S. aureus* mutant library, such as the Nebraska Transposon Mutant Library (NTML) (Yang et al., 2019). Alternatively, co-infection of neutrophils and pHrodo-labelled *S. aureus* mutants, combined with high content screening microscopy to screen *S. aureus* mutant library could allow the discovery of mutations that can collapse the *S. aureus* heterogeneity within neutrophils. Once mutant(s) are identified, assays such genetic complementation can be used to assess the selected mutants. It is also possible that the *S. aureus* heterogeneity within single neutrophil involves multiple genes, and this can be further interrogate using techniques such as real-time polymerase chain reaction (RT-PCR). Besides, RT-PCR could potentially reveal different levels of gene expression involved in the heterogenous phenotype.

To further probe the *S. aureus* heterogeneity and neutrophil dynamics, for example to investigate whether the lack of heterogeneity within neutrophils can alter the bacterial susceptibility to neutrophil killing, neutrophil intracellular killing assays can be performed. Fluorescence microscopy to visualise samples using GFP-labelled *S. aureus* strains, or live/dead bacterial viability kit, fixed at specific timepoints can be applied for further confirmation. Eventually, the multimodal imaging system presented in this thesis can be applied to observe long term live *S. aureus* within neutrophil at high resolution as further confirmation. Additionally, the flexibility of this imaging platform also present new grounds for technology development. For example, the system can be programmed to selectively visualise an area of interest in live cells 6.1. One proof of principle that can be performed is by visualising neutrophils that contain *S. aureus* at high resolution, while the surrounding areas with neutrophils only

is visualised at confocal or widefield mode using lower laser illumination. This can effectively reduce the overall photobleaching of samples. Furthermore, this selective targeting can be used to train a machine learning model to automate switching between imaging modalities. Alternatively, machine learning can be applied such that switching imaging modality is based on a change in an event, instead of a specific timepoint.

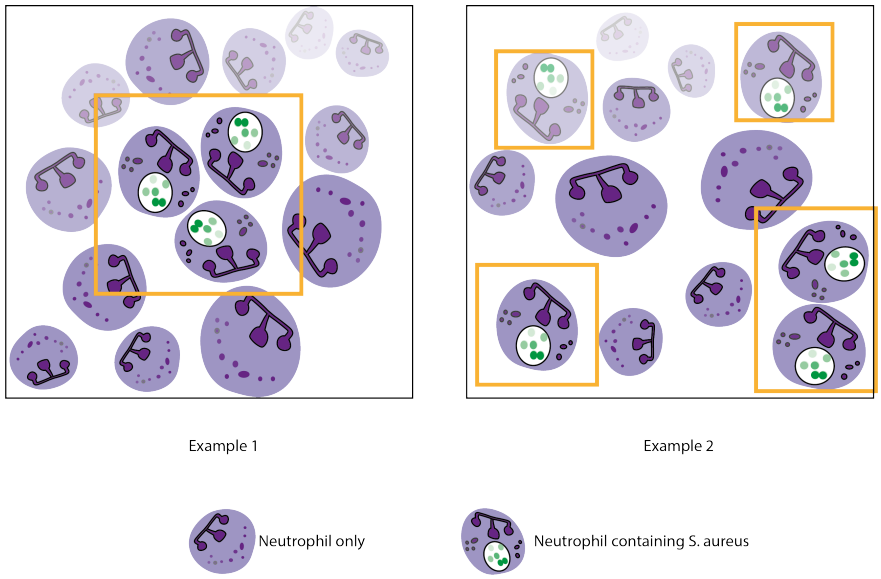

Fig. 6.1 **Selective illumination by multimodal system.** The multimodal imaging platform can be applied to perform selective illumination, in which area with neutrophils containing *S. aureus* is visualised at structured-illumination modality (orange boxes) to follow the intracellular bacterial dynamics at subcellular level, whereas the non bacterial-containing neutrophils are visualised in diffraction-limited modalities such as widefield modality using lower light illumination. This method of imaging will effectively lower the overall photobleaching of samples.

References

Abbe, E. (1873). Beiträge zur Theorie des Mikroskops und der mikroskopischen Wahrnehmung. Archiv für Mikroskopische Anatomie *9*, 413–468.

Aleyasin, H., Karuppagounder, S. S., Kumar, A., Sleiman, S., Basso, M., Ma, T., Siddiq, A., Chinta, S. J., Brochier, C., Langley, B., Haskew-Layton, R., Bane, S. L., Riggins, G. J., Gazaryan, I., Starkov, A. A., Andersen, J. K. and Ratan, R. R. (2015). Antihelminthic Benzimidazoles Are Novel HIF Activators That Prevent Oxidative Neuronal Death *via* Binding to Tubulin. Antioxidants & Redox Signaling *22*, 121–134.

Allen, L.-A. H. (2014). Immunofluorescence and Confocal Microscopy of Neutrophils. In Neutrophil Methods and Protocols, (Quinn, M. T. and DeLeo, F. R., eds), vol. 1124, pp. 251–268. Humana Press Totowa, NJ.

Bainton, D. F. (1971). The development of neutrophilic polymorphonuclear leukocytes in human bone marrow. Journal of Experimental Medicine *134*, 907–934.

Beavers, W. N. and Skaar, E. P. (2016). Neutrophil-generated oxidative stress and protein damage in *Staphylococcus aureus*. Pathogens and Disease *74*, ftw060.

Begleiter, A., Mowat, M., Israels, L. G. and Johnston, J. B. (1996). Chlorambucil in Chronic Lymphocytic Leukemia: Mechanism of Action. Leukemia & Lymphoma *23*, 187–201.

Berends, E. T. M., Zheng, X., Zwack, E. E., Ménager, M. M., Cammer, M., Shopsin, B. and Torres, V. J. (2019). *Staphylococcus aureus* Impairs the Function of and Kills Human Dendritic Cells via the LukAB Toxin. mBio *10*.

Berube, B. and Wardenburg, J. (2013). Staphylococcus aureus a-Toxin: Nearly a Century of Intrigue. Toxins *5*, 1140–1166.

Betzig, E., Patterson, G. H., Sougrat, R., Lindwasser, O. W., Olenych, S., Bonifacino, J. S., Davidson, M. W., Lippincott-Schwartz, J. and Hess, H. F. (2006). Imaging Intracellular Fluorescent Proteins at Nanometer Resolution. Science *313*, 1642–1645.

Blacker, T. S., Mann, Z. F., Gale, J. E., Ziegler, M., Bain, A. J., Szabadkai, G. and Duchen, M. R. (2014). Separating NADH and NADPH fluorescence in live cells and tissues using FLIM. Nature Communications *5*.

Boguslawski, K. M., McKeown, A. N., Day, C. J., Lacey, K. A., Tam, K., Vozhilla, N., Kim, S. Y., Jennings, M. P., Koralov, S. B., Elde, N. C. and Torres, V. J. (2020). Exploiting species specificity to understand the tropism of a human-specific toxin. Science Advances *6*, eaax7515.

Botos, I., Liu, L., Wang, Y., Segal, D. M. and Davies, D. R. (2009). The Toll-like receptor 3:dsRNA signaling complex. Biochimica et Biophysica Acta (BBA) - Gene Regulatory Mechanisms *1789*, 667–674.

Bottanelli, F., Kromann, E. B., Allgeyer, E. S., Erdmann, R. S., Wood Baguley, S., Sirinakis, G., Schepartz, A., Baddeley, D., Toomre, D. K., Rothman, J. E. and Bewersdorf, J. (2016). Two-colour live-cell nanoscale imaging of intracellular targets. Nature Communications *7*.

Bowker, K. E., Noel, A. R. and MacGowan, A. P. (2008). Pharmacodynamics of Minocycline against Staphylococcus aureus in an In Vitro Pharmacokinetic Model. Antimicrobial Agents and Chemotherapy *52*, 4370–4373.

Boyle-Vavra, S. and Daum, R. S. (2007). Community-acquired methicillin-resistant Staphylococcus aureus: the role of Panton–Valentine leukocidin. Laboratory Investigation *87*, 3–9.

Brinkmann, V. (2018). Neutrophil Extracellular Traps in the Second Decade. Journal of Innate Immunity *10*, 414–421.

Bronner, S., Monteil, H. and Prévost, G. (2004). Regulation of virulence determinants in *Staphylococcus aureus* : complexity and applications. FEMS Microbiology Reviews *28*, 183–200.

Bubeck Wardenburg, J., Bae, T., Otto, M., DeLeo, F. R. and Schneewind, O. (2007). Poring over pores: a-hemolysin and Panton-Valentine leukocidin in Staphylococcus aureus pneumonia. Nature Medicine *13*, 1405–1406.

Bubeck Wardenburg, J., Williams, W. A. and Missiakas, D. (2006). Host defenses against Staphylococcus aureus infection require recognition of bacterial lipoproteins. Proceedings of the National Academy of Sciences *103*, 13831–13836.

Carrington, W. A., Fogarty, K. E., Lifschitz, L. and Fay, F. S. (1990). Three-dimensional Imaging on Confocal and Wide-field Microscopes. In Handbook of Biological Confocal Microscopy, (Pawley, J. B., ed.), pp. 151–161. Springer US Boston, MA.

Chaili, S., Cheung, A. L., Bayer, A. S., Xiong, Y. Q., Waring, A. J., Memmi, G., Donegan, N., Yang, S.-J. and Yeaman, M. R. (2016). The GraS Sensor in Staphylococcus aureus Mediates Resistance to Host Defense Peptides Differing in Mechanisms of Action. Infection and Immunity *84*, 459–466.

Chakrabarti, S. (2005). Regulation of matrix metalloproteinase-9 release from IL-8-stimulated human neutrophils. Journal of Leukocyte Biology *78*, 279–288.

Chambers, H. F. and DeLeo, F. R. (2009). Waves of resistance: Staphylococcus aureus in the antibiotic era. Nature Reviews Microbiology *7*, 629–641.

Chang, J.-B., Chen, F., Yoon, Y.-G., Jung, E. E., Babcock, H., Kang, J. S., Asano, S., Suk, H.-J., Pak, N., Tillberg, P. W., Wassie, A. T., Cai, D. and Boyden, E. S. (2017). Iterative expansion microscopy. Nature Methods *14*, 593–599.

Chazotte, B. (2011). Labeling Nuclear DNA Using DAPI. Cold Spring Harbor Protocols *2011*, pdb.prot5556–pdb.prot5556.

Chen, B.-C., Legant, W. R., Wang, K., Shao, L., Milkie, D. E., Davidson, M. W., Janetopoulos, C., Wu, X. S., Hammer, J. A., Liu, Z., English, B. P., Mimori-Kiyosue, Y., Romero, D. P., Ritter, A. T., Lippincott-Schwartz, J., Fritz-Laylin, L., Mullins, R. D., Mitchell, D. M., Bembenek, J. N., Reymann, A.-C., Böhme, R., Grill, S. W., Wang, J. T., Seydoux, G., Tulu, U. S., Kiehart, D. P. and Betzig, E. (2014). Lattice light-sheet microscopy: Imaging molecules to embryos at high spatiotemporal resolution. Science *346*, 1257998.

Chen, F., Tillberg, P. W. and Boyden, E. S. (2015). Expansion microscopy. Science *347*, 543–548.

Cherla, R., Zhang, Y., Ledbetter, L. and Zhang, G. (2018). *Coxiella burnetii* Inhibits Neutrophil Apoptosis by Exploiting Survival Pathways and Antiapoptotic Protein Mcl-1. Infection and Immunity *86*, e00504–17.

Cheung, G. Y. C., Fisher, E. L., McCausland, J. W., Choi, J., Collins, J. W. M., Dickey, S. W. and Otto, M. (2018). Antimicrobial peptide resistance mechanism contributes to Staphylococcus aureus infection. The Journal of Infectious Diseases *0*.

Cho, J. S., Guo, Y., Ramos, R. I., Hebroni, F., Plaisier, S. B., Xuan, C., Granick, J. L., Matsushima, H., Takashima, A., Iwakura, Y., Cheung, A. L., Cheng, G., Lee, D. J., Simon, S. I. and Miller, L. S. (2012). Neutrophil-derived IL-1B Is Sufficient for Abscess Formation in Immunity against Staphylococcus aureus in Mice. PLoS Pathogens *8*, e1003047.

Combs, C. A. (2010). Fluorescence Microscopy: A Concise Guide to Current Imaging Methods. Current Protocols in Neuroscience *50*.

Conchello, J.-A. and Lichtman, J. W. (2005). Optical sectioning microscopy. Nature Methods *2*, 920–931.

Cowland, J. B. and Borregaard, N. (2016). Granulopoiesis and granules of human neutrophils. Immunological Reviews *273*, 11–28.

Culley, S., Albrecht, D., Jacobs, C., Pereira, P. M., Leterrier, C., Mercer, J. and Henriques, R. (2018a). Quantitative mapping and minimization of super-resolution optical imaging artifacts. Nature Methods *15*, 263–266.

Culley, S., Tosheva, K. L., Matos Pereira, P. and Henriques, R. (2018b). SRRF: Universal live-cell super-resolution microscopy. The International Journal of Biochemistry & Cell Biology *101*, 74–79.

Daigneault, M., Preston, J. A., Marriott, H. M., Whyte, M. K. B. and Dockrell, D. H. (2010). The Identification of Markers of Macrophage Differentiation in PMA-Stimulated THP-1 Cells and Monocyte-Derived Macrophages. PLoS ONE *5*, e8668.

Dancey, J. T., Deubelbeiss, K. A., Harker, L. A. and Finch, C. A. (1976). Neutrophil kinetics in man. Journal of Clinical Investigation *58*, 705–715.

David, M. Z., Boyle-Vavra, S., Zychowski, D. L. and Daum, R. S. (2011). Methicillin-Susceptible Staphylococcus aureus as a Predominantly Healthcare-Associated Pathogen: A Possible Reversal of Roles? PLoS ONE *6*, e18217.

de Jong, N. W. M., van Kessel, K. P. M. and van Strijp, J. A. G. (2019). Immune Evasion by Staphylococcus aureus. Microbiology Spectrum *7*.

Degterev, A., Hitomi, J., Germscheid, M., Ch'en, I. L., Korkina, O., Teng, X., Abbott, D., Cuny, G. D., Yuan, C., Wagner, G., Hedrick, S. M., Gerber, S. A., Lugovskoy, A. and Yuan, J. (2008). Identification of RIP1 kinase as a specific cellular target of necrostatins. Nature Chemical Biology *4*, 313–321.

Degterev, A., Huang, Z., Boyce, M., Li, Y., Jagtap, P., Mizushima, N., Cuny, G. D., Mitchison, T. J., Moskowitz, M. A. and Yuan, J. (2005). Chemical inhibitor of nonapoptotic cell death with therapeutic potential for ischemic brain injury. Nature Chemical Biology *1*, 112–119.

Delclaux, C., Delacourt, C., D'Ortho, M. P., Boyer, V., Lafuma, C. and Harf, A. (1996). Role of gelatinase B and elastase in human polymorphonuclear neutrophil migration across basement membrane. American Journal of Respiratory Cell and Molecular Biology *14*, 288–295.

DeLeo, F. R., Otto, M., Kreiswirth, B. N. and Chambers, H. F. (2010). Community-associated meticillin-resistant Staphylococcus aureus. The Lancet *375*, 1557–1568.

Dertinger, T., Colyer, R., Vogel, R., Heilemann, M., Sauer, M., Enderlein, J. and Weiss, S. (2012). Superresolution Optical Fluctuation Imaging (SOFI). In Nano-Biotechnology for Biomedical and Diagnostic Research, (Zahavy, E., Ordentlich, A., Yitzhaki, S. and Shafferman, A., eds), vol. 733, pp. 17–21. Springer Netherlands Dordrecht.

Dertinger, T., Pallaoro, A., Braun, G., Ly, S., Laurence, T. A. and Weiss, S. (2013). Advances in superresolution optical fluctuation imaging (SOFI). Quarterly Reviews of Biophysics *46*, 210–221.

Deurenberg, R. H. and Stobberingh, E. E. (2008). The evolution of Staphylococcus aureus. Infection, Genetics and Evolution *8*, 747–763.

Di Antonio, M., McLuckie, K. I. E. and Balasubramanian, S. (2014). Reprogramming the Mechanism of Action of Chlorambucil by Coupling to a G-Quadruplex Ligand. Journal of the American Chemical Society *136*, 5860–5863.

DuMont, A. L., Nygaard, T. K., Watkins, R. L., Smith, A., Kozhaya, L., Kreiswirth, B. N., Shopsin, B., Unutmaz, D., Voyich, J. M. and Torres, V. J. (2011). Characterization of a new cytotoxin that contributes to Staphylococcus aureus pathogenesis: The cytotoxin LukAB kills human phagocytes. Molecular Microbiology *79*, 814–825.

DuMont, A. L., Yoong, P., Surewaard, B. G. J., Benson, M. A., Nijland, R., van Strijp, J. A. G. and Torres, V. J. (2013). Staphylococcus aureus Elaborates Leukocidin AB To Mediate Escape from within Human Neutrophils. Infection and Immunity *81*, 1830–1841.

Edwards, A. M. and Massey, R. C. (2011). Invasion of Human Cells by a Bacterial Pathogen. Journal of Visualized Experiments , 2693.

Edwards, M. R., Pietzsch, C., Vausselin, T., Shaw, M. L., Bukreyev, A. and Basler, C. F. (2015). High-Throughput Minigenome System for Identifying Small-Molecule Inhibitors of Ebola Virus Replication. ACS Infectious Diseases *1*, 380–387.

Edwards, S. W. (1994). Biochemistry and Physiology of the Neutrophil. Cambridge University Press, Cambridge.

Eisenbeis, J., Saffarzadeh, M., Peisker, H., Jung, P., Thewes, N., Preissner, K. T., Herrmann, M., Molle, V., Geisbrecht, B. V., Jacobs, K. and Bischoff, M. (2018). The Staphylococcus aureus Extracellular Adherence Protein Eap Is a DNA Binding Protein Capable of Blocking Neutrophil Extracellular Trap Formation. Frontiers in Cellular and Infection Microbiology *8*.

El-Benna, J., Hurtado-Nedelec, M., Marzaioli, V., Marie, J.-C., Gougerot-Pocidalo, M.-A. and Dang, P. M.-C. (2016). Priming of the neutrophil respiratory burst: role in host defense and inflammation. Immunological Reviews *273*, 180–193.

Ellett, F., Jalali, F., Marand, A. L., Jorgensen, J., Mutlu, B. R., Lee, J., Raff, A. B. and Irimia, D. (2019). Microfluidic arenas for war games between neutrophils and microbes. Lab on a Chip *19*, 1205–1216.

Ettinger, A. and Wittmann, T. (2014). Fluorescence live cell imaging. In Methods in Cell Biology vol. 123, pp. 77–94. Elsevier.

Fabisiak, A., Murawska, N. and Fichna, J. (2016). LL-37: Cathelicidin-related antimicrobial peptide with pleiotropic activity. Pharmacological Reports *68*, 802–808.

Faurschou, M. and Borregaard, N. (2003). Neutrophil granules and secretory vesicles in inflammation. Microbes and Infection *5*, 1317–1327.

Flannagan, R. S., Kuiack, R. C., McGavin, M. J. and Heinrichs, D. E. (2018). *Staphylococcus aureus* Uses the GraXRS Regulatory System To Sense and Adapt to the Acidified Phagolysosome in Macrophages. mBio *9*.

Foote, J. R., Levine, A. P., Behe, P., Duchen, M. R. and Segal, A. W. (2017). Imaging the Neutrophil Phagosome and Cytoplasm Using a Ratiometric pH Indicator. Journal of Visualized Experiments *0*.

Forsgren, A. and Sjöquist, J. (1966). "Protein A" from S. aureus. I. Pseudo-immune reaction with human gamma-globulin. Journal of Immunology (Baltimore, Md.: 1950) *97*, 822–827.

Foster, T. J. (2005). Immune evasion by staphylococci. Nature Reviews Microbiology *3*, 948–958.

Foster, T. J., Geoghegan, J. A., Ganesh, V. K. and Höök, M. (2013). Adhesion, invasion and evasion: the many functions of the surface proteins of Staphylococcus aureus. Nature Reviews Microbiology *12*, 49–62.

Fox, S., Leitch, A. E., Duffin, R., Haslett, C. and Rossi, A. G. (2010). Neutrophil Apoptosis: Relevance to the Innate Immune Response and Inflammatory Disease. Journal of Innate Immunity *2*, 216–227.

Fricke, F., Beaudouin, J., Eils, R. and Heilemann, M. (2015). One, two or three? Probing the stoichiometry of membrane proteins by single-molecule localization microscopy. Scientific Reports *5*.

Galluzzi, L., Vitale, I., Aaronson, S. A., Abrams, J. M., Adam, D., Agostinis, P., Alnemri, E. S., Altucci, L., Amelio, I., Andrews, D. W., Annicchiarico-Petruzzelli, M., Antonov, A. V., Arama, E., Baehrecke, E. H., Barlev, N. A., Bazan, N. G., Bernassola, F., Bertrand, M. J. M., Bianchi, K., Blagosklonny, M. V., Blomgren, K., Borner, C., Boya, P., Brenner, C., Campanella, M., Candi, E., Carmona-Gutierrez, D., Cecconi, F., Chan, F. K.-M., Chandel, N. S., Cheng, E. H., Chipuk, J. E., Cidlowski, J. A., Ciechanover, A., Cohen, G. M., Conrad, M., Cubillos-Ruiz, J. R., Czabotar, P. E., D'Angiolella, V., Dawson, T. M., Dawson, V. L., De Laurenzi, V., De Maria, R., Debatin, K.-M., DeBerardinis, R. J., Deshmukh, M., Di Daniele, N., Di Virgilio, F., Dixit, V. M., Dixon, S. J., Duckett, C. S., Dynlacht, B. D., El-Deiry, W. S., Elrod, J. W., Fimia, G. M., Fulda, S., García-Sáez, A. J., Garg, A. D., Garrido, C., Gavathiotis, E., Golstein, P., Gottlieb, E., Green, D. R., Greene, L. A., Gronemeyer, H., Gross, A., Hajnoczky, G., Hardwick, J. M., Harris, I. S., Hengartner, M. O., Hetz, C., Ichijo, H., Jäättelä, M., Joseph, B., Jost, P. J., Juin, P. P., Kaiser, W. J., Karin, M., Kaufmann, T., Kepp, O., Kimchi, A., Kitsis, R. N., Klionsky, D. J., Knight, R. A., Kumar, S., Lee, S. W., Lemasters, J. J., Levine, B., Linkermann, A., Lipton, S. A., Lockshin, R. A., López-Otín, C., Lowe, S. W., Luedde, T., Lugli, E., MacFarlane, M., Madeo, F., Malewicz, M., Malorni, W., Manic, G., Marine, J.-C., Martin, S. J., Martinou, J.-C., Medema, J. P., Mehlen, P., Meier, P., Melino, S.,

Miao, E. A., Molkentin, J. D., Moll, U. M., Muñoz-Pinedo, C., Nagata, S., Nuñez, G., Oberst, A., Oren, M., Overholtzer, M., Pagano, M., Panaretakis, T., Pasparakis, M., Penninger, J. M., Pereira, D. M., Pervaiz, S., Peter, M. E., Piacentini, M., Pinton, P., Prehn, J. H., Puthalakath, H., Rabinovich, G. A., Rehm, M., Rizzuto, R., Rodrigues, C. M., Rubinsztein, D. C., Rudel, T., Ryan, K. M., Sayan, E., Scorrano, L., Shao, F., Shi, Y., Silke, J., Simon, H.-U., Sistigu, A., Stockwell, B. R., Strasser, A., Szabadkai, G., Tait, S. W., Tang, D., Tavernarakis, N., Thorburn, A., Tsujimoto, Y., Turk, B., Vanden Berghe, T., Vandenabeele, P., Vander Heiden, M. G., Villunger, A., Virgin, H. W., Vousden, K. H., Vucic, D., Wagner, E. F., Walczak, H., Wallach, D., Wang, Y., Wells, J. A., Wood, W., Yuan, J., Zakeri, Z., Zhivotovsky, B., Zitvogel, L., Melino, G. and Kroemer, G. (2018). Molecular mechanisms of cell death: recommendations of the Nomenclature Committee on Cell Death 2018. Cell Death & Differentiation *25*, 486–541.

Gardete, S. and Tomasz, A. (2014). Mechanisms of vancomycin resistance in Staphylococcus aureus. Journal of Clinical Investigation *124*, 2836–2840.

Geiger, T., Francois, P., Liebeke, M., Fraunholz, M., Goerke, C., Krismer, B., Schrenzel, J., Lalk, M. and Wolz, C. (2012). The Stringent Response of Staphylococcus aureus and Its Impact on Survival after Phagocytosis through the Induction of Intracellular PSMs Expression. PLoS Pathogens *8*, e1003016.

Genestier, A.-L., Michallet, M.-C., Prévost, G., Bellot, G., Chalabreysse, L., Peyrol, S., Thivolet, F., Etienne, J., Lina, G., Vallette, F. M., Vandenesch, F. and Genestier, L. (2005). Staphylococcus aureus Panton-Valentine leukocidin directly targets mitochondria and induces Bax-independent apoptosis of human neutrophils. Journal of Clinical Investigation *115*, 3117–3127.

Godin, A., Lounis, B. and Cognet, L. (2014). Super-resolution Microscopy Approaches for Live Cell Imaging. Biophysical Journal *107*, 1777–1784.

Goldblatt, D. and Thrasher, A. J. (2000). Chronic granulomatous disease. Immunodeficiency review. Clinical and Experimental Immunology *122*, 1–9.

Gordon, R. E. (2014). Electron Microscopy: A Brief History and Review of Current Clinical Application. In Histopathology, (Day, C. E., ed.), vol. 1180, pp. 119–135. Springer New York New York, NY. Series Title: Methods in Molecular Biology.

Goss, C. H. and Muhlebach, M. S. (2011). Review: Staphylococcus aureus and MRSA in cystic fibrosis. Journal of Cystic Fibrosis *10*, 298–306.

Gray, R. D., Hardisty, G., Regan, K. H., Smith, M., Robb, C. T., Duffin, R., Mackellar, A., Felton, J. M., Paemka, L., McCullagh, B. N., Lucas, C. D., Dorward, D. A., McKone, E. F., Cooke, G., Donnelly, S. C., Singh, P. K., Stoltz, D. A., Haslett, C., McCray, P. B., Whyte, M. K. B., Rossi, A. G. and Davidson, D. J. (2018). Delayed neutrophil apoptosis enhances NET formation in cystic fibrosis. Thorax *73*, 134–144.

Greenlee-Wacker, M. C., Kremserová, S. and Nauseef, W. M. (2017). Lysis of human neutrophils by community-associated methicillin-resistant *Staphylococcus aureus*. Blood *129*, 3237–3244.

Greenlee-Wacker, M. C., Rigby, K. M., Kobayashi, S. D., Porter, A. R., DeLeo, F. R. and Nauseef, W. M. (2014). Phagocytosis of Staphylococcus aureus by Human Neutrophils Prevents Macrophage Efferocytosis and Induces Programmed Necrosis. The Journal of Immunology *192*, 4709–4717.

Gregor, I. and Enderlein, J. (2019). Image scanning microscopy. Current Opinion in Chemical Biology *51*, 74–83.

Gresham, H. D., Lowrance, J. H., Caver, T. E., Wilson, B. S., Cheung, A. L. and Lindberg, F. P. (2000). Survival of Staphylococcus aureus Inside Neutrophils Contributes to Infection. The Journal of Immunology *164*, 3713–3722.

Grobelny, D., Poncz, L. and Galardy, R. E. (1992). Inhibition of human skin fibroblast collagenase, thermolysin, and Pseudomonas aeruginosa elastase by peptide hydroxamic acids. Biochemistry *31*, 7152–7154.

Guerra, F. E., Borgogna, T. R., Patel, D. M., Sward, E. W. and Voyich, J. M. (2017). Epic Immune Battles of History: Neutrophils vs. Staphylococcus aureus. Frontiers in Cellular and Infection Microbiology *7*.

Gustafsson, M. G. L. (2000). Surpassing the lateral resolution limit by a factor of two using structured illumination microscopy. SHORT COMMUNICATION. Journal of Microscopy *198*, 82–87.

Gustafsson, N., Culley, S., Ashdown, G., Owen, D. M., Pereira, P. M. and Henriques, R. (2016). Fast live-cell conventional fluorophore nanoscopy with ImageJ through super-resolution radial fluctuations. Nature Communications *7*, 12471.

Hammer, N. D. and Skaar, E. P. (2011). Molecular Mechanisms of *Staphylococcus aureus* Iron Acquisition. Annual Review of Microbiology *65*, 129–147.

Hamrick, T. S., Diaz, A. H., Havell, E. A., Horton, J. R. and Orndorff, P. E. (2003). Influence of Extracellular Bactericidal Agents on Bacteria within Macrophages. Infection and Immunity *71*, 1016–1019.

Hanley, Verveer, Gemkow, Arndt-Jovin and Jovin (1999). An optical sectioning programmable array microscope implemented with a digital micromirror device. Journal of Microscopy *196*, 317–331.

Harding, M. G., Zhang, K., Conly, J. and Kubes, P. (2014). Neutrophil Crawling in Capillaries; A Novel Immune Response to Staphylococcus aureus. PLoS Pathogens *10*, e1004379.

Haupt, K., Reuter, M., van den Elsen, J., Burman, J., Hälbich, S., Richter, J., Skerka, C. and Zipfel, P. F. (2008). The Staphylococcus aureus Protein Sbi Acts as a Complement Inhibitor and Forms a Tripartite Complex with Host Complement Factor H and C3b. PLoS Pathogens *4*, e1000250.

Hayashi, F. (2003). Toll-like receptors stimulate human neutrophil function. Blood *102*, 2660–2669.

Hell, S. W. (2009). Microscopy and its focal switch. Nature Methods *6*, 24–32.

Hell, S. W. and Wichmann, J. (1994). Breaking the diffraction resolution limit by stimulated emission: stimulated-emission-depletion fluorescence microscopy. Optics Letters *19*, 780.

Hellebrekers, P., Hietbrink, F., Vrisekoop, N., Leenen, L. P. H. and Koenderman, L. (2017). Neutrophil Functional Heterogeneity: Identification of Competitive Phagocytosis. Frontiers in Immunology *8*.

Henry, K. M., Loynes, C. A., Whyte, M. K. B. and Renshaw, S. A. (2013). Zebrafish as a model for the study of neutrophil biology. Journal of Leukocyte Biology *94*, 633–642.

Herdendorf, T. J. and Geisbrecht, B. V. (2018). Investigation of Human Neutrophil Elastase Inhibition by *Staphylococcus aureus* EapH1: The Key Role Played by Arginine 89. Biochemistry *57*, 6888–6896.

Herdendorf, T. J., Stapels, D. A., Rooijakkers, S. H. and Geisbrecht, B. V. (2020). Local structural plasticity of the *Staphylococcus aureus* evasion protein EapH1 enables engagement with multiple neutrophil serine proteases. Journal of Biological Chemistry *0*, jbc.RA120.013601.

Hoppenbrouwers, T., Sultan, A. R., Abraham, T. E., Lemmens-den Toom, N. A., Hansenová Maňásková, S., van Cappellen, W. A., Houtsmuller, A. B., van Wamel, W. J. B., de Maat, M. P. M. and van Neck, J. W. (2018). Staphylococcal Protein A Is a Key Factor in Neutrophil Extracellular Traps Formation. Frontiers in Immunology *9*.

Huang, B. (2010). Super-resolution optical microscopy: multiple choices. Current Opinion in Chemical Biology *14*, 10–14.

Huang, B., Bates, M. and Zhuang, X. (2009). Super-Resolution Fluorescence Microscopy. Annual Review of Biochemistry *78*, 993–1016.

Huff, J. (2015). The Airyscan detector from ZEISS: confocal imaging with improved signal-to-noise ratio and super-resolution. Nature Methods *12*, i–ii.

Huff, J. (2019). The Airyscan Detector: Confocal Microscopy Evolution for the Neurosciences. In Advanced Optical Methods for Brain Imaging, (Kao, F.-J., Keiser, G. and Gogoi, A., eds), vol. 5, pp. 83–102. Springer Singapore Singapore.

Huynh, M.-L. N., Fadok, V. A. and Henson, P. M. (2002). Phosphatidylserine-dependent ingestion of apoptotic cells promotes TGF-B1 secretion and the resolution of inflammation. Journal of Clinical Investigation *109*, 41–50.

Iba, T., Hashiguchi, N., Nagaoka, I., Tabe, Y. and Murai, M. (2013). Neutrophil cell death in response to infection and its relation to coagulation. Journal of Intensive Care *1*, 13.

Inoué, S. and Inoué, T. (2002). Direct-View High-Speed Confocal Scanner: The CSU-10. In Methods in Cell Biology vol. 70, pp. 87–127. Elsevier.

Introne, W., Boissy, R. E. and Gahl, W. A. (1999). Clinical, Molecular, and Cell Biological Aspects of Chediak–Higashi Syndrome. Molecular Genetics and Metabolism *68*, 283–303.

Itoh, S., Hamada, E., Kamoshida, G., Takeshita, K., Oku, T. and Tsuji, T. (2010). Staphylococcal Superantigen-Like Protein 5 Inhibits Matrix Metalloproteinase 9 from Human Neutrophils. Infection and Immunity *78*, 3298–3305.

J Cox, I., Sheppard, C. and Wilson, T. (1982). Super-resolution by confocal fluorescent microscopy. Optik - International Journal for Light and Electron Optics *60*, 391–396.

Jankowski, A. and Grinstein, S. (2002). Modulation of the Cytosolic and Phagosomal pH by the NADPH Oxidase. Antioxidants & Redox Signaling *4*, 61–68.

Jasper, A. E., McIver, W. J., Sapey, E. and Walton, G. M. (2019). Understanding the role of neutrophils in chronic inflammatory airway disease. F1000Research *8*, 557.

Jensen, E. C. (2013). Overview of Live-Cell Imaging: Requirements and Methods Used. The Anatomical Record: Advances in Integrative Anatomy and Evolutionary Biology *296*, 1–8.

Jin, T., Bokarewa, M., Foster, T., Mitchell, J., Higgins, J. and Tarkowski, A. (2004). Staphylococcus aureus resists human defensins by production of staphylokinase, a novel bacterial evasion mechanism. Journal of Immunology (Baltimore, Md.: 1950) *172*, 1169–1176.

Johnson, M. B. and Criss, A. K. (2013). Fluorescence microscopy methods for determining the viability of bacteria in association with mammalian cells. Journal of Visualized Experiments: JoVE .

Jubrail, J., Morris, P., Bewley, M. A., Stoneham, S., Johnston, S. A., Foster, S. J., Peden, A. A., Read, R. C., Marriott, H. M. and Dockrell, D. H. (2016). Inability to

sustain intraphagolysosomal killing of *Staphylococcus aureus* predisposes to bacterial persistence in macrophages: *S. aureus* killing by macrophages. Cellular Microbiology *18*, 80–96.

Jungmann, R., Avendaño, M. S., Woehrstein, J. B., Dai, M., Shih, W. M. and Yin, P. (2014). Multiplexed 3D cellular super-resolution imaging with DNA-PAINT and Exchange-PAINT. Nature Methods *11*, 313–318.

Jungmann, R., Steinhauer, C., Scheible, M., Kuzyk, A., Tinnefeld, P. and Simmel, F. C. (2010). Single-Molecule Kinetics and Super-Resolution Microscopy by Fluorescence Imaging of Transient Binding on DNA Origami. Nano Letters *10*, 4756–4761.

Kaiser, W. J., Sridharan, H., Huang, C., Mandal, P., Upton, J. W., Gough, P. J., Sehon, C. A., Marquis, R. W., Bertin, J. and Mocarski, E. S. (2013). Toll-like Receptor 3-mediated Necrosis via TRIF, RIP3, and MLKL. Journal of Biological Chemistry *288*, 31268–31279.

Karavolos, M. H. (2003). Role and regulation of the superoxide dismutases of Staphylococcus aureus. Microbiology *149*, 2749–2758.

Kennedy, A. D. and DeLeo, F. R. (2009). Neutrophil apoptosis and the resolution of infection. Immunologic Research *43*, 25–61.

Kim, T.-W. (2015). Drug Repositioning Approaches for the Discovery of New Therapeutics for Alzheimer's Disease. Neurotherapeutics *12*, 132–142.

Kitur, K., Parker, D., Nieto, P., Ahn, D. S., Cohen, T. S., Chung, S., Wachtel, S., Bueno, S. and Prince, A. (2015). Toxin-Induced Necroptosis Is a Major Mechanism of Staphylococcus aureus Lung Damage. PLOS Pathogens *11*, e1004820.

Kitur, K., Wachtel, S., Brown, A., Wickersham, M., Paulino, F., Peñaloza, H., Soong, G., Bueno, S., Parker, D. and Prince, A. (2016). Necroptosis Promotes Staphylococcus aureus Clearance by Inhibiting Excessive Inflammatory Signaling. Cell Reports *16*, 2219–2230.

Klebanoff, S. J. (2005). Myeloperoxidase: friend and foe. Journal of Leukocyte Biology *77*, 598–625.

Kobayashi, S. D., Braughton, K. R., Palazzolo-Ballance, A. M., Kennedy, A. D., Sampaio, E., Kristosturyan, E., Whitney, A. R., Sturdevant, D. E., Dorward, D. W., Holland, S. M., Kreiswirth, B. N., Musser, J. M. and DeLeo, F. R. (2010). Rapid Neutrophil Destruction following Phagocytosis of Staphylococcus aureus. Journal of Innate Immunity *2*, 560–575.

Kolaczkowska, E. and Kubes, P. (2013). Neutrophil recruitment and function in health and inflammation. Nature Reviews Immunology *13*, 159–175.

Kolenc, O. I. and Quinn, K. P. (2019). Evaluating Cell Metabolism Through Autofluorescence Imaging of NAD(P)H and FAD. Antioxidants & Redox Signaling *30*, 875–889.

Koymans, K., Bisschop, A., Vughs, M., van Kessel, K., de Haas, C. and van Strijp, J. (2016). Staphylococcal Superantigen-Like Protein 1 and 5 (SSL1 & SSL5) Limit Neutrophil Chemotaxis and Migration through MMP-Inhibition. International Journal of Molecular Sciences *17*, 1072.

Krismer, B., Weidenmaier, C., Zipperer, A. and Peschel, A. (2017). The commensal lifestyle of Staphylococcus aureus and its interactions with the nasal microbiota. Nature Reviews Microbiology *15*, 675–687.

Kubica, M., Guzik, K., Koziel, J., Zarebski, M., Richter, W., Gajkowska, B., Golda, A., Maciag-Gudowska, A., Brix, K., Shaw, L., Foster, T. and Potempa, J. (2008). A Potential New Pathway for Staphylococcus aureus Dissemination: The Silent Survival of S. aureus Phagocytosed by Human Monocyte-Derived Macrophages. PLoS ONE *3*, e1409.

Kuru, E., Hughes, H. V., Brown, P. J., Hall, E., Tekkam, S., Cava, F., dePedro, M. A., Brun, Y. V. and VanNieuwenhze, M. S. (2012). In Situ Probing of Newly Synthesized Peptidoglycan in Live Bacteria with Fluorescent-d -Amino Acids. Angewandte Chemie International Edition *51*, 12519–12523.

Kwiecinski, J. M. and Horswill, A. R. (2020). Staphylococcus aureus bloodstream infections: pathogenesis and regulatory mechanisms. Current Opinion in Microbiology *53*, 51–60.

Laarman, A. J., Mijnheer, G., Mootz, J. M., van Rooijen, W. J. M., Ruyken, M., Malone, C. L., Heezius, E. C., Ward, R., Milligan, G., van Strijp, J. A. G., de Haas, C. J. C., Horswill, A. R., van Kessel, K. P. M. and Rooijakkers, S. H. M. (2012). *Staphylococcus aureus* Staphopain A inhibits CXCR2-dependent neutrophil activation and chemotaxis: CXCR2 inhibition by Staphopain A. The EMBO Journal *31*, 3607–3619.

Laky, M., Sjöquist, J., Moraru, I. and Gheţie, V. (1985). Mutual inhibition of the binding of Clq and protein A to rabbit IgG immune complexes. Molecular Immunology *22*, 1297–1302.

Lawrence, S. M., Corriden, R. and Nizet, V. (2020). How Neutrophils Meet Their End. Trends in Immunology -.

Lee, A. S., de Lencastre, H., Garau, J., Kluytmans, J., Malhotra-Kumar, S., Peschel, A. and Harbarth, S. (2018). Methicillin-resistant Staphylococcus aureus. Nature Reviews Disease Primers *4*.

Levine, A. P., Duchen, M. R., de Villiers, S., Rich, P. R. and Segal, A. W. (2015). Alkalinity of Neutrophil Phagocytic Vacuoles Is Modulated by HVCN1 and Has Consequences for Myeloperoxidase Activity. PLOS ONE *10*, e0125906.

Lichtman, J. W. and Conchello, J.-A. (2005). Fluorescence microscopy. Nature Methods *2*, 910–919.

Lieschke, G. J., Oates, A. C., Crowhurst, M. O., Ward, A. C. and Layton, J. E. (2001). Morphologic and functional characterization of granulocytes and macrophages in embryonic and adult zebrafish. Blood *98*, 3087–3096.

Lin, M., Jackson, P., Tester, A. M., Diaconu, E., Overall, C. M., Blalock, J. E. and Pearlman, E. (2008). Matrix Metalloproteinase-8 Facilitates Neutrophil Migration through the Corneal Stromal Matrix by Collagen Degradation and Production of the Chemotactic Peptide Pro-Gly-Pro. The American Journal of Pathology *173*, 144–153.

Liu, G. Y., Essex, A., Buchanan, J. T., Datta, V., Hoffman, H. M., Bastian, J. F., Fierer, J. and Nizet, V. (2005). *Staphylococcus aureus* golden pigment impairs neutrophil killing and promotes virulence through its antioxidant activity. The Journal of Experimental Medicine *202*, 209–215.

Liu, T.-L., Upadhyayula, S., Milkie, D. E., Singh, V., Wang, K., Swinburne, I. A., Mosaliganti, K. R., Collins, Z. M., Hiscock, T. W., Shea, J., Kohrman, A. Q., Medwig, T. N., Dambournet, D., Forster, R., Cunniff, B., Ruan, Y., Yashiro, H., Scholpp, S., Meyerowitz, E. M., Hockemeyer, D., Drubin, D. G., Martin, B. L., Matus, D. Q., Koyama, M., Megason, S. G., Kirchhausen, T. and Betzig, E. (2018). Observing the cell in its native state: Imaging subcellular dynamics in multicellular organisms. Science *360*, eaaq1392.

Lodge, K. M., Cowburn, A. S., Li, W. and Condliffe, A. M. (2020). The Impact of Hypoxia on Neutrophil Degranulation and Consequences for the Host. International Journal of Molecular Sciences *21*, 1183.

Lu, T., Porter, A. R., Kennedy, A. D., Kobayashi, S. D. and DeLeo, F. R. (2014). Phagocytosis and Killing of ***Staphylococcus aureus*** by Human Neutrophils. Journal of Innate Immunity *6*, 639–649.

Lund, V. A., Wacnik, K., Turner, R. D., Cotterell, B. E., Walther, C. G., Fenn, S. J., Grein, F., Wollman, A. J., Leake, M. C., Olivier, N., Cadby, A., Mesnage, S., Jones, S. and Foster, S. J. (2018). Molecular coordination of Staphylococcus aureus cell division. eLife *7*.

Malachowa, N., Kobayashi, S. D., Freedman, B., Dorward, D. W. and DeLeo, F. R. (2013). Staphylococcus aureus Leukotoxin GH Promotes Formation of Neutrophil Extracellular Traps. The Journal of Immunology *191*, 6022–6029.

Mandal, P., Berger, S., Pillay, S., Moriwaki, K., Huang, C., Guo, H., Lich, J., Finger, J., Kasparcova, V., Votta, B., Ouellette, M., King, B., Wisnoski, D., Lakdawala, A., DeMartino, M., Casillas, L., Haile, P., Sehon, C., Marquis, R., Upton, J., Daley-Bauer, L., Roback, L., Ramia, N., Dovey, C., Carette, J., Chan, F.-M., Bertin, J., Gough, P., Mocarski, E. and Kaiser, W. (2014). RIP3 Induces Apoptosis Independent of Pronecrotic Kinase Activity. Molecular Cell *56*, 481–495.

Mandell, G. L. (1975). Catalase, superoxide dismutase, and virulence of Staphylococcus aureus. In vitro and in vivo studies with emphasis on staphylococcal–leukocyte interaction. Journal of Clinical Investigation *55*, 561–566.

Margraf, A., Ley, K. and Zarbock, A. (2019). Neutrophil Recruitment: From Model Systems to Tissue-Specific Patterns. Trends in Immunology *40*, 613–634.

Martin Thomas (2017). Optical Arrangement For Digital Micromirror Device.

Mayadas, T. N., Cullere, X. and Lowell, C. A. (2014). The Multifaceted Functions of Neutrophils. Annual Review of Pathology: Mechanisms of Disease *9*, 181–218.

McCracken, J. M. and Allen, L.-A. H. (2014). Regulation of Human Neutrophil Apoptosis and Lifespan in Health and Disease. Journal of Cell Death *7*, JCD.S11038.

McGuinness, W., Kobayashi, S. and DeLeo, F. (2016). Evasion of Neutrophil Killing by Staphylococcus aureus. Pathogens *5*, 32.

Menegazzi, R., Decleva, E. and Dri, P. (2012). Killing by neutrophil extracellular traps: fact or folklore? Blood *119*, 1214–1216.

Millar, A. W., Brown, P. D., Moore, J., Galloway, W. A., Cornish, A. G., Lenehan, T. J. and Lynch, K. P. (1998). Results of single and repeat dose studies of the oral matrix metalloproteinase inhibitor marimastat in healthy male volunteers. British Journal of Clinical Pharmacology *45*, 21–26.

Mitra, K. and Lippincott-Schwartz, J. (2010). Analysis of Mitochondrial Dynamics and Functions Using Imaging Approaches. Current Protocols in Cell Biology *46*.

Moore, K. L., Patel, K. D., Bruehl, R. E., Li, F., Johnson, D. A., Lichenstein, H. S., Cummings, R. D., Bainton, D. F. and McEver, R. P. (1995). P-selectin glycoprotein ligand-1 mediates rolling of human neutrophils on P-selectin. The Journal of Cell Biology *128*, 661–671.

Morel, F., Doussiere, J. and Vignais, P. V. (1991). The superoxide-generating oxidase of phagocytic cells. Physiological, molecular and pathological aspects. European Journal of Biochemistry *201*, 523–546.

Mulcahy, M. E. and McLoughlin, R. M. (2016). Host–Bacterial Crosstalk Determines Staphylococcus aureus Nasal Colonization. Trends in Microbiology *24*, 872–886.

Murdoch, C. and Finn, A. (2000). Chemokine receptors and their role in inflammation and infectious diseases. Blood *95*, 3032–3043.

Murphy, B. M., O'Neill, A. J., Adrain, C., Watson, R. W. G. and Martin, S. J. (2003). The Apoptosome Pathway to Caspase Activation in Primary Human Neutrophils Exhibits Dramatically Reduced Requirements for Cytochrome c. Journal of Experimental Medicine *197*, 625–632.

Müller, C. B. and Enderlein, J. (2010). Image Scanning Microscopy. Physical Review Letters *104*.

Müller, T., Schumann, C. and Kraegeloh, A. (2012). STED Microscopy and its Applications: New Insights into Cellular Processes on the Nanoscale. ChemPhysChem *13*, 1986–2000.

Navegantes, K. C., de Souza Gomes, R., Pereira, P. A. T., Czaikoski, P. G., Azevedo, C. H. M. and Monteiro, M. C. (2017). Immune modulation of some autoimmune diseases: the critical role of macrophages and neutrophils in the innate and adaptive immunity. Journal of Translational Medicine *15*.

Neubert, E., Meyer, D., Kruss, S. and Erpenbeck, L. (2020). The power from within – understanding the driving forces of neutrophil extracellular trap formation. Journal of Cell Science *133*, jcs241075.

Neubert, E., Meyer, D., Rocca, F., Günay, G., Kwaczala-Tessmann, A., Grandke, J., Senger-Sander, S., Geisler, C., Egner, A., Schön, M. P., Erpenbeck, L. and Kruss, S. (2018). Chromatin swelling drives neutrophil extracellular trap release. Nature Communications *9*.

Nguyen, G. T., Green, E. R. and Mecsas, J. (2017). Neutrophils to the ROScue: Mechanisms of NADPH Oxidase Activation and Bacterial Resistance. Frontiers in Cellular and Infection Microbiology *7*.

Niemann, S., Bertling, A., Brodde, M. F., Fender, A. C., Van de Vyver, H., Hussain, M., Holzinger, D., Reinhardt, D., Peters, G., Heilmann, C., Löffler, B. and Kehrel, B. E. (2018). Panton-Valentine Leukocidin associated with S. aureus osteomyelitis activates platelets via neutrophil secretion products. Scientific Reports *8*.

Nieuwenhuizen, R. P. J., Lidke, K. A., Bates, M., Puig, D. L., Grünwald, D., Stallinga, S. and Rieger, B. (2013). Measuring image resolution in optical nanoscopy. Nature Methods *10*, 557–562.

Nieves, D., Gaus, K. and Baker, M. (2018). DNA-Based Super-Resolution Microscopy: DNA-PAINT. Genes *9*, 621.

Nijnik, A. and Hancock, R. E. (2009). The roles of cathelicidin LL-37 in immune defences and novel clinical applications:. Current Opinion in Hematology *16*, 41–47.

Njoroge, J., Mitchell, L., Centola, M., Kastner, D., Raffeld, M. and Miller, J. (2001). Characterization of viable autofluorescent macrophages among cultured peripheral blood mononuclear cells. Cytometry *44*, 38–44.

Nordenfelt, P. and Tapper, H. (2011). Phagosome dynamics during phagocytosis by neutrophils. Journal of Leukocyte Biology *90*, 271–284.

Oliveira, D., Borges, A. and Simões, M. (2018). Staphylococcus aureus Toxins and Their Molecular Activity in Infectious Diseases. Toxins *10*, 252.

Oogai, Y., Matsuo, M., Hashimoto, M., Kato, F., Sugai, M. and Komatsuzawa, H. (2011). Expression of Virulence Factors by Staphylococcus aureus Grown in Serum. Applied and Environmental Microbiology *77*, 8097–8105.

O'Riordan, K. and Lee, J. C. (2004). Staphylococcus aureus Capsular Polysaccharides. Clinical Microbiology Reviews *17*, 218–234.

Otto, M. (2010). Basis of Virulence in Community-Associated Methicillin-Resistant *Staphylococcus aureus*. Annual Review of Microbiology *64*, 143–162.

Otto, M. (2013). Community-associated MRSA: What makes them special? International Journal of Medical Microbiology *303*, 324–330.

Ovesný, M., Křížek, P., Borkovec, J., Švindrych, Z. and Hagen, G. M. (2014). ThunderSTORM: a comprehensive ImageJ plug-in for PALM and STORM data analysis and super-resolution imaging. Bioinformatics *30*, 2389–2390.

Papayannopoulos, V., Metzler, K. D., Hakkim, A. and Zychlinsky, A. (2010). Neutrophil elastase and myeloperoxidase regulate the formation of neutrophil extracellular traps. The Journal of Cell Biology *191*, 677–691.

Papayannopoulos, V. and Zychlinsky, A. (2009). NETs: a new strategy for using old weapons. Trends in Immunology *30*, 513–521.

Peedikakkal, L. V., Furley, A. and Cadby, A. J. (2018). A Multimodal Adaptive Super-Resolution and Confocal Microscope. preprint Biophysics.

Peschel, A., Jack, R. W., Otto, M., Collins, L. V., Staubitz, P., Nicholson, G., Kalbacher, H., Nieuwenhuizen, W. F., Jung, G., Tarkowski, A., van Kessel, K. P. and van Strijp, J. A. (2001). *Staphylococcus aureus* Resistance to Human Defensins and Evasion of Neutrophil Killing via the Novel Virulence Factor Mprf Is Based on Modification of Membrane Lipids with l-Lysine. The Journal of Experimental Medicine *193*, 1067–1076.

Pilsczek, F. H., Salina, D., Poon, K. K. H., Fahey, C., Yipp, B. G., Sibley, C. D., Robbins, S. M., Green, F. H. Y., Surette, M. G., Sugai, M., Bowden, M. G., Hussain, M., Zhang, K. and Kubes, P. (2010). A Novel Mechanism of Rapid Nuclear Neutrophil

Extracellular Trap Formation in Response to Staphylococcus aureus. The Journal of Immunology *185*, 7413–7425.

Portlock, C. S., Fischer, D. S., Cadman, E., Lundberg, W. B., Levy, A., Bobrow, S., Bertino, J. R. and Farber, L. (1987). High-dose pulse chlorambucil in advanced, low-grade non-Hodgkin's lymphoma. Cancer Treatment Reports *71*, 1029–1031.

Postma, B., Poppelier, M. J., van Galen, J. C., Prossnitz, E. R., van Strijp, J. A. G., de Haas, C. J. C. and van Kessel, K. P. M. (2004). Chemotaxis inhibitory protein of Staphylococcus aureus binds specifically to the C5a and formylated peptide receptor. Journal of Immunology (Baltimore, Md.: 1950) *172*, 6994–7001.

Prajsnar, T. K., Cunliffe, V. T., Foster, S. J. and Renshaw, S. A. (2008). A novel vertebrate model of *Staphylococcus aureus* infection reveals phagocyte-dependent resistance of zebrafish to non-host specialized pathogens. Cellular Microbiology *10*, 2312–2325.

Prajsnar, T. K., Hamilton, R., Garcia-Lara, J., McVicker, G., Williams, A., Boots, M., Foster, S. J. and Renshaw, S. A. (2012). A privileged intraphagocyte niche is responsible for disseminated infection of *Staphylococcus aureus* in a zebrafish model: Modelling *S. aureus* infection in zebrafish. Cellular Microbiology *14*, 1600–1619.

Prajsnar, T. K., Serba, J. J., Dekker, B. M., Gibson, J. F., Masud, S., Fleming, A., Johnston, S. A., Renshaw, S. A. and Meijer, A. H. (2020). The autophagic response to *Staphylococcus aureus* provides an intracellular niche in neutrophils. Autophagy *NA*, 1–15.

Prince, L. R., Prosseda, S. D., Higgins, K., Carlring, J., Prestwich, E. C., Ogryzko, N. V., Rahman, A., Basran, A., Falciani, F., Taylor, P., Renshaw, S. A., Whyte, M. K. B. and Sabroe, I. (2017). NR4A orphan nuclear receptor family members, NR4A2 and NR4A3, regulate neutrophil number and survival. Blood *130*, 1014–1025.

Progatzky, F., Dallman, M. J. and Lo Celso, C. (2013). From seeing to believing: labelling strategies for *in vivo* cell-tracking experiments. Interface Focus *3*, 20130001.

Rashidfarrokhi, A., Richina, V. and Tafesse, F. G. (2017). Visualizing the Early Stages of Phagocytosis. Journal of Visualized Experiments *0*.

Rayleigh, L. (1903). On the Theory of Optical Images, with special reference to the Microscope. Journal of the Royal Microscopical Society *23*, 474–482.

Reeves, E. P., Lu, H., Jacobs, H. L., Messina, C. G. M., Bolsover, S., Gabella, G., Potma, E. O., Warley, A., Roes, J. and Segal, A. W. (2002). Killing activity of neutrophils is mediated through activation of proteases by K+ flux. Nature *416*, 291–297.

Rempel, S. A. and Mikkelsen, T. (2006). Tumor Invasiveness and Anti-invasion Strategies. In Handbook of Brain Tumor Chemotherapy pp. 193–218. Elsevier.

Rigby, K. M. and DeLeo, F. R. (2012). Neutrophils in innate host defense against Staphylococcus aureus infections. Seminars in Immunopathology *34*, 237–259.

Rock, K. L. and Kono, H. (2008). The Inflammatory Response to Cell Death. Annual Review of Pathology: Mechanisms of Disease *3*, 99–126.

Rosenfeldt, M., Valentino, M., Labruzzo, S., Scudder, L., Pavlaki, M., Cao, J., Vacirca, J., Bahou, W. and Zucker, S. (2005). The organomercurial 4-aminophenylmercuric acetate, independent of matrix metalloproteinases, induces dose-dependent activation/ inhibition of platelet aggregation. Thrombosis and Haemostasis *93*, 326–330.

Rust, M. J., Bates, M. and Zhuang, X. (2006). Sub-diffraction-limit imaging by stochastic optical reconstruction microscopy (STORM). Nature Methods *3*, 793–796.

Sabroe, I., Prince, L. R., Jones, E. C., Horsburgh, M. J., Foster, S. J., Vogel, S. N., Dower, S. K. and Whyte, M. K. B. (2003). Selective Roles for Toll-Like Receptor (TLR)2 and TLR4 in the Regulation of Neutrophil Activation and Life Span. The Journal of Immunology *170*, 5268–5275.

Sanderson, M. J., Smith, I., Parker, I. and Bootman, M. D. (2014). Fluorescence Microscopy. Cold Spring Harbor Protocols *2014*, pdb.top071795–pdb.top071795.

Sandri, A., Ortombina, A., Boschi, F., Cremonini, E., Boaretti, M., Sorio, C., Melotti, P., Bergamini, G. and Lleo, M. (2018). Inhibition of *Pseudomonas aeruginosa* secreted virulence factors reduces lung inflammation in CF mice. Virulence *9*, 1008–1018.

Saraiva, B. M., Sorg, M., Pereira, A. R., Ferreira, M. J., Caulat, L. C., Reichmann, N. T. and Pinho, M. G. (2020). Reassessment of the distinctive geometry of Staphylococcus aureus cell division. Nature Communications *11*.

Sarkar, A., Hellberg, L., Bhattacharyya, A., Behnen, M., Wang, K., Lord, J. M., Möller, S., Kohler, M., Solbach, W. and Laskay, T. (2012). Infection with Anaplasma phagocytophilum Activates the Phosphatidylinositol 3-Kinase/Akt and NF-kB Survival Pathways in Neutrophil Granulocytes. Infection and Immunity *80*, 1615–1623.

Sarma, J. V. and Ward, P. A. (2011). The complement system. Cell and Tissue Research *343*, 227–235.

Savill, J. S., Wyllie, A. H., Henson, J. E., Walport, M. J., Henson, P. M. and Haslett, C. (1989). Macrophage phagocytosis of aging neutrophils in inflammation. Programmed cell death in the neutrophil leads to its recognition by macrophages. Journal of Clinical Investigation *83*, 865–875.

Schermelleh, L., Ferrand, A., Huser, T., Eggeling, C., Sauer, M., Biehlmaier, O. and Drummen, G. P. C. (2019). Super-resolution microscopy demystified. Nature Cell Biology *21*, 72–84.

Schindelin, J., Arganda-Carreras, I., Frise, E., Kaynig, V., Longair, M., Pietzsch, T., Preibisch, S., Rueden, C., Saalfeld, S., Schmid, B., Tinevez, J.-Y., White, D. J., Hartenstein, V., Eliceiri, K., Tomancak, P. and Cardona, A. (2012). Fiji: an open-source platform for biological-image analysis. Nature Methods *9*, 676–682.

Schnitzbauer, J., Strauss, M. T., Schlichthaerle, T., Schueder, F. and Jungmann, R. (2017). Super-resolution microscopy with DNA-PAINT. Nature Protocols *12*, 1198–1228.

Schwartz, J., Leidal, K. G., Femling, J. K., Weiss, J. P. and Nauseef, W. M. (2009). Neutrophil Bleaching of GFP-Expressing Staphylococci: Probing the Intraphagosomal Fate of Individual Bacteria. The Journal of Immunology *183*, 2632–2641.

Schönbeck, U., Mach, F. and Libby, P. (1998). Generation of biologically active IL-1 beta by matrix metalloproteinases: a novel caspase-1-independent pathway of IL-1 beta processing. Journal of Immunology (Baltimore, Md.: 1950) *161*, 3340–3346.

Segal, A. W., Dorling, J. and Coade, S. (1980). Kinetics of fusion of the cytoplasmic granules with phagocytic vacuoles in human polymorphonuclear leukocytes. Biochemical and morphological studies. The Journal of Cell Biology *85*, 42–59.

Seilie, E. S. and Bubeck Wardenburg, J. (2017). Staphylococcus aureus pore-forming toxins: The interface of pathogen and host complexity. Seminars in Cell & Developmental Biology *72*, 101–116.

Semerad, C. L., Liu, F., Gregory, A. D., Stumpf, K. and Link, D. C. (2002). G-CSF is an essential regulator of neutrophil trafficking from the bone marrow to the blood. Immunity *17*, 413–423.

Sharonov, A. and Hochstrasser, R. M. (2006). Wide-field subdiffraction imaging by accumulated binding of diffusing probes. Proceedings of the National Academy of Sciences *103*, 18911–18916.

Sheshachalam, A., Srivastava, N., Mitchell, T., Lacy, P. and Eitzen, G. (2014). Granule Protein Processing and Regulated Secretion in Neutrophils. Frontiers in Immunology *5*.

Siegrist, M. S., Whiteside, S., Jewett, J. C., Aditham, A., Cava, F. and Bertozzi, C. R. (2013). d -Amino Acid Chemical Reporters Reveal Peptidoglycan Dynamics of an Intracellular Pathogen. ACS Chemical Biology *8*, 500–505.

Sieprawska-Lupa, M., Mydel, P., Krawczyk, K., Wojcik, K., Puklo, M., Lupa, B., Suder, P., Silberring, J., Reed, M., Pohl, J., Shafer, W., McAleese, F., Foster, T., Travis, J. and Potempa, J. (2004). Degradation of Human Antimicrobial Peptide LL-37 by Staphylococcus aureus-Derived Proteinases. Antimicrobial Agents and Chemotherapy *48*, 4673–4679.

Simons, M. P., Nauseef, W. M., Griffith, T. S. and Apicella, M. A. (2006). Neisseria gonorrhoeae delays the onset of apoptosis in polymorphonuclear leukocytes. Cellular Microbiology *8*, 1780–1790.

Smigiel, K. S. and Parks, W. C. (2017). Matrix Metalloproteinases and Leukocyte Activation. In Progress in Molecular Biology and Translational Science vol. 147, pp. 167–195. Elsevier.

Sodeoka, M. and Dodo, K. (2010). Development of selective inhibitors of necrosis. The Chemical Record *10*, 308–314.

Soehnlein, O., Steffens, S., Hidalgo, A. and Weber, C. (2017). Neutrophils as protagonists and targets in chronic inflammation. Nature Reviews Immunology *17*, 248–261.

St. Croix, C. M., Shand, S. H. and Watkins, S. C. (2005). Confocal microscopy: comparisons, applications, and problems. BioTechniques *39*, S2–S5.

Stapels, D. A. C., Ramyar, K. X., Bischoff, M., von Kockritz-Blickwede, M., Milder, F. J., Ruyken, M., Eisenbeis, J., McWhorter, W. J., Herrmann, M., van Kessel, K. P. M., Geisbrecht, B. V. and Rooijakkers, S. H. M. (2014). Staphylococcus aureus secretes a unique class of neutrophil serine protease inhibitors. Proceedings of the National Academy of Sciences *111*, 13187–13192.

Steele, A. J., Prentice, A. G., Hoffbrand, A. V., Yogashangary, B. C., Hart, S. M., Nacheva, E. P., Howard-Reeves, J. D., Duke, V. M., Kottaridis, P. D., Cwynarski, K., Vassilev, L. T. and Wickremasinghe, R. G. (2008). p53-mediated apoptosis of CLL cells: evidence for a transcription-independent mechanism. Blood *112*, 3827–3834.

Stephan, T., Roesch, A., Riedel, D. and Jakobs, S. (2019). Live-cell STED nanoscopy of mitochondrial cristae. Scientific Reports *9*.

Stephens, D. J. (2003). Light Microscopy Techniques for Live Cell Imaging. Science *300*, 82–86.

Stryjewski, M. and Chambers, H. (2008). Skin and Soft-Tissue Infections Caused by Community-Acquired Methicillin-Resistant *Staphylococcus aureus*. Clinical Infectious Diseases *46*, S368–S377.

Summers, C., Rankin, S. M., Condliffe, A. M., Singh, N., Peters, A. M. and Chilvers, E. R. (2010). Neutrophil kinetics in health and disease. Trends in Immunology *31*, 318–324.

Surewaard, B. G. J., de Haas, C. J. C., Vervoort, F., Rigby, K. M., DeLeo, F. R., Otto, M., van Strijp, J. A. G. and Nijland, R. (2013). Staphylococcal alpha-phenol soluble modulins contribute to neutrophil lysis after phagocytosis: *S. aureus* a-PSMs lyse neutrophils from within. Cellular Microbiology *15*, 1427–1437.

Sydor, A. M., Czymmek, K. J., Puchner, E. M. and Mennella, V. (2015). Super-Resolution Microscopy: From Single Molecules to Supramolecular Assemblies. Trends in Cell Biology *25*, 730–748.

Tam, K. and Torres, V. J. (2019). Staphylococcus aureus Secreted Toxins and Extracellular Enzymes. Microbiology Spectrum *7*.

Tangy, F., Moukkadem, M., Vindimian, E., Capmau, M.-L. and Goffic, F. (1985). Mechanism of action of gentamicin components. Characteristics of their binding to Escherichia coli ribosomes. European Journal of Biochemistry *147*, 381–386.

Tester, A. M., Cox, J. H., Connor, A. R., Starr, A. E., Dean, R. A., Puente, X. S., López-Otín, C. and Overall, C. M. (2007). LPS Responsiveness and Neutrophil Chemotaxis In Vivo Require PMN MMP-8 Activity. PLoS ONE *2*, e312.

Thakker, M., Park, J. S., Carey, V. and Lee, J. C. (1998). Staphylococcus aureus serotype 5 capsular polysaccharide is antiphagocytic and enhances bacterial virulence in a murine bacteremia model. Infection and Immunity *66*, 5183–5189.

Thammavongsa, V., Kim, H. K., Missiakas, D. and Schneewind, O. (2015). Staphylococcal manipulation of host immune responses. Nature Reviews Microbiology *13*, 529–543.

Thammavongsa, V., Missiakas, D. M. and Schneewind, O. (2013). Staphylococcus aureus Degrades Neutrophil Extracellular Traps to Promote Immune Cell Death. Science *342*, 863–866.

Thiam, H. R., Wong, S. L., Qiu, R., Kittisopikul, M., Vahabikashi, A., Goldman, A. E., Goldman, R. D., Wagner, D. D. and Waterman, C. M. (2020). NETosis proceeds by cytoskeleton and endomembrane disassembly and PAD4-mediated chromatin decondensation and nuclear envelope rupture. Proceedings of the National Academy of Sciences *117*, 7326–7337.

Thorn, K. (2017). Genetically encoded fluorescent tags. Molecular Biology of the Cell *28*, 848–857.

Tong, S. Y. C., Davis, J. S., Eichenberger, E., Holland, T. L. and Fowler, V. G. (2015). Staphylococcus aureus Infections: Epidemiology, Pathophysiology, Clinical Manifestations, and Management. Clinical Microbiology Reviews *28*, 603–661.

Toomre, D. and Pawley, J. B. (2006). Disk-Scanning Confocal Microscopy. In Handbook Of Biological Confocal Microscopy, (Pawley, J. B., ed.), pp. 221–238. Springer US Boston, MA.

Torres, V. J., Stauff, D. L., Pishchany, G., Bezbradica, J. S., Gordy, L. E., Iturregui, J., Anderson, K., Dunman, P. M., Joyce, S. and Skaar, E. P. (2007). A Staphylococcus aureus Regulatory System that Responds to Host Heme and Modulates Virulence. Cell Host & Microbe *1*, 109–119.

Truckenbrodt, S., Sommer, C., Rizzoli, S. O. and Danzl, J. G. (2019). A practical guide to optimization in X10 expansion microscopy. Nature Protocols *14*, 832–863.

Trzcinski, K., Cooper, B. S., Hryniewicz, W. and Dowson, C. G. (2000). Expression of resistance to tetracyclines in strains of methicillin-resistant Staphylococcus aureus. Journal of Antimicrobial Chemotherapy *45*, 763–770.

Tuffs, S. W., James, D. B. A., Bestebroer, J., Richards, A. C., Goncheva, M. I., O'Shea, M., Wee, B. A., Seo, K. S., Schlievert, P. M., Lengeling, A., van Strijp, J. A., Torres, V. J. and Fitzgerald, J. R. (2017). The Staphylococcus aureus superantigen SElX is a bifunctional toxin that inhibits neutrophil function. PLOS Pathogens *13*, e1006461.

Udo, E. E., Pearman, J. W. and Grubb, W. B. (1993). Genetic analysis of community isolates of methicillin-resistant Staphylococcus aureus in Western Australia. The Journal of Hospital Infection *25*, 97–108.

van de Linde, S., Heilemann, M. and Sauer, M. (2012). Live-Cell Super-Resolution Imaging with Synthetic Fluorophores. Annual Review of Physical Chemistry *63*, 519–540.

van Kessel, K. P. M., Bestebroer, J. and van Strijp, J. A. G. (2014). Neutrophil-Mediated Phagocytosis of Staphylococcus aureus. Frontiers in Immunology *5*.

Vanbelkum, A., Melles, D., Nouwen, J., Vanleeuwen, W., Vanwamel, W., Vos, M., Wertheim, H. and Verbrugh, H. (2009). Co-evolutionary aspects of human colonisation and infection by Staphylococcus aureus. Infection, Genetics and Evolution *9*, 32–47.

Ventura, C. L., Malachowa, N., Hammer, C. H., Nardone, G. A., Robinson, M. A., Kobayashi, S. D. and DeLeo, F. R. (2010). Identification of a Novel Staphylococcus aureus Two-Component Leukotoxin Using Cell Surface Proteomics. PLoS ONE *5*, e11634.

Verveer, Hanley, Verbeek, Van Vliet and Jovin (1998). Theory of confocal fluorescence imaging in the programmable array microscope (PAM). Journal of Microscopy *189*, 192–198.

Voyich, J. M., Braughton, K. R., Sturdevant, D. E., Whitney, A. R., Said-Salim, B., Porcella, S. F., Long, R. D., Dorward, D. W., Gardner, D. J., Kreiswirth, B. N., Musser, J. M. and DeLeo, F. R. (2005). Insights into Mechanisms Used by Staphylococcus aureus to Avoid Destruction by Human Neutrophils. The Journal of Immunology *175*, 3907–3919.

Wang, X., Yousefi, S. and Simon, H.-U. (2018). Necroptosis and neutrophil-associated disorders. Cell Death & Disease *9*.

Wassie, A. T., Zhao, Y. and Boyden, E. S. (2019). Expansion microscopy: principles and uses in biological research. Nature Methods *16*, 33–41.

Wheeler, M. A., Smith, S. D., García-Cardeña, G., Nathan, C. F., Weiss, R. M. and Sessa, W. C. (1997). Bacterial infection induces nitric oxide synthase in human neutrophils. Journal of Clinical Investigation *99*, 110–116.

Winterbourn, C. C., Kettle, A. J. and Hampton, M. B. (2016). Reactive Oxygen Species and Neutrophil Function. Annual Review of Biochemistry *85*, 765–792.

Wu, Y. and Shroff, H. (2018). Faster, sharper, and deeper: structured illumination microscopy for biological imaging. Nature Methods *15*, 1011–1019.

Yang, D., Ho, Y. X., Cowell, L. M., Jilani, I., Foster, S. J. and Prince, L. R. (2019). A Genome-Wide Screen Identifies Factors Involved in S. aureus-Induced Human Neutrophil Cell Death and Pathogenesis. Frontiers in Immunology *10*.

Yang, D.-L., Xu, J.-W., Zhu, J.-G., Zhang, Y.-L., Xu, J.-B., Sun, Q., Cao, X.-N., Zuo, W.-L., Xu, R.-S., Huang, J.-H., Jiang, F.-N., Zhuo, Y.-J., Xiao, B.-Q., Liu, Y.-Z., Yuan, D.-B., Sun, Z.-L., He, H.-C., Lun, Z.-R., Zhong, W.-D. and Zhou, W.-L. (2017). Role of GPR30 in estrogen-induced prostate epithelial apoptosis and benign prostatic hyperplasia. Biochemical and Biophysical Research Communications *487*, 517–524.

Yaseen, R., Blodkamp, S., Lüthje, P., Reuner, F., Völlger, L., Naim, H. Y. and von Köckritz-Blickwede, M. (2017). Antimicrobial activity of HL-60 cells compared to primary blood-derived neutrophils against Staphylococcus aureus. Journal of Negative Results in BioMedicine *16*.

Yin, C. and Heit, B. (2018). Armed for destruction: formation, function and trafficking of neutrophil granules. Cell and Tissue Research *371*, 455–471.

Yoong, P. and Torres, V. J. (2015). Counter inhibition between leukotoxins attenuates Staphylococcus aureus virulence. Nature Communications *6*, 8125.

York, A. G., Chandris, P., Nogare, D. D., Head, J., Wawrzusin, P., Fischer, R. S., Chitnis, A. and Shroff, H. (2013). Instant super-resolution imaging in live cells and embryos via analog image processing. Nature Methods *10*, 1122–1126.

York, A. G., Parekh, S. H., Nogare, D. D., Fischer, R. S., Temprine, K., Mione, M., Chitnis, A. B., Combs, C. A. and Shroff, H. (2012). Resolution doubling in live, multicellular organisms via multifocal structured illumination microscopy. Nature Methods *9*, 749–754.

Zeng, Q., Chen, G. G., Vlantis, A. C. and van Hasselt, C. A. (2007). Oestrogen mediates the growth of human thyroid carcinoma cells via an oestrogen receptor – ERK pathway. Cell Proliferation *40*, 921–935.

Zhou, Y., Niu, C., Ma, B., Xue, X., Li, Z., Chen, Z., Li, F., Zhou, S., Luo, X. and Hou, Z. (2018). Inhibiting PSMa-induced neutrophil necroptosis protects mice with MRSA pneumonia by blocking the agr system. Cell Death & Disease *9*.

Zimmer, M. (2009). GFP: from jellyfish to the Nobel prize and beyond. Chemical Society Reviews *38*, 2823.

Zurek, O. W., Pallister, K. B. and Voyich, J. M. (2015). *Staphylococcus aureus* Inhibits Neutrophil-derived IL-8 to Promote Cell Death. Journal of Infectious Diseases *212*, 934–938.

Zysk, G., Bejo, L., Schneider-Wald, B. K., Nau, R. and Heinz, H.-P. (2000). Induction of necrosis and apoptosis of neutrophil granulocytes by Streptococcus pneumoniae. Clinical and Experimental Immunology *122*, 61–66.

Appendix A

Identifying hits from 1st round of screen

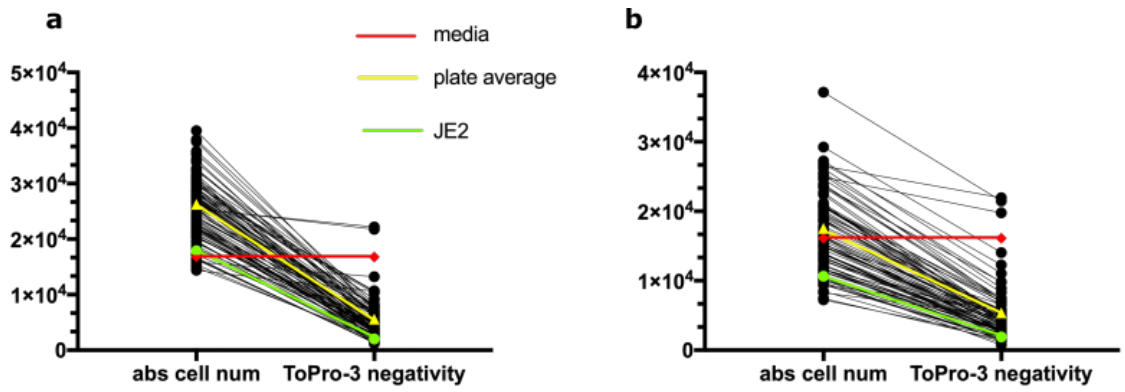

Fig. A.1 **Representative plots of plate 1.** Screen results from plate 1. The plate was screened twice using cells from two independent donors (n=2), a) donor 1 and b) donor 2. The yellow line indicated the threshold level, red line indicated uninfected neutrophils in media as control and the green line indicated untreated neutrophils co-infected with JE2. Each black line indicated the individual wells in each plate.

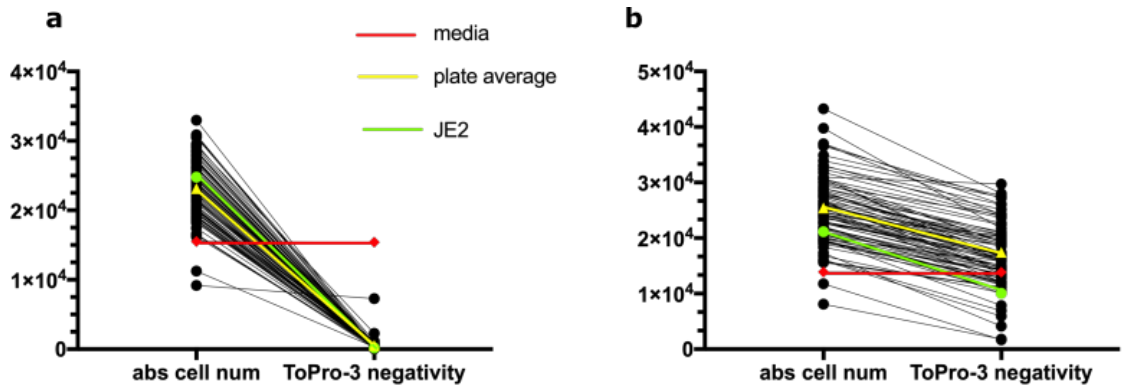

Fig. A.2 **Representative plots of plate 2.** Screen results from plate 2. The plate was screened twice using cells from two independent donors (n=2), a) donor 1 and b) donor 2. The yellow line indicated the threshold level, red line indicated uninfected neutrophils in media as control and the green line indicated untreated neutrophils co-infected with JE2. Each black line indicated the individual wells in each plate.

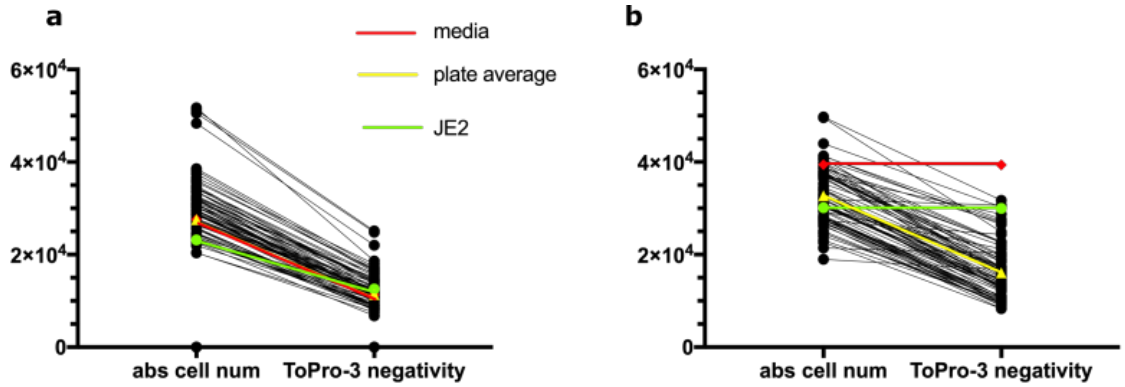

Fig. A.3 **Representative plots of plate 3.** Screen results from plate 3. The plate was screened twice using cells from two independent donors (n=2), a) donor 1 and b) donor 2. The yellow line indicated the threshold level, red line indicated uninfected neutrophils in media as control and the green line indicated untreated neutrophils co-infected with JE2. Each black line indicated the individual wells in each plate.

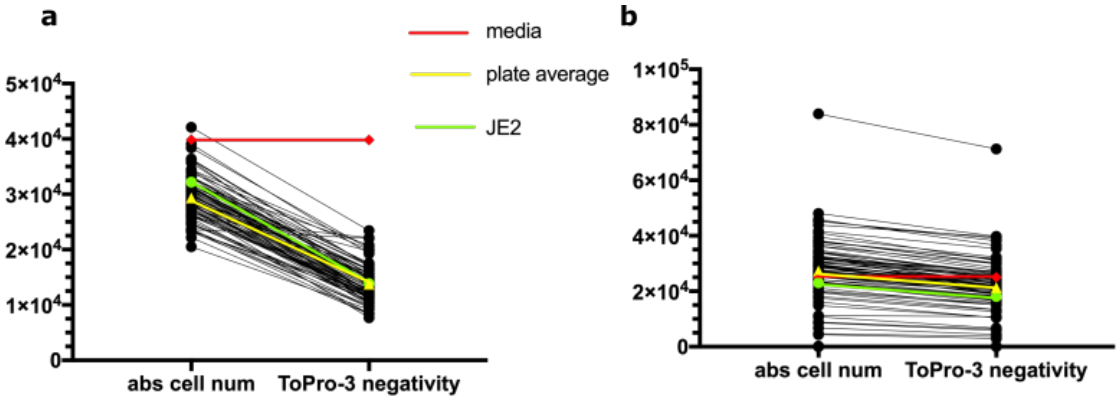

Fig. A.4 **Representative plots of plate 4.** Screen results from plate 4. The plate was screened twice using cells from two independent donors (n=2), a) donor 1 and b) donor 2. The yellow line indicated the threshold level, red line indicated uninfected neutrophils in media as control and the green line indicated untreated neutrophils co-infected with JE2. Each black line indicated the individual wells in each plate.

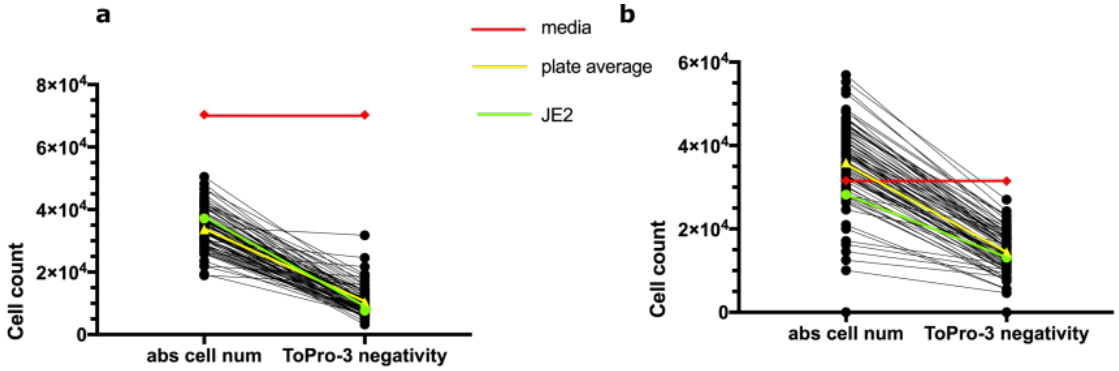

Fig. A.5 **Representative plots of plate 5.** Screen results from plate 5. The plate was screened twice using cells from two independent donors (n=2), a) donor 1 and b) donor 2. The yellow line indicated the threshold level, red line indicated uninfected neutrophils in media as control and the green line indicated untreated neutrophils co-infected with JE2. Each black line indicated the individual wells in each plate.

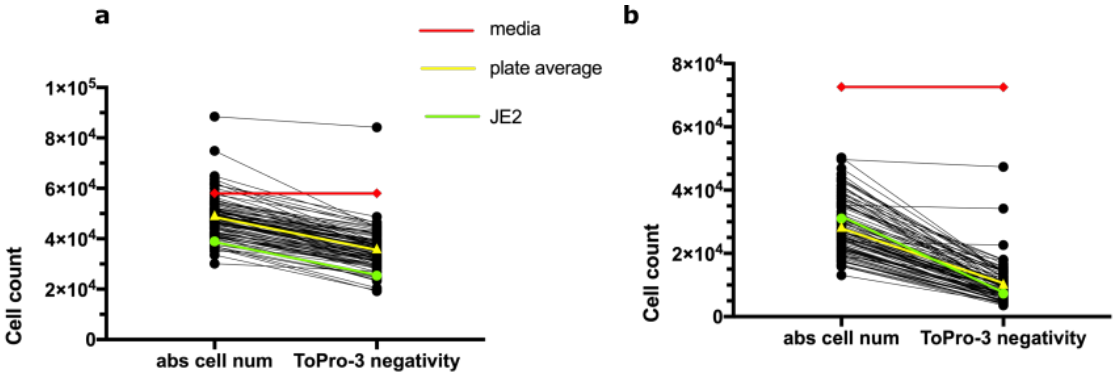

Fig. A.6 **Representative plots of plate 6.** Screen results from plate 6. The plate was screened twice using cells from two independent donors (n=2), a) donor 1 and b) donor 2. The yellow line indicated the threshold level, red line indicated uninfected neutrophils in media as control and the green line indicated untreated neutrophils co-infected with JE2. Each black line indicated the individual wells in each plate.

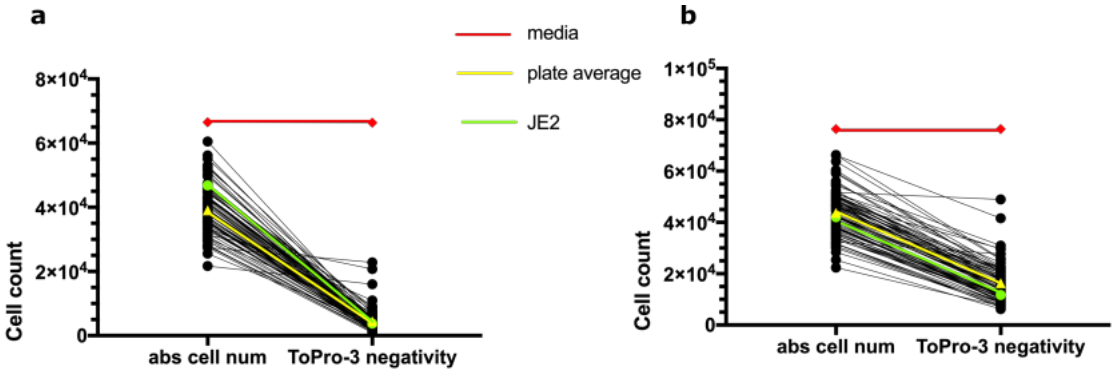

Fig. A.7 **Representative plots of plate 7.** Screen results from plate 7. The plate was screened twice using cells from two independent donors (n=2), a) donor 1 and b) donor 2. The yellow line indicated the threshold level, red line indicated uninfected neutrophils in media as control and the green line indicated untreated neutrophils co-infected with JE2. Each black line indicated the individual wells in each plate.

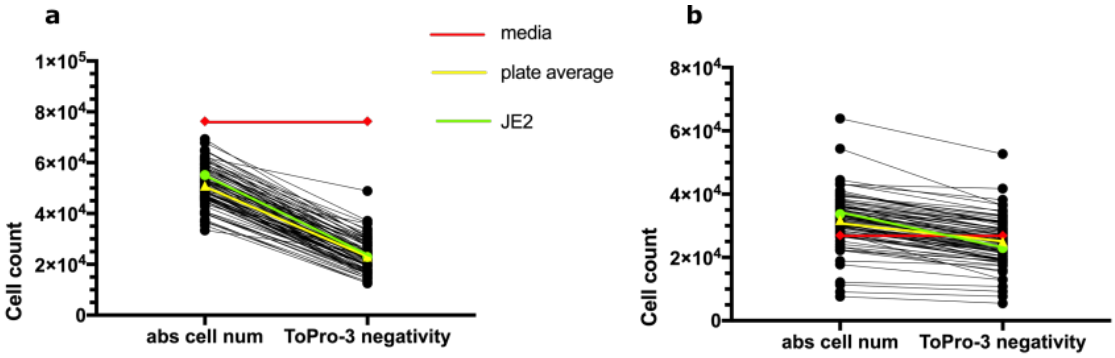

Fig. A.8 **Representative plots of plate 8.** Screen results from plate 8. The plate was screened twice using cells from two independent donors (n=2), a) donor 1 and b) donor 2. The yellow line indicated the threshold level, red line indicated uninfected neutrophils in media as control and the green line indicated untreated neutrophils co-infected with JE2. Each black line indicated the individual wells in each plate.

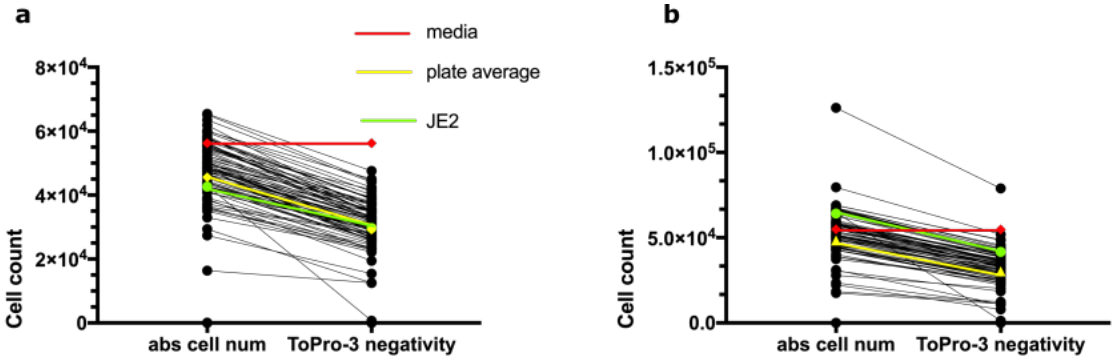

Fig. A.9 **Representative plots of plate 10.** Screen results from plate 10. The plate was screened twice using cells from two independent donors (n=2), a) donor 1 and b) donor 2. The yellow line indicated the threshold level, red line indicated uninfected neutrophils in media as control and the green line indicated untreated neutrophils co-infected with JE2. Each black line indicated the individual wells in each plate.

Appendix B

High throughput flow cytometry data analysis code

```
from openpyxl import load_workbook
wb=load_workbook(filename='281118P2n1.xlsx') #check file is in .xlsx
                                    not .xls format
wb.sheetnames
sheet=wb['281118P2n1']#check sheetname!
tuple(sheet['D2':'V289'])
# to extract the Name and Statistic data only
for NamesandStats in sheet['D2':'V289']:
    for names in NamesandStats:
        break

# Extract R1 data to look at the absolute cell number:
data=[NamesandStats]
all=[]
for i in range(3,289,3): #select all R1 data
    v2=[i,sheet.cell(row=i,column=4).value,sheet.cell(row=i,column=22
                                        ).value]
```

```
    all.append(v2)

#select control wells 1
    c1=[]
for k in range (3,289,36):
    c2=[k,sheet.cell(row=k,column=4).value,sheet.cell(row=k,column=22
                                        ).value]
    c1.append(c2)

#select control wells 12 (15/03/19)
    c12=[]
for j in range(36,289,36):
    c13=[j,sheet.cell(row=j,column=4).value,sheet.cell(row=j,column=
                                        22).value]
    c12.append(c13)

# remove control wells 1 from data
removeC1=[x for x in all if x not in c1]

# remove control wells 12 from data 15/03/19
compoundsOnly=[x for x in removeC1 if x not in c12]

# add all the numbers together, then get mean and s.d from there
sumAll=[]
value=0
for m in range(len(compoundsOnly)):
    m1=compoundsOnly[value]
    m2=m1[2]
    value+=1
    sumAll.append(m2)

import numpy as np
```

```
# mean=getMean(sumAll)
mean,std=np.mean(sumAll),np.std(sumAll)
print("R1 data analysis:")
print("Mean =",mean,", Standard deviation =",std)
# get threshold by 1.5s.d
setL1= (std/2)+std
setThreshold= mean+setL1
print("Threshold =",setThreshold)
# find values that are >= threshold value
hValue=[h for h in sumAll if h>= setThreshold]

#plot bar graph of R1 absolute cell num
import matplotlib.pyplot as plt
ypos=np.arange(len(sumAll))
plt.ylabel('absolute cell number')
plt.xlabel('Wells')
plt.bar(ypos,sumAll)
plt.axhline(y=setThreshold,linewidth=1,color='k')
plt.show()

#convert to dictionary to search hits
a1=tuple(removeC1)
a2=dict([ (k, [v, w]) for k, v, w in a1 ])
#convert to dataframe to make search easier?
import pandas as pd
df=pd.DataFrame(a2,columns=a2.keys())
df2=df.T
df2.columns=['Name','Stats']
# find the hits from dataframe
hit=df2.isin(hValue)
matchHit=df2[hit]
```

```
#find hits from the big list and return names that contain hit values
foundHit=pd.merge(df2,matchHit,on=['Stats'])
print ('Hits found: ',foundHit)

# Extract R2 data to look at the ToPro3 negativity:
dataR2=[NamesandStats]
allR2=[]
for i2 in range(4,290,3): #select all R2 data
    #print(i,sheet.cell(row=i,column=4).value,sheet.cell(row=i,column
                                        =21).value)
    vR2=[i2,sheet.cell(row=i2,column=4).value,sheet.cell(row=i2,
                                        column=22).value]
    allR2.append(vR2)
#select control wells 1
    cR1=[]
for k2 in range (4,290,36):
    cR2=[k2,sheet.cell(row=k2,column=4).value,sheet.cell(row=k2,
                                        column=22).value]
    cR1.append(cR2)

#select control wells 12 (15/03/19)
    cR12=[]
for j2 in range(37,290,36):
    cR13=[j2,sheet.cell(row=j2,column=4).value,sheet.cell(row=j2,
                                        column=22).value]
    cR12.append(cR13)

# remove control wells 1 and 12 from data
removeCR1=[y for y in allR2 if y not in cR1]
compoundsOnlyR2=[y for y in removeCR1 if y not in cR12]

# add all the numbers together, then get mean and s.d
```

```
sumAllR2=[]
valueR2=0
for mR in range(len(compoundsOnlyR2)):
    mR1=compoundsOnlyR2[valueR2]
    mR2=mR1[2]
    valueR2+=1
    sumAllR2.append(mR2)
# mean=getMean(sumAll)
mean1,std1=np.mean(sumAllR2),np.std(sumAllR2)
print("R2 data analysis:")
print("Mean =",mean1,", Standard deviation =",std1)
# get threshold by 1.5s.d
setLR1= (std1/2)+std1
setThreshold2= mean1+setLR1
print("Threshold =",setThreshold2)
# find values that are >= threshold value
hValueR2=[h2 for h2 in sumAllR2 if h2>= setThreshold2]
# plot bar graph of R2 \% ToPro3 negativity
import matplotlib.pyplot as plt
ypos=np.arange(len(sumAllR2))
plt.ylabel('ToPro3 negativity')
plt.xlabel('Wells')
plt.bar(ypos,sumAllR2)
plt.axhline(y=setThreshold2,linewidth=1,color='k')
plt.show()

#convert to dictionary to search hits
aR1=tuple(removeCR1)
aR2=dict([ (k1, [v1, w1]) for k1, v1, w1 in aR1 ])
#convert to dataframe to make search easier
import pandas as pd
dfR=pd.DataFrame(aR2,columns=aR2.keys())
```

```
dfR2=dfR.T
dfR2.columns=['Name','Stats']
# find the hits from dataframe
hitR2=dfR2.isin(hValueR2)
matchHitR2=dfR2[hitR2]
#find hits from the big list and return names that contain hit values
foundHitR2=pd.merge(dfR2,matchHitR2,on=['Stats'])
print ('Hits found: ',foundHitR2)
print("R1 data analysis:", "Mean =",mean,", Standard deviation =",std
                                    , '"Threshold =",setThreshold,
''Hits found: ',foundHit,' "R2 data analysis:",'"Mean =",mean1,",
                                    Standard deviation =",std1,'"
                                    Threshold =",setThreshold2,
''Hits found: ',foundHitR2,
file=open("281118P2n1_NewResults.txt", "a")#change the output name!
```